frontiers | Research Topics

Brain vs retina - differences and commonalities: The role of oxidative stress in neurodegenerative diseases

Edited by
Jose Hurst, Sven Schnichels, Ritushree Kukreti, Sandra Kuehn and Abel Santamaria

Published in
Frontiers in Neuroscience

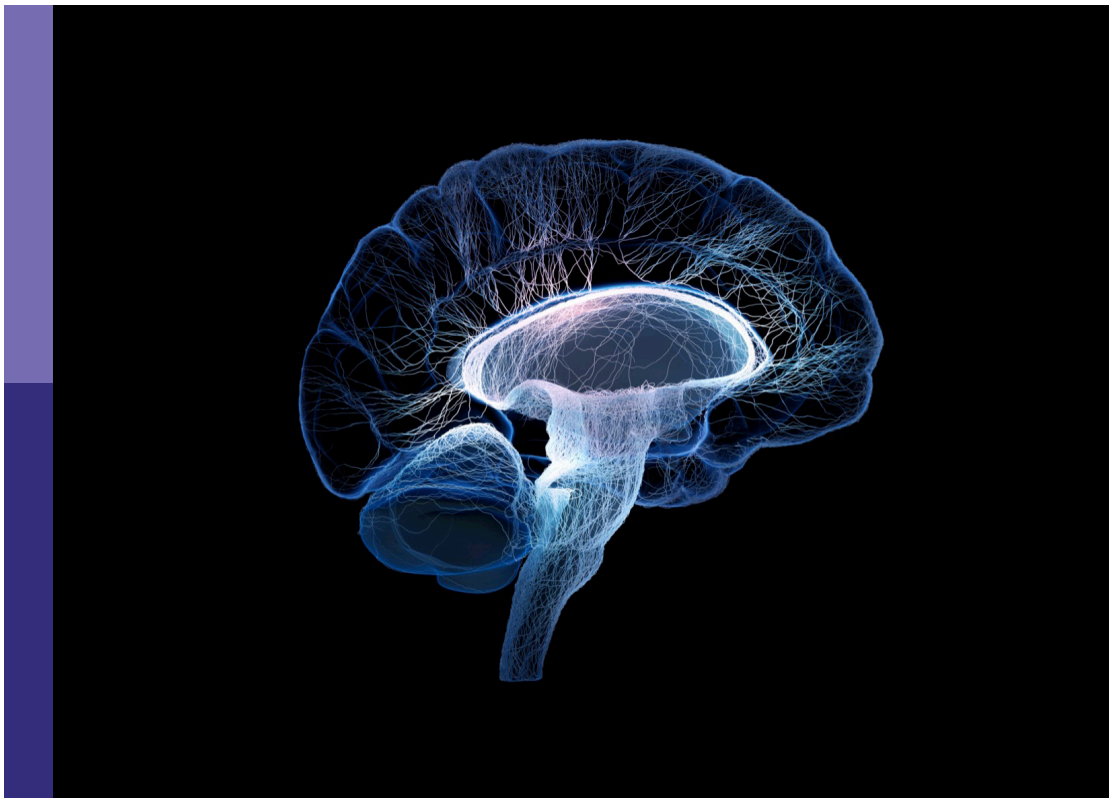

ISSN 1664-8714
ISBN 978-2-83252-025-3
DOI 10.3389/978-2-83252-025-3

About Frontiers

Frontiers is more than just an open access publisher of scholarly articles: it is a pioneering approach to the world of academia, radically improving the way scholarly research is managed. The grand vision of Frontiers is a world where all people have an equal opportunity to seek, share and generate knowledge. Frontiers provides immediate and permanent online open access to all its publications, but this alone is not enough to realize our grand goals.

Frontiers journal series

The Frontiers journal series is a multi-tier and interdisciplinary set of open-access, online journals, promising a paradigm shift from the current review, selection and dissemination processes in academic publishing. All Frontiers journals are driven by researchers for researchers; therefore, they constitute a service to the scholarly community. At the same time, the *Frontiers journal series* operates on a revolutionary invention, the tiered publishing system, initially addressing specific communities of scholars, and gradually climbing up to broader public understanding, thus serving the interests of the lay society, too.

Dedication to quality

Each Frontiers article is a landmark of the highest quality, thanks to genuinely collaborative interactions between authors and review editors, who include some of the world's best academicians. Research must be certified by peers before entering a stream of knowledge that may eventually reach the public - and shape society; therefore, Frontiers only applies the most rigorous and unbiased reviews. Frontiers revolutionizes research publishing by freely delivering the most outstanding research, evaluated with no bias from both the academic and social point of view. By applying the most advanced information technologies, Frontiers is catapulting scholarly publishing into a new generation.

What are Frontiers Research Topics?

Frontiers Research Topics are very popular trademarks of the *Frontiers journals series*: they are collections of at least ten articles, all centered on a particular subject. With their unique mix of varied contributions from Original Research to Review Articles, Frontiers Research Topics unify the most influential researchers, the latest key findings and historical advances in a hot research area.

Find out more on how to host your own Frontiers Research Topic or contribute to one as an author by contacting the Frontiers editorial office: frontiersin.org/about/contact

Brain vs retina - differences and commonalities: The role of oxidative stress in neurodegenerative diseases

Topic editors

Jose Hurst — University Hospital Tübingen, Germany
Sven Schnichels — University Hospital Tübingen, Germany
Ritushree Kukreti — Institute of Genomics and Integrative Biology, Council of Scientific and Industrial Research (CSIR), India
Sandra Kuehn — University of Oslo, Norway
Abel Santamaria — Manuel Velasco Suárez National Institute of Neurology and Neurosurgery, Mexico

Citation

Hurst, J., Schnichels, S., Kukreti, R., Kuehn, S., Santamaria, A., eds. (2023). *Brain vs retina - differences and commonalities: The role of oxidative stress in neurodegenerative diseases*. Lausanne: Frontiers Media SA.
doi: 10.3389/978-2-83252-025-3

Table of contents

frontiers | Frontiers in Neuroscience

TYPE Editorial
PUBLISHED 13 March 2023
DOI 10.3389/fnins.2023.1171235

OPEN ACCESS

EDITED AND REVIEWED BY
Wendy Noble,
King's College London, United Kingdom

*CORRESPONDENCE
José Hurst
✉ jose.hurst@med.uni-tuebingen.de

SPECIALTY SECTION
This article was submitted to Neurodegeneration, a section of the journal Frontiers in Neuroscience

RECEIVED 21 February 2023
ACCEPTED 27 February 2023
PUBLISHED 13 March 2023

CITATION
Hurst J and Schnichels S (2023) Editorial: Brain vs. retina - Differences and commonalities: The role of oxidative stress in neurodegenerative diseases. *Front. Neurosci.* 17:1171235. doi: 10.3389/fnins.2023.1171235

Editorial: Brain vs. retina - Differences and commonalities: The role of oxidative stress in neurodegenerative diseases

José Hurst* and Sven Schnichels

Center for Ophthalmology, University Eye Clinic, University Hospital Tübingen, Tübingen, Germany

KEYWORDS

neurodegeneration, oxidative stress, retina, ROS, neurological disorder

Editorial on the Research Topic
Brain vs. retina - Differences and commonalities: The role of oxidative stress in neurodegenerative diseases

The articles in this Research Topic shed light on the intricate relationship between oxidative stress and neurodegeneration in ophthalmic and neurological disorders. Oxidative stress is a hallmark of these disorders, and the articles highlight the importance of understanding the mechanisms of oxidative stress in order to develop effective therapeutic interventions. Both the brain and the retina are highly susceptible to oxidative stress, which can contribute to neurodegeneration (Wakamatsu et al., 2008; Angelova and Abramov, 2018; Domanskyi and Parlato, 2022). Oxidative stress is a condition with an imbalance between the production of reactive oxygen species (ROS) and the ability of cells to detoxify or repair the damage caused by ROS (Pizzino et al., 2017). Although the retina is the light sensitive part of the eye, it is also an extension of the brain as it contains central neural tissue and is directly connected to the brain *via* the optic nerve. So, while the retina is technically not a part of the brain, it is directly connected and dependent on the brain for its function in creating our visual perception (Rabin, 2013). Moreover, the exchange of (neurotrophic) factors between the eye and the brain is essential for survival and function of the connected cells, which means, if the counterpart dies, this has direct effects to the corresponding cells in the other organ and subsequently to their up- or downstream connected cells.

In the brain, oxidative stress can be caused by a number of factors, including inflammation, mitochondrial dysfunction and the accumulation of misfolded proteins such as amyloid beta and tau, which are hallmarks of Alzheimer's disease (Korovesis et al., 2023). ROS can damage proteins, lipids as well as DNA, and this damage can lead to neuronal dysfunction and death, which can contribute to the development and progression of neurodegenerative diseases (Pereira et al., 2012; Williams et al., 2013). In addition to Alzheimer's disease, other neurodegenerative diseases such as Parkinson's disease, multiple sclerosis, and Huntington's disease can also manifest in the eye or in its extensions (Archibald et al., 2009; Williams et al., 2013). For example, patients with Parkinson's disease may have visual hallucinations, whereas changes in visual acuity and contrast sensitivity are more common in multiple sclerosis (Zhang et al.).

In the retina, oxidative stress can also be caused by a number of factors, including age-related changes, light exposure and inflammation. The high metabolic rate and constant exposure to light renders the retina particularly vulnerable to oxidative stress, which can generate ROS (Sasaki et al., 2010; Williams et al., 2013). ROS can damage the cells of the retina, including the light-perceiving photoreceptors, and this damage can contribute to the development of age-related macular degeneration and other eye diseases such as glaucoma (Zanon-Moreno and Pinazo-Duran, 2008; Wiktorowska-Owczarek and Nowak, 2010; Marie et al., 2015). However, oxidative stress and inflammation play a role in the development and progression of other retinal diseases such as diabetic retinopathy, retinitis pigmentosa, or Leber's Hereditary Optic Neuropathy (LHON) (Kang and Yang, 2020; Gallenga et al., 2021; Rovcanin et al., 2021).

The article by Ryan et al. explores the role of oxidative stress in traumatic injury to the brain and retina. The study discovered that oxidative stress plays a critical role in neuronal death and tissue damage in the brain and retina after injury (Ryan et al.). Mitochondrial transplantation, as demonstrated in the second article by Lin et al., can mitigate these effects and improve locomotor function after spinal cord injury in rats. Similarly, the article by Zhou et al. reveals that superoxide dismutase 2 can ameliorate mitochondrial dysfunction in skin fibroblasts of patients with LHON, providing a potential therapeutic strategy for this genetic disorder.

In the context of retinal degeneration, the article by Gibbons et al. demonstrates that SARM1 promotes photoreceptor degeneration in an oxidative stress model of retinal degeneration. This finding highlights the importance of targeting SARM1 as a potential therapeutic strategy for retinal degenerative diseases (Gibbons et al.). In addition, the article by Wang et al. shows that complement C3a receptor inactivation can attenuate retinal degeneration induced by oxidative damage, providing further evidence for the role of oxidative stress in retinal degeneration.

The article by Constable et al. provides insights into the electroretinogram (ERG) characteristics of patients with autism spectrum disorder and attention deficit hyperactivity disorder. The study used discrete wavelet transform analysis to identify specific frequency bands that may be associated with these disorders (Constable et al.). Zhang et al. demonstrates a correlation between ophthalmologic problems and cognitive impairment in patients with Parkinson's disease, suggesting ophthalmic examinations may serve as a useful tool for monitoring cognitive decline in these patients. Finally, Wolfrum et al. shed light on the role of p53 in AMD and draw comparisons to the role of p53 in Alzheimer's and Parkinson's disease.

In conclusion, the close relationship between the eye and the brain provides an opportunity for researchers and clinicians to gain insight into the pathogenesis and progression of neurodegenerative diseases and develop novel diagnostic and therapeutic approaches. Collectively, these articles highlight the importance of oxidative stress in the pathogenesis of neurodegenerative and ophthalmic disorders. Future studies should focus on elucidating the mechanisms of oxidative stress and identifying effective therapeutic strategies that can mitigate the damaging effects of oxidative stress on the brain and retina.

Overall, this Research Topic provides a comprehensive overview of the current understanding of the interplay between oxidative stress and neurodegeneration in ophthalmic and neurological disorders. We hope that the findings presented here will inspire further research in this area and ultimately lead to the development of effective treatments for these devastating disorders. Additionally, due to several similarities between eye and brain disorders understanding similar pathomechanisms might lead to dual-use of therapeutics. Moreover, as the retina is visible from the outside, diagnostic techniques to not only diagnose eye diseases but also brain disease should be investigated with a greater extent.

Author contributions

All authors listed have made a substantial, direct, and intellectual contribution to the work and approved it for publication.

Conflict of interest

The authors declare that the research was conducted in the absence of any commercial or financial relationships that could be construed as a potential conflict of interest.

Publisher's note

References

Angelova, P. R., and Abramov, A. Y. (2018). Role of mitochondrial ROS in the brain: from physiology to neurodegeneration. *FEBS Lett.* 592, 692–702. doi: 10.1002/1873-3468.12964

Archibald, N. K., Clarke, M. P., Mosimann, U. P., and Burn, D. J. (2009). The retina in Parkinson's disease. *Brain* 132, 1128–1145. doi: 10.1093/brain/awp068

Domanskyi, A., and Parlato, R. (2022). Oxidative Stress in Neurodegenerative Diseases. *Antioxidants* 11, 504. doi: 10.3390/antiox11030504

Gallenga, C. E., Lonardi, M., Pacetti, S., Violanti, S. S., Tassinari, P., Virgilio, F. D., et al. (2021). Molecular mechanisms related to oxidative stress in retinitis pigmentosa. *Antioxidants* 10, 848. doi: 10.3390/antiox10060848

Kang, Q., and Yang, C. (2020). Oxidative stress and diabetic retinopathy: molecular mechanisms, pathogenetic role and therapeutic implications. *Redox Biol.* 37, 101799. doi: 10.1016/j.redox.2020.101799

Korovesis, D., Rubio-Tomas, T., and Tavernarakis, N. (2023). Oxidative stress in age-related neurodegenerative diseases: an overview of recent tools and findings. *Antioxidants* 12, 131. doi: 10.3390/antiox12010131

Marie, M., Bigot, K., Barrau, C., Gondouin, P., Pagan, D., Angebault-Prouteau, C., et al. (2015). Blue light induced oxidative stress in an *in vitro* model of AMD. *Invest. Ophthalmol. Vis. Sci.* 56, 4256.

Pereira, M. D., Ksiazek, K., and Menezes, R. (2012). Oxidative stress in neurodegenerative diseases and ageing. *Oxid. Med. Cell. Longev.* 2012, 796360. doi: 10.1155/2012/796360

Pizzino, G., Irrera, N., Cucinotta, M., Pallio, G., Mannino, F., Arcoraci, V., et al. (2017). Oxidative stress: harms and benefits for human health. *Oxid. Med. Cell. Longev.* 2017, 8416763. doi: 10.1155/2017/8416763

Rabin, J. C. (2013). The retina: an approachable part of the brain. *Optometr. Vis. Sci.* 90, e36. doi: 10.1097/OPX.0b013e3182805b2b

Rovcanin, B., Jancic, J., Pajic, J., Rovcanin, M., Samardzic, J., Djuric, V., et al. (2021). Oxidative stress profile in genetically confirmed cases of leber's hereditary optic neuropathy. *J. Mol. Neurosci.* 71, 1070–1081. doi: 10.1007/s12031-020-01729-y

Sasaki, M., Ozawa, Y., Kurihara, T., Kubota, S., Yuki, K., Noda, K., et al. (2010). Neurodegenerative influence of oxidative stress in the retina of a murine model of diabetes. *Diabetologia* 53, 971–979. doi: 10.1007/s00125-009-1655-6

Wakamatsu, T. H., Dogru, M., and Tsubota, K. (2008). Tearful relations: oxidative stress, inflammation and eye diseases. *Arq. Bras. Oftalmol.* 71, 72–79. doi: 10.1590/S0004-27492008000700015

Wiktorowska-Owczarek, A., and Nowak, J. Z. (2010). Pathogenesis and prophylaxis of AMD: focus on oxidative stress and antioxidants. *Postep. Hig. Med. Dosw.* 64, 333–343.

Williams, P. A., Thirgood, R. A., Oliphant, H., Frizzati, A., Littlewood, E., Votruba, M., et al. (2013). Retinal ganglion cell dendritic degeneration in a mouse model of Alzheimer's disease. *Neurobiol. Aging* 34, 1799–1806. doi: 10.1016/j.neurobiolaging.2013.01.006

Zanon-Moreno, V., and Pinazo-Duran, M. D. (2008). Oxidative stress theory of glaucoma. *J. Glaucoma* 17, 508–509. doi: 10.1097/IJG.0b013e318188b22f

frontiers | Frontiers in Neuroscience

BRIEF RESEARCH REPORT
published: 01 April 2022
doi: 10.3389/fnins.2022.852114

SARM1 Promotes Photoreceptor Degeneration in an Oxidative Stress Model of Retinal Degeneration

Luke Gibbons[1,2†], Ema Ozaki[1,2†], Chris Greene[3], Anne Trappe[4], Michael Carty[5,6], Judith A. Coppinger[4], Andrew G. Bowie[5,6], Matthew Campbell[3] and Sarah L. Doyle[1,2]*

[1] Trinity College Institute of Neuroscience, Trinity College Dublin, Dublin, Ireland, [2] Department of Clinical Medicine, School of Medicine, Trinity College Dublin, Dublin, Ireland, [3] Smurfit Institute of Genetics, Trinity College Dublin, Dublin, Ireland, [4] School of Pharmacy and Biomolecular Sciences, Royal College of Surgeons in Ireland, Dublin, Ireland, [5] School of Biochemistry and Immunology, Trinity College Dublin, Dublin, Ireland, [6] Trinity Biomedical Sciences Institute, Trinity College Dublin, Dublin, Ireland

OPEN ACCESS

Edited by:
Sandra Kuehn,
University of Oslo, Norway

Reviewed by:
Victoria Maneu,
University of Alicante, Spain
Michael B. Powner,
City University of London,
United Kingdom

***Correspondence:**
Sarah L. Doyle
sarah.doyle@tcd.ie

[†] These authors have contributed equally to this work

Specialty section:
This article was submitted to Neurodegeneration, a section of the journal Frontiers in Neuroscience

Received: 10 January 2022
Accepted: 04 March 2022
Published: 01 April 2022

Citation:
Gibbons L, Ozaki E, Greene C, Trappe A, Carty M, Coppinger JA, Bowie AG, Campbell M and Doyle SL (2022) SARM1 Promotes Photoreceptor Degeneration in an Oxidative Stress Model of Retinal Degeneration. Front. Neurosci. 16:852114. doi: 10.3389/fnins.2022.852114

SARM1 (sterile alpha and armadillo motif-containing protein) is a highly conserved Toll/IL-1 Receptor (TIR) adaptor with important roles in mediating immune responses. Studies in the brain have shown that SARM1 plays a role in induction of neuronal axon degeneration in response to a variety of injuries. We recently demonstrated that SARM1 is pro-degenerative in a genetic model of inherited retinopathy. This current study aimed to characterise the effect of SARM1 deletion in an alternative model of retinal degeneration (RD) in which the retinal pigment epithelium (RPE) fragments following administration of oxidising agent, sodium iodate ($NaIO_3$), leading to subsequent photoreceptor cell death. Following administration of $NaIO_3$, we observed no apparent difference in rate of loss of RPE integrity in SARM1 deficient mice compared to WT counterparts. However, despite no differences in RPE degeneration, photoreceptor cell number and retinal thickness were increased in *Sarm1*$^{-/-}$ mice compared to WT counterparts. This apparent protection of the photoreceptors in SARM1 deficient mice is supported by an observed decrease in pro-apoptotic caspase-3 in the photoreceptor layer of *Sarm1*$^{-/-}$ mice compared to WT. Together these data indicate a pro-degenerative role for SARM1 in the photoreceptors, but not in the RPE, in an oxidative stress induced model of retinal degeneration consistent with its known degenerative role in neurons in a range of neurodegenerative settings.

Keywords: SARM1, sodium iodate, retinal degeneration, photoreceptors, cell death, caspase-3

Abbreviations: ALS, amyotrophic lateral sclerosis; AMD, age related macular degeneration; GA, geographic atrophy; H&E, haematoxylin and eosin; HMOX1, heme oxygenase 1; NaIO3, sodium iodate; ONL, outer nuclear layer; PNA, Peanut agglutinin; RP, retinitis pigmentosa; SARM1, sterile alpha and toll/interleukin-1 receptor motif–containing 1; SD-OCT, spectral domain optical coherence tomography; TIR, toll-IL-1 receptor; TLR, toll like receptor; TUNEL, terminal deoxynucleotidyl transferase dUTP nick end labelling.

HIGHLIGHTS

- SARM1 is expressed in the neural retina, but not in the RPE/choroid of mice.
- Deletion of SARM1 has no effect on the pace of RPE degeneration in the $NaIO_3$ model.
- *Sarm1*$^{-/-}$ mice show reduced photoreceptor degeneration, markers of cell death, and retain photoreceptor segment length compared to WT counterparts.

INTRODUCTION

Retinal degenerative diseases, such as age-related macular degeneration (AMD) and retinitis pigmentosa (RP), represent one of the leading causes for incurable blindness worldwide. Although the risk factors and disease pathogenesis may differ greatly among these various diseases a common endpoint is the death of photoreceptors (Murakami et al., 2013). As these cells are responsible for the processing of light and initiation of visual signalling, photoreceptor cell death is detrimental to visual function and is ultimately the cause of vision loss in these diseases.

Retinal pigment epithelium (RPE) atrophy and photoreceptor degeneration are key features of late-stage disease in AMD termed geographic atrophy (GA). The RPE is a monolayer of pigmented cells separating the neuroretina and the choroid. It is of neuroectodermal origin and is therefore considered part of the retina. It plays a vital role in providing support for the photoreceptors and participates in the visual cycle, as such photoreceptor cell death occurs following RPE loss/dysfunction. Systemic administration of the oxidising agent sodium iodate ($NaIO_3$) in mice has been demonstrated to be an effective model for studying RPE atrophy *in vivo*, as in response to $NaIO_3$, RPE integrity is lost leading to subsequent secondary photoreceptor degeneration (Kiuchi et al., 2002). In this model it has been shown that RPE cells undergo cell death *via* necroptosis, an inflammatory form of regulated cell death, whereas the photoreceptor cells undergo apoptosis both as a direct effect of $NaIO_3$ administration and from the loss of the supporting RPE (Wang et al., 2014; Hanus et al., 2016).

SARM1 is a member of the Toll/IL-1 Receptor (TIR) domain containing superfamily of proteins and has a role in regulating signalling pathways downstream of Toll Like Receptors (TLRs; O'Neill et al., 2003; Carty et al., 2006). However, unlike other mammalian TIR proteins, SARM1 has a novel role in promoting degeneration of axons in injured neurons, with deletion of SARM1 leading to neuroprotection in mouse and Drosophila models of neurodegeneration (Osterloh et al., 2012). SARM1 activation has been implicated in a range of models of pathological neurodegeneration, including amyotrophic lateral sclerosis (ALS; White et al., 2019), traumatic brain injury (Marion et al., 2019), and chemotherapy induced peripheral neuropathy (Geisler et al., 2016; Bosanac et al., 2021).

This pro-degenerative function is mediated *via* an enzymatic NAD^+ cleavage site in the TIR domain of SARM1 (Gerdts et al., 2015; Essuman et al., 2017). Upon activation SARM1 consumes large amounts of NAD^+, an essential metabolite, leading to metabolic collapse and subsequent cell death/degeneration (Essuman et al., 2017). Such activation occurs in response to a variety of cellular insults, for example mitochondrial toxins, oxygen-glucose deprivation, trophic factor withdrawal, and injury. The precise mechanism by which these disparate factors trigger SARM1 activation is not fully understood (Kim et al., 2007; Tuttolomondo et al., 2009; Mukherjee et al., 2013; Summers et al., 2014), however, recent evidence has suggested that SARM1 acts as a metabolic sensor, becoming activated when the NMN:NAD^+ ratio within a cell becomes skewed toward the former, leading to consumption of the latter by activated SARM1 (Zhao et al., 2019; Figley et al., 2021).

Recently we identified a role for SARM1 in photoreceptor cell death, consistent with its pro-degenerative function in other neuronal cell types, in a mouse model of the inherited retinopathy retinitis pigmentosa (Ozaki et al., 2020). Here we demonstrate the pro-degenerative role of SARM1 in photoreceptors is maintained in the $NaIO_3$ model of retinal degeneration. Interestingly, the attenuation of photoreceptor cell death in the absence of SARM1 occurs despite the pace of RPE atrophy remaining apparently unaffected by the presence or absence of SARM1.

MATERIALS AND METHODS

$NaIO_3$ Model of Retinal Degeneration

All studies carried out in the Smurfit Institute of Genetics in TCD adhere to the principles laid out by the internal ethics committee at TCD, and all relevant national licences were obtained before commencement of all studies. Before experiments, all mice were kept on a 12-h light/dark cycle. Mice used were C57BL/6J mice and *Sarm1*$^{-/-}$ mice at 6–12 weeks old. $NaIO_3$ (40 mg/kg or 50 mg/kg) in 0.9% saline was administered to C57BL/6J and *Sarm1*$^{-/-}$ mice *via* a single intravenous injection (*via* tail vein). Control mice received an intravenous injection of 0.9% saline. Mice were euthanized at either 8 h, 3 days, or 7 days post injection of $NaIO_3$.

Optical Coherence Tomography and Fundus Imaging

Spectral domain optical coherence tomography (SD-OCT) and bright-field live fundus imaging was performed on mice using the image-guided OCT system (Micron IV, Phoenix Research Laboratories) and Micron Reveal software. Mouse pupils were dilated with 1% tropicamide and 2.5% phenylephrine and mice were anaesthetized using a mixture of ketamine/medetomidine (100/0.25 mg/kg). Vidisic lubricant was applied on the cornea of the anaesthetized mice, and the eye was positioned in front of the OCT camera. 50 frames were averaged along the horizontal axis above the optic disc from each eye. The thickness from the ONL to the RPE was measured at 1080 points along the retinal section using the InSight software.

Western Blot

Retinal tissue was lysed in RIPA lysis buffer with phosphatase and protease inhibitors (Sigma-Aldrich) and centrifuged at

15,000 *g* for 15 min. Protein lysates were resolved on a 12% polyacrylamide SDS-PAGE gel and transferred onto a PVDF membrane. Membranes were blocked for 1 h in 5% non-fat milk in Tris-buffered saline with 0.05% Tween-20 (TBST), and then incubated overnight at 4°C in primary antibody against SARM1 (1:1000, 13022, Cell Signalling Technology) and β-Actin (1:5000, Sigma-Aldrich). Membranes were washed three times with TBST and incubated with horseradish peroxidase-conjugated anti-rabbit or anti-mouse antibodies (1:2000, Sigma-Aldrich) in 5% non-fat milk in TBST for 1 h at room temperature. Membranes were washed three times with TBST. Membranes were developed using enhanced chemiluminescence (Advansta) with a Fujifilm LAS3000.

Mass Spectrometry

Retinas were lysed in 10 mM Tris-HCL, pH 7.4, 1 mM EDTA, 0.5% Triton X-100, 1 mM phenylmethylsulfonyl fluoride. Retinal samples were dissolved in 8 M urea, 100 mM Tris pH 8.5. Proteins were reduced with DTT and alkylated with IAA. Protein digestion was performed by overnight digestion with trypsin sequencing grade (Promega) resuspended in diluted TFA and stored at 4°C until MS analysis, where 10–20 μg of protein were ran on a Thermo Scientific Q Exactive mass spectrometer operated in positive ion mode and connected to a Dionex Ultimate 3000 (RSLCnano) chromatography system. All data was acquired while operating in automatic data dependent switching mode. A high-resolution (70,000) MS scan (300–1600 m/z) was performed to select the 12 most intense ions prior to MS/MS analysis using high-energy collision dissociation (HCD). Proteins were identified and quantified by MaxLFQ (Cox et al., 2014), termed MaxLFQ by searching with the MaxQuant version 1.5 against a human reference proteome database.

Modifications included C carbamlylation (fixed) and M oxidation (variable).

RT-qPCR Analysis

Total RNA was extracted from mouse retinas using Isolate II RNA extraction kit (Bioline) as per the manufacturer's instructions. RNA was reverse transcribed using MMLV Reverse Transcriptase (Promega). Target genes were amplified by real-time PCR with SensiFast SYBR Green (Bioline) using the ABI 7900HT system (Applied Biosystems). The comparative CT method was used for relative quantification after normalisation to the "housekeeping" gene Ubiquitin C. Primers used were as follows:

HMOX1	Forward	5′ – GAGCCTGAATCGAGCAGAAC
	Reverse	5′ – CCTTCAAGGCCTCAGACAAA
UBC	Forward	5′ – CCCAGTGTTACCACCAAGAAG
	Reverse	5′ – CCCCATCACACCCAAGAACA

Haematoxylin and Eosin Staining

$NaIO_3$ (50 mg/kg) was administered to C57BL/6J and *Sarm1*$^{-/-}$ mice *via* a single intravenous injection (*via* tail vein). Mice were euthanized 3- or 7-days post injection of $NaIO_3$, eyes were enucleated and fixed in Davidson's fixative for 24 h at 4°C, followed by 3 washes with PBS. Eyes were processed in a tissue processor under gentle agitation as follows: 70% ethanol for 1 h, 80% ethanol for 1 h, 95% ethanol for 1 h, 100% ethanol for 1 h, 100% ethanol for 1 h, 50% ethanol/xylene mix for 1 h, xylene for 1 h, xylene for 1 h, paraffin at 60°C for 1 h, and paraffin under vacuum at 60°C for 1 h. Eyes were then embedded in paraffin and 5 μm sections were collected onto Polysine slides using a microtome. Sections were deparaffinized by dipping ten times in Histo Clear (National Diagnostics). Followed by rehydration by ten dips each into 100, 90, and 70% ethanol. The slides were incubated in Haematoxylin solution for 6 min at room temperature, and subsequently rinsed in cold water, and incubated in Eosin solution for 3 min and rinsed again in water. Sections were dehydrated by tens dips each into 70, 90, and 100% ethanol and once into Histoclear. Slides were mounted onto coverslips using Sub-X mounting medium (VWR) and analysed under a light microscope (Olympus 1×81). Photoreceptor degeneration was quantified by counting the number of nuclei per row in the outer nuclear layer (ONL), by counting the number of nuclei in the ONL in an area of height 450 pixels in the centre of the ONL in each image, measuring the area of the ONL using ImageJ.

Immunohistochemistry

$NaIO_3$ (50 mg/kg) was administered to C57BL/6J and *Sarm1*$^{-/-}$ mice *via* a single intravenous injection (*via* tail vein). Mice were euthanized 3- or 7-days post injection of $NaIO_3$, eyes were enucleated and fixed in 4% paraformaldehyde for 1.5 h at room temperature. Eyes were washed 3 times with PBS. The lens and cornea were removed. Eyes were placed in 20% sucrose for 1 h at 4°C, followed by 30% sucrose overnight at 4°C. Eyes were embedded in OCT and frozen. 12 μm sections were collected onto Polysine slides (VWR) using a cryostat. Cryosections were blocked and permeabilized with 5% normal goat serum (NGS) (Sigma) and 0.05% Triton-X100 (Sigma) in PBS for 1 h at room temperature. Cryosections were incubated with primary antibody diluted in 5% NGS and 0.05% Triton-X100 in PBS overnight at 4°C in a humidity chamber. Primary antibody was cleaved caspase-3 (1:100, CST) and peanut agglutinin (PNA)-Alexa-568 (1:300; Invitrogen). Following three washes with PBS, cryosections were incubated with secondary antibody (AlexaFluor goat-anti rabbit 594, 1:500) for 2 h at room temperature. Cryosections were counterstained with Hoechst 33342 (1:10,000, Sigma) and washed 3 times with PBS. Slides were mounted onto coverslips with Hydromount (VWR) mounting medium and analysed using a confocal microscope (Zeiss LSM 710).

Terminal Deoxynucleotidyl Transferase dUTP Nick End Labelling Staining

Paraffin embedded sections from WT and *Sarm1*$^{-/-}$ mice were stained using *in situ* Cell Death Detection kit, TMR red (Roche) for 1 h at 37°C according to the manufacturer's protocol, and nuclei were stained with Hoechst 33342 (1:10,000, Sigma). Slides were mounted onto coverslips

with Hydromount (VWR) mounting medium and analysed using a confocal microscope (Zeiss LSM 710). The number of TUNEL positive nuclei in the ONL were counted at 3 points across the retina.

RESULTS

SARM1 Has No Effect on the Pace of Retinal Pigment Epithelium Degradation in the $NaIO_3$ Model of Retinal Degeneration

Given the importance of RPE function for photoreceptor health, and roles for SARM1 in non-neuronal cells (Strauss, 2005; Panneerselvam et al., 2013; Carty et al., 2019) we were interested to examine the effect of SARM1 deficiency on the RPE in a model of retinal degeneration that is thought to initiate with RPE loss. We have previously shown that the majority of SARM1 expressed in the neural retina is found in the photoreceptors. SARM1 mRNA was also detected by qPCR in the RPE/choroid of C57BL/6J mice, however, SARM1 protein expression in the RPE was not examined (Ozaki et al., 2020). We examined the expression of SARM1 protein in the mouse RPE/choroid tissue and neural retina. SARM1 was expressed in the neural retina, but was not present in the RPE when determined by Western blot **(Figure 1A)**. This pattern of expression was confirmed by mass spectrometry analysis **(Figure 1B)**. Consistent with the lack of SARM1 protein expression in the RPE/choroid, we observed no difference in RPE atrophy in the presence or absence of SARM1 following administration of $NaIO_3$. Fundus images taken at 3 and 7 days post administration of $NaIO_3$ showed no difference in the extent of pigmentary disruption between WT and *Sarm1*$^{-/-}$ mice **(Figure 1C)**. Additionally, there was similar upregulation of heme oxygenase 1 (HMOX1) in the retina in response to $NaIO_3$, in both WT and *Sarm1*$^{-/-}$ mice at 8 h post administration, indicating *Sarm1*$^{-/-}$ mice experience a similar level of oxidative stress to WT mice **(Figure 1D)**.

SARM1 Promotes Photoreceptor Cell Death in the $NaIO_3$ Model of Retinal Degeneration

Examination of retinal tissue sections from WT and *Sarm1*$^{-/-}$ mice at 3-days post administration of $NaIO_3$, stained with haematoxylin and eosin (H&E) **(Figure 2A)**, supported the observation by fundus imaging that the RPE is affected to a similar extent in WT **(Figure 2A**, left hand panel**)** and *Sarm1*$^{-/-}$ mice **(Figure 2A**, right hand panel**).** However, H&E staining also showed that there are more photoreceptor nuclei in *Sarm1*$^{-/-}$ mice. We observed that there are significantly more nuclei in ONL rows present in *Sarm1*$^{-/-}$ at 3 days post administration of $NaIO_3$ compared to WT counterparts **(Figure 2B)**. Similarly, the number of ONL nuclei in a set area at the central posterior region of each section **(Figure 2C)** and the area of the ONL **(Figure 2D)** are significantly increased in the absence of SARM1. Furthermore, PNA staining in the sub-retinal space indicates significantly more cone photoreceptor segments remain in *Sarm1*$^{-/-}$ mice compared with WT mice post administration of $NaIO_3$ **(Figures 2E,F)**.

SARM1 mediated neuronal degeneration does not require caspase-3 or RIPK3 to initiate cell death, however, it has been reported that photoreceptor cells undergo apoptosis following administration of $NaIO_3$ (Hanus et al., 2016). In order to determine whether loss of SARM1 affects photoreceptor apoptosis we utilised two markers of cell death: Terminal deoxynucleotidyl transferase dUTP nick end labelling (TUNEL) and cleaved caspase-3. We observed no significant difference in the number of TUNEL positive nuclei in the ONL of *Sarm1*$^{-/-}$ mice compared to WT counterparts **(Figures 2G,H)**. However, there are significantly higher amounts of cleaved caspase-3 positive nuclei in the ONL of WT mice, compared to *Sarm1*$^{-/-}$ mice, indicating decreased levels of photoreceptor apoptosis in the absence of SARM1 at this timepoint **(Figures 2I,J)**. Additionally, there is an increased number of immune cells infiltrating into the retina in WT mice compared to *Sarm1*$^{-/-}$ mice at 3 days following administration of $NaIO_3$, as observed by OCT imaging **(Figure 2K)**. Infiltrating cells were most abundant in WT mice around the optic nerve head and were present above the retinal ganglion cell layer of the retina **(Figure 2K)**. These data indicate that SARM1, among other cell death pathways, is promoting photoreceptor cell death in response to $NaIO_3$ administration, and that deletion of SARM1 can reduce these observed effects.

Loss of SARM1 Preserves Photoreceptor Number and Length in the $NaIO_3$ Model of Retinal Degeneration, Following Severe Retinal Pigment Epithelium Degradation

Haematoxylin and eosin stained retinal sections **(Figure 2A)** indicate that the RPE appears to remain largely intact at 3 days following administration of $NaIO_3$. To determine whether loss of SARM1 could confer protection against photoreceptor cell death following more severe degradation we examined H&E stained retinal sections at 7 days following administration of $NaIO_3$. At 7 days following administration of $NaIO_3$ there is a large degree of RPE degradation **(Figure 3A)**, despite this there is increased photoreceptor cell survival in *Sarm1*$^{-/-}$ mice compared to WT counterparts. Examination of H&E stained paraffin embedded retinal sections from WT and *Sarm1*$^{-/-}$ mice at 7 days following $NaIO_3$ administration shows that there are significantly more photoreceptor nuclei in the ONL, as measured by number of nuclei per row **(Figure 3B)**, the number of ONL nuclei in an area at the centre of each section **(Figure 3C)**, and ONL area **(Figure 3D)**. Using optical coherence tomography (OCT) we measured the thickness between the outer plexiform layer (which forms the interface between the bipolar cells and photoreceptors) and the RPE. This measurement gives the thickness of the entire photoreceptor length, inclusive of both the cell soma and photoreceptor segments. We observed a significant decrease in photoreceptor length in WT compared to *Sarm1*$^{-/-}$ mice at 7 days following $NaIO_3$ injection **(Figures 3E,F)**. These data indicate that the protection against photoreceptor cell death

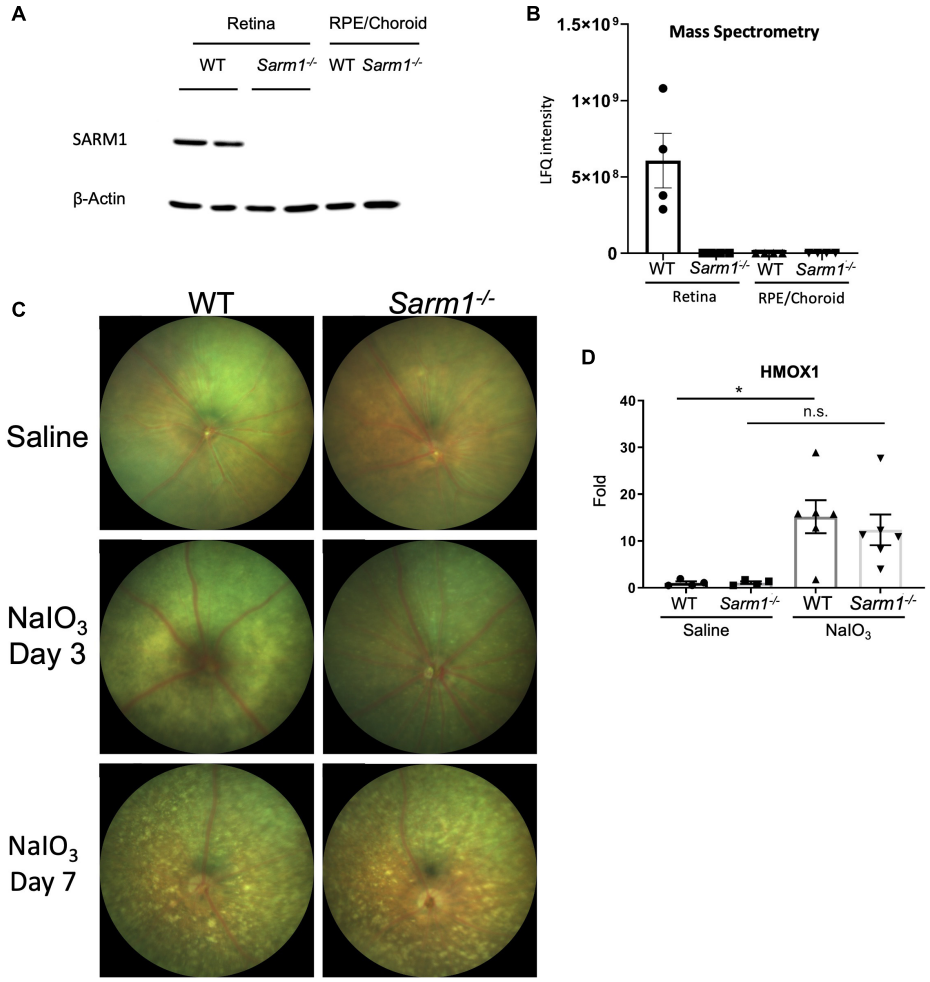

FIGURE 1 | SARM1 is expressed in the retina, not the RPE/choroid and has no effect on the pace of RPE degradation in the $NaIO_3$ model of retinal degeneration. Western blot analysis of SARM1 expression in the neural retina and RPE/choroid in C57BL/6J and *Sarm1*$^{-/-}$ mice, Beta-actin is the loading control **(A)**. Mass spectrometry analysis of SARM1 expression in the neural retina and RPE/choroid in C57BL/6J and *Sarm1*$^{-/-}$ mice, expression measured as label free quantification (LFQ) **(B)**. Colour fundus photographs of C57BL/6J and *Sarm1*$^{-/-}$ mice 3-days and 7-days following administration of saline or $NaIO_3$ (50 mg/kg) **(C)**. RT-qPCR analysis of HMOX1 transcript levels in the retina 8-h following administration of $NaIO_3$ or saline (*$P \leq 0.05$, by one-way ANOVA, $n = 4$ saline injected mice, $n = 6$ $NaIO_3$ injected mice) **(D)**.

conferred by deletion of SARM1 can persist following further degradation of the supporting RPE.

DISCUSSION

Previous studies from our lab (Ozaki et al., 2020) and others (Sasaki et al., 2020) have shown that SARM1 has a pro-degenerative role in inherited retinopathies, using models of retinitis pigmentosa and Leber Congenital Amaurosis (LCA). In this study, we have identified a similar, previously uncharacterised role for SARM1 in a model of RPE atrophy. We show that SARM1 promotes photoreceptor cell death, but has no obvious effect on degeneration of the RPE in the $NaIO_3$ model.

SARM1 has been previously shown to be highly expressed in neural tissues in comparison to other tissue types. Here, our data clearly demonstrates that in the eye SARM1 is expressed in the neural retina, but not in the RPE/choroid. As such, in the context of the $NaIO_3$ model, in which there is initially loss of RPE integrity followed by subsequent photoreceptor cell degeneration, any alterations to photoreceptor cell degeneration in *Sarm1*$^{-/-}$ mice are likely to be a direct consequence of loss of SARM1 in photoreceptor cells, rather than a direct effect on the supporting RPE. Indeed, SARM1 deficiency did not appear to slow the rate of pigmentary disruption as observed by fundus photography, and there was no apparent difference in the fragmentation of the RPE monolayer when observed by H&E staining in tissue sections at either timepoint post treatment with $NaIO_3$. Despite this balance in the acute loss of RPE integrity in both WT and *Sarm1*$^{-/-}$ mice, it is clear that SARM1 deficiency is protective for photoreceptor cells, as *Sarm1*$^{-/-}$ mice demonstrate a

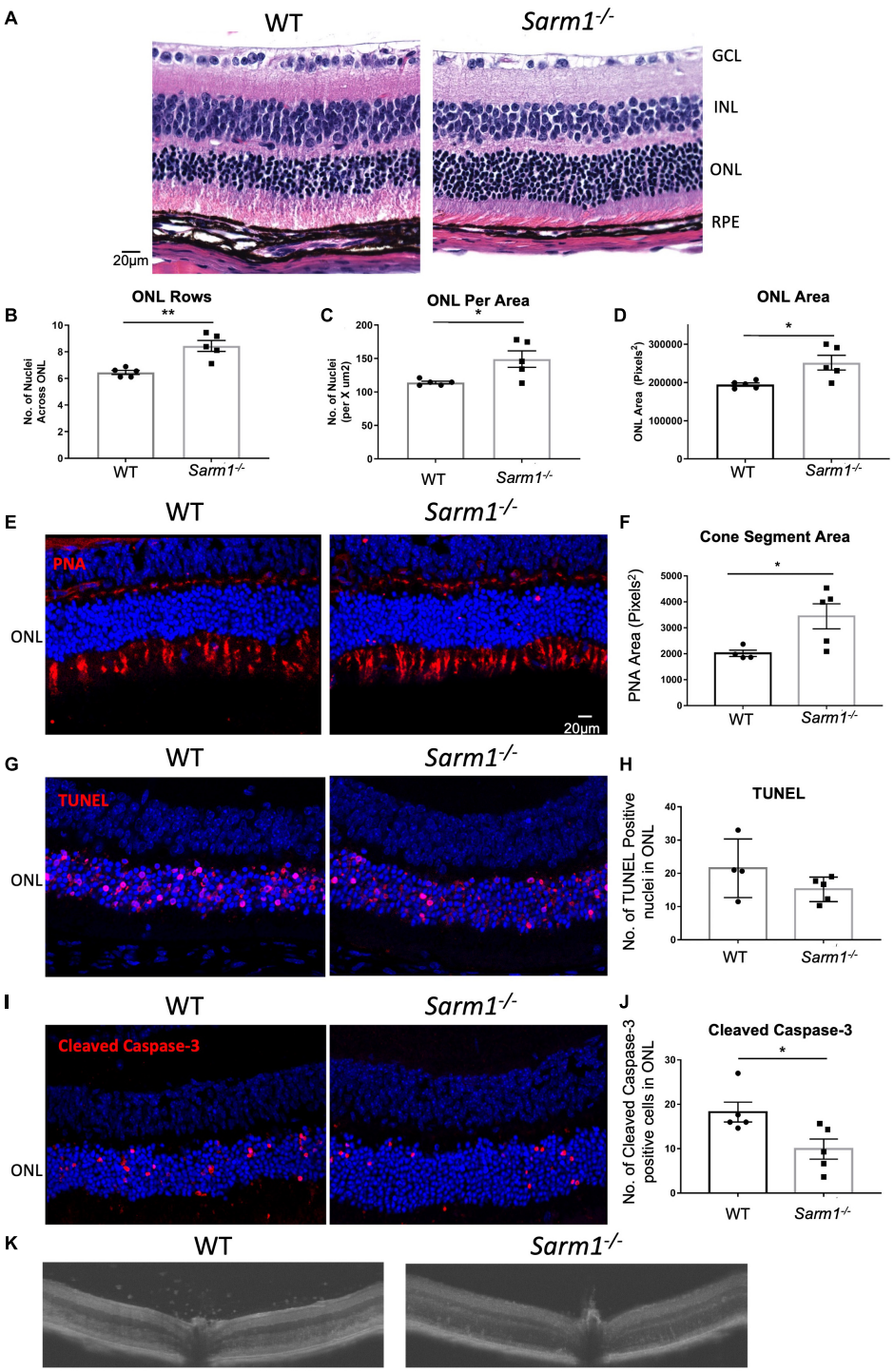

FIGURE 2 | SARM1 promotes photoreceptor cell death in the $NaIO_3$ model of retinal degeneration. Representative images of paraffin embedded retinal sections from WT and *Sarm1*$^{-/-}$ mice 3-days post administration of $NaIO_3$ stained with haematoxylin and eosin (H&E) **(A)**. Quantification of the number of nuclei per ONL row **(B)**, number of nuclei in the ONL in an area of height 450 pixels in the centre of the ONL in each image **(C)**, and ONL area (*$P \leq 0.05$, **$P \leq 0.01$, $n = 5$ mice) **(D)**. Representative images of retinal cryosections stained with PNA **(E)**. Quantification of area of PNA stained cone segments (*$P \leq 0.05$, $n = 4$ WT mice, $n = 5$ *Sarm1*$^{-/-}$ mice) **(F)**. Representative images of paraffin embedded retinal sections from WT and *Sarm1*$^{-/-}$ mice 3-days post administration of $NaIO_3$ stained with TUNEL (Red) and DAPI (Blue) **(G)**. Quantification of the number of TUNEL positive nuclei in the ONL ($n = 4$ WT mice, $n = 5$ *Sarm1*$^{-/-}$ mice) **(H)**. Representative images of retinal cryosections from WT and *Sarm1*$^{-/-}$ mice 3-days post administration of $NaIO_3$ stained with cleaved caspase-3 (Red) and DAPI (Blue) **(I)**. Quantification of the number of cleaved caspase-3 positive cells in the ONL (*$P \leq 0.05$, $n = 4$ WT mice, $n = 5$ *Sarm1*$^{-/-}$ mice) **(J)**. Optical coherence tomography (OCT) images taken *in vivo* from C57BL/6J and *Sarm1*$^{-/-}$ mice 3-days post administration of $NaIO_3$ (50 mg/kg) **(K)**.

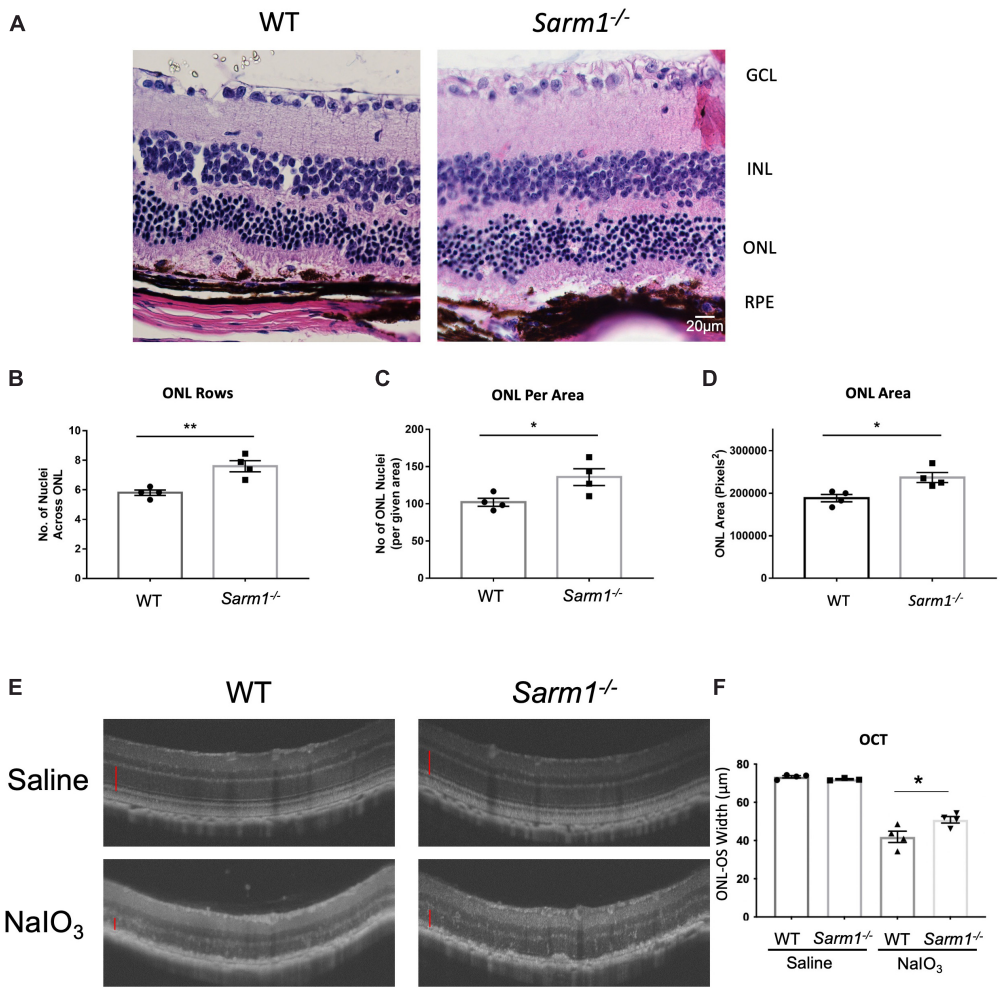

FIGURE 3 | Loss of SARM1 preserves photoreceptor number and length in the $NaIO_3$ model of retinal degeneration, following severe RPE degradation. Representative images of paraffin embedded retinal sections from WT and *Sarm1*$^{-/-}$ mice 7-days post administration of $NaIO_3$ stained with haematoxylin & eosin (H&E) **(A)**. Quantification of the number of nuclei per ONL row **(B)**, number of nuclei in the ONL in an area of height 450 pixels in the centre of the ONL in each image **(C)**, and ONL area **(D)** (*$P \leq 0.05$, **$P \leq 0.01$, $n = 4$ WT $NaIO_3$ mice, $n = 4$ *Sarm1*$^{-/-}$ $NaIO_3$ mice). Optical coherence tomography (OCT) images taken *in vivo* from C57BL/6J and *Sarm1*$^{-/-}$ mice 7-days post administration of $NaIO_3$ (50 mg/kg) **(E)**. Quantification of the distance of the ONL to the outer segments (OS) (marked with red line on OCT images) InSight (*$P \leq 0.05$, by Student's unpaired *t* test, $n = 4$ WT saline mice, $n = 3$ *Sarm1*$^{-/-}$ saline mice, $n = 4$ WT $NaIO_3$ mice, $n = 4$ *Sarm1*$^{-/-}$ mice) **(F)**.

decreased rate of thinning of the retina and reduced loss of photoreceptor cell nuclei.

The precise mechanism by which SARM1 promotes cell death in photoreceptors in this model remains to be described. We have previously shown that SARM1 cleaves NAD^+ in photoreceptor cells in a model of RP, and it is likely that a similar mechanism is at play here (Ozaki et al., 2020). This is also the mechanism observed in axonal degeneration of peripheral neurons (Gerdts et al., 2015; Essuman et al., 2017). However, it is clear that there is reduced cleaved caspase-3, a marker of apoptosis, in the photoreceptors in SARM1 deficient mice. This may be a consequence of SARM1 deficiency reducing extrinsic death ligands or intrinsic stress signalling and subsequently reducing activation of caspase-3, or it may indicate a role for caspase-3 in SARM1-mediated photoreceptor degeneration, akin to that described for SARM1- induction of mitochondrial apoptosis in activated CD8 T cells (Panneerselvam et al., 2013). Furthermore, in addition to loss of RPE trophic support, photoreceptor degeneration in the $NaIO_3$ model may be triggered by other factors, including direct effects of oxidising agent $NaIO_3$ on photoreceptors, and immune cell infiltration (Wang et al., 2014; Moriguchi et al., 2018). Indeed, SARM1 has been shown to induce chemokines CCL2, CCL7, and CCL12 in a model of peripheral nerve injury (Wang et al., 2018), these are distinct from the passenger mutations in Ccl3/4/5 carried by the *Sarm1*$^{-/-}$ mice (Uccellini et al., 2020) and interestingly, are key chemokines involved in mononuclear cell infiltration in the retina (Natoli et al., 2016; Karlen et al., 2018).

In this study, we also observed reduced immune cell infiltrate when assessed by OCT, which may account for some aspect of the delayed photoreceptor degeneration in the *Sarm1*$^{-/-}$ mice. However, it is not clear whether the cell infiltration is lessened in response to the reduced numbers of dying cells and consequent reduced inflammatory environment or is due to a direct effect of loss of chemokine signalling due to SARM1 deficiency. As such further investigation is required to fully describe the mechanism by which SARM1 becomes activated in this model and by which it promotes photoreceptor degeneration.

To date a number of studies have been published describing various molecules, such as zinc chloride and isoquinolines, that are capable of inhibiting the NAD^+ cleavage activity of SARM1, through a proposed mechanism involving interaction and possible modification of cysteine residues (Loring et al., 2020; Bosanac et al., 2021). These various inhibitors have been shown to prevent axonal degeneration induced by SARM1 following injury (Hughes et al., 2021) or in response to paclitaxel (Bosanac et al., 2021), both *in vitro* and *in vivo*. Our study adds to the growing body of data indicating that SARM1 inhibitors may also be of use in retinal degenerative diseases that have a SARM1 dependent component (Ozaki et al., 2020; Sasaki et al., 2020) making SARM1 a potential therapeutic target of interest for future study in retinal degeneration.

DATA AVAILABILITY STATEMENT

The original contributions presented in the study are included in the article/supplementary material, further inquiries can be directed to the corresponding author.

ETHICS STATEMENT

The animal study was reviewed and approved by Trinity College AREC.

AUTHOR CONTRIBUTIONS

LG, EO, CG, AT, and JC performed experiments. LG, EO, AB, and MC participated in the design of the study. SD conceived and designed the study. LG, EO, and SD wrote the manuscript. All authors read and approved the final manuscript.

FUNDING

This work was supported by HRB/MRCG-2018-08, SFI-15CDA/3497, IRCLA/2017/295, NCRC/18/10, ERC (Retina Rhythm – 864522). This work was also supported by Fighting Blindness Ireland and BrightFocus Foundation.

REFERENCES

Bosanac, T., Hughes, R. O., Engber, T., Devraj, R., Brearley, A., Danker, K., et al. (2021). Pharmacological SARM1 inhibition protects axon structure and function in paclitaxel-induced peripheral neuropathy. *Brain* 144, 3226–3238. doi: 10.1093/brain/awab184

Carty, M., Goodbody, R., Schroder, M., Stack, J., Moynagh, P. N., and Bowie, A. G. (2006). The human adaptor SARM negatively regulates adaptor protein TRIF-dependent Toll-like receptor signaling. *Nat. Immunol.* 7, 1074–1081. doi: 10.1038/ni1382

Carty, M., Kearney, J., Shanahan, K. A., Hams, E., Sugisawa, R., and Connolly, D. (2019). Cell survival and cytokine release after inflammasome activation is regulated by the Toll-IL-1R protein SARM. *Immunity* 50, 1412.e–1424.e. doi: 10.1016/j.immuni.2019.04.005

Cox, J., Hein, M. Y., Luber, C. A., Paron, I., Nagaraj, N., and Mann, M. (2014). Accurate proteome-wide label-free quantification by delayed normalization and maximal peptide ratio extraction, termed MaxLFQ. *Mol. Cell. Proteomics* 13, 2513–2526. doi: 10.1074/mcp.M113.031591

Essuman, K., Summers, D. W., Sasaki, Y., Mao, X. R., DiAntonio, A., and Milbrandt, J. (2017). The SARM1 toll/interleukin-1 receptor domain possesses intrinsic NAD^+ cleavage activity that promotes pathological axonal degeneration. *Neuron* 93, 1334–1343. doi: 10.1016/j.neuron.2017.02.022

Figley, M. D., Gu, W., Nanson, J. D., Shi, Y., Sasaki, Y., Cunnea, K., et al. (2021). SARM1 is a metabolic sensor activated by an increased NMN/NAD^+ ratio to trigger axon degeneration. *Neuron* 109, 1118–1136.e11.

Geisler, S., Doan, R. A., Strickland, A., Huang, X., Milbrandt, J., and DiAntonio, A. (2016). Prevention of vincristine-induced peripheral neuropathy by genetic deletion of SARM1 in mice. *Brain* 139, 3092–3108. doi: 10.1093/brain/aww251

Gerdts, J., Brace, E. J., Sasaki, Y., DiAntonio, A., and Milbrandt, J. (2015). SARM1 activation triggers axon degeneration locally via NAD^+ destruction. *Science* 348, 453–457. doi: 10.1126/science.1258366

Hanus, J., Anderson, C., Sarraf, D., Ma, J., and Wang, S. (2016). Retinal pigment epithelial cell necroptosis in response to sodium iodate. *Cell Death Discov.* 2:16054.

Hughes, R. O., Bosanac, T., Mao, X., Engber, T. M., DiAntonio, A., Milbrandt, J., et al. (2021). Small molecule SARM1 inhibitors recapitulate the SARM1$^{-/-}$ phenotype and allow recovery of a metastable pool of axons fated to degenerate. *Cell Rep.* 34:108588. doi: 10.1016/j.celrep.2020.108588

Karlen, S. J., Miller, E. B., Wang, X., Levine, E. S., Zawadzki, R. J., and Burns, M. E. (2018). Monocyte infiltration rather than microglia proliferation dominates the early immune response to rapid photoreceptor degeneration. *J. Neuroinflammation* 15:344. doi: 10.1186/s12974-018-1365-4

Kim, Y., Zhou, P., Qian, L., Chuang, J. Z., Lee, J., Li, C., et al. (2007). MyD88-5 links mitochondria, microtubules, and JNK3 in neurons and regulates neuronal survival. *J. Exp. Med.* 204, 2063–2074. doi: 10.1084/jem.20070868

Kiuchi, K., Yoshizawa, K., Shikata, N., Moriguchi, K., and Tsubura, A. (2002). Morphologic characteristics of retinal degeneration induced by sodium iodate in mice. *Curr. Eye Res.* 25, 373–379. doi: 10.1076/ceyr.25.6.373.14227

Loring, H. S., Parelkar, S. S., Mondal, S., and Thompson, P. R. (2020). Identification of the first noncompetitive SARM1 inhibitors. *Bioorg. Med. Chem.* 28:115644. doi: 10.1016/j.bmc.2020.115644

Marion, C. M., McDaniel, D. P., and Armstrong, R. C. (2019). Sarm1 deletion reduces axon damage, demyelination, and white matter atrophy after experimental traumatic brain injury. *Exp. Neurol.* 321:113040. doi: 10.1016/j.expneurol.2019.113040

Moriguchi, M., Nakamura, S., Inoue, Y., Nishinaka, A., Nakamura, M., Shimazawa, M., et al. (2018). Irreversible photoreceptors and RPE cells damage by intravenous sodium iodate in mice is related to macrophage accumulation. *Invest. Ophthalmol. Vis. Sci.* 59, 3476–3487. doi: 10.1167/iovs.17-23532

Mukherjee, P., Woods, T. A., Moore, R. A., and Peterson, K. E. (2013). Activation of the innate signaling molecule MAVS by bunyavirus infection upregulates the adaptor protein SARM1, leading to neuronal death. *Immunity* 38, 705–716. doi: 10.1016/j.immuni.2013.02.013

Murakami, Y., Notomi, S., Hisatomi, T., Nakazawa, T., Ishibashi, T., Miller, J. W., et al. (2013). Photoreceptor cell death and rescue in retinal detachment and degenerations. *Prog. Retin. Eye Res.* 37, 114–140. doi: 10.1016/j.preteyeres.2013.08.001

Natoli, R., Jiao, H., Barnett, N. L., Fernando, N., Valter, K., Provis, J. M., et al. (2016). A model of progressive photo-oxidative degeneration and inflammation in the pigmented C57BL/6J mouse retina. *Exp. Eye Res.* 147, 114–127. doi: 10.1016/j.exer.2016.04.015

O'Neill, L. A., Fitzgerald, K. A., and Bowie, A. G. (2003). The Toll–IL-1 receptor adaptor family grows to five members. *Trends Immunol.* 24, 286–289. doi: 10.1016/s1471-4906(03)00115-7

Osterloh, J. M., Yang, J., Rooney, T. M., Fox, A. N., Adalbert, R., Powell, E. H., et al. (2012). dSarm/Sarm1 is required for activation of an injury-induced axon death pathway. *Science* 337, 481–484. doi: 10.1126/science.1223899

Ozaki, E., Gibbons, L., Neto, N. G., Kenna, P., Carty, M., Humphries, M., et al. (2020). SARM1 deficiency promotes rod and cone photoreceptor cell survival in a model of retinal degeneration. *Life Sci. Alliance* 3:e201900618. doi: 10.26508/lsa.201900618

Panneerselvam, P., Singh, L. P., Selvarajan, V., Chng, W. J., Ng, S. B., Tan, N. S., et al. (2013). T-cell death following immune activation is mediated by mitochondria-localized SARM. *Cell Death Differ.* 20, 478–489. doi: 10.1038/cdd.2012.144

Sasaki, Y., Kakita, H., Kubota, S., Sene, A., Lee, T. J., Ban, N., et al. (2020). SARM1 depletion rescues NMNAT1-dependent photoreceptor cell death and retinal degeneration. *Elife* 9:e62027. doi: 10.7554/eLife.62027

Strauss, O. (2005). The retinal pigment epithelium in visual function. *Physiol. Rev.* 85, 845–881. doi: 10.1152/physrev.00021.2004

Summers, D. W., DiAntonio, A., and Milbrandt, J. (2014). Mitochondrial dysfunction induces Sarm1-dependent cell death in sensory neurons. *J. Neurosci.* 34, 9338–9350. doi: 10.1523/JNEUROSCI.0877-14.2014

Tuttolomondo, A., Di Sciacca, R., Di Raimondo, D., Arnao, V., Renda, C., Pinto, A., et al. (2009). Neuron protection as a therapeutic target in acute ischemic stroke. *Curr. Top. Med. Chem.* 9, 1317–1334. doi: 10.2174/156802609789869646

Uccellini, M. B., Bardina, S. V., Sanchez-Aparicio, M. T., White, K. M., Hou, Y. J., Lim, J. K., et al. (2020). Passenger mutations confound phenotypes of SARM1-deficient mice. *Cell Rep.* 31:107498. doi: 10.1016/j.celrep.2020.03.062

Wang, J., Iacovelli, J., Spencer, C., and Saint-Geniez, M. (2014). Direct effect of sodium iodate on neurosensory retina. *Invest. Ophthalmol. Vis. Sci.* 55, 1941–1953. doi: 10.1167/iovs.13-13075

Wang, Q., Zhang, S., Liu, T., Wang, H., Liu, K., Wang, Q., et al. (2018). Sarm1/Myd88-5 regulates neuronal intrinsic immune response to traumatic axonal injuries. *Cell Rep.* 23, 716–724. doi: 10.1016/j.celrep.2018.03.071

White, M. A., Lin, Z., Kim, E., Henstridge, C. M., Altamira, E. Pena, Hunt, C. K., et al. (2019). Sarm1 deletion suppresses TDP-43-linked motor neuron degeneration and cortical spine loss. *Acta Neuropathol. Commun.* 7:166. doi: 10.1186/s40478-019-0800-9

Zhao, Z. Y., Xie, X. J., Li, W. H., Liu, J., Chen, Z., Zhang, B., et al. (2019). A cell-permeant mimetic of NMN activates SARM1 to produce cyclic ADP-ribose and induce non-apoptotic cell death. *iScience* 15, 452–466. doi: 10.1016/j.isci.2019.05.001

Conflict of Interest: The authors declare that the research was conducted in the absence of any commercial or financial relationships that could be construed as a potential conflict of interest.

Publisher's Note: All claims expressed in this article are solely those of the authors and do not necessarily represent those of their affiliated organizations, or those of the publisher, the editors and the reviewers. Any product that may be evaluated in this article, or claim that may be made by its manufacturer, is not guaranteed or endorsed by the publisher.

frontiers | Frontiers in Neuroscience

ORIGINAL RESEARCH
published: 12 April 2022
doi: 10.3389/fnins.2022.800883

Mitochondrial Transplantation Attenuates Neural Damage and Improves Locomotor Function After Traumatic Spinal Cord Injury in Rats

*Ming-Wei Lin[1,2,3], Shih-Yuan Fang[4], Jung-Yu C. Hsu[5,6], Chih-Yuan Huang[7], Po-Hsuan Lee[7], Chi-Chen Huang[7], Hui-Fang Chen[5], Chen-Fuh Lam[1,8,9] and Jung-Shun Lee[5,6,7]**

[1] Department of Medical Research, E-Da Hospital, E-Da Cancer Hospital, Kaohsiung City, Taiwan, [2] Department of Nursing, College of Medicine, I-Shou University, Kaohsiung City, Taiwan, [3] Regenerative Medicine and Cell Therapy Research Center, Kaohsiung Medical University, Kaohsiung City, Taiwan, [4] Department of Anesthesiology, College of Medicine, National Cheng Kung University Hospital, National Cheng Kung University, Tainan City, Taiwan, [5] Department of Cell Biology and Anatomy, College of Medicine, National Cheng Kung University, Tainan City, Taiwan, [6] Institute of Basic Medical Sciences, College of Medicine, National Cheng Kung University, Tainan City, Taiwan, [7] Section of Neurosurgery, Department of Surgery, College of Medicine, National Cheng Kung University Hospital, National Cheng Kung University, Tainan City, Taiwan, [8] Department of Anesthesiology, E-Da Hospital, E-Da Cancer Hospital, Kaohsiung City, Taiwan, [9] College of Medicine, I-Shou University, Kaohsiung City, Taiwan

OPEN ACCESS

Edited by:
Bin Yu,
Nantong University, China

Reviewed by:
Guzal Khayrullina,
National Institutes of Health (NIH), United States
Diogo Trigo,
University of Aveiro, Portugal

***Correspondence:**
Jung-Shun Lee
nslee1218@gmail.com

Specialty section:
This article was submitted to Neurodegeneration, a section of the journal Frontiers in Neuroscience

Received: *24 October 2021*
Accepted: *18 March 2022*
Published: *12 April 2022*

Citation:
Lin M-W, Fang S-Y, Hsu J-YC, Huang C-Y, Lee P-H, Huang C-C, Chen H-F, Lam C-F and Lee J-S (2022) Mitochondrial Transplantation Attenuates Neural Damage and Improves Locomotor Function After Traumatic Spinal Cord Injury in Rats. Front. Neurosci. 16:800883. doi: 10.3389/fnins.2022.800883

Mitochondrial dysfunction is a hallmark of secondary neuroinflammatory responses and neuronal death in spinal cord injury (SCI). Even though mitochondria-based therapy is an attractive therapeutic option for SCI, the efficacy of transplantation of allogeneic mitochondria in the treatment of SCI remains unclear. Herein, we determined the therapeutic effects of mitochondrial transplantation in the traumatic SCI rats. Compressive SCI was induced by applying an aneurysm clip on the T10 spinal cord of rats. A 100-μg bolus of soleus-derived allogeneic mitochondria labeled with fluorescent tracker was transplanted into the injured spinal cords. The results showed that the transplanted mitochondria were detectable in the injured spinal cord up to 28 days after treatment. The rats which received mitochondrial transplantation exhibited better recovery of locomotor and sensory functions than those who did not. Both the expression of dynamin-related protein 1 and severity of demyelination in the injured cord were reduced in the mitochondrial transplanted groups. Mitochondrial transplantation also alleviated SCI-induced cellular apoptosis and inflammation responses. These findings suggest that transplantation of allogeneic mitochondria at the early stage of SCI reduces mitochondrial fragmentation, neuroapoptosis, neuroinflammation, and generation of oxidative stress, thus leading to improved functional recovery following traumatic SCI.

Keywords: allogenic mitochondria, mitochondrial dysfunction, mitochondrial transplantation, oxidative stress, spinal cord injury

INTRODUCTION

Traumatic spinal cord injury (SCI) often leads to devastating neural consequences, including partial or total paralysis (Mothe and Tator, 2012). The pathophysiology of traumatic SCI is initiated by a mechanical injury, followed by a series of neuroinflammatory events that result in secondary injuries. Increased expression of proinflammatory cytokines, ionic imbalance, mitochondrial dysfunctions, overproduction of oxygen and nitrogen radicals, and subsequent necrotic and apoptotic cell death are major features of the secondary injuries (Hausmann, 2003; Pineau and Lacroix, 2007). Considering the impact of profound neuroinflammation on the outcomes of traumatic SCI, numerous clinical trials have been conducted aiming to alleviate neuroinflammation; however, none of these approaches have been successful. This consequence could be attributed to the limitations imposed by the complicated spatiotemporal course of neuroinflammation in SCI (Hurlbert et al., 2015; Devaux et al., 2016; Colon et al., 2018), which complicates choosing a proper time window for treatment. Hence, exploring a novel strategy that effectively counteracts inflammation-induced secondary injuries is critical for treating traumatic SCI. Recently, a mitochondria-targeted treatment has emerged as a potential anti-inflammatory intervention (Wang et al., 2019; Lee et al., 2021).

Healthy mitochondria—which function as a powerhouse of cells—are essential for cell survival. They govern energy production, which is released in the form of adenosine triphosphate (ATP). Mitochondrial dysfunction promotes the overproduction of reactive oxygen and nitrogen species (RONS) and perturbs intracellular calcium homeostasis (Ide et al., 2001; Bolanos et al., 2009; McEwen et al., 2011; Ahuja et al., 2017) and is a common pathway preceding cell death and evident in several diseases (Swerdlow et al., 2010; Gollihue et al., 2018) especially neurological disorders-including ischemic stroke, epilepsy, and other neurodegenerative diseases (Wu et al., 2019), since the nervous system is enormously energy dependent. In the central nervous system, mitochondria are transportable between cells; neurons release damaged mitochondria to astrocytes either for disposal or recycling under normal conditions (Davis et al., 2014). These astrocytes can transfer viable mitochondria to the ischemic neurons during cerebral infarction to support both their viability and recovery (Hayakawa et al., 2016). Moreover, the neurorestorative effect of the transplantation of endothelial progenitor cells is primarily mediated through the release of the active extracellular mitochondria that derived from the progenitor cells in a rat model of ischemic stroke (Garbuzova-Davis et al., 2017; Russo et al., 2018). Furthermore, transferring exogenous mitochondria to the injured hippocampal neuronal cultures not only significantly increases neurite regrowth, but also restores their membrane potential (Chien et al., 2018). This transferable feature of mitochondria enlightens the innovation of mitochondrial transplantation (MT) treatments, which rapidly increases the mitochondrial density around the lesioned regions by direct administration of healthy mitochondria to replace the dysfunctional counterparts (McCully et al., 2017). The beneficial effects of MT on ischemia/reperfusion-induced myocardial injuries (McCully et al., 2009, 2017) have been proven in animal and human studies. However, studies testing the therapeutic effects of MT on SCI-induced functional impairments and neuroinflammation-related secondary insults are limited and the results remained conflicting.

Accordingly, to address this issue, we hypothesized that MT could alleviate SCI-induced functional and histological deficits and neuroinflammation-associated secondary injuries. To test this hypothesis, we made compressive traumatic SCI in rats by applying an aneurysm clip on their T10 spinal cord for 20 s. A 100 μg of soleus-derived allogeneic mitochondria labeled with fluorescent tracker, MitoTracker Deep Red FM (MTDR), was transplanted into the injured spinal cords of rats after the induction of traumatic SCI. The effects of MT on the SCI-induced impairments of somatosensory and locomotor functions were determined by performing somatosensory evoked potentials (SSEP) assay and Basso, Beattie, and Bresnahan (BBB) scoring, respectively. Luxol fast blue (LFB) staining was adopted to examine the degrees of demyelination in the injured spinal cord. The levels of neural apoptosis and neuroinflammation in the injured region were determined with Western blots, terminal deoxynucleotidyl transferase dUTP nick end labeling (TUNEL) assay, and enzyme-linked immunosorbent assay (ELISA).

MATERIALS AND METHODS

Animals

All experimental procedures were approved by the Institutional Animal Care and Use Committee. Adult Sprague–Dawley rats (220–250 g) were purchased from BioLASCO (Taipei, Taiwan) and maintained in the institutional Laboratory Animal Center. The rats were housed under an 11-h light/13-h dark cycle (lights on at 7 A.M.) at a stable temperature (24 ± 1°C) and humidity in the facility. The rats were given free access to food and water.

Fifty-six adult rats were used in this study. Six rats served as donors of allogeneic mitochondria and 40 rats were employed as experimental subjects. We used 10 rats to investigate the spatiotemporal distribution and viability of the transplanted mitochondria. These 10 rats were sacrificed on postinjury day (PID) 1, 3, 7, 10, 14, and 28 according to the experimental design. The remaining rats were used to investigate the effects of MT on the parameters of interest. They were randomly divided into four groups, i.e., sham laminectomy + vehicle control group, sham laminectomy + MT group, SCI + vehicle control group (Vehicle), and SCI + MT group. The MT rats were administered allogeneic mitochondria suspended in 1x phosphate-buffered saline (PBS), while the Vehicle rats were injected with an equal volume of 1x PBS. The details of MT were described in the following sections.

Allogeneic Mitochondria Isolation and Labeling

Allogeneic mitochondria were freshly isolated from the bilateral soleus muscles of healthy donor rats. The donor rat was placed in

a prone position under deep anesthesia with 4–5% of isoflurane (Panion & BF Biotech Inc., Taipei, Taiwan). An incision was made at the midline of the dorsal lower limb from its ankle to popliteal fossa. The superficial connective tissues and the gastrocnemius muscles were dissected to expose the soleus. Then, the bilateral soleus muscles were excised, immersed in 1x PBS, cut into tiny pieces, and homogenized with mitochondrial isolation solution (Cat. #: 89801, Thermo Fisher Scientific, Waltham, MA, United States) by a glass tissue grinder. The homogenates were centrifuged at 700 × *g* for 10 min at 4°C and the supernatants containing mitochondria were collected and centrifuged at 3,000 × *g* for 15 min at 4°C. After discarding the supernatants, the pellets were washed with wash buffer and centrifuged at 12,000 × *g* for 5 min at 4°C twice. Finally, the washed pellets were resuspended in 1x PBS and then stained with MTDR (Cat. #: M22425, Thermo Fisher Scientific) at 37°C for 30 min. The labeled mitochondria obtained from different donor rats were washed, suspended in 1x PBS, pooled together, and ready for further use.

Procedures of Induction of Traumatic Spinal Cord Injury and Mitochondrial Transplantation

The rats were anesthetized by an intraperitoneal injection (i.p.) of Zoletil® 50 (40 mg/kg; Virbac, Carros, France), administrated with enrofloxacin (5 mg/kg, Bayer, Leverkusen, Germany) and placed in a prone position. A 2-cm dorsal longitudinal incision was made over the T9-T10 vertebrae, dissected the paraspinal muscles, removed the spinal processes of T9-T10, and performed a laminectomy of the T10 vertebra to expose the spinal cord. Then, a new aneurysm clip (Model: No: 07-940-02, Sugita, Mizuho Logistics, Chiba, Japan) was extramurally applied on the T10 spinal cord for 20 s to elicit compressive traumatic SCI.

Following SCI, we used a microsyringe pump (Model: KDS101, KD Scientific, Holliston, MA, United States) to transplant mitochondria into the injured region of spinal cord of rats via the intraparenchymal route. Each rat received two injections which were conducted at 2 mm rostral and caudal to the epicenter of the injured site (0.6 mm in depth), respectively. The MT rats received administrations of mitochondria (50 μg in 1.5 μL 1x PBS, each shot), and the Vehicle rats received injections of equal volume of 1x PBS and served as controls. Then, the wound was closed in layers. The rats recovered from anesthesia under a warm blanket, housed individually, and had free access to water and chow. The urinary bladder of each rat was manually voided twice daily until the recovery of the bladder reflex.

Assessment of Sensory and Locomotor Functions of Rats

The sensory function of the hind limbs was evaluated using SSEP on PID 28 (Lee et al., 2012). The rats were anesthetized using Zoletil® 50 (40 mg/kg, i.p.; Virbac, Carros, France) and kept in a prone position. A needle electrode was inserted into the plantar aspect of the foot to stimulate the tibial nerve with rectangular pulses at a supramaximal intensity of 7 Hz for a duration of 0.2 ms. The needle electrode recorder was inserted into the C2-C3 interspinous ligament. The reference electrode was placed in the subcutaneous tissue next to the recording electrode. In contrast, the ground electrode was placed in the shoulder, ipsilateral to the side being stimulated. The recorded signals were averaged 20–50 times at a band-pass filter setting of 50–5,000 Hz, with a 20-ms time base. During the whole process, the heart rate, blood pressure, and core temperature of the rats were monitored.

The hindlimb locomotor function was independently evaluated by two observers which were blinded to the treatment groups using the BBB scale weekly (Lee et al., 2020).

Western Blotting

To collect spinal cord samples for Western blot, the rats were deeply anesthetized with Zoletil® 50 (40 mg/kg, i.p.; Virbac, Carros, France) and transcardially perfused with chilled normal saline. The 1-cm sections of the spinal cords centered at the epicenter of the injured site were dissected and homogenized with T-PER lysis buffer (Cat. #: 78510, Thermo Fisher Scientific Inc.) containing protease inhibitors (Cat. #: 04693116001, Roche, Basel, Switzerland) and phosphatase inhibitors (PHOSS-RO, Roche). After centrifuging at 15,000 × *g* for 15 min, the supernatants (25 μg) were loaded onto polyacrylamide gels (9–12%), electrophoresed with Mini-PROTEAN® tetra cell system (Bio-Rad Laboratories, Hercules, CA, United States), and transferred to PVDF membranes (Cat. #: IPVH00010, Merck-Millipore, Burlington, MA, United States) with wet transfer tank (Model: TE22 Mighty Small Transfer Tank, Hoefer, Holliston, MA, United States). The membranes were incubated overnight at 4°C with appropriate dilutions of primary antibodies, including cleaved caspase-3 (1:1,000; Cat. #: 9661, Cell Signaling Technology, Danvers, MA, United States), Bcl-2 (1:1,000; Cat. #: ab59348, Abcam, Cambridge, United Kingdom), BAX (1:1,000; Cat. #: 2772, Cell Signaling Technology), dynamin-related protein 1 (Drp1) (1:1,000; Cat. #: 8570, Cell Signaling Technology), tumor necrosis factor (TNF) (1:2,000, Cat. #: ab6671, Abcam), interleukin-6 (IL-6) (1:1,000, Cat. #: ab6672, Abcam), inducible nitric oxide synthase (iNOS) (1:1,000; Cat. #: A0312, ABclonal, Woburn, MA, United States), and β-actin (1:10,000; Cat. #: ab8227, Abcam). The band densities were measured using an image system (Model: Azure 280, Azure Biosystems, Dublin, CA, United States) and the densitometry was carried out using the ImageJ software (v2.0.0-rc-69/1.52p, U.S. National Institutes of Health). Relative protein expression was estimated by normalizing with the β-actin level. For re-probing, the membranes were incubated with a stripping buffer containing 2% SDS, 62.5 mM Tris, and 0.8% 2-mercaptoethanol for 20 min at 55°C to remove the bound antibodies.

Measurement of Nitric Oxide, 3-Nitrotyrosine, and Malondialdehyde

We determined the tissue concentrations of nitric oxide (NO), 3-nitrotyrosine (3-NT), and malondialdehyde in the spinal cord homogenates, respectively, using the Griess reagent kit (Cat. #: G7921, Sigma-Aldrich, St. Louis, MO, United States), 3-NT ELISA kit (Cat. #: ab113848, Abcam), and malondialdehyde

assay kit (Cat. #: NWK-MDA01, Northwest Life Science Specialties, Vancouver, WA, United States) according to the manufacturers' protocols.

Histological Examination

To determine the distribution of the transplanted mitochondria, the 1-cm sections of the spinal cords centered at the epicenter of the injured site were post-fixed with 4% paraformaldehyde and prepared into 20-μm thick horizontal sections using a cryostat. For the TUNEL assay and LFB staining, the spinal section was post-fixed with 4% paraformaldehyde and prepared into 20-μm thick transverse sections using a cryostat.

The TUNEL assay and LBF staining were carried out with commercial kits (TUNEL assay: Cat. #: S7165, Sigma-Aldrich; LFB staining: Cat. #: ab150675, Abcam). The labeled mitochondria and the TUNEL-positive nuclei were visualized under a fluorescence microscope (Nikon Microsystems). The LFB-stained sections were photographed at low magnification. Moreover, the ratio of the LFB-positive area to the total cross-sectional area of the spinal cord was quantified using ImageJ software and presented as a percentage. The images of the aforementioned experiments were captured with a fluorescence optical microscope (Model: ECLIPSE Ci, Nikon, Tokyo, Japan) equipped with a digital camera (Model: DS-Fi3, Nikon).

Statistical Analysis

All data are presented as the mean ± standard deviation. All statistical analyses were conducted using the Prism 7th edition.

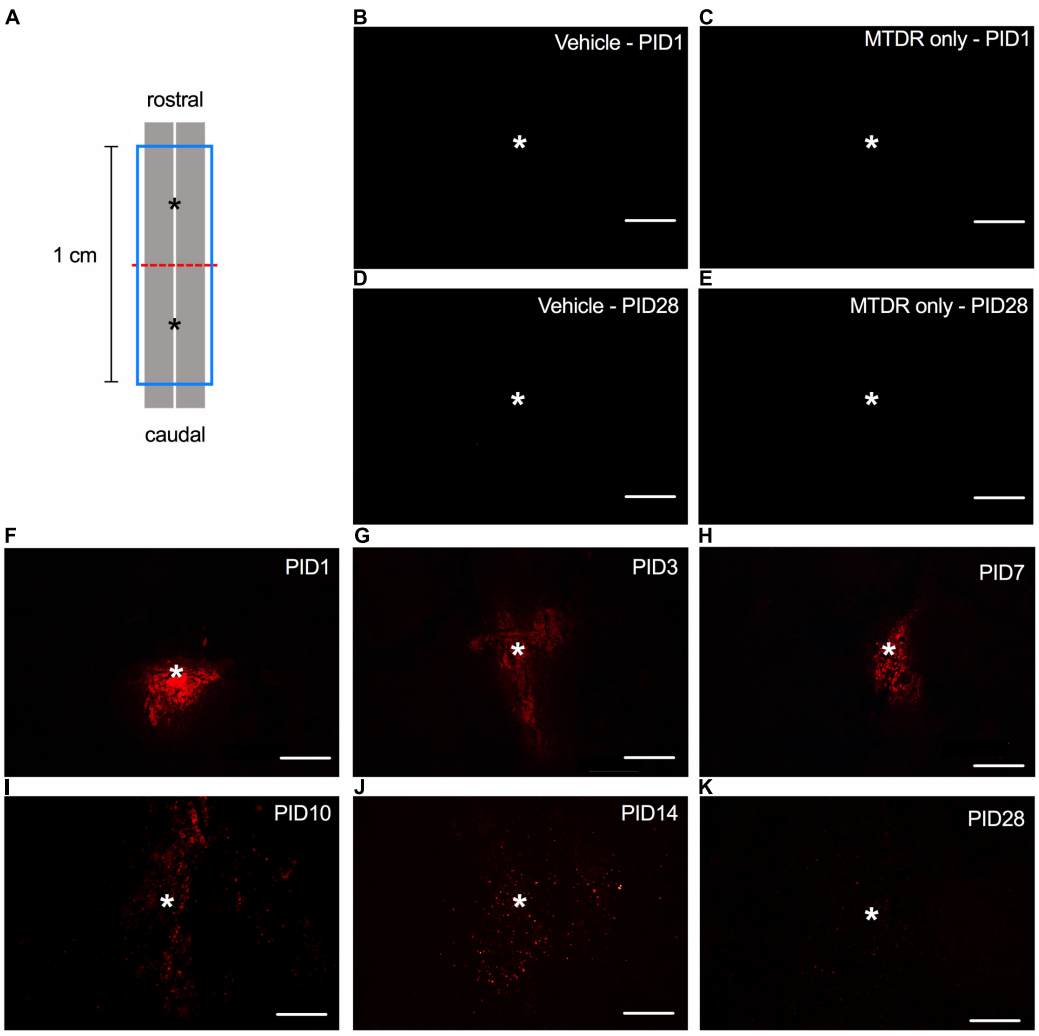

FIGURE 1 | The spatiotemporal distribution of transplanted mitochondria in the injured spinal cord of rats with traumatic SCI. **(A)** Diagram of the schematic spinal cord. The red dash line indicated the injury site. The blue frame indicated the 1-cm sampling area. The asterisks denoted the sites of administration of allogeneic mitochondria. **(B)** Representative micrograph of MTDR signals in the injured spinal cord of rat injected with 1x PBS vehicle on PID 1. **(C)** Representative micrograph of MTDR signals in the injured spinal cord of rat injected with MTDR dye on PID 1. **(D)** Representative micrograph of MTDR signals in the injured spinal cord of rat injected with 1x PBS vehicle on PID 28. **(E)** Representative micrograph of MTDR signals in the injured spinal cord of rat injected with MTDR dye on PID 28. **(F–K)** Representative micrograph of MTDR signals which were detected on PID1, 3, 7, 10, 14, and 28 in the injured spinal cord of rats injected with MTDR-labeled mitochondria. Horizontal sections were used. Scale bar = 100 μm. *N* = 1 rat per panel. The asterisks indicate the points of injection.

Two-tailed Student's *t*-test was used to compare means between two groups. The BBB scoring was analyzed by repeated-measures two-way ANOVA followed by Sidak's multiple comparisons. Significance was set at $p < 0.05$.

RESULTS

Spatiotemporal Distribution and Viability of the Transplanted Mitochondria in the Injured Spinal Cord

The amount (50 μg × 2, resuspended in 1x PBS) of transplanted mitochondria administered in this presented study was similar to the effective dosage characterized by Gollihue et al. (2018). Initially, we detected the MTDR signals in the horizontal sections of the injured spinal cord of rats (**Figure 1A**) that received MT to demonstrate the spatiotemporal distribution of transplanted mitochondria. No MTDR signal was detected in the injured spinal cord of rats injected with vehicle (**Figures 1B,D**) or MTDR dye (**Figures 1C,E**) on PID 1 and 28, suggesting that there was no obvious confoundedness of autofluorescence and that MTDR stained the exogenous mitochondria only. In the sections of the spinal cord with MTDR-labeled mitochondria, the MTDR signals were detectable at time points of PID 1, 3, 7, 10, 14, and 28 (**Figures 1F–K**). The exogenous MTDR-labeled mitochondria appeared as a cluster on PID 1 (**Figure 1F**) and gradually spread to the rostral and caudal ends of the lesion (**Figures 1G–K**).

Mitochondrial Transplantation Improves Recoveries of Sensory and Locomotor Functions in Rats With Traumatic Spinal Cord Injury

The effects of MT on the sensory function of traumatic SCI rats were examined by SSEP assessment performed on PID 28. Our results showed that there were no discriminable waveforms in the Vehicle group, whereas SSEPs were recognized in four out of five MT rats (**Figure 2A**). The locomotor functions of SCI rats were scored with the BBB test. Complete paralysis of the hind limbs in both groups was noted (BBB = 0) on PID 1 (**Figure 2B**). The MT rats showed better recovery of hindlimb locomotor function than the Vehicle ones in the BBB test carried out on PID 14 (3.60 ± 2.07 vs. 0.50 ± 0.58, score, MT vs. Vehicle, $p < 0.01$), 21 (4.60 ± 2.41 vs. 1.25 ± 0.50, score, MT vs. Vehicle, $p < 0.01$) and 28 (6.00 ± 2.00 vs. 1.50 ± 0.58, score, MT vs. Vehicle, $p < 0.0001$) (**Figure 2B**).

Mitochondrial Transplantation Protects Against Traumatic Spinal Cord Injury-Induced Demyelination in the Injured Spinal Cord of Rats

The results of LFB staining revealed that the severity of demyelination increased as the distance from the epicenter of the injured site decreased in both Vehicle and MT rats (**Figure 2C**). MT improved the preservation of white matter in the injured region (−1.6 mm: 86.39 ± 2.20 vs. 69.26 ± 7.57%, MT vs. Vehicle, $p < 0.01$; −0.8 mm: 50.96 ± 9.91 vs. 37.30 ± 7.26%, MT vs. Vehicle, $p < 0.05$; + 0.8 mm: 72.09 ± 5.89 vs. 36.07 ± 12.11%, MT vs. Vehicle, $p < 0.001$; + 1.6 mm: 72.39 ± 5.25 vs. 60.05 ± 7.10%, MT vs. Vehicle, $p < 0.05$) of spinal cords (**Figures 2C,D**).

Mitochondrial Transplantation Ameliorates Mitochondrial Fragmentation and Cellular Apoptosis in the Injured Spinal Cord of Rats With Traumatic Spinal Cord Injury

The mitochondrial dynamics of fusion and fission are crucial for mitochondrial homeostasis. It has been reported that mitochondrial fission occurs during early apoptosis and mitochondrial fragmentation-related mitochondrial dysfunction is linked to subsequent cell death (Liu et al., 2015; Jia et al., 2016). Accordingly, Western blotting was used to determine the protein level of Drp1, a marker of mitochondrial fission and fragmentation, in the injured sham control or injured spinal cords and found that MT rats had a lower Drp1 level (0.45 ± 0.12 vs. 1.00 ± 0.24, relative expression, MT vs. Vehicle, $p < 0.01$) than the Vehicle rats in the SCI groups on PID 1 (**Figure 3**).

Furthermore, we examined the effects of MT on cellular apoptosis in the injured spinal cord as well. First, we adopted immunoblotting to examine the expression of apoptosis regulatory proteins, i.e., cleaved caspase-3, Bcl-2, and BAX, in the regions of interest (**Figures 4A–H**) on PID 1. Quantitative results showed that apoptotic related proteins were not changed in sham control groups (**Figures 4A–D**). However, MT downregulated the expression of cleaved caspase-3 (0.68 ± 0.19 vs. 1.00 ± 0.18, relative expression, MT vs. Vehicle, $p < 0.05$) and BAX (0.71 ± 0.21 vs. 1.00 ± 0.07, relative expression, MT vs. Vehicle, $p < 0.05$) but upregulated the Bcl-2 (1.48 ± 0.27 vs. 1.00 ± 0.09, relative expression, MT vs. Vehicle, $p < 0.01$) level in the injured spinal cord of rats on PID 1 (**Figures 4E–H**). Second, TUNEL assay was performed to visualize the population of apoptotic cells in the injured spinal cord on PID 28. The results revealed that MT reduced the density of apoptotic cells (60.63 ± 14.46 vs. 107.74 ± 11.93, number/mm^2, MT vs. Vehicle, $p < 0.001$) in the injured spinal cord (**Figures 4I,J**).

Mitochondrial Transplantation Suppresses the Expression of Pro-inflammatory Cytokines in the Injured Spinal Cord of Rats With Traumatic Spinal Cord Injury

Neuroinflammation is accompanied by an increase of secretion of pro-inflammatory cytokines are critical hallmarks of secondary injury after SCI (Beattie et al., 2000; Bains and Hall, 2012). We confirmed that the inflammatory cytokines were not elevated after MT in sham control groups (**Figures 5A–C**). Moreover, we evaluated the levels of pro-inflammatory cytokines in the injured spinal cord after MT and demonstrated that MT rats had lower expression of TNF (0.57 ± 0.16 vs. 1.00 ± 0.10, relative

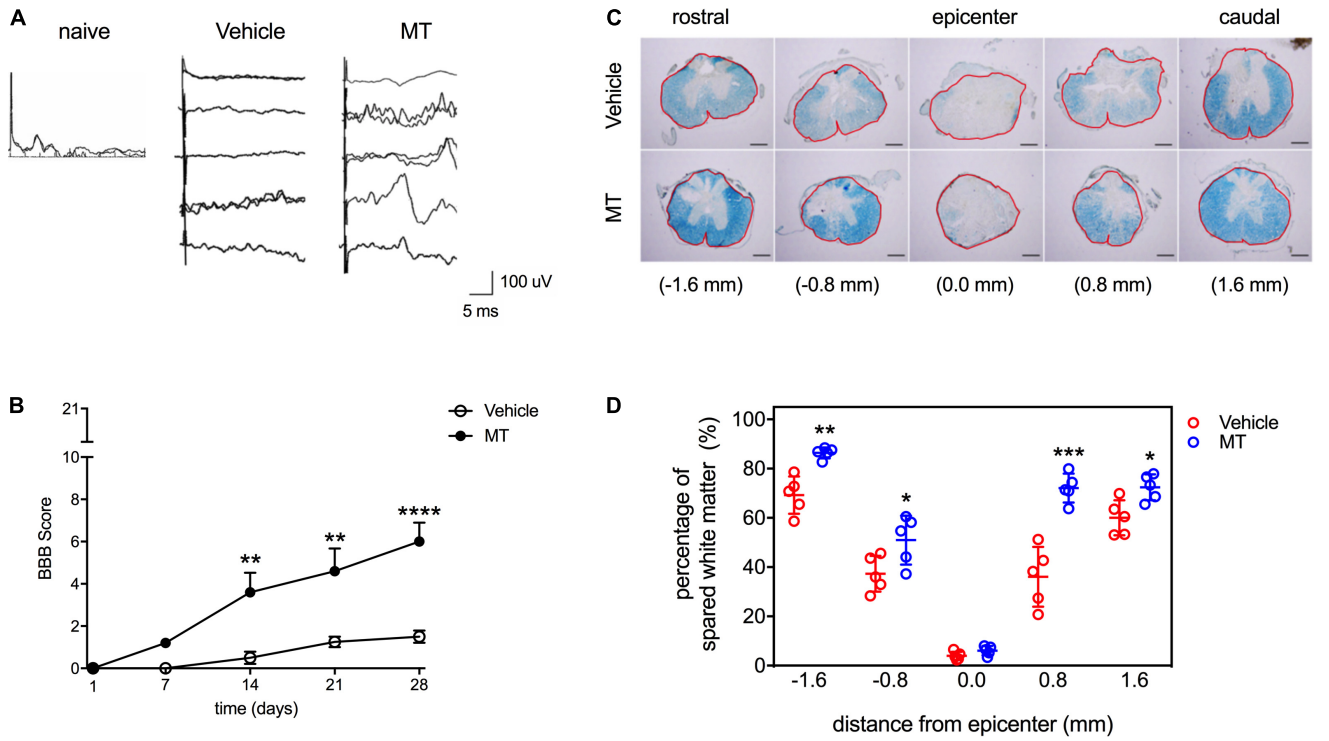

FIGURE 2 | Effects of mitochondrial transplantation on the sensory and locomotor functions and the white matter sparing in the injured spinal cord of rats with traumatic SCI. **(A)** Representative micrographs of SSEP traces recorded in SCI rats on PID 28. Scale = 100 μV/5 ms **(B)** Quantitative results of BBB scoring. $^{**}p < 0.01$, $^{****}p < 0.0001$, Sidak's multiple comparisons performed after the repeated measures two-way ANOVA. **(C)** Representative micrographs of LFB staining of transverse sections prepared from the injured spinal cords of rats. Scale bar = 100 μm. The red frames indicated the analyzed areas. **(D)** Quantitative results of percentage of LFB-positive area. $^{*}p < 0.05$, $^{**}p < 0.01$, $^{***}p < 0.001$, two-tailed Student's *t*-test. Data were expressed as mean ± standard deviation. $N = 5$. MT: mitochondria trans-plantation.

expression, MT vs. Vehicle, $p < 0.01$) and IL-6 (0.49 ± 0.20 vs. 1.00 ± 0.14, relative expression, MT vs. Vehicle, $p < 0.01$) than the Vehicle control rats (**Figures 5D–F**).

Mitochondrial Transplantation Attenuates Oxidative Damages in the Injured Spinal Cord of Rats With Traumatic Spinal Cord Injury

Overproduction of iNOS-derived NO and generation of 3-NT are signatures of oxidative damage during neuronal injury (Visavadiya et al., 2016). We investigated the effects of MT on the levels of these indicators of oxidative damage in the injured spinal cord on PID 1. The results demonstrated that the level of iNOS was not changed in the sham control groups (**Figures 6A,B**). In the injured groups, MT rats exhibited lower levels of iNOS (0.39 ± 0.06 vs. 1.00 ± 0.24, relative expression, MT vs. Vehicle, $p < 0.01$, **Figures 6C,D**), NO (2.41 ± 1.11 vs. 6.04 ± 0.25 μM, MT vs. Vehicle, $p < 0.001$, **Figure 6E**), and 3-NT (241.31 ± 121.06 vs. 467.33 ± 99.52 ng/ml, MT vs. Vehicle, $p < 0.001$, **Figure 6F**) than the Vehicle control rats on PID1. However, the concentrations of malondialdehyde, a marker for lipid peroxidation, were similar between the MT and Vehicle groups (**Figure 6G**).

DISCUSSION

This study was designed to elucidate the therapeutic effects of transplantation of allogeneic mitochondria on traumatic SCI. Our results showed that MT improved the recovery of somatosensory and locomotor functions after SCI and promoted the preservation of white matter in the injured spinal cord of rats with traumatic SCI. Attenuated mitochondrial fragmentation, cellular apoptosis, neuroinflammation, and oxidative stress were also evident in the spinal cord of rats that received MT. Moreover, by addressing the spatiotemporal distribution of the viable transplanted allogeneic mitochondria, we were able to newly demonstrate that transplanted allogeneic mitochondria survived in the lesioned region for at least 28 days in a rat model of traumatic SCI.

To the best of our knowledge, only two studies investigating the therapeutic effects of MT on traumatic SCI have been published (Li et al., 2015; Gollihue et al., 2018). Gollihue et al. (2018) first demonstrated that culture- and muscle-derived mitochondria, which were transplanted in the injured spinal cord, maintained their bioenergetics on PID 1. However, they did not identify any improving effect of MT on functional recovery in SCI rats (Gollihue et al., 2018). Conversely, Li et al. (2015) reported that the transplantation of mitochondria isolated from

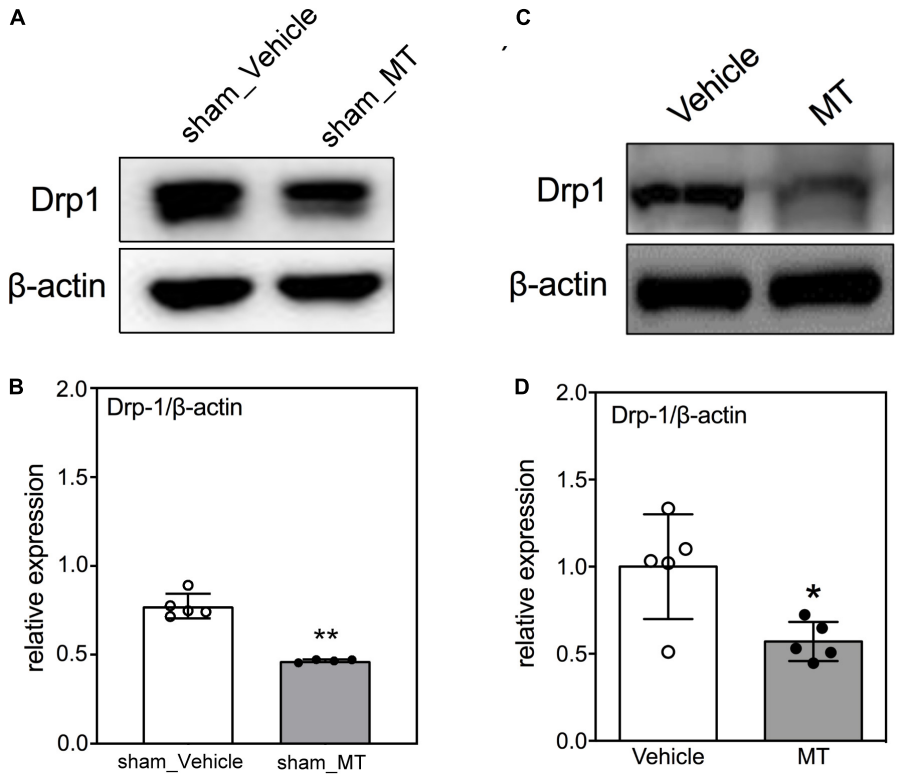

FIGURE 3 | Effects of mitochondrial transplantation on Drp1 expression in the injured spinal cord of rats with traumatic SCI on PID 1. **(A)** Representative micrograph of Western blot analysis of Drp1 in sham control groups. **(B)** Corresponding quantitative results of relative expression of Drp1 in sham control groups. **(C)** Representative micrograph of Western blot analysis of Drp1 in SCI groups on PID 1. **(D)** Corresponding quantitative results of relative expression of Drp1 in SCI groups on PID 1. The 1-cm spinal cord specimens centered at the epicenter of the injured site were used in Western blots. Data were expressed as mean ± standard deviation. $^{*}p < 0.05$, $^{**}p < 0.01$, two-tailed Student's *t*-test. $N = 5$. MT, mitochondria transplantation.

bone marrow mesenchymal stem cells to the injured spinal cord improved locomotor functional recovery in SCI rats, which is in line with our findings. These discrepancies may derive from the differences in the injecting site and the frequency of spinal cord puncture. First, intraparenchymal injection inevitably causes SCI. The midline of the dorsal spinal cord, the posterior median sulcus, has relatively fewer neural networks, compared with other parts of the spinal cord (Jacquesson et al., 2014; Mii et al., 2021). The midline incision is of paramount importance during surgery for intramedullary spinal pathologies. This can be attributed to its role in minimizing neural damage. Second, reduction in puncture time can mitigate tissue trauma. Therefore, we used a midline injection with two injection attempts, namely, rostral and caudal to the epicenter (Li et al., 2019), rather than a circumferential injection with four injection attempts (Gollihue et al., 2018).

It has been reported that transplanted mitochondria maintain their bioenergetics after transplantation (Garbuzova-Davis et al., 2017; Chien et al., 2018; Gollihue et al., 2018; Li et al., 2019); however, few studies have addressed their viability in the host. MTDR and mitochondria-targeting transgenically labeled green fluorescent protein (tGFP) are two widely used tools to label and trace the transplanted mitochondria. Given that the fluorescent signal of mitochondria-targeting tGFP decayed over time (Gollihue et al., 2018), we adopted MTDR to label the allogeneic transplanted mitochondria in this study. MTDR, a mitochondrial potential-dependent dye, stains viable mitochondria and sustains along with their viability (Xiao et al., 2016). Hence, MTDR is also suitable for detecting the viability of transplanted mitochondria. We found that the MTDR signals could be recognized in the injured spinal cord on PID 28, suggesting that the transplanted mitochondria survived for a least 28 days in the lesioned region. Our results were in line with a previous finding that transplanted xenogeneic mitochondria survived for 4 weeks in the myocardium of pigs with cardiac ischemia (Kaza et al., 2017). Furthermore, by characterizing the spatial distribution of the transplanted mitochondria, we also found that the spread region of the transplanted mitochondria was relatively restricted around the injection site. Hence, multiple and repeated administrations of allogeneic mitochondria may be required when dealing with a large volume of damaged tissue.

Intact mitochondrial function and bioenergetics depend on balanced mitochondrial fusion and fission. This mitochondrial dynamic is reactive to environmental changes. SCI leads to a shift from fusion to fission and subsequently results in neural death (Liu et al., 2015). It has been reported that the expression of mitochondrial fusion protein was increased, whereas the level of mitochondrial fission protein decreased in the spinal cord at 8 h after acute SCI (Jia et al., 2016). The expression

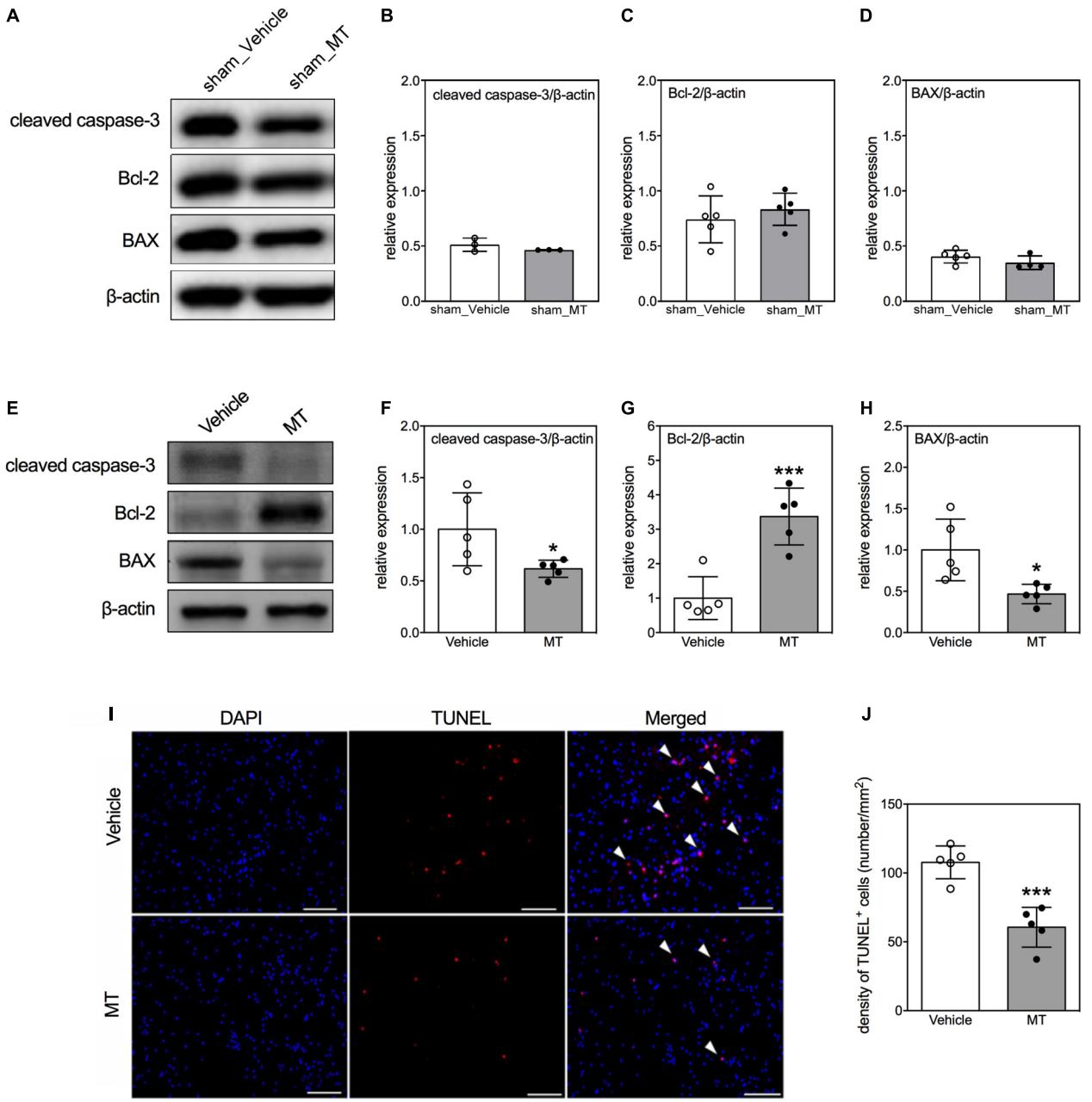

FIGURE 4 | Effects of mitochondrial transplantation on cellular apoptosis in the injured spinal cord of rats with traumatic SCI. **(A)** Representative micrograph of Western blots of cleaved caspase-3, Bcl-2, and BAX in sham control groups. **(B–D)** Corresponding quantitative results of relative expression of cleaved caspase-3, Bcl-2, and BAX in sham control groups. **(E)** Representative micrograph of Western blots of cleaved caspase-3, Bcl-2, and BAX in SCI groups on PID 1. **(F–H)** Corresponding quantitative results of relative expression of cleaved caspase-3, Bcl-2, and BAX in SCI groups on PID 1. The 1-cm spinal cord specimens centered at the epicenter of the injured site were used in Western blots. **(I)** Representative micrographs of TUNEL assay. The white arrowheads indicate both DAPI and TUNEL dual-positive cells. The sections used in TUNEL assay were obtained from the 1-cm spinal cord specimens centered at the epicenter of the injured site. Scale = 100 μm. **(J)** Quantitative results of the TUNEL assay. Data were expressed as mean ± standard deviation. $^{*}p < 0.05$, $^{***}p < 0.001$ two-tailed Student's *t*-test. *N* = 3–5. MT, mitochondria transplantation.

of the mitochondrial fusion protein was downregulated, but the level of mitochondrial fission protein was upregulated at 24 h after acute SCI (Jia et al., 2016). Herein, we assessed mitochondrial fission by determining Drp1 expression and found that MT suppressed the expression of Drp1 in the spinal cord of SCI rats, suggesting that MT alleviates injury-induced mitochondrial fission. Our results are consistent with reports of pharmacological inhibition of mitochondrial fission improving locomotor functions in several SCI models (Li et al., 2015; Liu et al., 2015). The ratio of fusion/fission protein expression

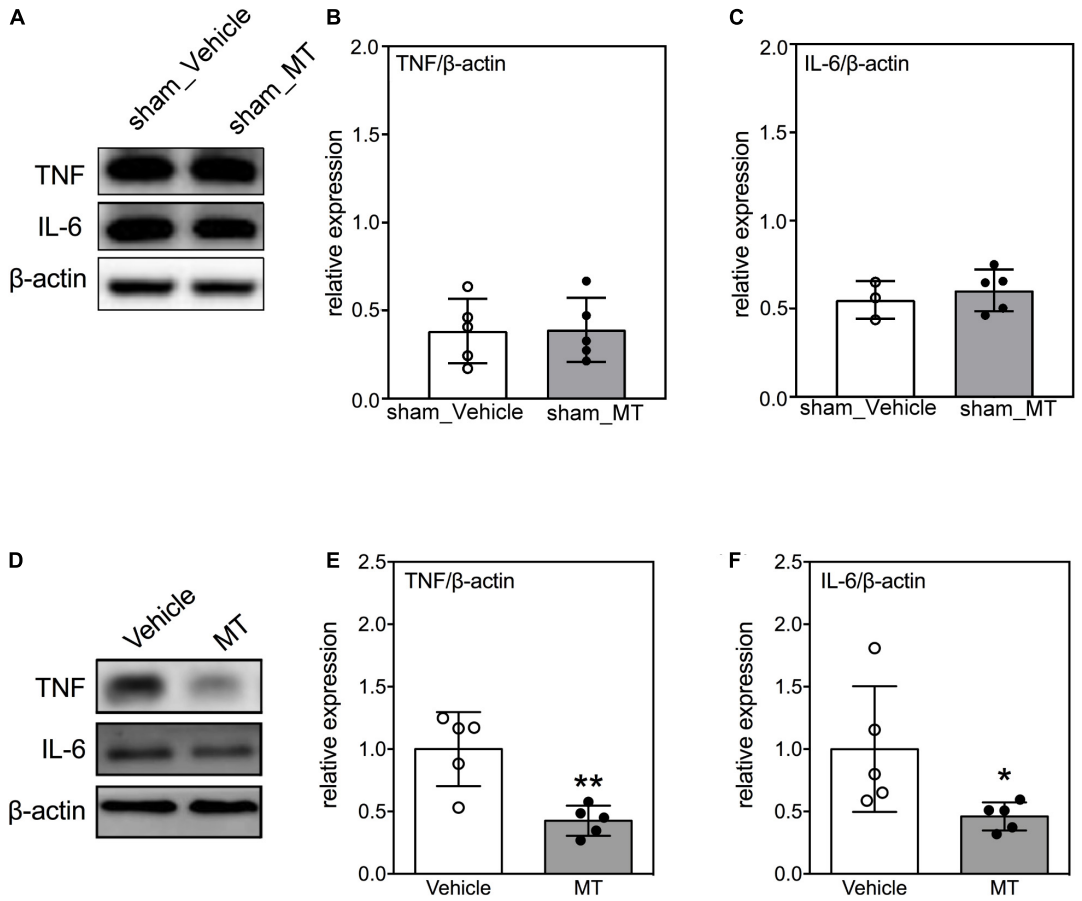

FIGURE 5 | Effects of mitochondrial transplantation on expression of pro-inflammatory cytokines in the injured spinal cord of rats with traumatic SCI on PID 1. **(A)** Representative micrograph of Western blots of TNF and IL-6 in sham control groups. **(B,C)** Quantitative results of relative expression of TNF and IL-6 in sham control groups. **(D)** Representative micrograph of Western blots of TNF and IL-6 in SCI groups on PID 1. **(E,F)** Quantitative results of relative expression of TNF and IL-6 in SCI groups on PID 1. The 1-cm spinal cord specimens centered at the epicenter of the injured site were used in Western blots. Data were expressed as mean ± standard deviation. $^{*}p < 0.05$, $^{**}p < 0.01$, two-tailed Student's *t*-test. $N = 3$–5. MT, mitochondria transplantation.

was suggested to be an important factor for maintenance of neuronal mitochondrial morphology and viability (Uo et al., 2009). We evaluated the ratio of Drp1/Mfn1 between the PBS and MT in the Sham and SCI groups. The results demonstrated that the ratio of Drp1/Mfn1 was decreased after MT in SCI group (**Supplementary Figure 1**). Our results were suggested the neuroprotection effects after MT in SCI rats.

Apoptosis, one of the leading causes of neural death in SCI, propagates from the injured site into the periphery and lasts for several weeks (Springer et al., 1999; Beattie et al., 2000). Inhibiting apoptosis improves locomotor functions in SCI models (Pei et al., 2017; Wei et al., 2018). Our results showed that MT repressed traumatic SCI-induced apoptosis by increasing the expression of anti-apoptotic protein, Bcl-2, and reducing the level of pro-apoptotic protein, BAX, the expression of apoptotic marker, cleaved caspase-3, and the TUNEL-positive cells. In line with our results, MT also exerted an anti-apoptotic effect in the model of cardiac ischemia (McCully et al., 2009, 2017). In SCI, apoptosis has been linked to mitochondrial fission according to the finding that the Drp1 inhibitor ameliorated SCI-induced apoptosis (Li et al., 2015). Thus, mitochondrial dynamics may be an upstream factor regulating the subsequent apoptosis. This relationship between mitochondrial fission and apoptosis was also evident in this study.

Mitochondria govern the homeostasis of cellular oxidative stress. An imbalance between the production and clearance of free radicals causes overwhelming injury to cells (Lobo et al., 2010). Since the mitochondrial content is relatively high in neurons, mitochondrial dysfunction following SCI elicits a huge accumulation of free radicals (Sullivan et al., 2007; Zhang et al., 2018). Antioxidant therapies are known to exert neuroprotective effects against SCI (Bains and Hall, 2012; Yang et al., 2016). In this study, we found that MT reduced the levels of NO, iNOS, and 3-NT in the injured spinal cord of rats. NO and iNOS are activators for the generation of RONS. 3-NT is a marker of protein oxidation in the injured spinal cord. Taken together, antioxidation may be involved in the mechanisms underlying the therapeutic effects of MT on traumatic SCI.

Activated microglia and infiltrating immune cells release a remarkable amount of pro-inflammatory mediators, such as

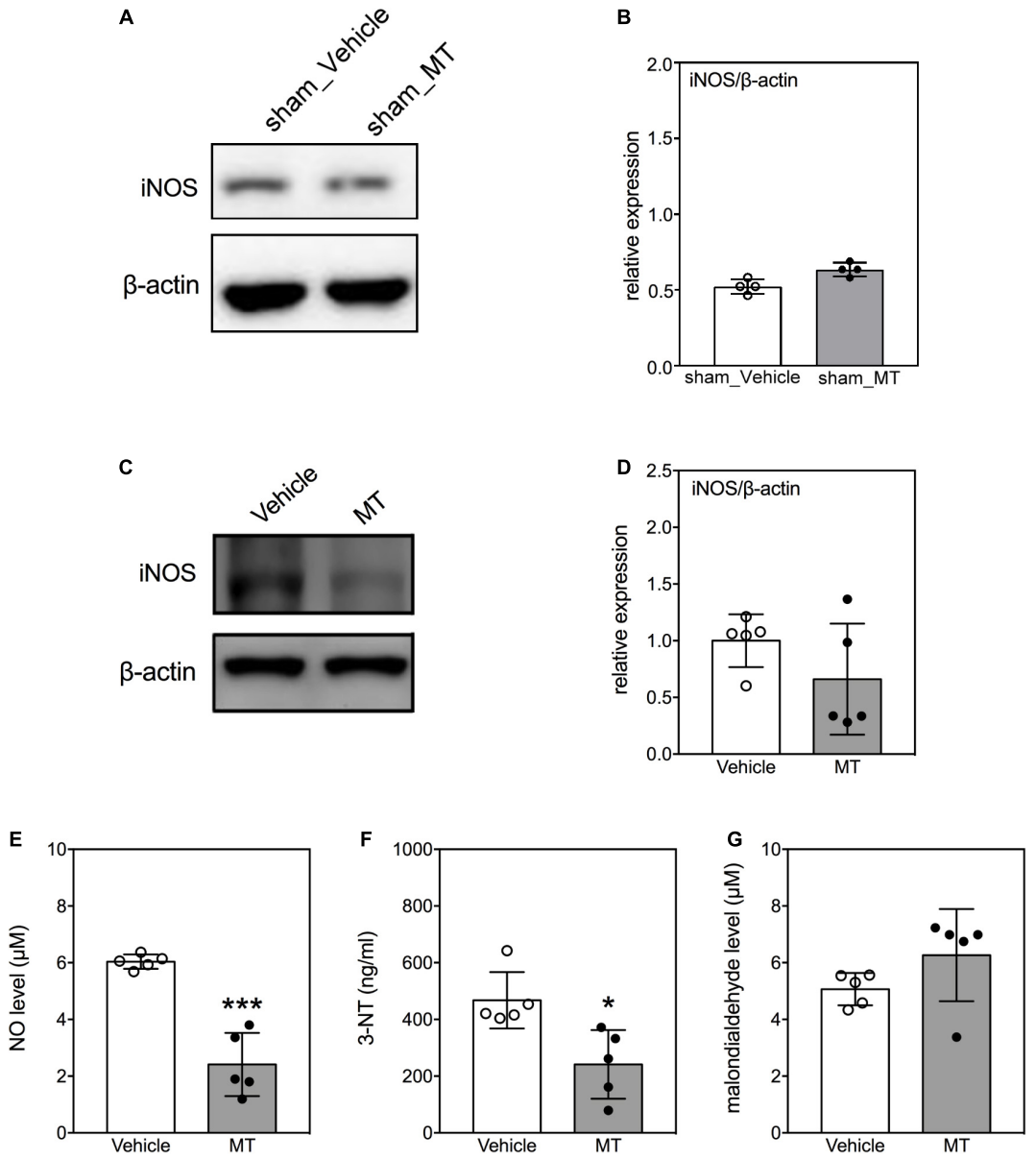

FIGURE 6 | Effects of mitochondrial transplantation on oxidative stress in the injured spinal cord of rats with traumatic SCI on PID 1. **(A)** Representative micrograph of Western blot of iNOS in sham control groups. **(B)** Quantitative results of relative expression of iNOS in sham control groups. **(C)** Representative micrograph of Western blot of iNOS in SCI groups on PID 1. **(D)** Quantitative results of relative expression of iNOS in SCI groups on PID 1. The 1-cm spinal cord specimens centered at the epicenter of the injured site were used in Western blots. **(E–G)** Quantitative results of the level of NO, 3-NT and malondialdehyde in SCI groups. Data were expressed as mean ± standard deviation. $^{*}p < 0.05$, $^{***}p < 0.001$, two-tailed Student's *t*-test. $N = 4–5$. MT, mitochondria transplantation.

TNF, IL-6, and NO, within hours after SCI and subsequently initiate a catastrophic secondary injury (Carlson et al., 1998; Hausmann, 2003; Pineau and Lacroix, 2007). Inhibiting the surge of inflammatory cytokines improves the functional outcomes in rats with SCI (Coelho-Santos et al., 2012; Guerrero et al., 2012; Wei et al., 2018). Herein, we observed a reduction in the TNF, IL-6, and NO levels in the injured spinal cords of MT rats, indicating reduction in inflammatory markers of MT. Similar to our findings, MT-induced downregulation of TNF and IL-6 has been also identified in a rabbit model of myocardial ischemia (Masuzawa et al., 2013). Our results suggested that anti-inflammation may be involved in the mechanisms underlying the therapeutic effects of MT on traumatic SCI. Moreover, it is noteworthy that IL-6 also behaves as a neurotrophic factor (Wagner, 1996; Erta et al., 2012) and promotes neuronal axon regeneration (Leibinger et al., 2013). Hence, the role of IL-6 in the MT-induced beneficial effects on SCI deserves further investigation.

Sirtuin 3 (SIRT3) has been identified as a stress-responsive deacetylase (Lombard et al., 2007), which shown to play a role

in protecting cells under stress in the mitochondria (Bause and Haigis, 2013). It can exhibit mighty anti-inflammation and anti-oxidation upon neuronal injury (Huang et al., 2019; Ye et al., 2019). Mitochondrial SIRT3 is known to act as a pro-survival factor, playing an essential role to protect neurons under excitotoxicity (Kim et al., 2011). Dai et al. show that SIRT3 attenuates oxidative stress-induced mitochondrial dysfunction via coordination of mitochondrial biogenesis and fission/fusion (Dai et al., 2014). Overexpression or activation of SIRT3 can provide an incremental protective effect against oxidative injury (Pillai et al., 2010; Dai et al., 2014). Although there was no significant change in anti-inflammatory markers, our results showed the increased expression of SIRT3 after MT in the SCI group (**Supplementary Figure 2**), which suggested that MT ameliorated SCI-induced neuronal injury may relate to the SIRT3-mediated anti-inflammatory pathway.

Previous *in vivo* and *in vitro* studies have reported evidence of intracellular transmission of mitochondria under normal physiological and pathological conditions via tunneling nanotubes, extracellular vesicles, cellular fusion, and gap junctions (Torralba et al., 2016). However, evidence of intercellular transmission of exogenous mitochondria following mitochondrial transplantation is still undetermined. Very limited number of exogenous mitochondria were internalized into the host cells in experimental models of spinal cord and myocardial injury (McCully et al., 2009; Li et al., 2019). Similarly, our results also showed that the regional administration of viable allogenic mitochondria dispersed into the periphery, where most of these exogenous organelles were located interstitially, rather than being internalized into the recipient cells (**Supplementary Figure 3**). Furthermore, the transplanted mitochondria have been hypothesized to increase ATP generation in the mitochondrial dysfunction tissues in order to support the injured cells. However, this hypothesis was not supported by the fact that administration of mitochondrial components or ATP/adenosine diphosphate failed to reproduce the therapeutic effects of MT on ischemic myocardial injury (McCully et al., 2009). On the other hand, recent reports showed that transplanted mitochondria suppressed the micro-environmental Ca^{2+} overload through the Ca^{2+}-buffering capacity to protect the neighboring cells (Chang et al., 2019). Additionally, Al Amir Dache et al. (2020) show human blood contains circulating cell-free respiratory competent mitochondria, which is suggestive of the maintenance of their bioenergetics under physiological calcium concentrations. However, the exact contribution of Ca^{2+}-buffering capacity of MT on attenuating neuroinflammation and apoptosis after SCI requires further investigations (Bertero et al., 2020; McCully et al., 2020).

CONCLUSION

We illustrated the therapeutic effects of transplantation of allogeneic mitochondria on traumatic SCI-induced somatosensory and functional impairments in rats. By determining the spatiotemporal distribution of viable transplanted mitochondria, we demonstrated the long-term survival of allogeneic mitochondria in the injured spinal cord of rats. Moreover, repressed mitochondrial fragmentation, apoptosis, oxidative stress, and inflammation may be likely involved in the mechanisms underlying the therapeutic effects of MT on SCI. Our findings provide basic evidence for the further translational application of MT in traumatic SCI. However, more detailed time-course studies on neuropathological changes after MT are needed, including the temporal expression of various pro-inflammatory cytokines and proteins associated with oxidative stress particularly at later stages of the injury, to better define the long-term therapeutic effects of MT on wound healing and functional improvements at the chronic stage after SCI.

DATA AVAILABILITY STATEMENT

The original contributions presented in the study are included in the article/**Supplementary Material**, further inquiries can be directed to the corresponding author.

ETHICS STATEMENT

The animal study was reviewed and approved by the National Cheng Kung University Institutional Animal Care and Use Committee (IACUC approval number: 107184).

AUTHOR CONTRIBUTIONS

M-WL, S-YF, C-FL, and J-SL: study design. S-YF, J-SL, C-YH, P-HL, and H-FC: conducting animal experiments and measurement of the motor function. M-WL, H-FC, and J-SL: conducting tissue collection and analysis. S-YF, J-YH, and J-SL: statistical analysis and data interpretation. M-WL, J-YH, C-FL, and J-SL: manuscript preparation. All authors contributed to the article and approved the submitted version.

FUNDING

This research was funded by the 2020 Higher Education Sprout Project, Ministry of Education, Taiwan, National Cheng Kung University Hospital-E-Da Hospital, Taiwan (grant number: NCKUEDA10705), and National Cheng Kung University Hospital, Taiwan (grant number: NCKUH-10904038).

ACKNOWLEDGMENTS

We are grateful to thank Yi-Ying Wu for English editing.

SUPPLEMENTARY MATERIAL

The Supplementary Material for this article can be found online at: https://www.frontiersin.org/articles/10.3389/fnins.2022.800883/full#supplementary-material

REFERENCES

Ahuja, C. S., Wilson, J. R., Nori, S., Kotter, M. R. N., Druschel, C., Curt, A., et al. (2017). Traumatic spinal cord injury. *Nat. Rev. Dis. Primers* 3:17018. doi: 10.1038/nrdp.2017.18

Al Amir Dache, Z., Otandault, A., Tanos, R., Pastor, B., Meddeb, R., Sanchez, C., et al. (2020). Blood contains circulating cell-free respiratory competent mitochondria. *FASEB J.* 34, 3616–3630. doi: 10.1096/fj.201901917RR

Bains, M., and Hall, E. D. (2012). Antioxidant therapies in traumatic brain and spinal cord injury. *Biochim. Biophys. Acta* 1822, 675–684. doi: 10.1016/j.bbadis.2011.10.017

Bause, A. S., and Haigis, M. C. (2013). SIRT3 regulation of mitochondrial oxidative stress. *Exp. Gerontol.* 48, 634–639. doi: 10.1016/j.exger.2012.08.007

Beattie, M. S., Farooqui, A. A., and Bresnahan, J. C. (2000). Review of current evidence for apoptosis after spinal cord injury. *J. Neurotrauma* 17, 915–925. doi: 10.1089/neu.2000.17.915

Bertero, E., O'Rourke, B., and Maack, C. (2020). Mitochondria do not survive calcium overload during transplantation. *Circ. Res.* 126, 784–786. doi: 10.1161/CIRCRESAHA.119.316291

Bolanos, J. P., Moro, M. A., Lizasoain, I., and Almeida, A. (2009). Mitochondria and reactive oxygen and nitrogen species in neurological disorders and stroke: therapeutic implications. *Adv. Drug Deliv. Rev.* 61, 1299–1315. doi: 10.1016/j.addr.2009.05.009

Carlson, S. L., Parrish, M. E., Springer, J. E., Doty, K., and Dossett, L. (1998). Acute inflammatory response in spinal cord following impact injury. *Exp. Neurol.* 151, 77–88. doi: 10.1006/exnr.1998.6785

Chang, C. Y., Liang, M. Z., and Chen, L. (2019). Current progress of mitochondrial transplantation that promotes neuronal regeneration. *Transl. Neurodegener.* 8:17. doi: 10.1186/s40035-019-0158-8

Chien, L., Liang, M. Z., Chang, C. Y., Wang, C., and Chen, L. (2018). Mitochondrial therapy promotes regeneration of injured hippocampal neurons. *Biochim. Biophys. Acta Mol. Basis Dis.* 1864(9 Pt B), 3001–3012. doi: 10.1016/j.bbadis.2018.06.012

Coelho-Santos, V., Goncalves, J., Fontes-Ribeiro, C., and Silva, A. P. (2012). Prevention of methamphetamine-induced microglial cell death by TNF-alpha and IL-6 through activation of the JAK-STAT pathway. *J. Neuroinflammation* 9:103. doi: 10.1186/1742-2094-9-103

Colon, J. M., Gonzalez, P. A., Cajigas, A., Maldonado, W. I., Torrado, A. I., Santiago, J. M., et al. (2018). Continuous tamoxifen delivery improves locomotor recovery 6h after spinal cord injury by neuronal and glial mechanisms in male rats. *Exp. Neurol.* 299(Pt A), 109–121. doi: 10.1016/j.expneurol.2017.10.006

Dai, S. H., Chen, T., Wang, Y. H., Zhu, J., Luo, P., Rao, W., et al. (2014). Sirt3 protects cortical neurons against oxidative stress via regulating mitochondrial Ca2+ and mitochondrial biogenesis. *Int. J. Mol. Sci.* 15, 14591–14609. doi: 10.3390/ijms150814591

Davis, C. H., Kim, K. Y., Bushong, E. A., Mills, E. A., Boassa, D., Shih, T., et al. (2014). Transcellular degradation of axonal mitochondria. *Proc. Natl. Acad. Sci. U.S.A.* 111, 9633–9638. doi: 10.1073/pnas.1404651111

Devaux, S., Cizkova, D., Quanico, J., Franck, J., Nataf, S., Pays, L., et al. (2016). Proteomic analysis of the spatio-temporal based molecular kinetics of acute spinal cord injury identifies a time- and segment-specific window for effective tissue repair. *Mol. Cell Proteomics* 15, 2641–2670. doi: 10.1074/mcp.M115.057794

Erta, M., Quintana, A., and Hidalgo, J. (2012). Interleukin-6, a major cytokine in the central nervous system. *Int. J. Biol. Sci.* 8, 1254–1266. doi: 10.7150/ijbs.4679

Garbuzova-Davis, S., Haller, E., Lin, R., and Borlongan, C. V. (2017). Intravenously transplanted human bone marrow endothelial progenitor cells engraft within brain capillaries, preserve mitochondrial morphology, and display pinocytotic activity toward blood-brain barrier repair in ischemic stroke rats. *Stem Cells* 35, 1246–1258. doi: 10.1002/stem.2578

Gollihue, J. L., Patel, S. P., Eldahan, K. C., Cox, D. H., Donahue, R. R., Taylor, B. K., et al. (2018). Effects of mitochondrial transplantation on bioenergetics. cellular incorporation, and functional recovery after spinal cord injury. *J. Neurotrauma* 35, 1800–1818. doi: 10.1089/neu.2017.5605

Guerrero, A. R., Uchida, K., Nakajima, H., Watanabe, S., Nakamura, M., Johnson, W. E., et al. (2012). Blockade of interleukin-6 signaling inhibits the classic pathway and promotes an alternative pathway of macrophage activation after spinal cord injury in mice. *J. Neuroinflammation* 9:40. doi: 10.1186/1742-2094-9-40

Hausmann, O. N. (2003). Post-traumatic inflammation following spinal cord injury. *Spinal Cord* 41, 369–378. doi: 10.1038/sj.sc.3101483

Hayakawa, K., Esposito, E., Wang, X., Terasaki, Y., Liu, Y., Xing, C., et al. (2016). Transfer of mitochondria from astrocytes to neurons after stroke. *Nature* 535, 551–555. doi: 10.1038/nature18928

Huang, D., Liu, M., and Jiang, Y. (2019). Mitochonic acid-5 attenuates TNF-alpha-mediated neuronal inflammation via activating Parkin-related mitophagy and augmenting the AMPK-Sirt3 pathways. *J. Cell Physiol.* 234, 22172–22182. doi: 10.1002/jcp.28783

Hurlbert, R. J., Hadley, M. N., Walters, B. C., Aarabi, B., Dhall, S. S., Gelb, D. E., et al. (2015). Pharmacological therapy for acute spinal cord injury. *Neurosurgery* 76(Suppl. 1), S71–S83. doi: 10.1227/01.neu.0000462080.04196.f7

Ide, T., Tsutsui, H., Hayashidani, S., Kang, D., Suematsu, N., Nakamura, K., et al. (2001). Mitochondrial DNA damage and dysfunction associated with oxidative stress in failing hearts after myocardial infarction. *Circ. Res.* 88, 529–535. doi: 10.1161/01.res.88.5.529

Jacquesson, T., Streichenberger, N., Sindou, M., Mertens, P., and Simon, E. (2014). What is the dorsal median sulcus of the spinal cord? Interest for surgical approach of intramedullary tumors. *Surg. Radiol. Anat.* 36, 345–351. doi: 10.1007/s00276-013-1194-1

Jia, Z. Q., Li, G., Zhang, Z. Y., Li, H. T., Wang, J. Q., Fan, Z. K., et al. (2016). Time representation of mitochondrial morphology and function after acute spinal cord injury. *Neural. Regen. Res.* 11, 137–143. doi: 10.4103/1673-5374.175061

Kaza, A. K., Wamala, I., Friehs, I., Kuebler, J. D., Rathod, R. H., Berra, I., et al. (2017). Myocardial rescue with autologous mitochondrial transplantation in a porcine model of ischemia/reperfusion. *J. Thorac. Cardiovasc. Surg.* 153, 934–943. doi: 10.1016/j.jtcvs.2016.10.077

Kim, S. H., Lu, H. F., and Alano, C. C. (2011). Neuronal Sirt3 protects against excitotoxic injury in mouse cortical neuron culture. *PLoS One* 6:e14731. doi: 10.1371/journal.pone.0014731

Lee, J. M., Hwang, J. W., Kim, M. J., Jung, S. Y., Kim, K. S., Ahn, E. H., et al. (2021). Mitochondrial transplantation modulates inflammation and apoptosis, alleviating tendinopathy both in vivo and in vitro. *Antioxidants (Basel)* 10:696. doi: 10.3390/antiox10050696

Lee, J. S., Hsu, Y. H., Chiu, Y. S., Jou, I. M., and Chang, M. S. (2020). Anti-IL-20 antibody improved motor function and reduced glial scar formation after traumatic spinal cord injury in rats. *J. Neuroinflammation* 17:156. doi: 10.1186/s12974-020-01814-4

Lee, J. S., Yang, C. C., Kuo, Y. M., Sze, C. I., Hsu, J. Y., Huang, Y. H., et al. (2012). Delayed granulocyte colony-stimulating factor treatment promotes functional recovery in rats with severe contusive spinal cord injury. *Spine* 37, 10–17. doi: 10.1097/BRS.0b013e31823b0440

Leibinger, M., Muller, A., Gobrecht, P., Diekmann, H., Andreadaki, A., and Fischer, D. (2013). Interleukin-6 contributes to CNS axon regeneration upon inflammatory stimulation. *Cell Death Dis.* 4:e609. doi: 10.1038/cddis.2013.126

Li, G., Jia, Z., Cao, Y., Wang, Y., Li, H., Zhang, Z., et al. (2015). Mitochondrial division inhibitor 1 ameliorates mitochondrial injury, apoptosis, and motor dysfunction after acute spinal cord injury in rats. *Neurochem. Res.* 40, 1379–1392. doi: 10.1007/s11064-015-1604-3

Li, H., Wang, C., He, T., Zhao, T., Chen, Y. Y., Shen, Y. L., et al. (2019). Mitochondrial transfer from bone marrow mesenchymal stem cells to motor neurons in spinal cord injury rats via gap junction. *Theranostics* 9, 2017–2035. doi: 10.7150/thno.29400

Liu, J. M., Yi, Z., Liu, S. Z., Chang, J. H., Dang, X. B., Li, Q. Y., et al. (2015). The mitochondrial division inhibitor mdivi-1 attenuates spinal cord ischemia-reperfusion injury both in vitro and in vivo: involvement of BK channels. *Brain Res.* 1619, 155–165. doi: 10.1016/j.brainres.2015.03.033

Lobo, V., Patil, A., Phatak, A., and Chandra, N. (2010). Free radicals, antioxidants and functional foods: impact on human health. *Pharmacogn. Rev.* 4, 118–126. doi: 10.4103/0973-7847.70902

Lombard, D. B., Alt, F. W., Cheng, H. L., Bunkenborg, J., Streeper, R. S., Mostoslavsky, R., et al. (2007). Mammalian Sir2 homolog SIRT3 regulates global mitochondrial lysine acetylation. *Mol. Cell Biol.* 27, 8807–8814. doi: 10.1128/MCB.01636-07

Masuzawa, A., Black, K. M., Pacak, C. A., Ericsson, M., Barnett, R. J., Drumm, C., et al. (2013). Transplantation of autologously derived mitochondria protects the

heart from ischemia-reperfusion injury. *Am. J. Physiol. Heart Circ. Physiol.* 304, H966–H982. doi: 10.1152/ajpheart.00883.2012

McCully, J. D., Cowan, D. B., Emani, S. M., and Del Nido, P. J. (2017). Mitochondrial transplantation: from animal models to clinical use in humans. *Mitochondrion* 34, 127–134. doi: 10.1016/j.mito.2017.03.004

McCully, J. D., Cowan, D. B., Pacak, C. A., Toumpoulis, I. K., Dayalan, H., and Levitsky, S. (2009). Injection of isolated mitochondria during early reperfusion for cardioprotection. *Am. J. Physiol. Heart Circ. Physiol.* 296, H94–H105. doi: 10.1152/ajpheart.00567.2008

McCully, J. D., Emani, S. M., and Del Nido, P. J. (2020). Letter by mccully et al regarding article, "mitochondria do not survive calcium overload". *Circ. Res.* 126, e56–e57. doi: 10.1161/CIRCRESAHA.120.316832

McEwen, M. L., Sullivan, P. G., Rabchevsky, A. G., and Springer, J. E. (2011). Targeting mitochondrial function for the treatment of acute spinal cord injury. *Neurotherapeutics* 8, 168–179. doi: 10.1007/s13311-011-0031-7

Mii, K., Yagishita, S., and Kumabe, T. (2021). Electron microscopic study of the median structure of the posterior column of the spinal cord of the adult rat with a special reference to the posterior median septum. *Anat. Rec. (Hoboken)* 304, 625–630. doi: 10.1002/ar.24569

Mothe, A. J., and Tator, C. H. (2012). Advances in stem cell therapy for spinal cord injury. *J. Clin. Invest.* 122, 3824–3834. doi: 10.1172/JCI64124

Pei, J. P., Fan, L. H., Nan, K., Li, J., Dang, X. Q., and Wang, K. Z. (2017). HSYA alleviates secondary neuronal death through attenuating oxidative stress, inflammatory response, and neural apoptosis in SD rat spinal cord compression injury. *J. Neuroinflammation* 14:97. doi: 10.1186/s12974-017-0870-1

Pillai, V. B., Sundaresan, N. R., Kim, G., Gupta, M., Rajamohan, S. B., Pillai, J. B., et al. (2010). Exogenous NAD blocks cardiac hypertrophic response via activation of the SIRT3-LKB1-AMP-activated kinase pathway. *J. Biol. Chem.* 285, 3133–3144. doi: 10.1074/jbc.M109.077271

Pineau, I., and Lacroix, S. (2007). Proinflammatory cytokine synthesis in the injured mouse spinal cord: multiphasic expression pattern and identification of the cell types involved. *J. Comp. Neurol.* 500, 267–285. doi: 10.1002/cne.21149

Russo, E., Nguyen, H., Lippert, T., Tuazon, J., Borlongan, C. V., and Napoli, E. (2018). Mitochondrial targeting as a novel therapy for stroke. *Brain Circ.* 4, 84–94. doi: 10.4103/bc.bc_14_18

Springer, J. E., Azbill, R. D., and Knapp, P. E. (1999). Activation of the caspase-3 apoptotic cascade in traumatic spinal cord injury. *Nat. Med.* 5, 943–946. doi: 10.1038/11387

Sullivan, P. G., Krishnamurthy, S., Patel, S. P., Pandya, J. D., and Rabchevsky, A. G. (2007). Temporal characterization of mitochondrial bioenergetics after spinal cord injury. *J. Neurotrauma* 24, 991–999. doi: 10.1089/neu.2006.0242

Swerdlow, R. H., Burns, J. M., and Khan, S. M. (2010). The Alzheimer's disease mitochondrial cascade hypothesis. *J. Alzheimers Dis.* 20(Suppl. 2), S265–S279. doi: 10.3233/JAD-2010-100339

Torralba, D., Baixauli, F., and Sanchez-Madrid, F. (2016). Mitochondria know no boundaries: mechanisms and functions of intercellular mitochondrial transfer. *Front. Cell Dev. Biol.* 4:107. doi: 10.3389/fcell.2016.00107

Uo, T., Dworzak, J., Kinoshita, C., Inman, D. M., Kinoshita, Y., Horner, P. J., et al. (2009). Drp1 levels constitutively regulate mitochondrial dynamics and cell survival in cortical neurons. *Exp. Neurol.* 218, 274–285. doi: 10.1016/j.expneurol.2009.05.010

Visavadiya, N. P., Patel, S. P., VanRooyen, J. L., Sullivan, P. G., and Rabchevsky, A. G. (2016). Cellular and subcellular oxidative stress parameters following severe spinal cord injury. *Redox. Biol.* 8, 59–67. doi: 10.1016/j.redox.2015.12.011

Wagner, J. A. (1996). Is IL-6 both a cytokine and a neurotrophic factor? *J. Exp. Med.* 183, 2417–2419. doi: 10.1084/jem.183.6.2417

Wang, Y., Ni, J., Gao, C., Xie, L., Zhai, L., Cui, G., et al. (2019). Mitochondrial transplantation attenuates lipopolysaccharide- induced depression-like behaviors. *Prog. Neuropsychopharmacol. Biol. Psychiatry* 93, 240–249. doi: 10.1016/j.pnpbp.2019.04.010

Wei, W., Shurui, C., Zipeng, Z., Hongliang, D., Hongyu, W., Yuanlong, L., et al. (2018). Aspirin suppresses neuronal apoptosis, reduces tissue inflammation, and restrains astrocyte activation by activating the Nrf2/HO-1 signaling pathway. *Neuroreport* 29, 524–531. doi: 10.1097/WNR.0000000000000969

Wu, Y., Chen, M., and Jiang, J. (2019). Mitochondrial dysfunction in neurodegenerative diseases and drug targets via apoptotic signaling. *Mitochondrion* 49, 35–45. doi: 10.1016/j.mito.2019.07.003

Xiao, B., Deng, X., Zhou, W., and Tan, E. K. (2016). Flow cytometry-based assessment of mitophagy using mitotracker. *Front. Cell Neurosci.* 10:76. doi: 10.3389/fncel.2016.00076

Yang, L., Yao, M., Lan, Y., Mo, W., Sun, Y. L., Wang, J., et al. (2016). Melatonin for spinal cord injury in animal models: a systematic review and network meta-analysis. *J. Neurotrauma* 33, 290–300. doi: 10.1089/neu.2015.4038

Ye, J. S., Chen, L., Lu, Y. Y., Lei, S. Q., Peng, M., and Xia, Z. Y. (2019). SIRT3 activator honokiol ameliorates surgery/anesthesia-induced cognitive decline in mice through anti-oxidative stress and anti-inflammatory in hippocampus. *CNS Neurosci. Ther.* 25, 355–366. doi: 10.1111/cns.13053

Zhang, G. F., Yang, P., Yin, Z., Chen, H. L., Ma, F. G., Wang, B., et al. (2018). Electroacupuncture preconditioning protects against focal cerebral ischemia/reperfusion injury via suppression of dynamin-related protein 1. *Neural. Regen. Res.* 13, 86–93. doi: 10.4103/1673-5374.224373

Conflict of Interest: The authors declare that the research was conducted in the absence of any commercial or financial relationships that could be construed as a potential conflict of interest.

Publisher's Note: All claims expressed in this article are solely those of the authors and do not necessarily represent those of their affiliated organizations, or those of the publisher, the editors and the reviewers. Any product that may be evaluated in this article, or claim that may be made by its manufacturer, is not guaranteed or endorsed by the publisher.

frontiers | Frontiers in Neuroscience

ORIGINAL RESEARCH
published: 06 June 2022
doi: 10.3389/fnins.2022.890461

Discrete Wavelet Transform Analysis of the Electroretinogram in Autism Spectrum Disorder and Attention Deficit Hyperactivity Disorder

Paul A. Constable[1], Fernando Marmolejo-Ramos[2], Mercedes Gauthier[3], Irene O. Lee[4], David H. Skuse[4] and Dorothy A. Thompson[5,6]*

[1] College of Nursing and Health Sciences, Caring Futures Institute, Flinders University, Adelaide, SA, Australia, [2] Centre for Change and Complexity in Learning, The University of South Australia, Adelaide, SA, Australia, [3] Department of Ophthalmology & Visual Sciences, Faculty of Medicine and Health Sciences, McGill University, Montréal, QC, Canada, [4] Behavioural and Brain Sciences Unit, Population, Policy and Practice Programme, UCL Great Ormond Street Institute of Child Health, University College London, London, United Kingdom, [5] The Tony Kriss Visual Electrophysiology Unit, Clinical and Academic Department of Ophthalmology, Great Ormond Street Hospital for Children NHS Trust, London, United Kingdom, [6] UCL Great Ormond Street Institute of Child Health, University College London, London, United Kingdom

OPEN ACCESS

Edited by:
Christian Casanova, Université de Montréal, Canada

Reviewed by:
Mirella Barboni, Semmelweis University, Hungary
Marina Vladimirovna Zueva, Helmholtz Moscow Research Institute of Eye Diseases (NMITS GB), Russia

****Correspondence:***
Paul A. Constable
Paul.Constable@flinders.edu.au

Specialty section:
This article was submitted to Neurodevelopment, a section of the journal Frontiers in Neuroscience

Received: *06 March 2022*
Accepted: *09 May 2022*
Published: *06 June 2022*

Citation:
Constable PA, Marmolejo-Ramos F, Gauthier M, Lee IO, Skuse DH and Thompson DA (2022) Discrete Wavelet Transform Analysis of the Electroretinogram in Autism Spectrum Disorder and Attention Deficit Hyperactivity Disorder. Front. Neurosci. 16:890461. doi: 10.3389/fnins.2022.890461

Background: To evaluate the electroretinogram waveform in autism spectrum disorder (ASD) and attention deficit hyperactivity disorder (ADHD) using a discrete wavelet transform (DWT) approach.

Methods: A total of 55 ASD, 15 ADHD and 156 control individuals took part in this study. Full field light-adapted electroretinograms (ERGs) were recorded using a Troland protocol, accounting for pupil size, with five flash strengths ranging from –0.12 to 1.20 log photopic cd.s.m^{-2}. A DWT analysis was performed using the Haar wavelet on the waveforms to examine the energy within the time windows of the a- and b-waves and the oscillatory potentials (OPs) which yielded six DWT coefficients related to these parameters. The central frequency bands were from 20–160 Hz relating to the a-wave, b-wave and OPs represented by the coefficients: a20, a40, b20, b40, op80, and op160, respectively. In addition, the b-wave amplitude and percentage energy contribution of the OPs (%OPs) in the total ERG broadband energy was evaluated.

Results: There were significant group differences ($p < 0.001$) in the coefficients corresponding to energies in the b-wave (b20, b40) and OPs (op80 and op160) as well as the b-wave amplitude. Notable differences between the ADHD and control groups were found in the b20 and b40 coefficients. In contrast, the greatest differences between the ASD and control group were found in the op80 and op160 coefficients. The b-wave amplitude showed both ASD and ADHD significant group differences from the control participants, for flash strengths greater than 0.4 log photopic cd.s.m^{-2} ($p < 0.001$).

Conclusion: This methodological approach may provide insights about neuronal activity in studies investigating group differences where retinal signaling may be

altered through neurodevelopment or neurodegenerative conditions. However, further work will be required to determine if retinal signal analysis can offer a classification model for neurodevelopmental conditions in which there is a co-occurrence such as ASD and ADHD.

Keywords: discrete wavelet transform, electroretinogram, retina, neurodevelopment, autism, attention deficit hyperactivity disorder

INTRODUCTION

Altered retinal signaling in neurodevelopmental conditions such as autism spectrum disorder (ASD) (Ritvo et al., 1988; Constable et al., 2016, 2020b), schizophrenia and bipolar disorder (Hébert et al., 2010, 2015, 2020; Lavoie et al., 2014; Maziade et al., 2022) have been reported with differences between these groups and controls in time-domain parameters of the electroretinogram (ERG) waveform. Whilst this method is widely employed in cardiology (Addison, 2005; Meziani et al., 2013) and neurology (Bullmore et al., 2003; Faust et al., 2015), wavelet analysis has not been used previously to study time-frequency domain of the ERG in the neurodevelopmental disorders ASD and Attention Deficit Hyperactivity Disorder (ADHD). Discrete Wavelet Transform (DWT) analysis may provide biomarkers that facilitate stratification of these neurodevelopmental conditions (Molloy and Gallagher, 2021) which are known to share substantial genetic risk (Rommelse et al., 2010; Brainstorm Consortium et al., 2018, Cao et al., 2022).

Autism spectrum disorder and ADHD are the main neurodevelopmental disorders diagnosed in early childhood with a global prevalence estimated at approximately 1 and 3.4%, respectively (Polanczyk et al., 2015; Nevison et al., 2018). The co-occurrence of neurodevelopmental conditions is high with approximately 1:3 children with ASD also meeting diagnostic criteria for ADHD (Berenguer-Forner et al., 2015). ASD and ADHD often present as co-occurrence in children (Russell et al., 2014; Mansour et al., 2017) as well as other co-occurrences of conditions such as anxiety, epilepsy, and sleep disorders (Bougeard et al., 2021). Visual perception in ASD shows superiority in visual search (Constable et al., 2020a) and abnormal electrophysiological cortical differences in global motion perception (van der Hallen et al., 2019), motion onset (Constable et al., 2012), and coherence thresholds perception (Robertson et al., 2014). For reviews of sensory and visual perception in ASD see Dakin and Frith (2005) and Robertson and Baron-Cohen (2017). Individuals with ADHD also display differences in visual tasks and perception relating to visual attention (Zarka et al., 2021) and visual search (Mullane and Klein, 2008). Sensory processing problems are common in both ASD and ADHD children and a measure of sensory function using the ERG may help our understanding of the differences and similarities of these two groups (Dellapiazza et al., 2021).

The retina has three cell types connected in a vertical signaling pathway from the photoreceptors to the bipolar cells and then to the ganglion cells. Lateral neurons modify this path at two points: horizontal cells feedback to regulate the signal between photoreceptors and bipolar cells and amacrine cells link bipolar and ganglion cells (Masland, 2012). The retinal signal in response to brief flashes of light is captured as the ERG waveform. This is composed of an initial a-wave, a negative deflection originating from the hyperpolarization of the photoreceptors. The b-wave is a positive peak following the a-wave and is formed principally by the depolarization of bipolar cells. The cone and rod bipolar cells contribute to either the ON- or OFF- pathways within the retina (Kaneda, 2013). The ON-bipolar cells use slower metabotropic glutamate receptors and respond to an increase in retinal illumination, whilst- the OFF-bipolar cells utilize faster ionotropic glutamate receptors and respond when there is a decrease in retinal illumination (Severns and Johnson, 1993; Hanna and Calkins, 2006, 2007). The a-wave of the light-adapted ERG is shaped principally by the hyperpolarization of the cones but also has post receptoral contributions from bipolar cells (Bush and Sieving, 1994; Robson et al., 2003; Friedburg et al., 2004). Inhibitory pathways are formed by the horizontal and amacrine cells that utilize GABA and dopamine as the principal inhibitory neurotransmitters respectively (Diamond, 2017). The Oscillatory Potentials (OPs) are high frequency waves that appear on the b-wave and contribute to its amplitude and are initiated by the amacrine cells with some ganglion and bipolar cell modulation (Wachtmeister, 1980, 1981, 1998, 2001).

The DWT allows the energy to be determined within frequency bands at discrete time windows within the whole ERG waveform. The method was first applied to the ERG by Gauvin et al. (2014) who used a DWT derived from a continuous wavelet transform function to extract the energy associated within the frequency bands centered on: 20, 40, 80 and 160 Hz within the a- and b-wave time windows. The group then quantified the relative contributions of the DWT coefficients within each frequency band to specific sub-components of the ON- (20 Hz) and OFF- (40 Hz) pathway responses within the a- and b-waves (termed a20, a40, b20, b40) as well as characterizing the slow and fast OPs at 80 (op80) and 160 Hz (op160), respectively (Gauvin et al., 2014, 2015, 2016, 2017). This work demonstrated the fundamental strength of the DWT analysis in its power to quantify the discrete energies related to the ON- and OFF-pathways and the OPs. Our study aimed to explore the ability of the DWT analysis to identify features in the ERG waveform that could distinguish the neurodevelopmental conditions ASD and ADHD from a control group.

MATERIALS AND METHODS

Participants

A total of 55 ASD, 15 ADHD, and 156 control individuals took part with mean age (years) ± SD of: ASD: 14.2 ± 4.9; range

(6.0–27.3), ADHD: 15.8 ± 3.2; range (8.4–21.8) and control: 13.2 ± 5.0; range (3.1–26.7) Kruskal–Wallis test ($p < 0.001$) although age would not be a factor in this young population with ERG amplitudes remaining stable from ages 15 to 24 years before media opacities influence the amount of light reaching the retina (Birch and Anderson, 1992). Within the control group 22 participants (14%) were siblings of an ASD participant which provided a more representative sample of the general population. The sex balance for each group was: ADHD 8 male: 7 female, control 50 male, and 112 female and in the ASD group 40 male and 15 females [$\chi^2(2)$, 28.1 $p < 0.001$].

All participants were recruited at two sites from existing databases or local autism groups and *via* social media. Electrophysiological testing typically occurred in the afternoon for the participants. All ASD participants met criteria for a diagnostic classification based on DSM-IV-TR (American Psychiatric Association [APA], 2000) or DSM-5 (American Psychiatric Association [APA], 2013) criteria. Clinical assessments were guided by a combination of standardized observation (Autism Diagnostic Observation Schedule; Lord et al., 1989 or ADOS-2, Gotham et al., 2007) and interview (Developmental, Dimensional and Diagnostic interview, Skuse et al., 2004). The clinical diagnosis of ADHD was based on ICD-10 Research Diagnostic Criteria, incorporating measures of Hyperactivity, Impulsivity and Inattention provided by parents/carers and schoolteachers. The diagnostic assessments were performed by pediatric psychiatrists or clinical psychologists in the social communication disorder clinics at Great Ormond Street Hospital for Children in the United Kingdom or local Child and Adolescent Mental Health clinics in South Australia.

Participants were excluded if there was a history of strabismus surgery, other syndromic or metabolic disorders, or if there was a history of brain injury. We excluded participants who had co-existing ASD and ADHD, ADD, or OCD. Cognitive abilities were measured by the age-appropriate Wechsler scales: ASD group (mean ± SD): 101 ± 20 [range 60–136 for $N = 41$ (measure available for 75% of the group)]; ADHD group: 88 ± 10 [range 72–105 for $N = 7$ (measure available for 47% of the group)].

Eight of seventy-five participants had taken a psychoactive medication on the day prior to testing; Seven (12%) in the ASD group and one participant had taken methylphenidate (6%) in the ADHD group (6%). One individual with ASD was on an antiepileptic medication but had been seizure free for 5 years. The study was approved by human research ethics committees at both sites and written informed consent was obtained from either the participant or parent/guardian/carer as required before testing.

Electrophysiology

The ERG recording protocol has been reported previously in more detail (Constable et al., 2020b, 2021) and followed the International Society for Clinical Electrophysiology of Vision guidelines (Robson et al., 2022). All recordings were taken under normal room luminance (350–450 Lux). Five white flash strengths at: –0.119, 0.398, 0.602, 0.949, and 1.204 log photopic cd.s.m^{-2} on a 40 cd.m^{-2} white background were randomly presented to the right and then to the left eye at 2 Hz with 60 averages per flash strength. Traces were rejected from the average if they fell above or below the 25th centile. Repeats of the recordings were made in each eye if required. The waveform data, iris color along with video and images of the electrode position below the eye were exported using the RFF extractor version 2.9.4.1 (LKC Technologies Inc., Gaithersburg, MD, United States). The iris color index is automatically reported by the RETeval as the ratio of the 25th centile gray scale between the iris and pupil at the midline. Measurements of the iris color allowed for this parameter to be accounted for given that individuals with darker irises have lower ERG amplitudes (Al Abdlseaed et al., 2010). In addition, the electrode height (Hobby et al., 2018) was accounted for from the photographic image and a scaled ruler for each eye at 5 levels from –2 to +2 representing the height of the electrode from the recommended position of 2 mm below the lid margin. A value of –1 represents the electrode placed 1 mm below the recommended position). If the electrode was positioned greater than 2 mm below the reference level, then the data were not included in the sample. The mean ± SD iris colors for the groups were: ASD 1.23 ± 0.11, ADHD 1.27 ± 0.12, and control 1.25 ± 0.12 [Kruskal–Wallis test ($p < 0.001$)]. Only waveforms with an a-wave amplitude >1 μV were included (see **Supplementary Material** for further details on methods).

Discrete Wavelet Transform Analysis

The DWT function (Eq. 1) where the *DWT(j,k)* represents the wavelet coefficients at discrete frequencies (*j*) and discrete time windows (*k*), for the raw signal *x(t)* of the ERG waveform of amplitude vs. time, with ψ representing the Haar square wavelet function (Mallat, 2009).

$$DWT\ (j,k) = \int_{-\infty}^{+\infty} x(t)\, 2^{-j/2} \psi\left(2^{-j}t - k\right) dt \qquad (1)$$

The coefficients within each time window represent the energy (μV.s) within the signal which were extracted for statistical analysis. A scalogram presents the energies within each frequency band centered on (20, 40, 80, and 160 Hz) within time windows between –20–17.5 and 0–17.5 ms (a-wave), 17.5–55 ms (b-wave), and 8.125–55 ms and 8.125–55 ms (OPs) (Gauvin et al., 2015).

The DWT analysis gives results for the energy in the 20 Hz (ON-pathway) and 40 Hz (OFF-pathway) for the a- and b-wave components (Gauvin et al., 2015; Gauvin et al., 2017) as well as the 80 and 160 Hz components of the OPs that quantify the energy within the slow and fast OPs. The %OPs are measured as the percentage of the OPs energy (i.e., the 80 ops + 160 ops coefficients) to the overall ERG energy (i.e., the 20b + 40b + 80ops + 160ops coefficients), as described by Gauvin et al. (2016).

The DWT analysis was performed in MATLAB (Mathworks Inc.). See (Gauvin et al., 2014, 2015, 2016, 2017) for detailed descriptions of the DWT methodology applied to the ERG waveform. Code is available on request from Dr. Mercedes Gauthier.

Statistical Analyses

Non-parametric pairwise comparisons were performed between groups (i.e., ASD, control, and ADHD) at each of the five

flash strengths for each of the six DWT-related dependent variables, the b-wave amplitude and %OPs. The method proposed by Noguchi et al. (2020) was used *via* the "mctp" function in the "nparcomp" R package with its default settings (Tukey-type contrast, global pseudo-rank estimation method, Fisher asymptotic approximation method, and with 95% CIs). In addition to the "mctp" adjusting *p*-values for multiple comparisons, a stringent $p < 0.005$ was adopted as a cut-off of statistical significance (Benjamin et al., 2018). Confidence limits around each estimator for comparisons between groups are provided in the statistical output section of the **Supplementary Material**.

See **Supplementary Material** for statistical output and further details on the methods. The data set is available at Flinders FigShare Repository: https://doi.org/10.25451/flinders.17712347.v3

RESULTS

Discrete Wavelet Transforms

Scalogram plots of the DWT coefficients are shown in **Figure 1** of the ERG and OPs waveforms normalized to the ADHD color scale for a representative individual in each group. Note the reduced energy in the OP waveform (op80 and op160) in the ASD group compared with the control but no difference in the energy levels in the ERG waveform in the b20 and b40 energies between the ASD and the control. In contrast, the energy in all the frequency bands representing the DWT coefficients is higher in the ADHD compared to the control and ASD participant in the ERG and OP waveforms. There were no significant group differences across flash strengths for the dependent variables (Mann–Whitney U test $p > 0.09$).

Pairwise Comparisons

Figure 2 illustrates the group characteristics for the five flash strengths with the b40 and op80 coefficients. The boxplots display the distribution of the data with a notch at the median and the interquartile range (shown by the box itself) enables visualization of the dispersion in the data. The maverick observations are shown as the squares (see **Supplementary Material** Statistical Outputs for all data).

Table 1 reports the pairwise *p*-values comparison between the three groups for each of the DWT coefficients and the b-wave amplitude (b_amp) and %OPs for the two main flash strengths of 1.204 and 0.602 log photopic cd.s.m^{-2} (see **Supplementary Material** for all strengths). For comparison at the 1.204 log cd.s.m^{-2} the b20, b40, op80, and op160 coefficients were all significantly greater than control ($p < 0.001$) for the ADHD group. The respective energies (μV.s) for ADHD and controls at this flash strength were: Median (95% CI) ADHD group: b20 104.1 (96.0–112.6), b40 93.1 (87.0–101.6), op80 30.8 (28.7–35.9), and op160 17.9 (16.6–18.9). For the control group: b20 68.6 (65.6–71.4), b40 62.8 (61.0–65.6), op80 23.6 (23.1–24.2), and op160 13.6 (13.1–13.9). In contrast, for the ASD and control group differences at 1.204 log photopic cd.s.m^{-2} there were no significant differences for the b20 and b40 coefficients ($p > 0.008$) but there were significant differences ($p < 0.001$) for the op80 and op160 coefficients with the ASD coefficient values being: b20 65.2 (62.6–70.2), b40 55.5 (52.3–60.9), op80 20.2 (19.0–21.4), and op160 10.8 (9.9–11.7).

The %OPs as a measure of the contribution of the OPs to the overall broadband ERG energy were significantly reduced for the ASD ($p < 0.003$) across several flash strengths but only at the highest flash strength of 1.204 log photopic cd.s.m^{-2} for ADHD ($p < 0.001$) with median (95% CI) values of: ASD 54.3 (53.7–55.2), control 57.1 (56.4–57.5), and ADHD 55.3 (53.8–55.5)%.

The a20 component representing the ON-response showed a significant increased energy for ADHD compared to the control group ($p < 0.001$) only for flash strengths from 0.398 to 1.204 log photopic cd.s.m^{-2} and at the maximal flash strength of 1.204 log photopic cd.s.m^{-2} the respective values for a20 for the ADHD and control groups were: [median (95% CI)]: 29.5 (27.2–35.3) μV.s and 22.5 (21.2–24.0) μV.s. The a40 component representing the OFF-pathway was also significantly lower ($p < 0.001$) for the ASD group compared to control at the 0.602 and 1.204 log photopic cd.s.m^{-2} flash strengths with significant group differences observed between the ADHD and control group only at the two weakest flash strengths of –0.119 and 0.398 log photopic cd.s.m^{-2} ($p < 0.001$).

As previously reported, the light-adapted b-wave amplitude was reduced for ASD compared to controls (Constable et al., 2016, 2020b) and increased for ADHD compared to controls ($p < 0.001$). For example, at the 1.204 cd.s.m^{-2} flash strength the b-wave amplitudes (μV) [median (95% CI)] were: ASD 23.5 (21.7–25.7), control 30.4 (28.4–31.3), and ADHD 37.2 (33.3–41.1). See **Supplementary Table 2** for all values.

There were no significant correlations between groups for the dependent variables ($p > 0.48$) using robust percentage bend correlation method (Wilcox, 2012). A larger sample and consistent diagnostic metrics would be required before any conclusions regarding correlations between the DWT parameters and severity could be applied. See **Supplementary Material** for details of the correlation analysis.

DISCUSSION

Ours is the first study to apply a DWT analysis of the ERG in individuals with a neurodevelopmental disorder. Our aim was to test the hypothesis that there would be underlying differences between ADHD and ASD in the light adapted ERG waveforms that we have previously reported as abnormal in ASD (Constable et al., 2016, 2020b). We did find a pattern of difference between the ASD and control groups OPs. Whilst some differences in the shape of the second light-adapted OP peak have been described previously in a small cohort of adults with ASD (Constable et al., 2016), we can now provide the first quantification of this component of the ERG in children with ASD. We propose that the reduced b-wave amplitude we found in association with ASD could be explained by reduced energy and contribution of the neural generators of the OPs. The OPs originate in the amacrine cells, which utilize dopamine as their main neurotransmitter (Wachtmeister, 1998, 2001). Genetic studies have suggested

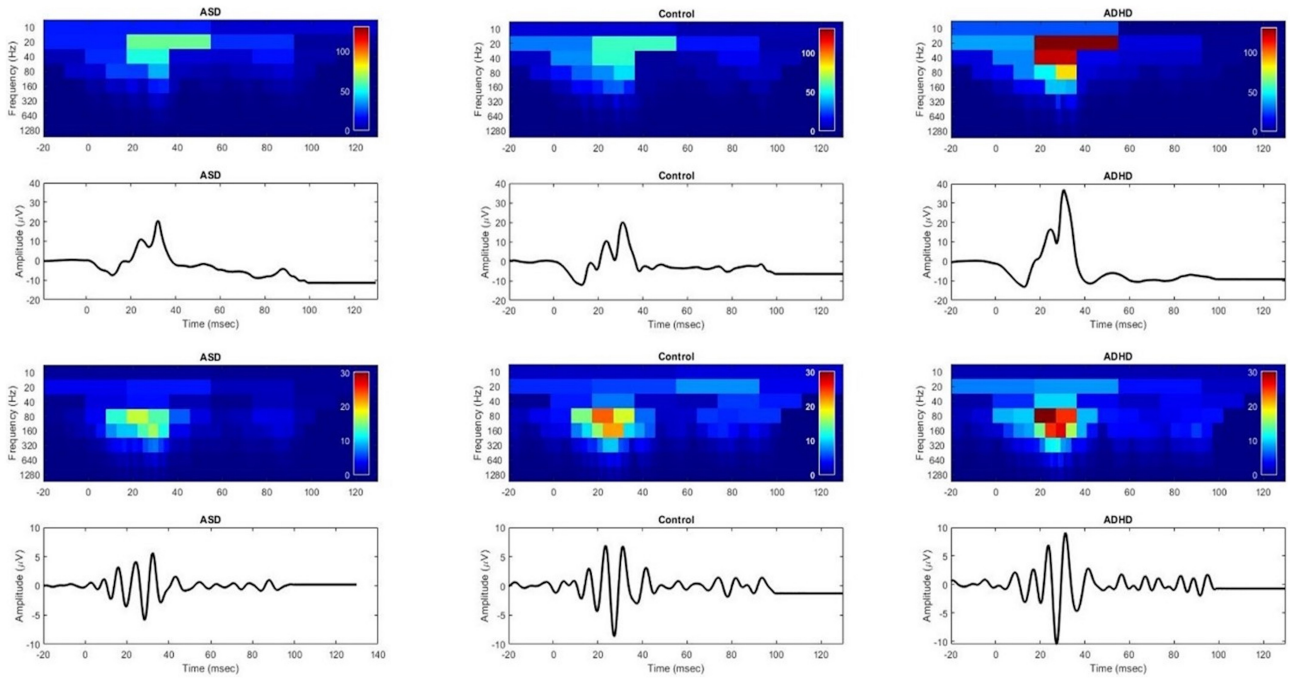

FIGURE 1 | DWT scalograms of the ERG and OPs waveforms for ASD, control and ADHD normalized to the color scale of the ADHD participant using a Flash Strength of log 1.204 photopic cd.s.m^{-2}. Red indicates greater energy levels and blue low energy levels. Upper panel shows the ERG waveforms and lower panels show the corresponding OP waveforms. In the upper panel the b20 and b40 bands of the ASD scalogram are not significantly different from that of the control. In contrast the ADHD participant's recording shows increased energy within all frequency bands of the scalogram compared to the ASD and control. The lower panels, show a reduced op80 and op160 energy in the ASD participant compared to the control.

dopamine regulation plays a role in ASD (Liu et al., 2021; Pavăl and Micluția, 2021). The characteristics of the coefficients op80, op160 and %OPs we observed, in relation to the b-wave, could be related to the amacrine cells and dopamine signaling, transport or storage (Wachtmeister and Dowling, 1978; Wachtmeister, 2001, 1981). Supportive evidence is provided by the observation that reduced retinal dopamine levels in Parkinson's disease are associated with lower b-wave amplitudes (Jackson et al., 2012; Nowacka et al., 2015).

Our findings in respect of ADHD concerned the b20 and b40 coefficients of the ERG, which relate to the ON- and OFF-pathways. These use glutamate as the principal neurotransmitter. There appears to be greater energy in those coefficients than in controls. The a20 coefficient was increased in ADHD compared with controls at flash strengths from 0.40 to 1.20 log cd.s.m^{-2} implying there is an ON-response difference between groups in this component. There is no direct involvement of the ON-pathway with the a-wave of the light-adapted ERG and the 20 Hz component is representative of the generalized on-response within the retina (Gauvin et al., 2015, 2017). In contrast, the a40 or OFF-pathway component to the a-wave did not differentiate these two groups at flash strengths greater than 0.60 log photopic cd.s.m^{-2} suggesting there is a relatively normal OFF-pathway response within the time window of the a-wave in children with ADHD. The post-receptor OFF-pathway normally contributes the amplitude of light-adapted a-wave (Bush and Sieving, 1994; Robson et al., 2003; Friedburg et al., 2004). The elevated energy in DWT coefficients that we observed may reflect alterations in bipolar cell functions that contribute to the b-wave. These implicate glutamate signaling and or transport/storage as the underlying cause, and glutamic gene function is associated with hyperactivity and impulsivity in ADHD (Naaijen et al., 2017). A polymorphism in metabotropic glutamate receptors predisposes to ADHD in the Chinese Han population (Zhang et al., 2021).

The %OPs were not significantly different between ADHD and control for flash strengths lower than 1.20 log photopic cd.s.m^{-2} ($p > 0.11$) with the main coefficients contributing to the elevated b-wave in ADHD being b20 and b40. In contrast, in keeping with the reduced op80 and op160 coefficients in ASD the %OPs were significantly lower for the ASD group compared to the control group for all flash strengths greater than 0.4 log photopic cd.s.m^{-2} ($p \geq 0.005$) supporting the reduced contribution of the OPs to the overall b-wave amplitude in ASD.

Evidence from mouse models also supports the clinical findings here. A recent study using the BTBR inbred mouse strain as an ASD model showed reductions in the b-wave response under dark and light adapted conditions (Cheng et al., 2020) as well as. Studies of an ADHD mouse model in which novel DA transporter had been knocked out have indicated ERG b-wave amplitudes are increased under light-adapted conditions, which is consistent with our findings (Dai et al., 2017). Offspring of mice exposed to valproic acid as an ASD model also show reduced dark-adapted ERG responses (Guimarães-Souza et al., 2019) in

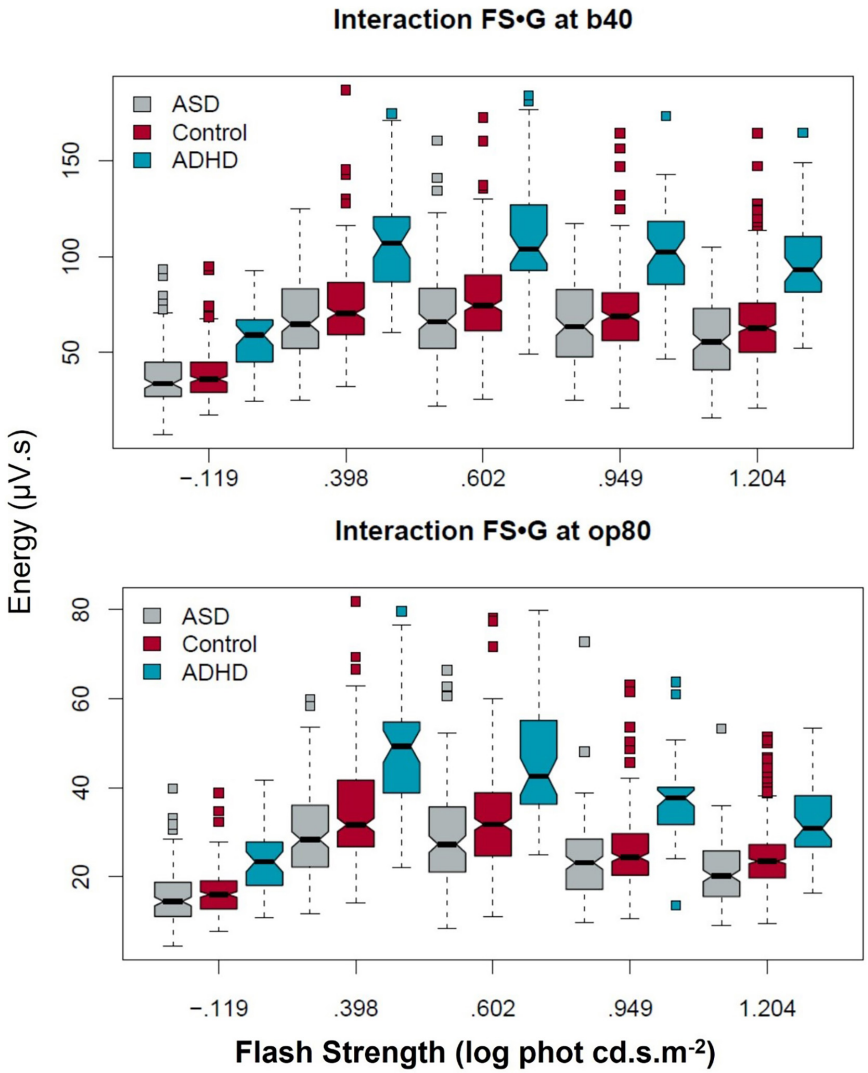

FIGURE 2 | Group differences in the b40 and op80 DWT coefficients across the five flash strengths. The ADHD group exhibited higher b40 and op80 energy levels across the flash series. In contrast the difference between ASD and controls was more significantly reduced for the op80 energy compared to the b40 at the higher flash strengths. Boxplots display ∼95% CIs around the median values.

support of previous findings of adults and children (Ritvo et al., 1988; Constable et al., 2016) and a deficit in ON-pathway retinal function. Currently no dark-adapted ERG studies have been performed in ADHD and this would be of interest to determine if the elevated ON-pathway response was also present under a different state of retinal adaptation.

The pathophysiology of ADHD and ASD remains a conundrum. There are no biomarkers for either condition, and we know multiple genetic and environmental factors contribute to the phenotypes (Geurts et al., 2013; Cooper et al., 2014; Kohls et al., 2014; Ronald et al., 2014; van Steijn et al., 2014; Naaijen et al., 2017). We provide some tentative evidence for neurophysiological changes that not only differentiate both conditions from typically developing children, but also evidence that they can be distinguished from each other based on ERG characteristics. Our findings suggest an elevation in the overall energy in the ERG within the b-wave and OPs in ADHD, which is consistent with reports of greater background retinal noise in this group (Bubl et al., 2015; Lee et al., 2022). In contrast, we report a reduction in the OPs contribution to the b-wave in ASD. We suggest this could account for the reduction in the b-wave amplitude previously reported in those with ASD, under dark and light adapted conditions (Ritvo et al., 1988; Constable et al., 2016, 2020b, 2021; Lee et al., 2022).

Discrete wavelet transform analysis has been applied to other clinical conditions. For instance, the multifocal ERG and the pattern ERG reveal a positive association with primary open angle glaucoma (Brandao et al., 2017; Hassankarimi et al., 2019). In congenital stationary night blindness, DWT analysis of the ERG and multifocal ERG highlighted the known absence of the ON-pathway involvement in the waveforms (Dorfman et al., 2020). A DWT analysis of low contrast pattern reversal

TABLE 1 | Median (Mdn) and lower (L) and upper (U) 95% confidence intervals for the three groups (ASD) autism spectrum disorder, control, and attention deficit hyperactivity disorder (ADHD) at each flash strength (FS) in log photopic cd.s.m^{-2}.

		ASD (a)			Control (c)			ADHD (A)			Contrast (*p*-value)		
FS	**Parameter**	**Mdn**	**L**	**U**	**Mdn**	**L**	**U**	**Mdn**	**L**	**U**	**c v a**	**A v a**	**A v c**
0.602	b wave amplitude	27.9	25.3	30.4	33.4	32.5	35.0	40.1	37.3	44.1	$2.5e^{-5}$	$< 10^{-16}$	$1.9e^{-10}$
	a20 Energy	14.8	13.7	16.0	15.0	13.9	15.8	19.4	16.2	22.4	0.74	0.005	$7.3e^{-4}$
	a40 Energy	17.2	15.7	18.6	19.6	19.0	20.5	23.4	21.0	27.8	$9.7e^{-5}$	$2.5e^{-4}$	0.11
	b20 Energy	63.7	60.5	68.6	65.2	63.1	68.9	95.3	89.3	100.3	0.15	$< 10^{-16}$	$<10^{-16}$
	b40 Energy	66.3	62.2	69.5	72.7	70.5	75.1	104.0	99.3	118.0	0.004	$< 10^{-16}$	$<10^{-16}$
	op80 Energy	27.3	24.9	29.8	29.4	28.0	30.4	42.6	39.7	46.5	$8.3e^{-4}$	$< 10^{-16}$	$6.9e^{-14}$
	op160 Energy	13.5	12.6	14.3	16.8	16.1	17.3	19.4	18.1	21.7	$1.2e^{-5}$	$3.2e^{-15}$	$2.4e^{-7}$
	%OPs	60.4	59.6	61.2	61.6	61.2	62.0	60.7	59.6	61.6	003	0.80	0.11
1.204	b wave amplitude	23.5	21.7	25.7	29.3	28.4	30.3	36.9	33.3	41.1	$1.3e^{-6}$	$1.4e^{-12}$	$6.3e^{-6}$
	a20 Energy	21.4	20.2	23.8	22.5	21.2	24.0	29.5	27.2	35.3	0.65	$1.3e^{-6}$	$3.4e^{-9}$
	a40 Energy	21.9	19.7	23.3	26.9	25.9	27.5	27.3	22.0	31.1	$6.7e^{-7}$	0.004	0.99
	b20 Energy	65.2	62.6	70.2	68.6	65.6	71.4	104.1	96.0	112.6	0.72	$< 10^{-16}$	$<10^{-16}$
	b40 Energy	55.5	52.3	60.9	62.8	61.0	65.6	93.1	87.0	101.6	0.008	$< 10^{-16}$	$<10^{-16}$
	op80 Energy	20.2	19.0	21.4	23.6	23.1	24.2	30.8	28.7	35.9	$1.5e^{-5}$	$< 10^{-16}$	$4.9e^{-12}$
	op160 Energy	10.8	9.9	11.7	13.6	13.1	13.9	17.9	16.6	18.9	$2.7e^{-7}$	$9.0e^{-13}$	$1.4e^{-7}$
	%OPs	54.3	53.7	55.2	57.1	56.4	57.5	55.3	53.8	55.5	$2.4e^{-9}$	0.85	$4.0e^{-4}$

Results of non-parametric multiple comparisons between groups at each flash strength in each of the ERG-related measures at $p < 0.005$. c, control; a, ASD; A, ADHD. The b-wave amplitude (μV) (b_amp) and the DWT solutions for b20, b40, op80, op160 (μV.s), and %OPs (no units).

visual evoked potentials at different spatial frequencies found the DWT coefficients showed greater significant differences than time domain or fast Fourier transform parameters for describing the evoked potentials (Hassankarimi et al., 2020). In cardiac disease, wavelet analysis has been used extensively for analysis of the ECG and cardiac arrhythmia (Rahul and Sharma, 2021; Li et al., 2022). It has also been used to analyze EEG signals in epilepsy (Zarei and Asl, 2021) and Parkinson's disease (Liu et al., 2017). The application of retinal signal analysis may provide a new marker for the classification of neurodevelopmental and neurodegenerative disorders given the broad heterogeneity and the lack of sufficient objective clinical and neuroscientific evidence within current classifications (Molloy and Gallagher, 2021). There is a need for a different approach that can support more reliable diagnoses, prognoses, and better targeted treatments. The DWT methodology has the potential to provide a "biotype" based on retinal signal analysis (Clementz et al., 2016; Cuthbert, 2020) and contribute to this field. Signal analysis of the ERG waveform may also provide more subtle functional insights into the structural changes within the retina which have been documented in longitudinal studies of Alzheimer's or Parkinson's disease using retinal imaging techniques (Kashani et al., 2021). It may also provide a sensitive method to monitor the effects of clinical trials of pharmacological and gene therapy to manage retinal and ophthalmic diseases (Yu-Wai-Man et al., 2020; Maguire et al., 2021; Gajendran et al., 2022).

Analysis of the ERG waveform using wavelet functions [as well as other signal analysis techniques such as Variable Frequency Complex Demodulation (VFCDM), (Chon et al., 2009), or Functional Data Analysis (Calle-Saldarriaga et al., 2021)] could provide better characterization of the heterogeneity inherent within the neurodevelopmental disorders that share common clinical traits (Thapar et al., 2017; Molloy and Gallagher, 2021). Of these, VFCDM can provide one of the highest time-frequency resolutions (Chon et al., 2009) and has been used to analyze other physiological signals (Wang et al., 2006; Siu et al., 2009, Posada-Quintero et al., 2016; Hossain et al., 2021). VFCDM uses a bank of low-pass filters to decompose the signal into a suite of band-limited signals. These can estimate instantaneous amplitude, frequency, and phase within each frequency band with higher resolution than DWT. VFCDM may offer an additional process to unlock the hidden signals within the ERG of neurological and retinal conditions.

This study is the first to apply a wavelet transform approach to analyzing clinical waveforms in neurodevelopmental conditions using the ERG. The method allows an objective description of the ON- and OFF- pathways as well as the contribution of the OPs to the overall ERG signal. A combination of time domain (b-wave amplitude) and time-frequency domain parameters (b20, b40, op80, op160) may assist with developing classification models of ADHD and ASD in the future, as well as providing a simple method to extract information on the underlying contributions of the ON- and OFF- pathways without the need for modeling luminance-response functions across several flash strengths (Hamilton et al., 2007; Hébert et al., 2017; Constable et al., 2020b). We speculate that the wavelet approach may in future aid in the study of retinal neurophysiology in schizophrenia and bipolar disorder (Hébert et al., 2015, 2020) as well as neurodegenerative conditions such as Parkinson's disease (Garcia-Martin et al., 2014; Nowacka et al., 2015). Further work will be required to establish abnormalities in these retinal signals are specific to neurodevelopmental disorders and what effects may be observed in the case of co-occurrence of other conditions (Silverstein and Thompson, 2020).

DATA AVAILABILITY STATEMENT

The datasets presented in this study can be found in online repositories. The names of the repository/repositories and accession number(s) can be found below: https://doi.org/10.25451/flinders.17712347.v3.

ETHICS STATEMENT

This study was reviewed and approved by the Flinders University Human Research Ethics Committee and the South East Scotland Research Ethics Committee in the United Kingdom. Written informed consent to participate in this study for those under 16 years of age was provided by the participants' legal guardian/next of kin.

AUTHOR CONTRIBUTIONS

PC wrote the first draft and collected ERG recordings with IL and DT. FM-R conducted the statistical analysis. DS contributed to the main discussion and clinical assessments. PC and MG performed the DWT analysis. All authors contributed equally to the final manuscript.

FUNDING

This study was funded by the Alan B. Slifka Foundation.

ACKNOWLEDGMENTS

We thank the participants and their families for their support. Quentin Davis and Joshua Santosa of LKC Technologies for programming the RETeval custom protocol.

SUPPLEMENTARY MATERIAL

The Supplementary Material for this article can be found online at: https://www.frontiersin.org/articles/10.3389/fnins.2022.890461/full#supplementary-material

REFERENCES

Addison, P. S. (2005). Wavelet transforms and the ECG: a review. *Physiol. Meas.* 26, R155–R199. doi: 10.1088/0967-3334/26/5/r01

Al Abdlseaed, A., McTaggart, Y., Ramage, T., Hamilton, R., and McCulloch, D. L. (2010). Light- and dark-adapted electroretinograms (ERGs) and ocular pigmentation: comparison of brown- and blue-eyed cohorts. *Doc. Ophthalmol.* 121, 135–146. doi: 10.1007/s10633-010-9240-3

American Psychiatric Association [APA] (2000). *Diagnostic and Statistical Manual of Mental Disorders (DSM-IV-TR)*. Washington DC: American Psychiatric Association.

American Psychiatric Association [APA] (2013). *Diagnostic and Statistical Manual of Mental Disorders V*, ed. R. Adamczyk (Arlington VA: American Psychiatric Association).

Benjamin, D. J., Berger, J. O., Johannesson, M., Nosek, B. A., Wagenmakers, E. J., Berk, R., et al. (2018). Redefine statistical significance. *Nat. Hum. Behav.* 2, 6–10. doi: 10.1038/s41562-017-0189-z

Berenguer-Forner, C., Miranda-Casas, A., Pastor-Cerezuela, G., and Roselló-Miranda, R. (2015). Comorbidity of autism spectrum disorder and attention deficit with hyperactivity. A review study. *Rev. Neurol.* 60, S37–43.

Birch, D. G., and Anderson, J. L. (1992). Standardized full-field electroretinography. Normal values and their variation with age. *Arch. Ophthalmol.* 110, 1571–1576. doi: 10.1001/archopht.1992.01080230071024

Bougeard, C., Picarel-Blanchot, F., Schmid, R., Campbell, R., and Buitelaar, J. (2021). Prevalence of autism spectrum disorder and co-morbidities in children and adolescents: a systematic literature review. *Front. Psychiatry* 12:744709. doi: 10.3389/fpsyt.2021.744709

Brainstorm Consortium, Anttila, V., Bulik-Sullivan, B., Finucane, H. K., Walters, R. K., Bras, J., et al. (2018). Analysis of shared heritability in common disorders of the brain. *Science* 360:eaa8757. doi: 10.1126/science.aap8757

Brandao, L. M., Monhart, M., Schötzau, A., Ledolter, A. A., and Palmowski-Wolfe, A. M. (2017). Wavelet decomposition analysis in the two-flash multifocal ERG in early glaucoma: a comparison to ganglion cell analysis and visual field. *Doc. Ophthalmol.* 135, 29–42. doi: 10.1007/s10633-017-9593-y

Bubl, E., Dörr, M., Riedel, A., Ebert, D., Philipsen, A., Bach, M., et al. (2015). Elevated background noise in adult attention deficit hyperactivity disorder is associated with inattention. *PLoS One* 10:e0118271. doi: 10.1371/journal.pone.0118271

Bullmore, E., Fadili, J., Breakspear, M., Salvador, R., Suckling, J., and Brammer, M. (2003). Wavelets and statistical analysis of functional magnetic resonance images of the human brain. *Stat. Methods Med. Res.* 12, 375–399. doi: 10.1191/0962280203sm339ra

Bush, R. A., and Sieving, P. A. (1994). A proximal retinal component in the primate photopic ERG a-wave. *Invest. Ophthalmol. Vis. Sci.* 35, 635–645.

Calle-Saldarriaga, A., Laniado, H., Zuluaga, F., and Leiva, V. (2021). Homogeneity tests for functional data based on depth-depth plots with chemical applications. *Chemometr. Intell. Lab. Syst.* 219:104420. doi: 10.1016/j.chemolab.2021.104420

Cao, H., Wang, J., Baranova, A., and Zhang, F. (2022). Classifying major mental disorders genetically. *Prog. Neuropsychopharmacol. Biol. Psychiatry* 112:110410. doi: 10.1016/j.pnpbp.2021.110410

Cheng, N., Pagtalunan, E., Abushaibah, A., Naidu, J., Stell, W. K., Rho, J. M., et al. (2020). Atypical visual processing in a mouse model of autism. *Sci. Rep.* 10:12390. doi: 10.1038/s41598-020-68589-9

Chon, K. H., Dash, S., and Ju, K. (2009). Estimation of respiratory rate from photoplethysmogram data using time–frequency spectral estimation. *IEEE Trans. Biomed. Eng.* 56, 2054–2063. doi: 10.1109/TBME.2009.2019766

Clementz, B. A., Sweeney, J. A., Hamm, J. P., Ivleva, E. I., Ethridge, L. E., Pearlson, G. D., et al. (2016). Identification of distinct psychosis biotypes using brain-based biomarkers. *Am. J. Psychiatry* 173, 373–384. doi: 10.1176/appi.ajp.2015.14091200

Constable, P. A., Bailey, K., Beck, A., Borrello, D., Kozman, M., and Schneider, K. (2020a). Effect size of search superiority in autism spectrum disorder. *Clin. Exp. Optom.* 103, 296–306. doi: 10.1111/cxo.12940

Constable, P. A., Ritvo, E. R., Ritvo, A. R., Lee, I. O., McNair, M. L., Stahl, D., et al. (2020b). Light-adapted electroretinogram differences in autism spectrum disorder. *J. Autism Dev. Disord.* 50, 2874–2885. doi: 10.1007/s10803-020-04396-5

Constable, P. A., Gaigg, S. B., Bowler, D. M., Jägle, H., and Thompson, D. A. (2016). Full-field electroretinogram in autism spectrum disorder. *Doc. Ophthalmol.* 132, 83–99. doi: 10.1007/s10633-016-9529-y

Constable, P. A., Gaigg, S. B., Bowler, D. M., and Thompson, D. A. (2012). Motion and pattern cortical potentials in adults with high-functioning autism spectrum disorder. *Doc. Ophthalmol.* 125, 219–227. doi: 10.1007/s10633-012-9349-7

Constable, P. A., Lee, I. O., Marmolejo-Ramos, F., Skuse, D. H., and Thompson, D. A. (2021). The photopic negative response in autism spectrum disorder. *Clin. Exp. Optom.* 104, 841–847. doi: 10.1080/08164622.2021.1903808

Cooper, M., Martin, J., Langley, K., Hamshere, M., and Thapar, A. (2014). Autistic traits in children with ADHD index clinical and cognitive problems. *Eur. Child Adolesc. Psychiatry* 23, 23–34. doi: 10.1007/s00787-013-0398-6

Cuthbert, B. N. (2020). The role of RDoC in future classification of mental disorders. *Dialogues Clin. Neurosci.* 22, 81–85. doi: 10.31887/DCNS.2020.22.1/bcuthbert

Dai, H., Jackson, C. R., Davis, G. L., Blakely, R. D., and McMahon, D. G. (2017). Is dopamine transporter-mediated dopaminergic signaling in the retina a noninvasive biomarker for attention-deficit/ hyperactivity disorder? A study in a novel dopamine transporter variant Val559 transgenic mouse model. *J. Neurodev. Disord.* 9:38. doi: 10.1186/s11689-017-9215-8

Dakin, S., and Frith, U. (2005). Vagaries of visual perception in autism. *Neuron* 48, 497–507. doi: 10.1016/j.neuron.2005.10.018

Dellapiazza, F., Michelon, C., Vernhet, C., Muratori, F., Blanc, N., Picot, M. C., et al. (2021). Sensory processing related to attention in children with ASD, ADHD, or typical development: results from the ELENA cohort. *Eur. Child Adolesc. Psychiatry* 30, 283–291. doi: 10.1007/s00787-020-01516-5

Diamond, J. S. (2017). Inhibitory interneurons in the retina: types, circuitry, and function. *Annu. Rev. Vis. Sci.* 3, 1–24. doi: 10.1146/annurev-vision-102016-061345

Dorfman, A. L., Gauvin, M., Vatcher, D., Little, J. M., Polomeno, R. C., and Lachapelle, P. (2020). Ring analysis of multifocal oscillatory potentials (mfOPs) in cCSNB suggests near-normal ON-OFF pathways at the fovea only. *Doc. Ophthalmol.* 141, 99–109. doi: 10.1007/s10633-020-09755-2

Faust, O., Acharya, U. R., Adeli, H., and Adeli, A. (2015). Wavelet-based EEG processing for computer-aided seizure detection and epilepsy diagnosis. *Seizure* 26, 56–64. doi: 10.1016/j.seizure.2015.01.012

Friedburg, C., Allen, C. P., Mason, P. J., and Lamb, T. D. (2004). Contribution of cone photoreceptors and post-receptoral mechanisms to the human photopic electroretinogram. *J. Physiol.* 556, 819–834. doi: 10.1113/jphysiol.2004.061523

Gajendran, M. K., Rohowetz, L. J., Koulen P., and Mehdizadeh, A. (2022). Novel machine-learning based framework using electroretinography data for the detection of early-stage glaucoma. *Front. Neurosci.* 16:869137. doi: 10.3389/fnins.2022.869137

Garcia-Martin, E., Rodriguez-Mena, D., Satue, M., Almarcegui, C., Dolz, I., Alarcia, R., et al. (2014). Electrophysiology and optical coherence tomography to evaluate Parkinson disease severity. *Invest. Ophthalmol. Vis. Sci.* 55, 696–705. doi: 10.1167/iovs.13-13062

Gauvin, M., Dorfman, A. L., Trang, N., Gauthier, M., Little, J. M., Lina, J. M., et al. (2016). Assessing the contribution of the oscillatory potentials to the genesis of the photopic ERG with the Discrete Wavelet Transform. *Biomed. Res. Int.* 2016:2790194. doi: 10.1155/2016/2790194

Gauvin, M., Lina, J. M., and Lachapelle, P. (2014). Advance in ERG analysis: from peak time and amplitude to frequency, power, and energy. *Biomed. Res. Int.* 2014:246096. doi: 10.1155/2014/246096

Gauvin, M., Little, J. M., Lina, J. M., and Lachapelle, P. (2015). Functional decomposition of the human ERG based on the discrete wavelet transform. *J. Vis.* 15:14. doi: 10.1167/15.16.14

Gauvin, M., Sustar, M., Little, J. M., Brecelj, J., Lina, J. M., and Lachapelle, P. (2017). Quantifying the ON and OFF contributions to the flash ERG with the Discrete Wavelet Transform. *Transl. Vis. Sci. Technol.* 6:3. doi: 10.1167/tvst.6.1.3

Geurts, H. M., Ridderinkhof, K. R., and Scholte, H. S. (2013). The relationship between grey-matter and ASD and ADHD traits in typical adults. *J. Autism Dev. Disord.* 43, 1630–1641. doi: 10.1007/s10803-012-1708-4

Gotham, K., Risi, S., Pickles, A., and Lord, C. (2007). The autism diagnostic observation schedule: revised algorithms for improved diagnostic validity. *J. Autism Dev. Disord.* 37, 613–627. doi: 10.1007/s10803-006-0280-1

Guimarães-Souza, E. M., Joselevitch, C., Britto, L. R. G., and Chiavegatto, S. (2019). Retinal alterations in a pre-clinical model of an autism spectrum disorder. *Mol. Autism* 10:19. doi: 10.1186/s13229-019-0270-8

Hamilton, R., Bees, M. A., Chaplin, C. A., and McCulloch, D. L. (2007). The luminance-response function of the human photopic electroretinogram: a mathematical model. *Vis. Res.* 47, 2968–2972. doi: 10.1016/j.visres.2007.04.020

Hanna, M. C., and Calkins, D. J. (2006). Expression and sequences of genes encoding glutamate receptors and transporters in primate retina determined using 3'-end amplification polymerase chain reaction. *Mol. Vis.* 12, 961–976.

Hanna, M. C., and Calkins, D. J. (2007). Expression of genes encoding glutamate receptors and transporters in rod and cone bipolar cells of the primate retina determined by single-cell polymerase chain reaction. *Mol. Vis.* 13, 2194–2208.

Hassankarimi, H., Jafarzadehpur, E., Mohammadi, A., and Noori, S. M. R. (2020). Low-contrast pattern-reversal visual evoked potential in different spatial frequencies. *J. Ophthalmic Vis. Res.* 15, 362–371. doi: 10.18502/jovr.v15i3.7455

Hassankarimi, H., Noori, S. M. R., Jafarzadehpour, E., Yazdani, S., and Radinmehr, F. (2019). Analysis of pattern electroretinogram signals of early primary open-angle glaucoma in discrete wavelet transform coefficients domain. *Int. Ophthalmol.* 39, 2373–2383. doi: 10.1007/s10792-019-01077-w

Hébert, M., Gagné, A. M., Paradis, M. E., Jomphe, V., Roy, M. A., Mérette, C., et al. (2010). Retinal response to light in young nonaffected offspring at high genetic risk of neuropsychiatric brain disorders. *Biol. Psychiatry* 67, 270–274. doi: 10.1016/j.biopsych.2009.08.016

Hébert, M., Mérette, C., Gagné, A. M., Paccalet, T., Moreau, I., Lavoie, J., et al. (2020). The electroretinogram may differentiate schizophrenia from bipolar disorder. *Biol. Psychiatry* 87, 263–270. doi: 10.1016/j.biopsych.2019.06.014

Hébert, M., Mérette, C., Paccalet, T., Emond, C., Gagné, A. M., Sasseville, A., et al. (2015). Light evoked potentials measured by electroretinogram may tap into the neurodevelopmental roots of schizophrenia. *Schizophr. Res.* 162, 294–295. doi: 10.1016/j.schres.2014.12.030

Hébert, M., Mérette, C., Paccalet, T., Gagné, A. M., and Maziade, M. (2017). Electroretinographic anomalies in medicated and drug free patients with major depression: tagging the developmental roots of major psychiatric disorders. *Prog. Neuropsychopharmacol. Biol. Psychiatry* 75, 10–15. doi: 10.1016/j.pnpbp.2016.12.002

Hobby, A. E., Kozareva, D., Yonova-Doing, E., Hossain, I. T., Katta, M., Huntjens, B., et al. (2018). Effect of varying skin surface electrode position on electroretinogram responses recorded using a handheld stimulating and recording system. *Doc. Ophthalmol.* 137, 79–86. doi: 10.1007/s10633-018-9652-z

Hossain, M. B., Bashar, S. K., Lazaro, J., Reljin, N., Noh, Y., and Chon, K. H. (2021). A robust ECG denoising technique using variable frequency complex demodulation. *Comput. Methods Programs Biomed.* 200:105856. doi: 10.1016/j.cmpb.2020.105856

Jackson, C. R., Ruan, G.-X., Aseem, F., Abey, J., Gamble, K., Stanwood, G., et al. (2012). Retinal dopamine mediates multiple dimensions of light-adapted vision. *J. Neurosci.* 32, 9359–9368. doi: 10.1523/JNEUROSCI.0711-12.2012

Kaneda, M. (2013). Signal processing in the mammalian retina. *J. Nippon Med. Sch.* 80, 16–24. doi: 10.1272/jnms.80.16

Kashani, A. H., Asanad, S., Chan, J. W., Singer, M. B., Zhang, J., Sharifi, M., et al. (2021). Past, present and future role of retinal imaging in neurodegenerative disease. *Prog. Retin. Eye Res.* 83:100938. doi: 10.1016/j.preteyeres.2020.100938

Kohls, G., Thönessen, H., Bartley, G. K., Grossheinrich, N., Fink, G. R., Herpertz-Dahlmann, B., et al. (2014). Differentiating neural reward responsiveness in autism versus ADHD. *Dev. Cogn. Neurosci.* 10, 104–116. doi: 10.1016/j.dcn.2014.08.003

Lavoie, J., Illiano, P., Sotnikova, T. D., Gainetdinov, R. R., Beaulieu, J. M., and Hébert, M. (2014). The electroretinogram as a biomarker of central dopamine and serotonin: potential relevance to psychiatric disorders. *Biol. Psychiatry* 75, 479–486. doi: 10.1016/j.biopsych.2012.11.024

Lee, I. O., Skuse, D. H., Constable, P. A., Marmolejo-Ramos, F., Olsen, L. R., and Thompson, D. A. (2022). The electroretinogram b-wave amplitude: a differential physiological measure for Attention Deficit Hyperactivity Disorder and Autism Spectrum Disorder. *J. Neurodev. Disord.* 14:30. doi: 10.1186/s11689-022-09440-2

Li, Y., Qian, R., and Li, K. (2022). Inter-patient arrhythmia classification with improved deep residual convolutional neural network. *Comput. Methods Programs Biomed.* 214:106582. doi: 10.1016/j.cmpb.2021.106582

Liu, G., Zhang, Y., Hu, Z., Du, X., Wu, W., Xu, C., et al. (2017). Complexity analysis of electroencephalogram dynamics in patients with Parkinson's disease. *Parkinsons Dis.* 2017:8701061. doi: 10.1155/2017/8701061

Liu, J., Fu, H., Kong, J., Yu, H., and Zhang, Z. (2021). Association between autism spectrum disorder and polymorphisms in genes encoding serotine and dopamine receptors. *Metab. Brain Dis.* 36, 865–870. doi: 10.1007/s11011-021-00699-3

Lord, C., Rutter, M., Goode, S., Heemsbergen, J., Jordan, H., Mawhood, L., et al. (1989). Autism diagnostic observation schedule: a standardized observation of communicative and social behavior. *J. Autism Dev. Disord.* 19, 185–212. doi: 10.1007/bf02211841

Maguire, A. M., Russell, S., Chung, D. C., Yu, Z. F., Tillman, A., Drack, A. V., et al. (2021). Durability of voretigene neparvovec for biallelic RPE65-mediated inherited retinal disease: phase 3 Results at 3 and 4 Years. *Ophthalmology* 128, 1460–1468. doi: 10.1016/j.ophtha.2021.03.031

Mallat, S. G. (2009). *A Wavelet Tour of Signal Processing. The Sparse way*, 3rd Edn. Houston TX: Academic Press.

Mansour, R., Dovi, A. T., Lane, D. M., Loveland, K. A., and Pearson, D. A. (2017). ADHD severity as it relates to comorbid psychiatric symptomatology in children with Autism Spectrum Disorders (ASD). *Res. Dev. Disabil.* 60, 52–64. doi: 10.1016/j.ridd.2016.11.009

Masland, R. H. (2012). The neuronal organization of the retina. *Neuron* 76, 266–280. doi: 10.1016/j.neuron.2012.10.002

Maziade, M., Bureau, A., Jomphe, V., and Gagné, A. M. (2022). Retinal function and preclinical risk traits in children and adolescents at genetic risk of schizophrenia and bipolar disorder. *Prog. Neuropsychopharmacol. Biol. Psychiatry* 112:110432. doi: 10.1016/j.pnpbp.2021.110432

Meziani, F., Debbal, S. M., and Atbi, A. (2013). Analysis of the pathological severity degree of aortic stenosis (AS) and mitral stenosis (MS) using the discrete wavelet transform (DWT). *J. Med. Eng. Technol.* 37, 61–74. doi: 10.3109/03091902.2012.733058

Molloy, C. J., and Gallagher, L. (2021). Can stratification biomarkers address the heterogeneity of autism spectrum disorder? *Ir. J. Psychol. Med.* doi: 10.1017/ipm.2021.73 [Epub ahead of print].

Mullane, J. C., and Klein, R. M. (2008). Literature review: visual search by children with and without ADHD. *J. Atten. Disord.* 12, 44–53. doi: 10.1177/1087054707305116

Naaijen, J., Bralten, J., Poelmans, G., IMAGE consortium, Glennon, J., Franke, B., et al. (2017). Glutamatergic and GABAergic gene sets in attention-deficit/hyperactivity disorder: association to overlapping traits in ADHD and autism. *Transl. Psychiatry* 7:e999. doi: 10.1038/tp.2016.273

Nevison, C., Blaxill, M., and Zahorodny, W. (2018). California autism prevalence trends from 1931 to 2014 and comparison to national ASD data from IDEA and ADDM. *J. Autism Dev. Disord.* 48, 4103–4117. doi: 10.1007/s10803-018-3670-2

Noguchi, K., Abel, A. S., Marmolejo-Ramos, F., and Konietschke, F. (2020). Nonparametric multiple comparisons. *Behav. Res. Methods* 52, 489–502. doi: 10.3758/s13428-019-01247-9

Nowacka, B., Lubinski, W., Honczarenko, K., Potemkowski, A., and Safranow, K. (2015). Bioelectrical function and structural assessment of the retina in patients with early stages of Parkinson's disease (PD). *Doc. Ophthalmol.* 131, 95–104. doi: 10.1007/s10633-015-9503-0

Pavăl, D., and Micluţia, I. V. (2021). The dopamine hypothesis of autism spectrum disorder revisited: current status and future prospects. *Dev. Neurosci.* 43, 73–83. doi: 10.1159/000515751

Polanczyk, G. V., Salum, G. A., Sugaya, L. S., Caye, A., and Rohde, L. A. (2015). Annual research review: a meta-analysis of the worldwide prevalence of mental disorders in children and adolescents. *J. Child Psychol. Psychiatry* 56, 345–365. doi: 10.1111/jcpp.12381

Posada-Quintero, H. F., Florian, J. P., Orjuela-Cañón, Á. D., and Chon, K. H. (2016). Highly sensitive index of sympathetic activity based on time-frequency spectral analysis of electrodermal activity. *Am. J. Physiol.* 311, R582–R591. doi: 10.1152/ajpregu.00180.2016

Rahul, J., and Sharma, L. D. (2021). An enhanced T-wave delineation method using phasor transform in the electrocardiogram. *Biomed. Phys. Eng. Express* 7:045015. doi: 10.1088/2057-1976/ac0502

Ritvo, E. R., Creel, D., Realmuto, G., Crandall, A. S., Freeman, B. J., Bateman, J. B., et al. (1988). Electroretinograms in autism: a pilot study of b-wave amplitudes. *Am. J. Psychiatry* 145, 229–232. doi: 10.1176/ajp.145.2.229

Robertson, C. E., and Baron-Cohen, S. (2017). Sensory perception in autism. *Nat. Rev. Neurosci.* 18, 671–684. doi: 10.1038/nrn.2017.112

Robertson, C. E., Thomas, C., Kravitz, D. J., Wallace, G. L., Baron-Cohen, S., Martin, A., et al. (2014). Global motion perception deficits in autism are reflected as early as primary visual cortex. *Brain* 137, 2588–2599. doi: 10.1093/brain/awu189

Robson, A. G., Frishman, L. J., Grigg, J., Hamilton, R., Jeffrey, B. G., Kondo, M. et al. (2022). ISCEV standard for full-field clinical electroretinography (2022 update). *Doc. Ophthalmol.* doi: 10.1007/s10633-022-09872-0

Robson, J. G., Saszik, S. M., Ahmed, J., and Frishman, L. J. (2003). Rod and cone contributions to the a-wave of the electroretinogram of the macaque. *J. Physiol.* 547(Pt 2), 509–530. doi: 10.1113/jphysiol.2002.030304

Rommelse, N. N., Franke, B., Geurts, H. M., Hartman, C. A., and Buitelaar, J. K. (2010). Shared heritability of attention-deficit/hyperactivity disorder and autism spectrum disorder. *Eur. Child Adolesc. Psychiatry* 19, 281–295. doi: 10.1007/s00787-010-0092-x

Ronald, A., Larsson, H., Anckarsater, H., and Lichtenstein, P. (2014). Symptoms of autism and ADHD: a Swedish twin study examining their overlap. *J. Abnorm. Psychol.* 123, 440–451. doi: 10.1037/a0036088

Russell, G., Rodgers, L. R., Ukoumunne, O. C., and Ford, T. (2014). Prevalence of parent-reported ASD and ADHD in the UK: findings from the Millennium Cohort Study. *J. Autism Dev. Disord.* 44, 31–40. doi: 10.1007/s10803-013-1849-0

Severns, M. L., and Johnson, M. A. (1993). The variability of the b-wave of the electroretinogram with stimulus luminance. *Doc. Ophthalmol.* 84, 291–299.

Silverstein, S. M., and Thompson, J. L. (2020). Progress, possibilities, and pitfalls in electroretinography research in psychiatry. *Biol. Psychiatry* 87, 202–203. doi: 10.1016/j.biopsych.2019.10.028

Siu, K. L., Sung, B., Cupples, W. A., Moore, L. C., and Chon, K. H. (2009). Detection of low-frequency oscillations in renal blood flow. *Am. J. Physiol.* 297, F155–F162. doi: 10.1152/ajprenal.00114.2009

Skuse, D., Warrington, R., Bishop, D., Chowdhury, U., Lau, J., Mandy, W., et al. (2004). The developmental, dimensional and diagnostic interview (3di): a novel computerized assessment for autism spectrum disorders. *J. Am. Acad. Child Adolesc. Psychiatry* 43, 548–558. doi: 10.1097/00004583-200405000-00008

Thapar, A., Cooper, M., and Rutter, M. (2017). Neurodevelopmental disorders. *Lancet Psychiatry* 4, 339–346. doi: 10.1016/s2215-0366(16)30376-5

van der Hallen, R., Manning, C., Evers, K., and Wagemans, J. (2019). Global motion perception in autism spectrum disorder: a meta-analysis. *J. Autism Dev. Disord.* 49, 4901–4918. doi: 10.1007/s10803-019-04194-8

van Steijn, D. J., Oerlemans, A. M., van Aken, M. A., Buitelaar, J. K., and Rommelse, N. N. (2014). The reciprocal relationship of ASD, ADHD, depressive symptoms and stress in parents of children with ASD and/or ADHD. *J. Autism Dev. Disord.* 44, 1064–1076. doi: 10.1007/s10803-013-1958-9

Wachtmeister, L. (1980). Further studies of the chemical sensitivity of the oscillatory potentials of the electroretinogram (ERG) I. GABA- and glycine antagonists. *Acta. Ophthalmol.* 58, 712–725. doi: 10.1111/j.1755-3768.1980.tb06684.x

Wachtmeister, L. (1981). Further studies of the chemical sensitivity of the oscillatory potentials of the electroretinogram (ERG). II. Glutamate-aspartate- and dopamine antagonists. *Acta. Ophthalmol.* 59, 247–258. doi: 10.1111/j.1755-3768.1981.tb02987.x

Wachtmeister, L. (1998). Oscillatory potentials in the retina: what do they reveal. *Prog. Retin. Eye Res.* 17, 485–521. doi: 10.1016/s1350-9462(98)00006-8

Wachtmeister, L. (2001). Some aspects of the oscillatory response of the retina. *Prog. Brain Res.* 131, 465–474. doi: 10.1016/s0079-6123(01)31037-3

Wachtmeister, L., and Dowling, J. E. (1978). The oscillatory potentials of the mudpuppy retina. *Invest. Ophthalmol. Vis. Sci.* 17, 1176–1188.

Wang, H., Siu, K., Ju, K., and Chon, K. H. (2006). A high resolution approach to estimating time-frequency spectra and their amplitudes. *Ann. Biomed. Eng.* 34, 326–338. doi: 10.1007/s10439-005-9035-y

Wilcox, R. (2012). *Introduction to Robust Estimation and Hypothesis Testing*, 3rd Edn. Amsterdam: Elsevier.

Yu-Wai-Man, P., Newman, N. J., Carelli, V., Moster, M. L., Biousse, V., Sadun, A. A., et al. (2020). Bilateral visual improvement with unilateral gene therapy injection for Leber hereditary optic neuropathy. *Sci. Transl. Med.* 12:eaaz7423. doi: 10.1126/scitranslmed.aaz7423

Zarei, A., and Asl, B. M. (2021). Automatic seizure detection using orthogonal matching pursuit, discrete wavelet transform, and entropy based features of

EEG signals. *Comput. Biol. Med.* 131:104250. doi: 10.1016/j.compbiomed.2021.104250

Zarka, D., Leroy, A., Cebolla, A. M., Cevallos, C., Palmero-Soler, E., and Cheron, G. (2021). Neural generators involved in visual cue processing in children with attention-deficit/hyperactivity disorder (ADHD). *Eur. J. Neurosci.* 53, 1207–1224. doi: 10.1111/ejn.15040

Zhang, Q., Chen, X., Li, S., Yao, T., and Wu, J. (2021). Association between the group III metabotropic glutamate receptor gene polymorphisms and attention-deficit/hyperactivity disorder and functional exploration of risk loci. *J. Psychiatr. Res.* 132, 65–71. doi: 10.1016/j.jpsychires.2020.09.035

Conflict of Interest: The authors declare that the research was conducted in the absence of any commercial or financial relationships that could be construed as a potential conflict of interest.

Publisher's Note: All claims expressed in this article are solely those of the authors and do not necessarily represent those of their affiliated organizations, or those of the publisher, the editors and the reviewers. Any product that may be evaluated in this article, or claim that may be made by its manufacturer, is not guaranteed or endorsed by the publisher.

frontiers | Frontiers in Neuroscience

TYPE Original Research
PUBLISHED 08 August 2022
DOI 10.3389/fnins.2022.949129

OPEN ACCESS

EDITED BY
Jian Wang,
Zhengzhou University, China

REVIEWED BY
Berislav Zlokovic,
University of Southern California, United States
Zixuan Lin,
Johns Hopkins University, United States
Sandeepa Sur,
Johns Hopkins Medicine, United States

*CORRESPONDENCE
Jianping Jia
jjp@ccmu.edu.cn

SPECIALTY SECTION
This article was submitted to Neurodegeneration, a section of the journal Frontiers in Neuroscience

RECEIVED 20 May 2022
ACCEPTED 18 July 2022
PUBLISHED 08 August 2022

CITATION
Gong M and Jia J (2022) Contribution of blood-brain barrier-related blood-borne factors for Alzheimer's disease vs. vascular dementia diagnosis: A pilot study. *Front. Neurosci.* 16:949129. doi: 10.3389/fnins.2022.949129

Contribution of blood-brain barrier-related blood-borne factors for Alzheimer's disease vs. vascular dementia diagnosis: A pilot study

Min Gong[1] and Jianping Jia[1,2,3,4,5]*

[1]Innovation Center for Neurological Disorders and Department of Neurology, Xuanwu Hospital, Capital Medical University, National Clinical Research Center for Geriatric Diseases, Beijing, China, [2]Beijing Key Laboratory of Geriatric Cognitive Disorders, Beijing, China, [3]Clinical Center for Neurodegenerative Disease and Memory Impairment, Capital Medical University, Beijing, China, [4]Center of Alzheimer's Disease, Beijing Institute of Brain Disorders, Collaborative Innovation Center for Brain Disorders, Capital Medical University, Beijing, China, [5]Key Laboratory of Neurodegenerative Diseases, Ministry of Education, Beijing, China

Background: Alzheimer's disease (AD) and vascular dementia (VaD) are the two most common types of neurodegenerative dementia among the elderly with similar symptoms of cognitive decline and overlapping neuropsychological profiles. Biological markers to distinguish patients with VaD from AD would be very useful. We aimed to investigate the expression of blood-brain barrier (BBB)-related blood-borne factors of soluble low-density lipoprotein receptor-related protein 1 (sLRP1), cyclophilin A (CyPA), and matrix metalloproteinase 9 (MMP9) and its correlation with cognitive function between patients with AD and VaD.

Materials and methods: Plasma levels of sLRP1, CyPA, and MMP9 were analyzed in 26 patients with AD, 27 patients with VaD, and 27 normal controls (NCs). Spearman's rank correlation analysis was used to explore the relationships among biomarker levels, cognitive function, and imaging references. Receiver operating characteristic (ROC) curve analysis was used to discriminate the diagnosis of AD and VaD.

Results: Among these BBB-related factors, plasma CyPA levels in the VaD group were significantly higher than that in the AD group ($p < 0.05$). Plasma sLRP1 levels presented an increasing trend in VaD while maintaining slightly low levels in patients with AD ($p > 0.05$). Plasma MMP9 in different diagnostic groups displayed the following trend: VaD group > AD group > NC group, but the difference was not statistically significant ($p > 0.05$). Furthermore, plasma sLRP1 levels were positively related to MoCA scores, and plasma CyPA levels were significantly correlated with MTA scores ($p < 0.05$) in the AD group. Plasma MMP9 levels were negatively correlated with MoCA scores ($p < 0.05$) in the VaD groups. No significant correlation was detected between the other factors and different cognitive scores ($p > 0.05$). ROC analysis showed

a good preference of plasma CyPA [AUC = 0.725, 95% CI (0.586–0.865); p = 0.0064] in diagnosis.

Conclusion: The plasma CyPA level is a reference index when distinguishing between an AD and subcortical ischemic vascular dementia (SIVD) diagnosis. Blood-derived factors associated with the BBB may provide new insights into the differential diagnosis of neurodegenerative dementia and warrant further investigation.

KEYWORDS

vascular dementia (VaD), Alzheimer's disease (AD), blood-brain barrier, low-density lipoprotein receptor-related protein, cyclophilin A, matrix metalloproteinase-9

Introduction

Dementia manifests as global cognitive decline and significantly impairs daily activities, which has imposed a heavy burden on the public and healthcare systems as society ages (Jia et al., 2020). Alzheimer's disease (AD) and vascular dementia (VaD) are the two most common types of neurodegenerative dementia among the elderly. AD has a slow course characterized by gradual deterioration of cognitive function. VaD has a variable course presented by a stepwise worsening of executive function, which can have a sudden or slow onset (O'Brien and Thomas, 2015). Although these two types of dementia share many clinical features, including symptoms of cognitive decline and overlapping neuropsychological profiles, the underlying pathophysiological mechanisms are different. Efficient therapy depends on accurate diagnosis, thus it is crucial to distinguish between VaD and AD (Neto et al., 2015; Tachibana et al., 2016). Despite advances in molecular neuroimaging, the understanding of clinicopathological relevance and the development of novel biomarkers have been limited in the last decade (Park and Moon, 2016; Bjerke and Engelborghs, 2018). Moreover, imaging is relatively expensive and invasive and is usually not immediately available for such a diagnosis. As another option, lumbar puncture is an invasive procedure, which requires written informed consent. Clinicians still need reliable and non-invasive molecular markers for the differential diagnosis of neurodegenerative dementia. Blood testing is an economical, minimally invasive and more accessible procedure and is more suitable for investigating these pathological mechanisms and distinguishing between different forms, at least as a primary screening test.

Although the etiology of AD and VaD may differ, the overall mechanisms of subsequent neurovascular dysfunction are similar, with defective blood-brain barrier (BBB) function. BBB failure is considered to be a core mechanism in vascular-related diseases and neurodegenerative dementia, driving disease pathology and progression (Yamazaki and Kanekiyo, 2017; Cai et al., 2018; Ueno et al., 2019; Uemura et al., 2020). The breakdown of the BBB is caused by the degeneration of pericytes and endothelial cells, loss of tight junctions, and brain capillary leakages, which cause toxic molecules from the blood to enter the brain and initiate multiple neurodegenerative pathways (Bell et al., 2010; Zlokovic, 2011; Nelson et al., 2016; Storck et al., 2016; Montagne et al., 2020). Currently, it is speculated that low-density lipoprotein receptor-related protein 1 (LRP1), cyclophilin A (CyPA), and matrix metallopeptidase 9 (MMP9) are involved in the regulation of BBB permeability (Bell et al., 2012; Halliday et al., 2016). Soluble LRP1 (sLRP1) circulates freely in plasma and is primarily responsible for peripheral Aβ clearance (Quinn et al., 1997). Several studies have reported a significant reduction in LRP1 expression in brain microvascular endothelial cells in AD (Shibata et al., 2000; Deane et al., 2004; Donahue et al., 2006). Circulating sLRP in the plasma binds Aβ and prevents brain reentry across the BBB, producing a peripheral sink that promotes the outflow of Aβ from the brain (Sagare et al., 2007, 2012; Deane et al., 2008). Plasma sLRP1 levels and Aβ binding to sLRP1 are significantly reduced due to increased levels of oxidized sLRP1, which does not bind Aβ, resulting in an increase in free Aβ levels in plasma to return to the brain *via* the receptor for advanced glycation end products (RAGE) in patients with AD (Deane et al., 2003; Sagare et al., 2007, 2011). CyPA is secreted by activated macrophages, lymphocytes, and platelets and mediates the harmful effects of pericytes on BBB disruption (Seizer et al., 2010, 2015, 2016; Pan et al., 2020). Previous studies have shown that the plasma CyPA level is a new biomarker for the diagnosis of coronary artery disease (CAD) and renal disease progression and is used as a prognostic factor in patients with ruptured intracranial aneurysms (Satoh et al., 2013; Ramachandran et al., 2014; Kao et al., 2015; El-Ebidi et al., 2020; Rath et al., 2020). MMP9 is involved in the increase of BBB permeability during AD, which accelerates its onset (Barr et al., 2010; Shackleton et al., 2019). These results provide support for the use of BBB-related blood-borne factors as sensitive predictors of neurodegenerative dementia (specifically BBB dysfunction-related cognitive decline) because they are tentatively present in biofluids and are involved in BBB function. Few studies have analyzed the correlation

between BBB-related blood-borne factors (sLRP1, CyPA, and MMP9) and dementias.

In this clinical study, we aimed to measure plasma sLRP1, CyPA, and MMP9 levels in patients with AD, patients with VaD, and healthy controls and to evaluate their correlation with cognitive function to assist the discovery of new biomarkers.

Materials and methods

Study populations

A total of 80 participants were enrolled in our research who were admitted to the Department of Xuanwu Hospital, Capital Medical University from July 2019 to July 2021. More specifically, 26 patients with AD, 27 patients with subcortical ischemic vascular dementia (SIVD), and 27 age-matched cognitive normal controls (NC) were recruited. The diagnosis of AD was performed according to the National Institute on Aging and the Alzheimer's Association (NIA-AA) criteria (Jack et al., 2011). The diagnosis of SIVD was performed according to the modified National Institute of Neurological Disorders and Stroke and the Association Internationale pour la Recherche et l'Enseignement en Neurosciences (NINDS-AIREN) and has evidence of ischemic lesions on brain magnetic resonance imaging (Erkinjuntti, 2003). Moreover, healthy individuals, not affected by neurodegenerative diseases, were recruited as NC. This study was approved by the ethics committee. Written informed consent was obtained before enrollment. The details of inclusion/exclusion criteria for AD and VD are shown in the **Supplementary material**.

Plasma sample processing

Blood samples were taken in the morning after a 12-h fast. Notably, 6 ml of whole blood were drawn from each subject and stored in a polypropylene tube containing EDTA. Plasma separation was performed by centrifugation at 1,880 $\times$ *g* for 15 min. Finally, plasma was collected in centrifugal tubes and stored at -80°C until analysis.

Measurements

The levels of sLRP1, CyPA, and MMP9 were measured in plasma using a commercially available enzyme-linked immunosorbent assay (ELISA) (LRP1: IC-LRP1-Hu, ImmunoClone, United States; CyPA: KE1726, immunoway, United States; and MMP9: KE1407, immunoway, United States) according to the manufacturer's instructions, and the dilution concentrations of sLPR1, CYPA, and MMP9 were 1:2,000, 1:10, and 1:50, respectively. The cognition of participants was assessed using the Mini-Mental State Examination (MMSE) and the Montreal Cognitive Assessment (MoCA). Total cholesterol (TC), triglyceride (TG), low-density lipoprotein cholesterol (LDL), and high-density lipoprotein cholesterol (HDL) were measured by the clinical levorotary testing center. Periventricular hyperintensity (PVH) and deep white matter hyperintense signals (DWMH) were evaluated using the Fazekas scale, and the scores of these two parts were summarized to obtain the total score (the lowest total score is 0, and the highest is 6) (Fazekas et al., 1987). A high Fazekas score is clinically associated with the diagnosis of individuals at high risk of cerebrovascular disease (Hilal et al., 2021). Concordantly, a high Fazekas score can successfully predict the cognitive function of patients with dementia in a clinical setting (Lam et al., 2021). Another, medial temporal lobe atrophy (MTA) visual rating scale has been shown to have high diagnostic accuracy for AD (Cavedo et al., 2014). It has also been reported in patients with VaD (Barber et al., 2000). In our study, ratings of PVH (0 = absence, 1 = "caps" or pencil-thin lining, 2 = smooth "halo," and 3 = irregular) and DWMH (0 = absence, 1 = punctate foci, 2 = beginning confluence of foci, and 3 = large confluent areas) were summarized into total Fazekas scores using the axial fluid-attenuated inversion recovery (FLAIR) images from a 3T MRI and were classified into low WMSA burden (Fazekas scores $<$ 3) and high WMSA burden (Fazekas scores $\geq$ 3). MTA was dichotomized into groups of 0–1 (none to mild) vs. 2–4 (moderate to severe) by analyzing the width of the choroidal fissure, the width of the temporal horn of the lateral ventricle, and the height of the hippocampus on T1-weighted coronal sections. The total score of each patient was approved by two experienced neurologists who were blind to the clinical data. The typical images of MTA/white matter hyperintensity from patients have shown in **Supplementary Figure 1**.

Statistical analysis

Descriptive statistics were used to summarize the participant characteristics. For normally distributed data, including the variables of age, TC, HDL, MMSE scores, and MoCA scores, the means $\pm$ standard deviation (SD) was used to describe the quantitative variables. The two groups were compared using *t*-test, among groups were compared using ANOVA, and the differences between the groups were statistically significant based on further pairwise comparison *t*-test with normal distributions. For non-normally distributed data, including the variables of TG, LDL, years of education, sLRP1, CyPA, and MMP9 levels, we used medians and interquartile ranges to describe the quantitative variables. Baseline characteristics were compared using the independent-sample Kruskal-Wallis

TABLE 1 Participant characteristics.

Characteristics	AD (n = 26)	SIVD (n = 27)	NC (n = 27)	P
Age, Mean ± SD (year)	66.65 ± 9.53	65.37 ± 9.93	65.04 ± 6.12	0.708
Male, N (%)	11(42.3)	18 (66.7)	10 (37.0)	0.068
Education, median (Q25, Q75) (year)	12.00 (9.00, 15.00)	12.00 (9.00, 13.00)	12.00 (9.00, 12.00)	0.163
TC, Mean ± SD (mmol/L)	4.50 ± 1.09	4.07 ± 1.46	4.06 ± 0.87	0.262
TG, median (Q25, Q75) (mmol/L)	1.20 (1.01, 1.74)	1.34 (1.03, 1.72)	1.02 (0.79, 1.38)	0.060
LDL, median (Q25, Q75) (mmol/L)	2.55 (1.92, 3.22)	1.77 (1.35, 3.18)	2.52 (1.83, 2.95)	0.414
HDL, Mean ± SD (mmol/L)	1.32 ± 0.38	1.20 ± 0.43	1.25 ± 0.38	0.537
Hypertension, N (%)	11 (42.3)	17 (63.0)	20 (74.1)	0.057
Diabetes, N (%)	6 (23.1)	7 (25.9)	9 (33.3)	0.687
Hyperlipidemia, N (%)	3 (11.5)	5 (18.5)	9 (33.3)	0.139
MMSE, Mean ± SD (score)	19.12 ± 5.69$^{\#}$	21.09 ± 8.32$^{\#}$	27.63 ± 1.28	<0.001
MoCA, Mean ± SD (score)	13.60 ± 4.87$^{\#}$	16.27 ± 7.32$^{\#}$	25.07 ± 1.04	<0.001
Fazekas WMSA burden, N (%)				<0.001
High (3–6 scores)	1 (3.8)*	23 (85.7)	NA	
Low (0–2 scores)	25 (96.2)	4 (14.3)	NA	
MTA, N (%)				0.128
None to mild (0–1 scores)	8 (30.8)	14 (52.2)	NA	
Moderate to severe (2–4 scores)	18 (69.2)	13 (47.8)	NA	

Data are shown as mean ± SD and N (%).
*Compared with the subcortical ischemic vascular dementia (SIVD) group, the difference was significant ($p < 0.05$).
$^{\#}$Compared with the NC group, the difference was significant ($p < 0.05$).

TABLE 2 sLRP1, CyPA, and MMP9 values by diagnostic groups.

Characteristics	AD (n = 26)	SIVD (n = 27)	NC (n = 27)	H	P
sLRP1, median (Q25, Q75) (ng/ml)	2409.65 (1544.57, 3732.41)	2896.88^{a} (2353.69, 4694.35)	2639.14 (2042.29, 3564.04)	3.817	0.148
CyPA, median (Q25, Q75) (ng/ml)	18.95*^{b} (10.46, 35.05)	36.57 (17.51, 73.32)	30.78^{b} (21.00, 49.15)	8.302	0.016
MMP9, median (Q25, Q75) (pg/ml)	15076.43^{c} (9873.41,20403.41)	17076.83 (10679.13, 26947.31)	10699.70*^{c} (8450.16, 20368.37)	3.778	0.151

Data are shown as medians (IQR).
*Compared with the subcortical ischemic vascular dementia (SIVD) group, the difference was significant ($p < 0.05$); ^{a}Delete 2 Outliers; ^{b}Delete 3 Outliers; ^{c}Delete 5 Outliers. *$p < 0.05$.

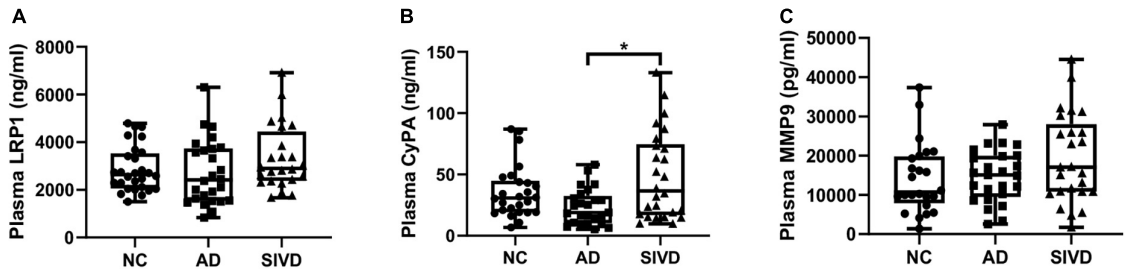

FIGURE 1
Box and dot plots of plasma **(A)** sLRP1, **(B)** CyPA, and **(C)** MMP9 per diagnostic group. Analytes with significant differences between diagnostic groups are shown. *p = 0.018.

test. Categorical data were presented as proportions, and among groups were compared using the chi-square test. The Spearman correlation analysis was performed to assess the correlation between two quantitative variables, adjusted for age, sex, and education. The diagnostic value of AD and SIVD was estimated by the area under the curve (AUC) using the receiver operating characteristic (ROC) curve. $p < 0.05$ was considered to indicate significant results. p-values were corrected using the Bonferroni method for multiple comparison corrections. All statistical analyses were performed using SPSS version 23.0 (SPSS Inc., Chicago, IL, United States).

Results

Demographics

The demographic and clinical characteristics of each diagnostic group are described in Table 1. No significant difference was found between the groups in age, gender distribution, education, and others. The differences in the MMSE, MoCA scores, and Fazekas WMSA burden among the different groups were presented (refer to Table 1).

Differences in sLRP1, CyPA, and MMP9 levels between diagnostic groups

Plasma sLRP1, CyPA, and MMP9 levels in the diagnostic group are shown in Table 2. Plasma sLRP1 levels in the AD group showed a decreasing trend compared with that in the NC group, but the difference was not statistically significant (H = 3.817, p = 0.148). The difference in plasma CyPA levels was statistically significant across the three groups (H = 8.302, p = 0.016). Further pairwise comparison showed that plasma CyPA levels in the SIVD group were significantly higher than that in the AD group (p = 0.018). The differences in the plasma MMP9 levels were not statistically significant (H = 3.778, p = 0.151). Figure 1 shows the plasma sLRP1, CyPA, and MMP9 levels in each group.

The correlation of plasma biomarker levels with cognition score

Spearman correlation analysis found that plasma sLRP1 levels were positively related to MoCA (r = 0.414, p = 0.040) scores in the AD groups, and plasma MMP9 levels and MoCA (r = −0.528, p = 0.014) scores showed a significant negative correlation in the SIVD groups; however, CyPA levels were not significantly correlated with cognitive scores (Table 3 and Supplementary Figure 2). Correlation analysis showed a significant correlation between plasma CyPA levels and MTA scores in the AD group (r = 0.464, p = 0.017). No significant correlation was detected between the other biomarkers and imaging parameters (p > 0.05) (Table 3). The correlation of plasma biomarkers with other factors is shown in the Supplementary Tables 1–4.

Differential diagnostic value of CyPA concentrations

The ROC analysis was finally performed to assess the differential diagnosis value in patients with AD and SIVD group using CyPA concentration; the performance was found to be good [AUC = 0.725, 95% CI (0.586–0.865); p = 0.0064]. ROC analysis identified a cutoff value for CyPA of 60.15 ng/ml (Figure 2).

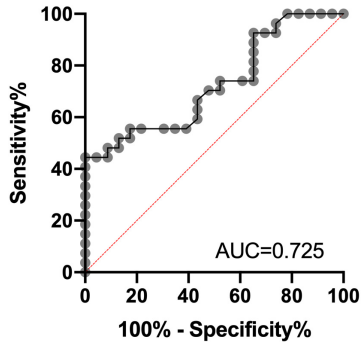

FIGURE 2
Receiver operating characteristic (ROC) analysis of CyPA concentrations in plasma as a candidate biomarker of differential diagnosis for Alzheimer's disease (AD) and subcortical ischemic vascular dementia (SIVD). AUC, area under the curve.

Discussion

Our study aimed to explore the levels of BBB-related blood-borne factors sLRP1, CyPA, and MMP9 in AD, SIVD, and NC. Furthermore, the association of BBB-related factors with cognitive function and imaging parameters was evaluated. To the best of our knowledge, this study is the first to demonstrate that BBB-related blood-borne factors are associated with different types of dementia. Our results support the use of blood-borne factors as potential biomarkers for the differential diagnosis of dementia.

This study showed that plasma CyPA levels presented a decreasing trend in the AD group, and an increasing trend in the SIVD group compared with the NC group, and the plasma CyPA level in the SIVD group was significantly higher than that in the AD group. We used plasma CyPA as a reference index for the differential diagnosis of SIVD and AD. To date, studies have shown that CyPA secretion is increased in patients with central nervous system diseases, such as cerebrovascular disease, brain trauma, and obstructive sleep apnoea with mild cognitive impairment (MCI) (Redell et al., 2007; Chang et al., 2018, 2020; Li et al., 2021). These studies have confirmed that CyPA is critical for brain damage. Furthermore, CyPA levels in endothelial cells and pericytes of the brain are elevated in patients with AD (Halliday et al., 2016). Associations between serum CyPA levels and regional gray matter volume indicated that blood levels of CyPA may reflect the pathological mechanism of AD in

TABLE 3 Correlation of plasma biomarker levels with cognitive scores and imaging parameters.

Factors	sLRP1		CyPA		MMP9	
	r	*P*	r	*P*	r	*P*
The whole sample						
MMSE	0.167	0.152	0.066	0.571	−0.128	0.276
MoCA	0.169	0.149	0.077	0.514	−0.182	0.123
Fazekas	0.089	0.543	0.185	0.203	0.151	0.309
MTA	−0.010	0.945	−0.086	0.558	−0.007	0.961
The AD groups						
MMSE	0.303	0.141	0.085	0.685	0.108	0.606
MoCA	0.414	0.040*	0.237	0.254	−0.017	0.937
Fazekas	0.053	0.797	0.259	0.201	0.167	0.416
MTA	0.346	0.083	0.464	0.017*	0.000	1.000
The SIVD groups						
MMSE	0.314	0.145	−0.139	0.527	−0.325	0.140
MoCA	0.228	0.308	−0.397	0.067	−0.528	0.014*
Fazekas	0.001	0.998	0.195	0.398	−0.248	0.278
MTA	0.197	0.367	−0.157	0.476	0.142	0.529

Adjusted for age, sex, and education.
*The correlation of plasma biomarker levels with cognitive scores and imaging parameters, the difference was significant ($p < 0.05$).

the brain (Choi et al., 2021). Given our study of CyPA, we postulate that plasma CyPA exerts a crucial association with dementia, especially when comparing AD vs. VaD. The molecular mechanisms underlying the effects of CyPA on AD and SIVD are not yet fully understood. *In vitro* studies have shown that CyPA induces endothelial dysfunction, the proliferation of vascular smooth muscle cells, and the migration of inflammatory cells and promotes the development of atherosclerosis (Nigro et al., 2011; Satoh et al., 2011). Pan et al. (2020) demonstrated that CyPA mediates the destruction of brain BBB by pericytes through CD147/NF-κB/MMP9 signaling and junction protein degradation, which may provide a new insights into the management by targeting CyPA and pericytes. *APOE* protein can control BBB integrity *via* the inhibition of CypA-MMP9 signaling cascades (Halliday et al., 2016; Montagne et al., 2020, 2021). Bell et al. also found that the level of CyPA in the cerebral microvessels of *APOE* ε*4* and *APOE*−/− mice was five to six times higher than that in the control group of *APOE* ε*2* and *APOE* ε*3* mice. Knocking out CyPA could eliminate BBB damage caused by *APOE* ε*4* and *APOE*−/− mice. Moreover, treating *APOE* ε*4* mice with low doses of cyclosporine was shown to eliminate BBB damage, indicating that the change in CyPA on the BBB is reversible, and CyPA may be a therapeutic target that causes BBB destruction (Bell et al., 2012; Montagne et al., 2021). Taken together, these results indicate that CyPA controls cerebrovascular integrity. In conjunction with our study, although the number of patients in this study was small, the differences between patients with VaD and AD were significant. These results suggest that plasma CyPA measurements, while not diagnostic, might be combined with psychometric and imaging references to improve the early differentiation between VaD and AD, which may help to better select patients in future clinical trials. To the best of our knowledge, this is the first study to describe elevated plasma CyPA levels in patients with VaD.

Our results provide evidence of differences in plasma CyPA in AD vs. VaD. We also found that plasma CyPA levels were associated with MTA scores in the AD group; however, CyPA levels were not significantly correlated with cognitive scores. The breakdown of the BBB initially occurs in the hippocampus during normal aging, which is a key area for memory. Disruption of the BBB in the hippocampus is associated with MCI, which is in turn associated with damage to pericytes (Montagne et al., 2015). Individuals with early cognitive impairment, regardless of changes in Aβ and/or tau biomarkers of AD, develop brain capillary damage and disruption of the hippocampal BBB, indicating that BBB disruption is an early biomarker of human cognitive dysfunction independent of Aβ and tau (Nation et al., 2019). These results indicate that CyPA is involved in the brain structure of the hippocampus *via* the BBB, which may be an early event in the aging human brain that begins in the hippocampus and is reflected by CyPA. Thus, CyPA may predict early BBB dysfunction in the hippocampus in AD; however, the mechanism requires further exploration. Another study showed that CyPA and MMP9 levels in serum were associated with cognitive impairment and white matter signal abnormalities, which is controversial in our study (Li et al., 2021). The

correlation between CyPA levels and cognitive function requires further verification.

Lipoprotein receptor-related protein 1, a major transporter in the brain-to-blood clearance of Aβ across the BBB, is associated with cognitive decline in AD (Deane et al., 2004; Storck et al., 2016; Ma et al., 2018). Our study found that lower plasma sLRP1 levels were associated with cognitive decline in patients with AD. A previous study showed that cannabinoid treatment enhanced Aβ transfer at the BBB, accompanied by increased brain and plasma sLRP1 levels (Bachmeier et al., 2013). This finding is consistent with those of this study. Another study found that BBB-associated pericytes cleared Aβ aggregation through LRP1/*APOE* subtype-specific mechanisms, supporting the role of the LRP1/*APOE* interaction as a potential therapeutic target for controlling Aβ clearance in AD (Ma et al., 2018). Masaya et al. identified LRP1 as the potential molecular mechanism by which *APOE ε4* in patients with AD intensifies the deposition of Aβ protein in the brain, which was seen both in a mouse model of AD and in autopsies of patients with AD (Tachibana et al., 2019). Halliday et al. also suggested that *APOE ε4* leads to the accelerated loss of the LRP1-dependent CyPA-MMP9 BBB degradation pathway in pericytes and endothelial cells (Halliday et al., 2016; Nikolakopoulou et al., 2021). A recent study suggested that the loss of brain endothelial LRP1 results in the loss of BBB integrity, neuronal loss, and cognitive deficits in mice, which could be reversed by endothelial-specific LRP1 gene therapy (Nikolakopoulou et al., 2021). Thus, increased cerebral LRP1 and plasma sLRP may explain the increased Aβ BBB transport and may provide an effective strategy to reduce the Aβ burden in the AD brain. At present, many studies have focused on the inhibition of Aβ production. However, the occurrence and development of AD are believed to be due to the reduction in Aβ, rather than the excessive production of Aβ (Mawuenyega et al., 2010; Xiang et al., 2015; Wang et al., 2017). Our study focused on Aβ clearance-related proteins and enzymes in AD, which can help discover their potential in the development of AD drugs and provide an optimistic prospect for future therapeutic targets. Furthermore, previous studies found downregulation of LRP1 protein and mRNA expression in VaD rats *via* the IKK/NF-κB signaling pathway (Cai et al., 2020; Wang et al., 2020). Nevertheless, Mercedes et al. proposed that serum sLRP1 can serve as a candidate marker to differentiate AD from mixed dementia phenotypes, with a significant increase in sLRP1 serum protein levels in subjects with mixed dementia and relatively normal levels in AD (Lachén-Montes et al., 2021). Our study also showed that plasma sLRP1 levels presented an increasing trend in VaD while maintaining slightly low levels in patients with AD. This inconsistency may be attributed to the relatively small sample size, different samples, and methods used. Further research is needed to determine whether and how sLRP1 in the blood affects cognitive preference in patients with dementia.

Matrix metallopeptidase 9 is a major protein related to brain disorders and the BBB (Rempe et al., 2016). Inhibition of MMP prevented tight junction protein loss, suggesting that MMP interferes with barrier integrity by degrading tight junction proteins (Yang et al., 2007). Previous studies have found that plasma MMP-9 levels of patients with AD are higher than those in normal controls through an increase in BBB permeability (Lorenzl et al., 2003, 2008). However, Horstmann et al. (2010) showed that plasma MMP9 activity was decreased by 41% in patients with AD compared with that in normal controls. Another study verified that the damage of MMP9 to neurovascular units is thought to be related to vascular cognitive dysfunction by increasing the BBB opening (Candelario-Jalil et al., 2011). The level of MMP9 in the CSF of patients with VaD was higher than that in the AD and normal control groups (Adair et al., 2004). In this study, plasma MMP9 in different diagnostic groups displayed the following trend: SIVD group > AD group > NC group, and higher plasma MMP9 was correlated with cognitive decline, which was broadly consistent with previous studies. MMP9 may increase the permeability of the BBB, activate inflammatory factors, cause various inflammatory responses in cells, and accelerate the onset of disease. Thus, MMP9 may contribute to the course of senile neurodegenerative dementia and may play a role in predicting cognitive function in the periphery. Further studies are required to explore the role of MMP in AD progression.

Our study has some limitations. First, due to the relatively small number of experimental studies and limited research participants, the quality of the statistical analysis may be affected; second, cross-sectional studies have limited causality, and a longitudinal follow-up study is needed to elucidate the relationship between CyPA, sLRP1, and MMP9 levels and disease progression; third, the diagnostic value of a single biomarker is limited, and combinations with other biomarkers should be considered in the future to be used to predict the diagnosis of neurodegenerative dementia; fourth, considering the effect of *APOE* on neurovascular injury and neuronal dysfunction, clarifying the relationship of BBB-related blood-borne factors with *APOE* genotypes is required in the future; fifth, as the assessment of imaging parameters uses visual rating, adding some quantitative volumetric analysis such as hippocampal volume would be informative in future validation studies; the assessment of scales for other cognitive domains and their correlations with biomarkers should also be considered; and finally, we did not have additional information to clarify the mechanism of BBB dysfunction.

In summary, our study suggests that the plasma CyPA level is a reference index when distinguishing between an AD and SIVD diagnosis. sLRP1 and MMP-9 may be ideal biomarkers of cognitive decline. Our findings highlight that blood-derived factors associated with the BBB may provide new insights into the differential diagnosis of neurodegenerative dementia and warrant further investigation.

Data availability statement

The raw data supporting the conclusions of this article will be made available by the authors, without undue reservation.

Ethics statement

The studies involving human participants were reviewed and approved by the Ethics Review Board of the Xuanwu Hospital. The patients/participants provided their written informed consent to participate in this study.

Author contributions

JJ supervised and obtained funding for this study. MG did the statistical analysis. Both authors designed the study, critically revised and drafted the manuscript, contributed to the collection, analysis, and interpretation of data, and approved the final version of the manuscript.

Funding

This study was supported by the Key Project of the National Natural Science Foundation of China (U20A20354), the Beijing Brain Initiative from Beijing Municipal Science & Technology Commission (Z201100005520016 and Z201100005520017), the National Major R&D Projects of China-Scientific Technological Innovation 2030 (2021ZD0201802), the National Key Scientific Instrument and Equipment Development Project (31627803), and the Key Project of the National Natural Science Foundation of China (81530036).

Acknowledgments

We thank the patients for their participation.

Conflict of interest

The authors declare that the research was conducted in the absence of any commercial or financial relationships that could be construed as a potential conflict of interest.

Publisher's note

Supplementary material

The Supplementary Material for this article can be found online at: https://www.frontiersin.org/articles/10.3389/fnins.2022.949129/full#supplementary-material

References

Adair, J. C., Charlie, J., Dencoff, J. E., Kaye, J. A., Quinn, J. F., Camicioli, R. M., et al. (2004). Measurement of gelatinase B (MMP-9) in the cerebrospinal fluid of patients with vascular dementia and Alzheimer disease. *Stroke* 35, e159–62. doi: 10.1161/01.Str.0000127420.10990.76

Bachmeier, C., Beaulieu-Abdelahad, D., Mullan, M., and Paris, D. (2013). Role of the cannabinoid system in the transit of beta-amyloid across the blood-brain barrier. *Mol. Cell. Neurosci.* 56, 255–262. doi: 10.1016/j.mcn.2013.06.004

Barber, R., Ballard, C., McKeith, I. G., Gholkar, A., and O'Brien, J. T. (2000). MRI volumetric study of dementia with Lewy bodies: A comparison with AD and vascular dementia. *Neurology* 54, 1304–1309. doi: 10.1212/wnl.54.6.1304

Barr, T. L., Latour, L. L., Lee, K. Y., Schaewe, T. J., Luby, M., Chang, G. S., et al. (2010). Blood-brain barrier disruption in humans is independently associated with increased matrix metalloproteinase-9. *Stroke* 41, e123–8. doi: 10.1161/strokeaha.109.570515

Bell, R. D., Winkler, E. A., Sagare, A. P., Singh, I., LaRue, B., Deane, R., et al. (2010). Pericytes control key neurovascular functions and neuronal phenotype in the adult brain and during brain aging. *Neuron* 68, 409–427. doi: 10.1016/j.neuron.2010.09.043

Bell, R. D., Winkler, E. A., Singh, I., Sagare, A. P., Deane, R., Wu, Z., et al. (2012). Apolipoprotein E controls cerebrovascular integrity via cyclophilin A. *Nature* 485, 512–516. doi: 10.1038/nature11087

Bjerke, M., and Engelborghs, S. (2018). Cerebrospinal Fluid Biomarkers for Early and Differential Alzheimer's Disease Diagnosis. *J. Alzheimers Dis.* 62, 1199–1209. doi: 10.3233/jad-170680

Cai, H., Cai, T., Zheng, H., Liu, L., Zhou, L., Pang, X., et al. (2020). The Neuroprotective Effects of Danggui-Shaoyao San on Vascular Cognitive Impairment: Involvement of the Role of the Low-Density Lipoprotein Receptor-Related Protein. *Rejuvenation Res.* 23, 420–433. doi: 10.1089/rej.2019.2182

Cai, Z., Qiao, P. F., Wan, C. Q., Cai, M., Zhou, N. K., and Li, Q. (2018). Role of Blood-Brain Barrier in Alzheimer's Disease. *J. Alzheimers Dis.* 63, 1223–1234. doi: 10.3233/jad-180098

Candelario-Jalil, E., Thompson, J., Taheri, S., Grossetete, M., Adair, J. C., Edmonds, E., et al. (2011). Matrix metalloproteinases are associated with increased blood-brain barrier opening in vascular cognitive impairment. *Stroke* 42, 1345–1350. doi: 10.1161/strokeaha.110.600825

Cavedo, E., Pievani, M., Boccardi, M., Galluzzi, S., Bocchetta, M., Bonetti, M., et al. (2014). Medial temporal atrophy in early and late-onset Alzheimer's disease. *Neurobiol. Aging* 35, 2004–2012. doi: 10.1016/j.neurobiolaging.2014.03.009

Chang, C. S., Kuo, C. L., Huang, C. S., Cheng, Y. S., Lin, S. S., and Liu, C. S. (2020). Association of cyclophilin A level and pulse pressure in predicting recurrence of cerebral infarction. *Kaohsiung J. Med. Sci.* 36, 122–128. doi: 10.1002/kjm2.12143

Chang, C. S., Su, S. L., Kuo, C. L., Huang, C. S., Tseng, W. M., Lin, S. S., et al. (2018). Cyclophilin A: A Predictive Biomarker of Carotid Stenosis in Cerebral Ischemic Stroke. *Curr. Neurovasc. Res.* 15, 111–119. doi: 10.2174/1567202615666180516120959

Choi, H. I., Kim, K., Lee, J., Chang, Y., Rhee, H. Y., Park, S., et al. (2021). Relationship between Brain Tissue Changes and Blood Biomarkers of Cyclophilin A, Heme Oxygenase-1, and Inositol-Requiring Enzyme 1 in Patients with Alzheimer's Disease. *Diagnostics* 11:740. doi: 10.3390/diagnostics11050740

Deane, R., Du Yan, S., Submamaryan, R. K., LaRue, B., Jovanovic, S., Hogg, E., et al. (2003). RAGE mediates amyloid-beta peptide transport across the blood-brain barrier and accumulation in brain. *Nat. Med.* 9, 907–913. doi: 10.1038/nm890

Deane, R., Sagare, A., and Zlokovic, B. V. (2008). The role of the cell surface LRP and soluble LRP in blood-brain barrier Abeta clearance in Alzheimer's disease. *Curr. Pharm. Des.* 14, 1601–1605. doi: 10.2174/138161208784705487

Deane, R., Wu, Z., Sagare, A., Davis, J., Du Yan, S., Hamm, K., et al. (2004). LRP/amyloid beta-peptide interaction mediates differential brain efflux of Abeta isoforms. *Neuron* 43, 333–344. doi: 10.1016/j.neuron.2004.07.017

Donahue, J. E., Flaherty, S. L., Johanson, C. E., Duncan, J. A. III, Silverberg, G. D., Miller, M. C., et al. (2006). RAGE, LRP-1, and amyloid-beta protein in Alzheimer's disease. *Acta Neuropathol.* 112, 405–415. doi: 10.1007/s00401-006-0115-3

El-Ebidi, A. M., Saleem, T. H., Saadi, M. G. E., Mahmoud, H. A., Mohamed, Z., and Sherkawy, H. S. (2020). Cyclophilin A (CyPA) as a Novel Biomarker for Early Detection of Diabetic Nephropathy in an Animal Model. *Diabetes Metab. Syndr. Obes.* 13, 3807–3819. doi: 10.2147/dmso.S260293

Erkinjuntti, T. (2003). Subcortical ischemic vascular disease and dementia. *Int. Psychogeriatr.* 15, 23–26. doi: 10.1017/s1041610203008925

Fazekas, F., Chawluk, J. B., Alavi, A., Hurtig, H. I., and Zimmerman, R. A. (1987). MR signal abnormalities at 1.5 T in Alzheimer's dementia and normal aging. *AJR Am. J. Roentgenol.* 149, 351–356. doi: 10.2214/ajr.149.2.351

Halliday, M. R., Rege, S. V., Ma, Q., Zhao, Z., Miller, C. A., Winkler, E. A., et al. (2016). Accelerated pericyte degeneration and blood-brain barrier breakdown in apolipoprotein E4 carriers with Alzheimer's disease. *J. Cereb. Blood Flow Metab.* 36, 216–227. doi: 10.1038/jcbfm.2015.44

Hilal, S., Liu, S., Wong, T. Y., Vrooman, H., Cheng, C. Y., Venketasubramanian, N., et al. (2021). White matter network damage mediates association between cerebrovascular disease and cognition. *J. Cereb. Blood Flow Metab.* 41, 1858–1872. doi: 10.1177/0271678x21990980

Horstmann, S., Budig, L., Gardner, H., Koziol, J., Deuschle, M., Schilling, C., et al. (2010). Matrix metalloproteinases in peripheral blood and cerebrospinal fluid in patients with Alzheimer's disease. *Int. Psychogeriatr.* 22, 966–972. doi: 10.1017/s1041610210000827

Jack, C. R. Jr., Albert, M. S., Knopman, D. S., McKhann, G. M., Sperling, R. A., Carrillo, M. C., et al. (2011). Introduction to the recommendations from the National Institute on Aging-Alzheimer's Association workgroups on diagnostic guidelines for Alzheimer's disease. *Alzheimers Dement.* 7, 257–262. doi: 10.1016/j.jalz.2011.03.004

Jia, L., Quan, M., Fu, Y., Zhao, T., Li, Y., Wei, C., et al. (2020). Dementia in China: Epidemiology, clinical management, and research advances. *Lancet Neurol.* 19, 81–92. doi: 10.1016/s1474-4422(19)30290-x

Kao, H. W., Lee, K. W., Chen, W. L., Kuo, C. L., Huang, C. S., Tseng, W. M., et al. (2015). Cyclophilin A in Ruptured Intracranial Aneurysm: A Prognostic Biomarker. *Medicine* 94:e1683. doi: 10.1097/md.0000000000001683

Lachén-Montes, M., Íñigo-Marco, I., Cartas-Cejudo, P., Fernández-Irigoyen, J., and Santamaría, E. (2021). Olfactory Bulb Proteomics Reveals Widespread Proteostatic Disturbances in Mixed Dementia and Guides for Potential Serum Biomarkers to Discriminate Alzheimer Disease and Mixed Dementia Phenotypes. *J. Pers. Med.* 11:503. doi: 10.3390/jpm11060503

Lam, S., Lipton, R. B., Harvey, D. J., Zammit, A. R., and Ezzati, A. (2021). White matter hyperintensities and cognition across different Alzheimer's biomarker profiles. *J. Am. Geriatr. Soc.* 69, 1906–1915. doi: 10.1111/jgs.17173

Li, M., Sun, H., Shen, T., Xue, S., Zhao, Y., Leng, B., et al. (2021). Increased serum levels of cyclophilin a and matrix metalloproteinase-9 are associated with cognitive impairment in patients with obstructive sleep apnea. *Sleep Med.* 93, 75–83. doi: 10.1016/j.sleep.2021.10.009

Lorenzl, S., Albers, D. S., Relkin, N., Ngyuen, T., Hilgenberg, S. L., Chirichigno, J., et al. (2003). Increased plasma levels of matrix metalloproteinase-9 in patients with Alzheimer's disease. *Neurochem. Int.* 43, 191–196. doi: 10.1016/s0197-0186(03)00004-4

Lorenzl, S., Buerger, K., Hampel, H., and Beal, M. F. (2008). Profiles of matrix metalloproteinases and their inhibitors in plasma of patients with dementia. *Int. Psychogeriatr.* 20, 67–76. doi: 10.1017/s1041610207005790

Ma, Q., Zhao, Z., Sagare, A. P., Wu, Y., Wang, M., Owens, N. C., et al. (2018). Blood-brain barrier-associated pericytes internalize and clear aggregated amyloid-β42 by LRP1-dependent apolipoprotein E isoform-specific mechanism. *Mol. Neurodegener.* 13:57. doi: 10.1186/s13024-018-0286-0

Mawuenyega, K. G., Sigurdson, W., Ovod, V., Munsell, L., Kasten, T., Morris, J. C., et al. (2010). Decreased clearance of CNS beta-amyloid in Alzheimer's disease. *Science* 330:1774. doi: 10.1126/science.1197623

Montagne, A., Barnes, S. R., Sweeney, M. D., Halliday, M. R., Sagare, A. P., Zhao, Z., et al. (2015). Blood-brain barrier breakdown in the aging human hippocampus. *Neuron* 85, 296–302. doi: 10.1016/j.neuron.2014.12.032

Montagne, A., Nation, D. A., Sagare, A. P., Barisano, G., Sweeney, M. D., Chakhoyan, A., et al. (2020). APOE4 leads to blood-brain barrier dysfunction predicting cognitive decline. *Nature* 581, 71–76. doi: 10.1038/s41586-020-2247-3

Montagne, A., Nikolakopoulou, A. M., Huuskonen, M. T., Sagare, A. P., Lawson, E. J., Lazic, D., et al. (2021). APOE4 accelerates advanced-stage vascular and neurodegenerative disorder in old Alzheimer's mice via cyclophilin A independently of amyloid-β. *Nat. Aging* 1, 506–520. doi: 10.1038/s43587-021-00073-z

Nation, D. A., Sweeney, M. D., Montagne, A., Sagare, A. P., D'Orazio, L. M., Pachicano, M., et al. (2019). Blood-brain barrier breakdown is an early biomarker of human cognitive dysfunction. *Nat. Med.* 25, 270–276. doi: 10.1038/s41591-018-0297-y

Nelson, A. R., Sweeney, M. D., Sagare, A. P., and Zlokovic, B. V. (2016). Neurovascular dysfunction and neurodegeneration in dementia and Alzheimer's disease. *Biochim. Biophys. Acta* 1862, 887–900. doi: 10.1016/j.bbadis.2015.12.016

Neto, E., Allen, E. A., Aurlien, H., Nordby, H., and Eichele, T. (2015). EEG Spectral Features Discriminate between Alzheimer's and Vascular Dementia. *Front. Neurol.* 6:25. doi: 10.3389/fneur.2015.00025

Nigro, P., Satoh, K., O'Dell, M. R., Soe, N. N., Cui, Z., Mohan, A., et al. (2011). Cyclophilin A is an inflammatory mediator that promotes atherosclerosis in apolipoprotein E-deficient mice. *J. Exp. Med.* 208, 53–66. doi: 10.1084/jem.20101174

Nikolakopoulou, A. M., Wang, Y., Ma, Q., Sagare, A. P., Montagne, A., Huuskonen, M. T., et al. (2021). Endothelial LRP1 protects against neurodegeneration by blocking cyclophilin A. *J. Exp. Med.* 218:e20202207. doi: 10.1084/jem.20202207

O'Brien, J. T., and Thomas, A. (2015). Vascular dementia. *Lancet* 386, 1698–1706. doi: 10.1016/s0140-6736(15)00463-8

Pan, P., Zhao, H., Zhang, X., Li, Q., Qu, J., Zuo, S., et al. (2020). Cyclophilin a signaling induces pericyte-associated blood-brain barrier disruption after subarachnoid hemorrhage. *J. Neuroinflammation* 17:16. doi: 10.1186/s12974-020-1699-6

Park, M., and Moon, W. J. (2016). Structural MR Imaging in the Diagnosis of Alzheimer's Disease and Other Neurodegenerative Dementia: Current Imaging Approach and Future Perspectives. *Korean J. Radiol.* 17, 827–845. doi: 10.3348/kjr.2016.17.6.827

Quinn, K. A., Grimsley, P. G., Dai, Y. P., Tapner, M., Chesterman, C. N., and Owensby, D. A. (1997). Soluble low density lipoprotein receptor-related protein (LRP) circulates in human plasma. *J. Biol. Chem.* 272, 23946–23951. doi: 10.1074/jbc.272.38.23946

Ramachandran, S., Venugopal, A., Kutty, V. R., Chitrasree, V., Mullassari, A., Pratapchandran, N. S., et al. (2014). Plasma level of cyclophilin A is increased in patients with type 2 diabetes mellitus and suggests presence of vascular disease. *Cardiovasc. Diabetol.* 13:38. doi: 10.1186/1475-2840-13-38

Rath, D., von Ungern-Sternberg, S., Heinzmann, D., Sigle, M., Monzien, M., Horstmann, K., et al. (2020). Platelet surface expression of cyclophilin A is associated with increased mortality in patients with symptomatic coronary artery disease. *J. Thromb. Haemost.* 18, 234–242. doi: 10.1111/jth.14635

Redell, J. B., Zhao, J., and Dash, P. K. (2007). Acutely increased cyclophilin a expression after brain injury: A role in blood-brain barrier function and tissue preservation. *J. Neurosci. Res.* 85, 1980–1988. doi: 10.1002/jnr.21324

Rempe, R. G., Hartz, A. M. S., and Bauer, B. (2016). Matrix metalloproteinases in the brain and blood-brain barrier: Versatile breakers and makers. *J. Cereb. Blood Flow Metab.* 36, 1481–1507. doi: 10.1177/0271678x16655551

Sagare, A., Deane, R., Bell, R. D., Johnson, B., Hamm, K., Pendu, R., et al. (2007). Clearance of amyloid-beta by circulating lipoprotein receptors. *Nat. Med.* 13, 1029–1031. doi: 10.1038/nm1635

Sagare, A. P., Deane, R., Zetterberg, H., Wallin, A., Blennow, K., and Zlokovic, B. V. (2011). Impaired lipoprotein receptor-mediated peripheral binding of plasma amyloid-β is an early biomarker for mild cognitive impairment preceding Alzheimer's disease. *J Alzheimers Dis.* 24, 25–34. doi: 10.3233/jad-2010-101248

Sagare, A. P., Deane, R., and Zlokovic, B. V. (2012). Low-density lipoprotein receptor-related protein 1: A physiological Aβ homeostatic mechanism with multiple therapeutic opportunities. *Pharmacol. Ther.* 136, 94–105. doi: 10.1016/j.pharmthera.2012.07.008

Satoh, K., Fukumoto, Y., Sugimura, K., Miura, Y., Aoki, T., Nochioka, K., et al. (2013). Plasma cyclophilin A is a novel biomarker for coronary artery disease. *Circ. J.* 77, 447–455. doi: 10.1253/circj.cj-12-0805

Satoh, K., Nigro, P., Zeidan, A., Soe, N. N., Jaffré, F., Oikawa, M., et al. (2011). Cyclophilin A promotes cardiac hypertrophy in apolipoprotein E-deficient mice. *Arterioscler. Thromb. Vasc. Biol.* 31, 1116–1123. doi: 10.1161/atvbaha.110.214601

Seizer, P., Fuchs, C., Ungern-Sternberg, S. N., Heinzmann, D., Langer, H., Gawaz, M., et al. (2016). Platelet-bound cyclophilin A in patients with stable coronary artery disease and acute myocardial infarction. *Platelets* 27, 155–158. doi: 10.3109/09537104.2015.1051466

Seizer, P., Schönberger, T., Schött, M., Lang, M. R., Langer, H. F., Bigalke, B., et al. (2010). EMMPRIN and its ligand cyclophilin A regulate MT1-MMP, MMP-9 and M-CSF during foam cell formation. *Atherosclerosis* 209, 51–57. doi: 10.1016/j.atherosclerosis.2009.08.029

Seizer, P., Ungern-Sternberg, S. N., Schönberger, T., Borst, O., Münzer, P., Schmidt, E. M., et al. (2015). Extracellular cyclophilin A activates platelets via EMMPRIN (CD147) and PI3K/Akt signaling, which promotes platelet adhesion and thrombus formation in vitro and in vivo. *Arterioscler. Thromb. Vasc. Biol.* 35, 655–663. doi: 10.1161/atvbaha.114.305112

Shackleton, B., Ringland, C., Abdullah, L., Mullan, M., Crawford, F., and Bachmeier, C. (2019). Influence of Matrix Metallopeptidase 9 on Beta-Amyloid Elimination Across the Blood-Brain Barrier. *Mol. Neurobiol.* 56, 8296–8305. doi: 10.1007/s12035-019-01672-z

Shibata, M., Yamada, S., Kumar, S. R., Calero, M., Bading, J., Frangione, B., et al. (2000). Clearance of Alzheimer's amyloid-ss(1-40) peptide from brain by LDL receptor-related protein-1 at the blood-brain barrier. *J. Clin. Invest.* 106, 1489–1499. doi: 10.1172/jci10498

Storck, S. E., Meister, S., Nahrath, J., Meißner, J. N., Schubert, N., Di Spiezio, A., et al. (2016). Endothelial LRP1 transports amyloid-β(1-42) across the blood-brain barrier. *J. Clin. Invest.* 126, 123–136. doi: 10.1172/jci81108

Tachibana, H., Washida, K., Kowa, H., Kanda, F., and Toda, T. (2016). Vascular Function in Alzheimer's Disease and Vascular Dementia. *Am. J. Alzheimers Dis. Other Demen.* 31, 437–442. doi: 10.1177/1533317516653820

Tachibana, M., Holm, M. L., Liu, C. C., Shinohara, M., Aikawa, T., Oue, H., et al. (2019). APOE4-mediated amyloid-β pathology depends on its neuronal receptor LRP1. *J. Clin. Invest.* 129, 1272–1277. doi: 10.1172/jci124853

Uemura, M. T., Maki, T., Ihara, M., Lee, V. M. Y., and Trojanowski, J. Q. (2020). Brain Microvascular Pericytes in Vascular Cognitive Impairment and Dementia. *Front. Aging Neurosci.* 12:80. doi: 10.3389/fnagi.2020.00080

Ueno, M., Chiba, Y., Murakami, R., Matsumoto, K., Fujihara, R., Uemura, N., et al. (2019). Disturbance of Intracerebral Fluid Clearance and Blood-Brain Barrier in Vascular Cognitive Impairment. *Int. J. Mol. Sci.* 20:2600. doi: 10.3390/ijms20102600

Wang, J., Gu, B. J., Masters, C. L., and Wang, Y. J. (2017). A systemic view of Alzheimer disease - insights from amyloid-β metabolism beyond the brain. *Nat. Rev. Neurol.* 13, 612–623. doi: 10.1038/nrneurol.2017.111

Wang, J. J., Wu, S. B., Cheng, H. L., Yang, C., Chen, Y., and Yang, J. (2020). [Effect of moxibustion on expression of RAGE and LRP-1 and neuronal ultrastructure of frontal cortex and hippocampus in vascular dementia rats]. *Zhen Ci Yan Jiu* 45, 33–39. doi: 10.13702/j.1000-0607.1902956

Xiang, Y., Bu, X. L., Liu, Y. H., Zhu, C., Shen, L. L., Jiao, S. S., et al. (2015). Physiological amyloid-beta clearance in the periphery and its therapeutic potential for Alzheimer's disease. *Acta Neuropathol.* 130, 487–499. doi: 10.1007/s00401-015-1477-1

Yamazaki, Y., and Kanekiyo, T. (2017). Blood-Brain Barrier Dysfunction and the Pathogenesis of Alzheimer's Disease. *Int. J. Mol. Sci.* 18:1965. doi: 10.3390/ijms18091965

Yang, Y., Estrada, E. Y., Thompson, J. F., Liu, W., and Rosenberg, G. A. (2007). Matrix metalloproteinase-mediated disruption of tight junction proteins in cerebral vessels is reversed by synthetic matrix metalloproteinase inhibitor in focal ischemia in rat. *J. Cereb. Blood Flow Metab.* 27, 697–709. doi: 10.1038/sj.jcbfm.9600375

Zlokovic, B. V. (2011). Neurovascular pathways to neurodegeneration in Alzheimer's disease and other disorders. *Nat. Rev. Neurosci.* 12, 723–738. doi: 10.1038/nrn3114

frontiers | Frontiers in Neuroscience

TYPE Original Research
PUBLISHED 09 August 2022
DOI 10.3389/fnins.2022.917348

OPEN ACCESS

EDITED BY
Jose Hurst,
University Hospital Tübingen, Germany

REVIEWED BY
Daniela Valenti,
Department of Biomedical Sciences, Institute of Biomembranes, Bioenergetics and Molecular Biotechnologies (CNR), Italy
Jingfa Zhang,
Shanghai General Hospital, China
Haiwei Xu,
Army Medical University, China

*CORRESPONDENCE
Bo Lei
bolei99@126.com

†These authors have contributed equally to this work and share first authorship

SPECIALTY SECTION
This article was submitted to Neurodegeneration, a section of the journal Frontiers in Neuroscience

RECEIVED 11 April 2022
ACCEPTED 22 July 2022
PUBLISHED 09 August 2022

CITATION
Zhou Q, Yao S, Yang M, Guo Q, Li Y, Li L and Lei B (2022) Superoxide dismutase 2 ameliorates mitochondrial dysfunction in skin fibroblasts of Leber's hereditary optic neuropathy patients.
Front. Neurosci. 16:917348.
doi: 10.3389/fnins.2022.917348

Superoxide dismutase 2 ameliorates mitochondrial dysfunction in skin fibroblasts of Leber's hereditary optic neuropathy patients

Qingru Zhou[1†], Shun Yao[1,2†], Mingzhu Yang[1,2], Qingge Guo[1,2], Ya Li[1,2], Lei Li[3] and Bo Lei[1,2*]

[1]Henan Provincial People's Hospital, Zhengzhou University People's Hospital, Zhengzhou, China, [2]Henan Eye Hospital, Henan Provincial People's Hospital, Henan Eye Institute, Zhengzhou, China, [3]Xinxiang Medical University, Xinxiang, China

Background: In Leber's hereditary optic neuropathy (LHON), mtDNA mutations mediate mitochondrial dysfunction and apoptosis of retinal ganglion cells. Mitochondrial superoxide dismutase 2 (SOD2) is a crucial antioxidase against reactive oxygen species (ROS). This study aims to investigate whether SOD2 could ameliorate mtDNA mutation mediated mitochondrial dysfunction in skin fibroblasts of LHON patients and explore the underlying mechanisms.

Methods: The skin of normal healthy subjects and severe LHON patients harboring m.11778G > A mutation was taken to prepare immortalized skin fibroblast cell lines (control-iFB and LHON-iFB). LHON-iFB cells were transfected with SOD2 plasmid or negative control plasmid, respectively. In addition, human neuroblastoma SH-SY5Y cells and human primary retinal pigmental epithelium (hRPE) cells were stimulated by H_2O_2 after gene transfection. The oxygen consumption rate (OCR) was measured with a Seahorse extracellular flux analyzer. The level of ATP production, mitochondrial membrane potential, ROS and malondialdehyde (MDA) were measured separately with the corresponding assay kits. The expression level of SOD2, inflammatory cytokines and p-IκBα/IκBα was evaluated by western-blot. Assessment of apoptosis was performed by TUNEL assay.

Results: LHON-iFB exhibited lower OCR, ATP production, mitochondrial membrane potential but higher level of ROS and MDA than control-iFB. Western-blot revealed a significantly increased expression of IL-6 and p-IκBα/IκBα in LHON-iFB. Compared with the negative control, SOD2 overexpression increased OCR, ATP production and elevated mitochondrial membrane potential, but impaired ROS and MDA production. Besides, western-blot demonstrated exogenous SOD2 reduced the protein level of IL-6 and p-IκBα/IκBα. TUNEL assays suggested SOD2 inhibited cells apoptosis. Analogously, in SH-SY5Y and hRPE cells, SOD2 overexpression increased ATP

production and mitochondrial membrane potential, but decreased ROS, MDA levels and suppressed apoptosis.

Conclusion: SOD2 upregulation inhibited cells apoptosis through ameliorating mitochondrial dysfunction and reducing NF-κB associated inflammatory response. This study further support exogenous SOD2 may be a promising therapy for the treatment of LHON.

KEYWORDS

SOD2, LHON, mitochondrial dysfunction, oxidative stress, retinal ganglion cell

Introduction

With a prevalence of about 1/30,000, Leber's hereditary optic neuropathy (LHON) is a maternally inherited disease characterized by irreversible loss of vision and atrophy of the optic nerve (Yu-Wai-Man et al., 2011). The visual prognosis is usually poor and causes legal blindness. At present, it is still an incurable condition due to the lack of effective treatments. Three mutations (MTND1-3460, MTND4-11778, and MTND6-14484) account for 95% of European cases and MTND4-11778 alone for 80% of Japanese cases (Yen et al., 2006). These mutations change the function of mitochondrial respiratory chain complex I and lead to bioenergetic defect (Lopez Sanchez et al., 2020).

Mitochondrion contains the key structure of energy production, involved in both energy metabolism and free radical metabolism. By generating almost 90% of the total amount of cellular ROS, it is the major source of ROS under normal physiological conditions (Balaban et al., 2005; Sarewicz et al., 2010; Kausar et al., 2018). ROS is produced as a result of electronic leakage from the mitochondrial respiratory chain during oxidative phosphorylation (OXPHOS) and is responsible for oxidative damage mediated by permanently modifying proteins, lipids, and mtDNA (Islam, 2017; Schofield and Schafer, 2021). In LHON, abnormal function and structure of mitochondrial respiratory chain complex I generates excessive ROS (Carelli et al., 2009; Hayashi and Cortopassi, 2015; Lopez Sanchez et al., 2016). The accumulation of ROS plays an important role in the development of LHON and other neurodegenerative diseases (Singh et al., 2019; Liskova et al., 2021).

By transforming superoxide radicals into hydrogen peroxide and oxygen, superoxide dismutase (SOD) enzymes are among the most important defense systems against oxygen radicals. Three isoforms of SOD exist in mammals, including cytoplasmic superoxide dismutase (SOD1), mitochondrial superoxide dismutase (SOD2) and extracellular superoxide dismutase (SOD3) (Sheng et al., 2014; Rosa et al., 2021). Since mitochondria are involved in the pathogenesis of LHON, we verified the hypothesis that SOD2 might protect against mitochondrial dysfunction by inhibiting oxidative stress and prevent cell death. Free radicals and other oxidants are critical determinants of the cellular signaling pathways involved in the pathogenesis of several human diseases including inflammatory diseases. SOD plays an essential pathogenic role in the inflammatory diseases by not only catalyzing the conversion of the superoxide to hydrogen peroxide and oxygen but also affecting immune responses (Hernandez-Saavedra et al., 2005; Kwon et al., 2012; Nguyen et al., 2020). Thus, we detected inflammatory cytokine expression and explored the anti-inflammatory effect in LHON is mediated by NF-κB signaling. Because it is impossible to obtain retinal ganglion cells from the patients, we constructed fibroblastic cells derived from patients' skin tissues, which have recently been used to explore the mechanisms and therapeutic effects by other groups (Chao de la Barca et al., 2016; Morvan and Demidem, 2018; Zhou et al., 2020). To further confirm the results, additional tests were performed in human neuroblastoma SH-SY5Y cells and in human primary retinal pigmental epithelium (hRPE) cells.

Abbreviations: LHON, Leber's hereditary optic neuropathy; SOD, mitochondrial superoxide dismutase; ROS, reactive oxygen species; mtDNA, mitochondrial DNA; iFB, fibroblasts; hRPE, human primary retinal pigmental epithelium; OCR, oxygen consumption rate; ATP, adenosine triphosphate; MDA, malondialdehyde; TUNEL, terminal-deoxynucleoitidyl transferase mediated nick end labeling; OXPHOS, oxidative phosphorylation; CDS, coding sequence; FCCP, carbonyl cyanide 4-(trifluoromethoxy) phenylhydrazone; MMP, mitochondrial membrane potential; TBA, thiobarbituric acid; PBS, Phosphate Buffered Saline; PMSF, phenylmethylsulfonyl fluoride; WB, western blot; IP, immunoprecipitation; BCA, bicinchoninic acid; PVDF, polyvinylidene difluoride; TBST, tris buffered saline with tween-20.

Materials and methods

Subjects and cell culture

This study was conducted followed the Declaration of Helsinki. All protocols in this study were approved by Ethic Committees of Henan Eye Hospital [IRB approval number:

HNEECKY-2019 (12)]. Informed consents were obtained from all participants. Two genetically unrelated Chinese LHON subjects carrying mutation m.11778G > A, aged 28 and 31 years old, respectively, and an age-matched (30 years old) healthy control subject without mtDNA mutation were recruited at Henan Eye Hospital. One subject carried only one mutation m.11778G > A, and the other carried multiple variants LHON associated mutations including m.11778G > A, m.10398A > G and m.4833A > G. All patients presented typical clinical manifestations of LHON. The healthy control subject did not have any ophthalmic condition and was excluded for any other diseases. The immortalized fibroblast cell lines (LHON-iFB and control-iFB) were conducted as following. The volume of 2 mm^3 skin tissues were obtained from volunteers and soak in 75% alcohol for 2 min. The tissues were cut into pieces and washed repeatedly, followed by incubating in complete medium at 37°C for 30–60 min. A small piece was clamped into a culture flask and cultured with 2 ml complete fibroblast medium in a 5% CO_2 incubator for 2 h. The medium was changed every 3 days until the tissue blocks grow around it. After removing tissue pieces, the cells were trypsinized and incubated with complete medium for 1 week. Cells were infected with SV40-overexpressing lentivirus (EF1α-SV40-IRES-puromycin) and puromycin was used for selection until the cells were tolerant. The successfully screened cells were expanded and subjected to experiments. The complete fibroblast medium contains DMEM/F12 medium supplemented with 10% fetal bovine serum, 10 ng/ml basic fibroblast growth factor (Labsystech, Shanghai, China) and 1% penicillin and streptomycin (Solarbio, Shanghai, China).

Primary human RPE (hRPE) cells were prepared from donor eyes from the Henan Eye Bank based on our previous protocols (Fu et al., 2017; Qiu et al., 2021; Jin et al., 2022). None of the donors had a history of eye diseases. SH-SY5Y cells were purchased from the American Type Culture Collection (ATCC, Manassas, VA, United States). The cells were cultured with DMEM medium (Invitrogen, Carlsbad, CA, United States) supplemented with 10% fetal bovine serum (Corning, Tewksbury, MA, United States), 100 U/ml penicillin and 100 U/ml streptomycin (Solarbio) in 37°C incubator.

Plasmids and transfection

The CDS (coding sequence) of the human SOD2 gene with a flag tag at the C-terminal was synthesized and subcloned into the pcDNA3.1 (+) expression vector (Invitrogen). All plasmids were confirmed by DNA sequencing and WB analysis. When cells grow to 80% confluence, transfection was performed using Lipofectamine 3000 (Invitrogen). After transfection, the cells were harvested at 48 h for protein extraction and further analysis.

Measurements of oxygen consumption

The rates of oxygen consumption (OCR) in fibroblast cell lines were measured with a Seahorse Bioscience XFe96 extracellular flux analyzer (Agilent, Santa Clara, CA, United States) (Dranka et al., 2011). Fibroblast cells were seeded at a density of 2.5×10^4 cells per well on the polystyrene tissue culture plates. Inhibitors were added with the following concentrations: oligomycin (1.5 μM), carbonyl cyanide 4-(trifluoromethoxy) phenylhydrazone (FCCP; 1 μM), antimycin A and rotenone (0.5 μM).

Determination of mitochondrial membrane potential

Mitochondrial membrane potential (MMP) was detected with a JC-1 Staining Kit (Beyotime, Shanghai, China). Skin fibroblast cells, hRPE cells and SH-SY5Y cells were cultured in 12-well plates separately. After treatments, cells were washed with PBS (phosphate buffer saline) and incubated with JC-1 staining fluid in darkness at 37°C for 30 min. Then, the cells were washed with cold staining buffer. Fluorescent cells were visualized using an Olympus confocal microscope. Cellular mitochondria with normal MMP emitted red fluorescence (J-aggregate), while those with abnormal MMP showed green fluorescence (J-monomer). Fluorescence intensity was quantified using Image-J software (National Institutes of Health, Bethesda, MD, United States). The MMP was reflected by ratio of red/green fluorescence intensity.

Reactive oxygen species level detection

Skin fibroblast, hRPE and SH-SY5Y cells were subjected to reactive oxygen species (ROS) assay, respectively, according to the manufacturer's instruction (Beyotime). Briefly, cells were incubated with corresponding serum-free medium containing with DCFH-DA at 37°C for 30 min. DCFH-DA was removed and washed with serum-free medium for three times. Fluorescence of DCF was detected using fluorescence microscope analysis (Olympus, TKY, Japan). The average optical density of each group was measured with Image-J software.

Adenosine triphosphate and malondialdehyde assay

The ATP levels in various cells were determined by the Enhanced ATP Assay Kit (Beyotime) according to the manufacturer's instructions. The luminescence was read on a microplate reader (Bio-Tek, Winooski, VT, United States) and

the content of ATP was calculated according to ATP standard curve. ATP levels were normalized to μmol/mg protein. The lipid peroxidation levels of various cells were examined using a Lipid Peroxidation MDA Assay kit (Beyotime). The preparation of thiobarbituric acid (TBA) stock solution and MDA working solution, as well as the dilution of the standard substances were all performed in accordance with the product manual. The MDA content was measured at 532 nm using a microplate reader (Bio Tek). ATP levels and MDA levels were normalized to mmol/mg protein.

Terminal-deoxynucleoitidyl transferase mediated nick end labeling assay

Cell apoptosis was determined by using the One-step TUNEL cell apoptosis detection kits (Beyotime) following manufacturer's protocols. Various cells were seeded in 12-well plates separately. After treatments, cells were fixed with 4% paraformaldehyde for 30 min and washed twice using PBS. Cells were permeabilized with PBS containing 0.3% Triton X-100 at room temperature for 5 min and washed twice with PBS. A total of 50 μl TUNEL detection solution was added to the sample and incubated in the darkness at 37°C for 60 min. Every sample was photographed by a fluorescent microscope.

Extraction of mitochondrial proteins

Mitochondrial proteins were extracted by the Cell Mitochondria Isolation kit (Beyotime). Cells were collected and resuspended in 2.5 ml of mitochondrial separation reagent containing 1 mM phenylmethylsulfonyl fluoride (PMSF). After incubation on ice for 15 min, the cell resuspension was homogenized by a glass homogenizer and centrifuged at 600 g for 10 min at 4°C. The supernatant was centrifuged at 11,000 g for 10 min at 4°C. The supernatant was discarded, whereas the precipitate containing the mitochondria was washed and re-suspended in 100 μl lysis solution with 1 mM PMSF. The lysed solution was centrifuged again and the supernatant containing mitochondrial proteins was collected for western blotting.

Western blotting analysis

Skin fibroblast cells were washed with PBS (Solarbio) for three times and lysed with RIPA lysis buffer for WB/IP assays (Yesen, Shanghai, China) containing 1% pro-tease inhibitor cocktail (ApexBio, Housto, TX, United States) on the ice for 30 min. The supernatants were collected after centrifuging at 12,000 rpm for 15 min. The protein concentration was detected by using a bicinchoninic acid (BCA) protein kit (Beyotime). All samples were diluted with 5 × SDS loading buffer (EpiZyme, Shanghai, China) and boiled at 95°C for 5 min. Equal amounts of total protein were separated on a 10% SDS-polyacrylamide gel and transferred to polyvinylidene difluoride (PVDF) membranes (Millipore, Billerica, MA, United States). After blocking with 5% non-fat milk for 1.5 h, the membranes were incubated with specific primary antibodies against flag (1:1,000, Abcam, Cambridge, United Kingdom), p-IκB-α (1:500, Abcam), IκB-α (1:1,000, Abcam), IL-6 (1:500, Abcam), and β-actin (1:1,000, Abcam) overnight at 4°C. After washed with TBST (containing 1% Tween-20, Solarbio) for three times, the membranes were incubated with secondary antibody (1:10,000, Millipore) at room temperature for 1.5 h. The membranes were washed with TBST (containing 1% Tween-20) for three times. Signals were developed with ECL kit (Millipore), and band densitometry was performed using the AlphaView SA Software (ProteinSimple, San Jose, CA, United States). β-Actin was used as loading control. Measurements were repeated three times for each experiment. Band intensity was analyzed using the Image-J software (Fu et al., 2017; Lei et al., 2017; Qiu et al., 2021).

Statistical Analysis

Statistical analysis was performed by using the GraphPad Prism 7 (GraphPad Software, San Jose, CA, United States). Experimental data were analyzed by Student's *t*-test or one-way analysis of variance (ANOVA) followed by Bonferroni correction. *P*-value less than 0.05 was considered statistically significant. All data are presented as the mean ± standard deviation.

Results

Leber's hereditary optic neuropathy-fibroblasts presented mitochondrial dysfunction, oxidative stress, inflammatory response, and increased apoptosis

LHON-WJ was a 28-year-old male carrying mutation m.11778G > A. His BCVA was 0.25 in the right and 0.20 in the left eye. LHON-MZT, aged 31 years old, had BCVA of 0.02 in both eyes and carried LHON associated mutations m.11778G > A, m.10398A > G, and m.4833A > G. SS-OCT revealed the retinal nerve fiber layer decreased in both cases.

As measured by the Seahorse XFe96 extracellular flux analyzer and microplate reader, LHON-iFBs from both patients had considerably lower OCR, particularly for maximal respiration (**Figures 1A,B**, $n = 3$), and ATP level (**Figure 1C**, $n = 4$) as compared to control-iFB. JC-1 fluorescence images and quantitative analysis revealed that LHON-iFBs

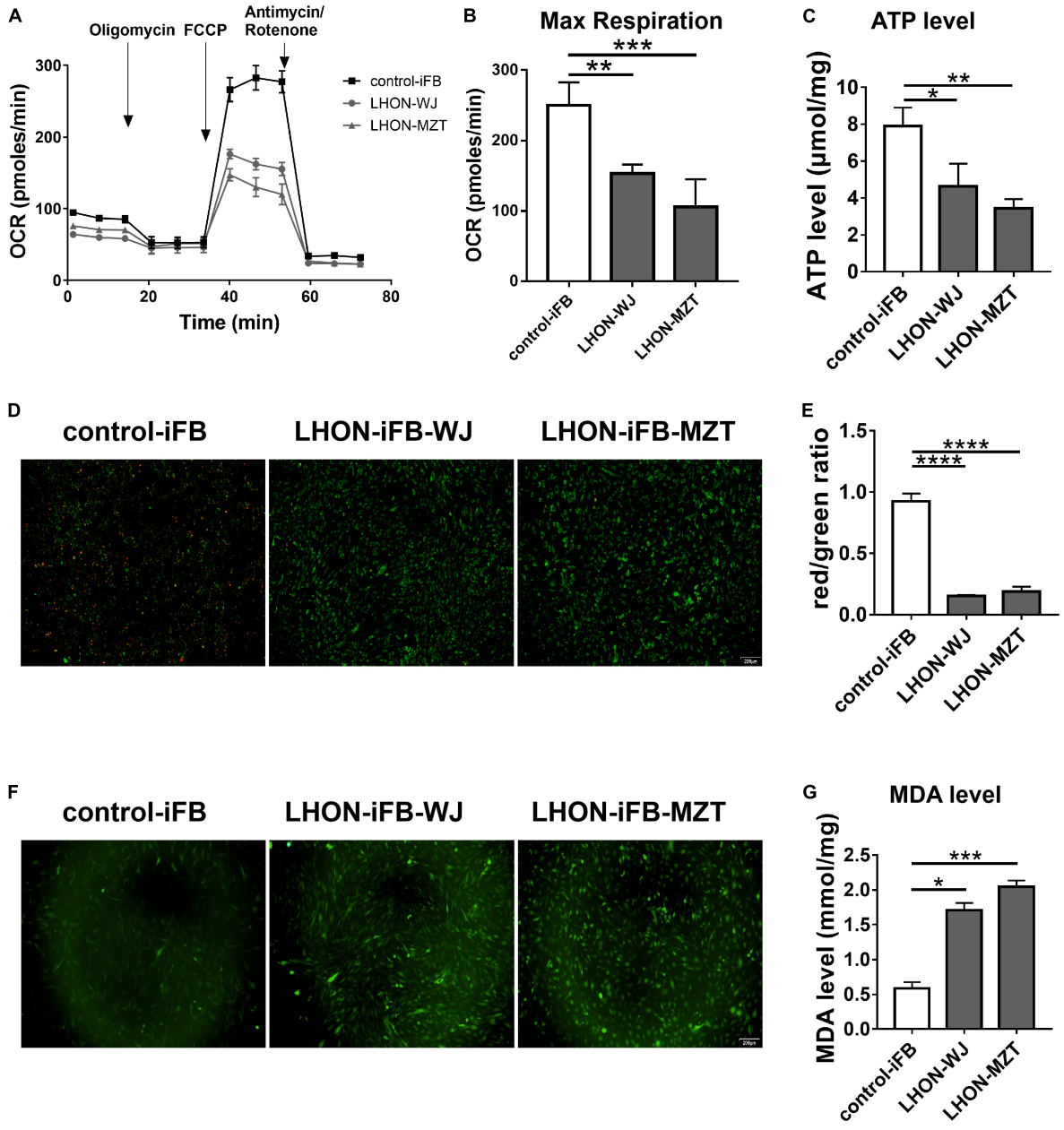

FIGURE 1
LHON-iFBs presented mitochondrial dysfunction and oxidative stress. **(A,B)** OCR, **(C)** ATP level, **(D,E)** mitochondrial membrane potential, and **(F)** ROS level in LHON-iFBs and control-iFB were measured immediately after samples were prepared from each group. **(G)** The level of MDA in fibroblasts were detected, respectively. The results (mean ± SD) were statistically significant (*$p < 0.05$, **$p < 0.01$, ***$p < 0.001$, ****$p < 0.0001$, $n = 3–5$) by using one-way ANOVA with Bonferroni correction, and the assays were performed three times.

displayed higher green fluorescence intensity, but much weaker red fluorescence intensity than the control-iFB, indicating a significant drop of mitochondrial membrane potential (Figures 1D,E, $n = 4$). These results indicated mitochondrial dysfunction in both LHON-iFBs.

ROS and MDA measurements were performed in LHON-iFBs to assess oxidative stress. ROS level was detected by the DCFH-DA fluorescent probe. The averaged fluorescent intensity in the LHON fibroblast cell lines was higher than that in control fibroblasts (Figure 1F, $n = 4$), indicating overproduction of ROS in LHON fibroblasts. In addition, MDA, a product of lipid peroxidation, in LHON-iFBs were higher than in control-iFB (Figure 1G, $n = 5$). These results suggested that LHON-iFBs were at a higher status of oxidative stress.

Western blot revealed that the ratio of p-IκBα to IκBα protein, and the expression of IL-6 increased significantly

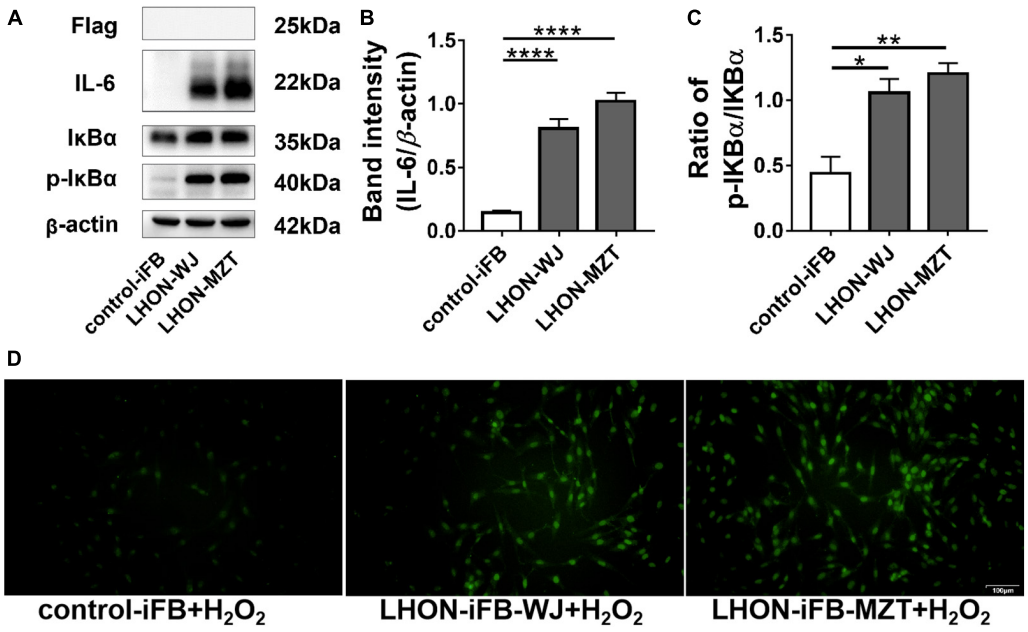

FIGURE 2
LHON-iFBs presented inflammatory response and increased apoptosis. Western blot showed that **(A,B)** protein levels of IL-6 and **(A,C)** the ratio of p-IκBα to IκBα were upregulated robustly in LHON-iFB compared to control-iFB. **(D)** TUNEL assay was performed in LHON-iFBs and control-iFB treated with same concentration of hydrogen peroxide for 12 h. The results (mean ± SD) were statistically significant (*$p < 0.05$, **$p < 0.01$, ****$p < 0.0001$, $n = 3–4$) by using one-way ANOVA with Bonferroni correction, and the assays were performed three times.

in LHON-iFBs compared to the control-iFB, indicating that phosphorylation of IκBα and the secretion of the inflammatory cytokine were upregulated in LHON-iFBs (Figures 2A–C, $n = 4$). The fibroblasts from LHON patients presented higher inflammatory response.

To explore the apoptosis status in LHON-iFBs, we performed the TUNEL assay. Hydrogen peroxide treatment was used to induce apoptosis before measurements (Miyoshi et al., 2006; Cerella et al., 2009; Fan et al., 2020). TUNEL-positive cells (indicating apoptosis) were much more in LHON-iFBs as compared with control-iFB (Figure 2D, $n = 3$), demonstrating cells bearing mtDNA mutation were more susceptible to the insult.

Exogenous superoxide dismutase 2 protected Leber's hereditary optic neuropathy-fibroblasts by ameliorating oxidative stress, mitochondrial dysfunction, inflammatory response and apoptosis

Next, we assessed the protective effects of exogenous SOD2. Firstly, we confirmed the overexpression of SOD2 mediated by plasmid (Figure 3A, $n = 3$). Subsequently, we found that compared with cells treated with negative control plasmid, LHON-iFBs transfected with SOD2 showed significantly decreased ROS (Figure 3B, $n = 4$) and MDA level (Figure 3C, $n = 5$), suggesting SOD2 suppressed oxidative stress in LHON fibroblasts.

Mitochondrial energy metabolism analysis showed the OCR, particularly maximal respiration (Figures 3D,E, $n = 3$), and ATP levels (Figure 3F, $n = 3$) were significantly increased in the SOD2 treated group when compared with the negative control group. JC-1 fluorescence revealed that the SOD2 group displayed weaker green fluorescence intensity and stronger red fluorescence intensity than the negative control group, indicating SOD2 ameliorated the decrease of mitochondrial membrane potential (Figure 3G, $n = 5$). SOD2 protected mitochondrial dysfunction in LHON fibroblasts.

In addition, LHON-iFB group transfected with SOD2 displayed decreased ratio of p-IκBα to IκBα protein and the level of IL-6 (Figures 4A–C, $n = 4$), which indicated that SOD2 downregulated the phosphorylation of IκBα and the secretion of inflammatory cytokines IL-6.

LHON-iFBs were transfected with SOD2 plasmid or negative control plasmid for 48 h, respectively, before exposure to hydrogen peroxide for 12 h. LHON fibroblasts overexpressed with exogenous SOD2 displayed weaker fluorescence of apoptosis marker than the negative control group (Figure 4D, $n = 3$). SOD2 reduced hydrogen peroxide-induced apoptosis in LHON-iFBs.

Superoxide dismutase 2 prevented hydrogen peroxide induced oxidative stress, mitochondrial dysfunction and apoptosis in human primary retinal pigmental epithelium and SH-SY5Y cells

To further confirm the protective effects of SOD2 in neurons, we repeated hydrogen peroxide-induced oxidative stress in other two cell models. Primary human retinal pigment epitheliums (hRPE) and human neuroblastoma cells (SH-SY5Y) were transfected with SOD2 or negative control plasmids for 48 h, respectively, before exposure to hydrogen peroxide for 12 h. SOD2 overexpressed substantially in gene transfected hRPE and SH-SY5Y cells (**Figure 5A**, $n = 5$).

Compared with the control group, SOD2 significantly decreased ROS (**Figure 5B**, $n = 3$) and MDA levels (**Figure 5C**, $n = 5$) in hRPE and SH-SY5Y cells treated with hydrogen peroxide.

Then we examined the effects of SOD2 on mitochondrial membrane potential and ATP levels in hRPE and SH-SY5Y cells underwent oxidative stress. In concert with the above findings, weaker green fluorescence intensity and stronger red fluorescence intensity was evident in the SOD2 group than the negative control group, which meant higher membrane potentials (**Figure 5D**, $n = 3$). Similarly, the level of ATP (**Figure 5E**, $n = 4$) was higher in the SOD2 treated group. These data indicated that hydrogen peroxide induced mitochondrial dysfunction in hRPE and SH-SY5Y cells was alleviated by exogenous SOD2.

Hydrogen peroxide (400 μM/2 h) increased TUNEL-positive cells as compared with the PBS treated hRPE and SH-SY5Y cells. However, cells transfected with SOD2 exhibited weaker staining (**Figure 5F**, $n = 3$). SOD2 reduced hydrogen peroxide-induced apoptosis in hRPE and SH-SY5Y cells.

Discussion

The majority of LHON pathogenic mutations affect a single subunit of mitochondrial complex I (mitochondrial NADH dehydrogenase), causing dysfunction of electron transport chain. Complex I is the largest and most intricate mitochondrial OXPHOS complexes. It is comprised of 45 subunits, 7 (ND-1, −2, −3, −4, −4L, −5, and −6) of which are coded by the mtDNA (Hirst, 2009). Complex I transfers electrons from NADH to ubiquinone, and the energy release is coupled to proton translocations, which contributes to the generation and maintenance of membrane potential (DiMauro et al., 2013). LHON mutations variably affect Complex I, ultimately resulting in energetic deficiency and redox imbalance (Yu-Wai-Man et al., 2011).

In a damaged respiratory chain, electrons overflow and react with molecular oxygen, and eventually lead to the generation of ROS. Excessive ROS production may damage the respiratory subunits and other mitochondrial enzymes, causes lipid membrane peroxidation and apoptosis. These effects lead to cell energy failure and cell death (Yu-Wai-Man et al., 2011; DiMauro et al., 2013).

Recently, Rovcanin et al. (2021) reported increased oxidative stress level in the plasma of LHON patients. Investigations in mouse and transmitochondrial cytoplasmic hybrid (cybrid) model showed similar features resembling LHON, indicating oxidative stress played a critical role in the pathophysiology of LHON (Brown et al., 2000; Lin et al., 2012). On the other hand, previous studies have tested the therapeutic effects in LHON patients and several models. It was suggested that antioxidants including SOD2, coenzyme Q10, idebenone, and EPI-743 could reduce oxidative stress in this condition (Jurkute et al., 2019). In LHON cybrid cell model, estrogens reduced ROS production and apoptosis by activating mitochondrial biosynthesis and improving the metabolic defect (Giordano et al., 2011).

Retinal ganglion cells (RGC) are the main target of LHON, which are not accessible for experiment (Zhang et al., 2010). Various alternative strategies have been developed for LHON research due to the lack of access to RGCs. At present, iPS-RGC cells are a favored emerging cell model (Peron et al., 2020; Harvey et al., 2022; Singh et al., 2022). Fibroblasts have been induced into RGC-like cells by reprogramming of factors stimulation (Peron et al., 2020) or Sendai virus infection (Wu et al., 2018) and these cells present mitochondrial damage phenotype (Wu et al., 2018; Yang et al., 2020). This strategy allows us to obtain a cell model similar to optic nerve tissue for study. However, some limitations still exist. For example, the clone number was insufficient after differentiation due to immature technology (Peron et al., 2021), and mutated mtDNA might be missed in partial RGCs differentiated from iPSC{Peron, 2021 #79}. Skin-derived fibroblasts are a proven alternative cell model (Jankauskaite et al., 2017). As cells do not undergo differentiation processes, the genetic background is more stable. And fibroblasts have the advantages of easy obtaining and culture. Although fibroblasts cannot used for the study of axon degeneration and neural signaling, multiple studies demonstrated that they can be used as a valuable strategy for studying mitochondrial impairment in neurological disorders (Olesen et al., 2022). In addition, our previous study (Yao et al., 2022) and the current manuscript have proved that fibroblasts could reflect some cellular phenotypes of RGC cells with LHON, such as energy metabolism, mitochondrial dysfunction, and oxidative stress, which was consistent with iPSC. Therefore, in this study, we conducted LHON patients' skin derived fibroblasts for the study of mitochondria function and inflammation. Nevertheless, iPS cell is still a cell model of significant potential in the future with its unique advantages.

10.3389/fnins.2022.917348

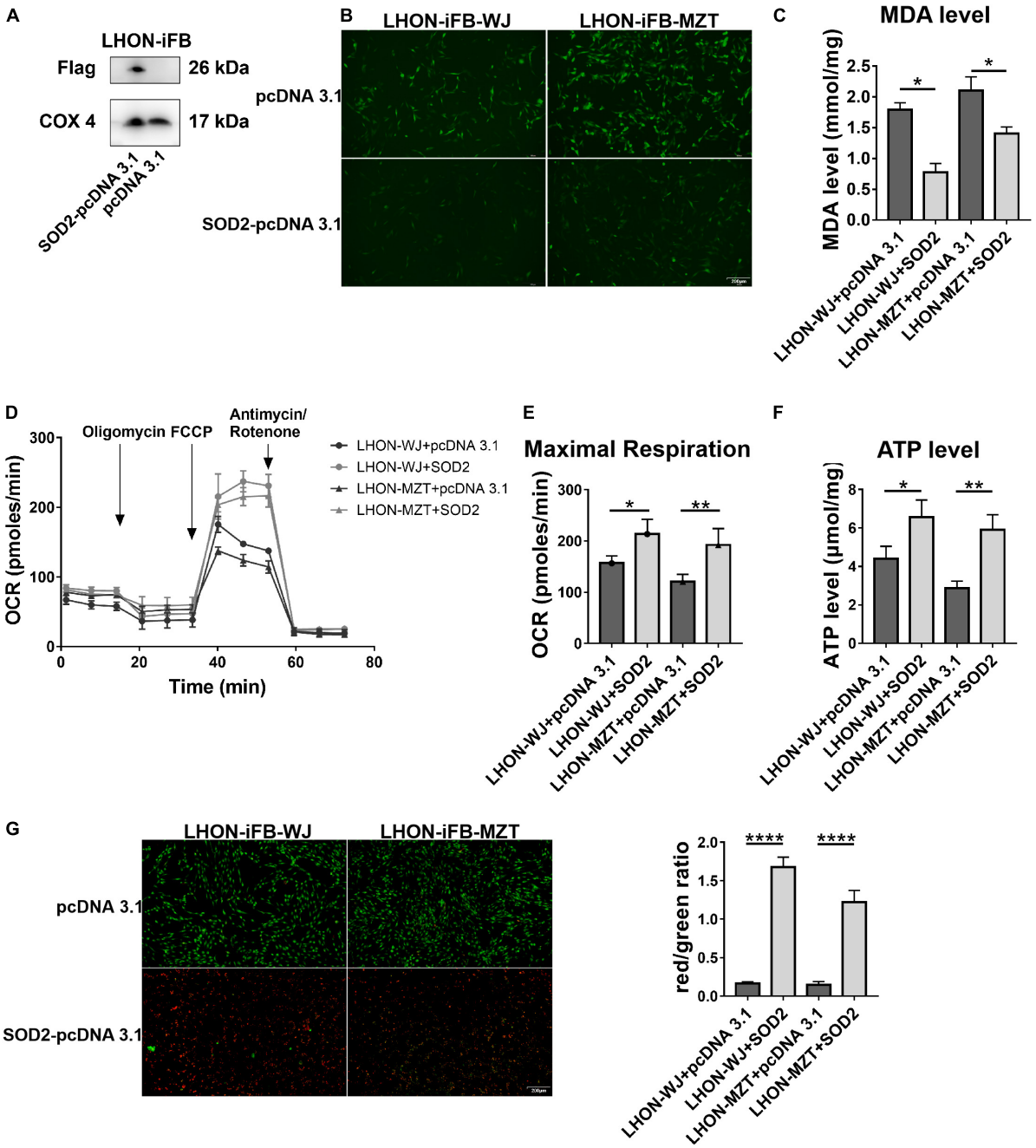

FIGURE 3
Protective effects of SOD2 on oxidative stress and mitochondrial dysfunction in LHON-iFBs. **(A)** The protein levels of exogenous SOD2 in mitochondria were detected by Western blot. The **(B)** ROS level, **(C)** MDA level, **(D,E)** OCR, and **(F)** ATP level in LHON-iFBs were measured immediately after samples were prepared from each group. **(G)** Representative fluorescence intensity images and red/green ratio of JC-1 fluorescence and from mitochondria in each group. The results (mean ± SD) were statistically significant (*$p < 0.05$, **$p < 0.01$, ****$p < 0.0001$, $n = 3–5$) by using one-way ANOVA with Bonferroni correction, and the assays were performed three times.

We constructed immortalized skin fibroblasts LHON-iFB derived from severe LHON patients. These cells presented mitochondrial dysfunction, oxidative stress and NF-κB associated inflammatory response. We further showed that SOD2 ameliorated oxidative stress, mitochondrial dysfunction, inflammatory response, and apoptosis in the LHON-iFBs. To further prove the protective effects of SOD2, we constructed additional oxidative stress cell models. Overexpression of SOD2 alleviated oxidative stress, mitochondrial dysfunction and apoptosis in hRPE and SH-SY5Y cells exposed to

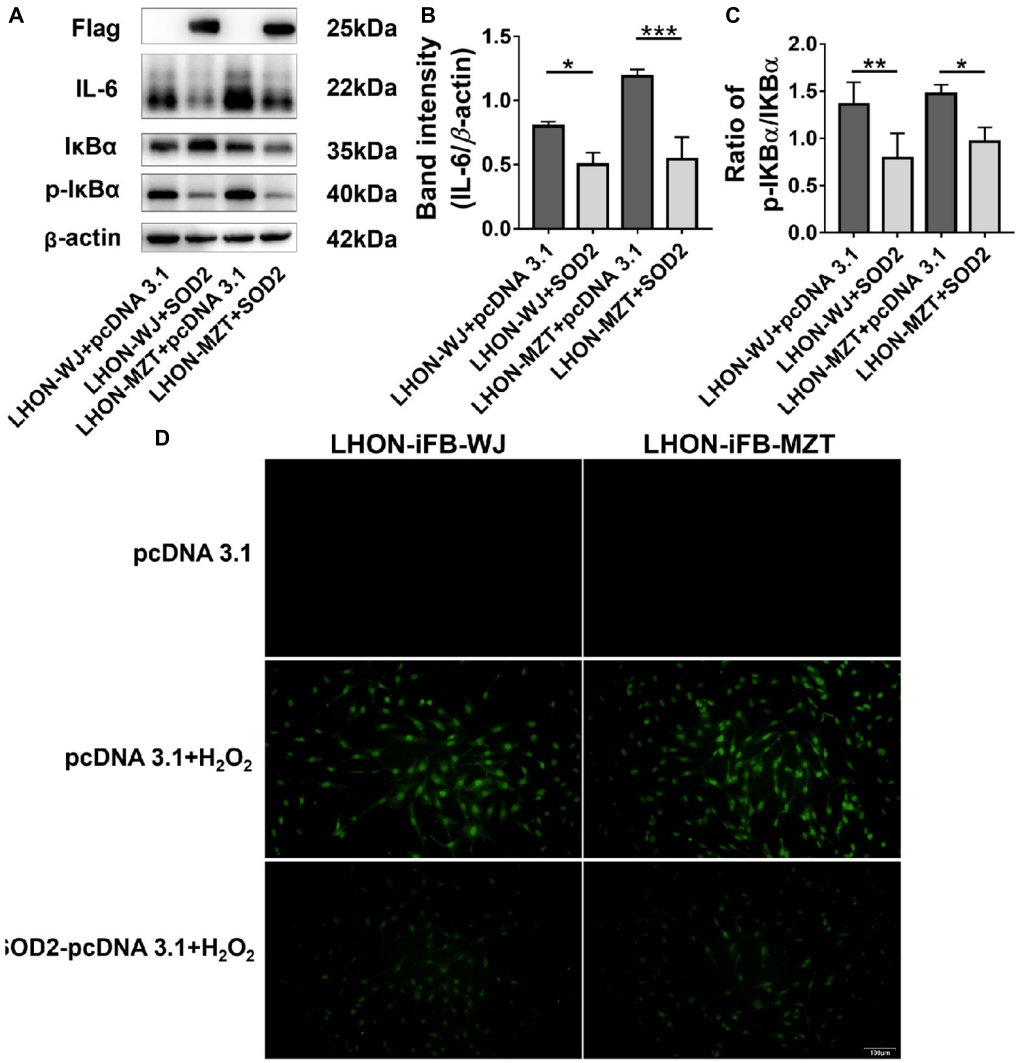

FIGURE 4
Protective effects of SOD2 on inflammatory response and apoptosis in LHON-iFBs. Western blot showed that **(A,B)** protein levels of IL-6 and **(A,C)** the ratio of p-IκBα to IκBα were inhibited by SOD2 significantly in LHON-iFBs transfected with SOD2 plasmid. **(D)** TUNEL staining demonstrated cell apoptosis in LHON-iFBs transfected with SOD2 plasmid or negative control plasmid for 48 h, respectively, before exposure to hydrogen peroxide for 12 h. The results (mean ± SD) were statistically significant (*$p < 0.05$, **$p < 0.01$, ***$p < 0.001$, $n = 3–4$) by using one-way ANOVA with Bonferroni correction, and the assays were performed three times.

hydrogen peroxide. These data further supported the protective effects of SOD2.

A large number of studies have demonstrated that inflammatory response plays a critical role in neurodegenerative disorders (Glass et al., 2010; van Horssen et al., 2019). However, reports that inflammatory response is involved in the pathophysiology of LHON are limited. We observed that the ratio of p-IκBα to IκBα protein and the level of IL-6 increased in LHON-iFBs. These results could be direct evidence that NF-κB associated inflammatory response were involved in LHON. However, the detailed role of inflammatory response in LHON is still unknown. As a possible interpretation, inflammatory responses might be a consequence of mitochondrial dysfunction. Released during severe injury induced by stress or infection, macromolecules damage-associated molecular patterns (DAMPs) are capable of eliciting a strong local inflammatory response (Chen and Nunez, 2010). Mitochondrion is a source of DAMPs. As such, mitochondrial dysfunction results in the release of DAMPs within the cytosol or in the extracellular environment thereby eliciting innate immune activation (Tait and Green, 2012). We speculate that energetic deficiency and redox imbalance increases mitochondrial membrane permeability and induces the release of mitochondrial components, such as mtDNA or cardiolipin, which in turn elicited inflammatory response. Inflammatory response seen in LHON models is an interesting

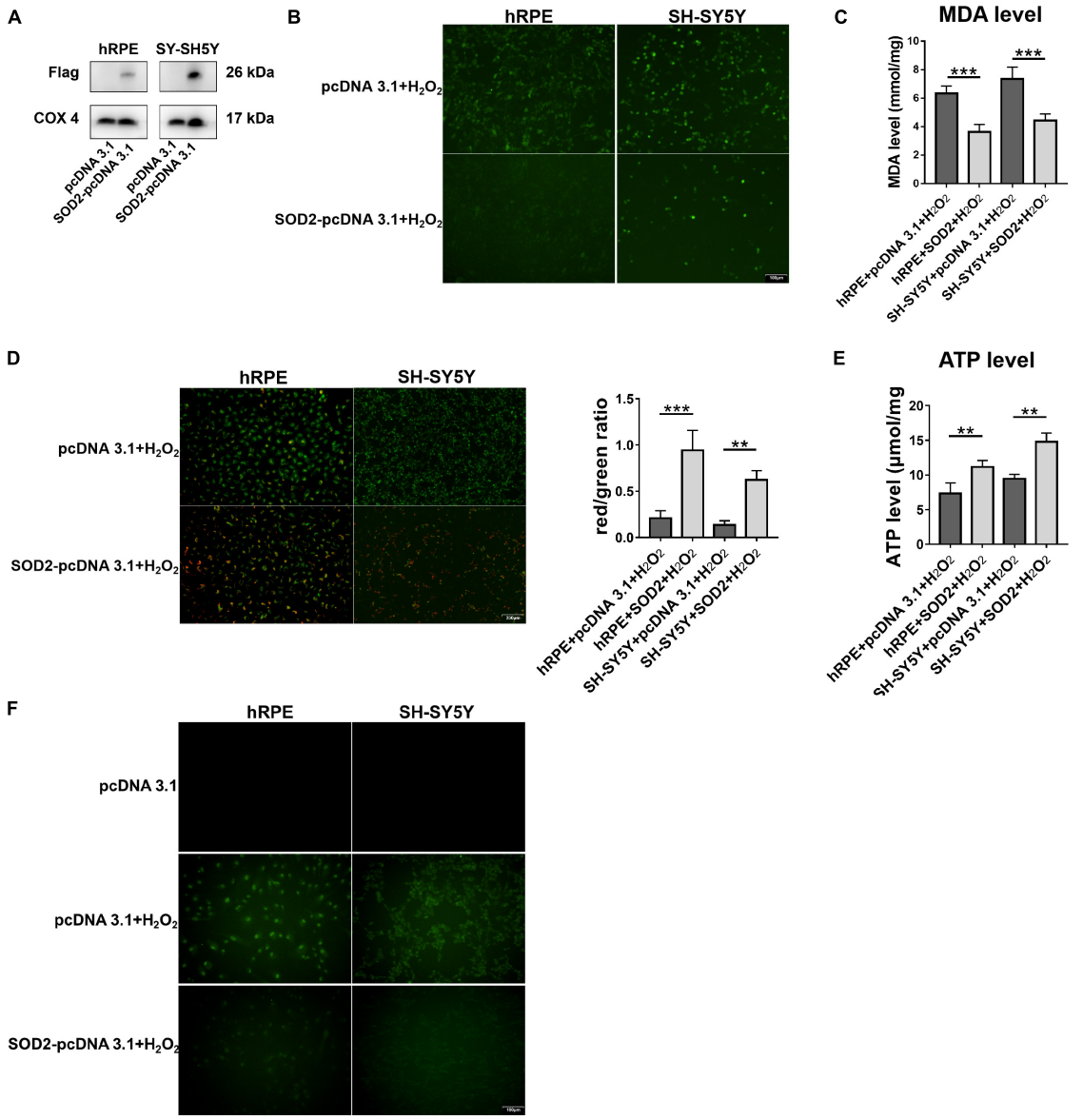

FIGURE 5
Protective effects of SOD2 on hydrogen peroxide-induced oxidative stress, mitochondrial dysfunction and cell apoptosis in hRPE and SH-SY5Y. **(A)** The protein levels of exogenous SOD2 in mitochondria were detected by Western blot. The **(B)** ROS level and **(C)** MDA level in hRPE and SH-SY5Y were measured immediately after samples were prepared from each group. **(D)** Representative fluorescence intensity images and red/green ratio of JC-1 fluorescence from mitochondria in each group. **(E)** ATP level was detected in hRPE and SH-SY5Y cells. **(F)** TUNEL staining demonstrated cell apoptosis in hRPE and SH-SY5Y. The results (mean ± SD) were statistically significant (**$p < 0.01$, ***$p < 0.001$, $n = 3–5$) by using one-way ANOVA with Bonferroni correction, and the assays were performed three times.

phenomenon. Clearly, extensive experiments are necessary to further verify it and its underlying mechanisms.

In conclusion, skin derived LHON-iFB presented some crucial pathophysiologic features of LHON including mitochondrial dysfunction, oxidative stress, inflammatory response and susceptibility to insult. Mitochondria-targeted antioxidase SOD2 ameliorated mitochondrial dysfunction by inhibiting oxidative stress and cell death. Our data further support the notion that augment of exogenous SOD2 may be a promising therapy for the treatment of LHON (Qi et al., 2007).

Conclusion

The results showed LHON-iFB presented mitochondrial dysfunction and increased ROS, suggesting the skin fibroblasts derived from the patients may be a valuable model to

study LHON. Exogenous SOD2 ameliorated mitochondrial dysfunction by inhibiting oxidative stress and preventing oxidative stress-induced cell death. The protective effects might be associated with reducing inflammatory response and inhibiting NF-κB signaling. The data further support exogenous SOD2 may be a promising therapy for the treatment of LHON.

Data availability statement

The original contributions presented in this study are included in the article/supplementary material, further inquiries can be directed to the corresponding author/s.

Ethics statement

The studies involving human participants were reviewed and approved by the Ethics Committee of Henan Eye Hospital [IRB approval number: HNEECKY-2019 (12)]. The patients/participants provided their written informed consent to participate in this study. Written informed consent was obtained from the individual(s) for the publication of any potentially identifiable images or data included in this article.

Author contributions

BL and QZ designed the study and wrote the manuscript. QZ and SY performed the experiments and analyzed the data. LL helped in performing the experiments. MY, QG, and YL collected patients' information, prepared the fibroblasts, and RPE cells. BL revised the manuscript, supervised the study, and provided financial support. All authors read and approved the final manuscript.

Funding

This research was funded by the National Natural Science Foundation of China Grant (82071008) and the Henan Key Laboratory of Ophthalmology and Vision Science.

Acknowledgments

We thank the patients and their family members for participation in this study.

Conflict of interest

The authors declare that the research was conducted in the absence of any commercial or financial relationships that could be construed as a potential conflict of interest.

Publisher's note

References

Balaban, R. S., Nemoto, S., and Finkel, T. (2005). Mitochondria, oxidants, and aging. *Cell* 120, 483–495. doi: 10.1016/j.cell.2005.02.001

Brown, M. D., Trounce, I. A., Jun, A. S., Allen, J. C., and Wallace, D. C. (2000). Functional analysis of lymphoblast and cybrid mitochondria containing the 3460, 11778, or 14484 Leber's hereditary optic neuropathy mitochondrial DNA mutation. *J. Biol. Chem.* 275, 39831–39836. doi: 10.1074/jbc.M006476200

Carelli, V., La Morgia, C., Valentino, M. L., Barboni, P., Ross-Cisneros, F. N., and Sadun, A. A. (2009). Retinal ganglion cell neurodegeneration in mitochondrial inherited disorders. *Biochim. Biophys. Acta* 1787, 518–528. doi: 10.1016/j.bbabio.2009.02.024

Cerella, C., Coppola, S., Maresca, V., De Nicola, M., Radogna, F., and Ghibelli, L. (2009). Multiple mechanisms for hydrogen peroxide-induced apoptosis. *Ann. N. Y. Acad. Sci.* 1171, 559–563. doi: 10.1111/j.1749-6632.2009.04901.x

Chao de la Barca, J. M., Simard, G., Amati-Bonneau, P., Safiedeen, Z., Prunier-Mirebeau, D., Chupin, S., et al. (2016). The metabolomic signature of Leber's hereditary optic neuropathy reveals endoplasmic reticulum stress. *Brain* 139, 2864–2876. doi: 10.1093/brain/aww222

Chen, G. Y., and Nunez, G. (2010). Sterile inflammation: sensing and reacting to damage. *Nat. Rev. Immunol.* 10, 826–837. doi: 10.1038/nri2873

DiMauro, S., Schon, E. A., Carelli, V., and Hirano, M. (2013). The clinical maze of mitochondrial neurology. *Nat. Rev. Neurol.* 9, 429–444. doi: 10.1038/nrneurol.2013.126

Dranka, B. P., Benavides, G. A., Diers, A. R., Giordano, S., Zelickson, B. R., Reily, C., et al. (2011). Assessing bioenergetic function in response to oxidative stress by metabolic profiling. *Free Radic Biol. Med.* 51, 1621–1635. doi: 10.1016/j.freeradbiomed.2011.08.005

Fan, Y., Xing, Y., Xiong, L., and Wang, J. (2020). Sestrin2 overexpression alleviates hydrogen peroxide-induced apoptosis and oxidative stress in retinal ganglion cells by enhancing Nrf2 activation via Keap1 downregulation. *Chem. Biol. Interact.* 324:109086. doi: 10.1016/j.cbi.2020.109086

Fu, X., Lin, R., Qiu, Y., Yu, P., and Lei, B. (2017). Overexpression of angiotensin-converting enzyme 2 ameliorates amyloid beta-induced inflammatory response in human primary retinal pigment epithelium. *Invest. Ophthalmol. Vis. Sci.* 58, 3018–3028. doi: 10.1167/iovs.17-21546

Giordano, C., Montopoli, M., Perli, E., Orlandi, M., Fantin, M., Ross-Cisneros, F. N., et al. (2011). Oestrogens ameliorate mitochondrial dysfunction in Leber's hereditary optic neuropathy. *Brain* 134(Pt 1), 220–234. doi: 10.1093/brain/awq276

Glass, C. K., Saijo, K., Winner, B., Marchetto, M. C., and Gage, F. H. (2010). Mechanisms underlying inflammation in neurodegeneration. *Cell* 140, 918–934. doi: 10.1016/j.cell.2010.02.016

Harvey, J. P., Sladen, P. E., Yu-Wai-Man, P., and Cheetham, M. E. (2022). Induced pluripotent stem cells for inherited optic neuropathies-disease modeling and therapeutic development. *J. Neuroophthalmol.* 42, 35–44. doi: 10.1097/WNO.0000000000001375

Hayashi, G., and Cortopassi, G. (2015). Oxidative stress in inherited mitochondrial diseases. *Free Radic Biol. Med.* 88(Pt A), 10–17. doi: 10.1016/j.freeradbiomed.2015.05.039

Hernandez-Saavedra, D., Zhou, H., and McCord, J. M. (2005). Anti-inflammatory properties of a chimeric recombinant superoxide dismutase: SOD2/3. *Biomed. Pharmacother.* 59, 204–208. doi: 10.1016/j.biopha.2005.03.001

Hirst, J. (2009). Towards the molecular mechanism of respiratory complex I. *Biochem. J.* 425, 327–339. doi: 10.1042/BJ20091382

Islam, M. T. (2017). Oxidative stress and mitochondrial dysfunction-linked neurodegenerative disorders. *Neurol. Res.* 39, 73–82. doi: 10.1080/01616412.2016.1251711

Jankauskaite, E., Bartnik, E., and Kodron, A. (2017). Investigating Leber's hereditary optic neuropathy: cell models and future perspectives. *Mitochondrion* 32, 19–26. doi: 10.1016/j.mito.2016.11.006

Jin, X., Liu, J., Wang, W., Li, J., Liu, G., Qiu, R., et al. (2022). Identification of age-associated proteins and functional alterations in human retinal pigment epithelium. *Genom. Proteom. Bioinform.* Online ahead of print. doi: 10.1016/j.gpb.2022.06.001

Jurkute, N., Harvey, J., and Yu-Wai-Man, P. (2019). Treatment strategies for Leber hereditary optic neuropathy. *Curr. Opin. Neurol.* 32, 99–104. doi: 10.1097/WCO.0000000000000646

Kausar, S., Wang, F., and Cui, H. (2018). The role of mitochondria in reactive oxygen species generation and its implications for neurodegenerative diseases. *Cells* 7:274. doi: 10.3390/cells7120274

Kwon, M. J., Han, J., Kim, B. H., Lee, Y. S., and Kim, T. Y. (2012). Superoxide dismutase 3 suppresses hyaluronic acid fragments mediated skin inflammation by inhibition of toll-like receptor 4 signaling pathway: superoxide dismutase 3 inhibits reactive oxygen species-induced trafficking of toll-like receptor 4 to lipid rafts. *Antioxid. Redox. Signal.* 16, 297–313. doi: 10.1089/ars.2011.4066

Lei, C., Lin, R., Wang, J., Tao, L., Fu, X., Qiu, Y., et al. (2017). Amelioration of amyloid beta-induced retinal inflammatory responses by a LXR agonist TO901317 is associated with inhibition of the NF-kappaB signaling and NLRP3 inflammasome. *Neuroscience* 360, 48–60. doi: 10.1016/j.neuroscience.2017.07.053

Lin, C. S., Sharpley, M. S., Fan, W., Waymire, K. G., Sadun, A. A., Carelli, V., et al. (2012). Mouse mtDNA mutant model of Leber hereditary optic neuropathy. *Proc. Natl. Acad. Sci. U S A.* 109, 20065–20070. doi: 10.1073/pnas.1217113109

Liskova, A., Samec, M., Koklesova, L., Kudela, E., Kubatka, P., and Golubnitschaja, O. (2021). Mitochondriopathies as a clue to systemic disorders-analytical tools and mitigating measures in context of predictive. preventive, and personalized (3p) medicine. *Int. J. Mol. Sci.* 22:2007. doi: 10.3390/ijms22042007

Lopez Sanchez, M. I., Crowston, J. G., Mackey, D. A., and Trounce, I. A. (2016). Emerging mitochondrial therapeutic targets in optic neuropathies. *Pharmacol. Ther.* 165, 132–152. doi: 10.1016/j.pharmthera.2016.06.004

Lopez Sanchez, M. I. G., Van Bergen, N. J., Kearns, L. S., Ziemann, M., Liang, H., Hewitt, A. W., et al. (2020). OXPHOS bioenergetic compensation does not explain disease penetrance in Leber hereditary optic neuropathy. *Mitochondrion* 54, 113–121. doi: 10.1016/j.mito.2020.07.003

Miyoshi, N., Oubrahim, H., Chock, P. B., and Stadtman, E. R. (2006). Age-dependent cell death and the role of ATP in hydrogen peroxide-induced apoptosis and necrosis. *Proc. Natl. Acad. Sci. U S A.* 103, 1727–1731. doi: 10.1073/pnas.0510346103

Morvan, D., and Demidem, A. (2018). NMR metabolomics of fibroblasts with inherited mitochondrial complex I mutation reveals treatment-reversible lipid and amino acid metabolism alterations. *Metabolomics* 14:55. doi: 10.1007/s11306-018-1345-1349

Nguyen, N. H., Tran, G. B., and Nguyen, C. T. (2020). Anti-oxidative effects of superoxide dismutase 3 on inflammatory diseases. *J. Mol. Med.* 98, 59–69. doi: 10.1007/s00109-019-01845-1842

Olesen, M. A., Villavicencio-Tejo, F., and Quintanilla, R. A. (2022). The use of fibroblasts as a valuable strategy for studying mitochondrial impairment in neurological disorders. *Transl. Neurodegener.* 11:36. doi: 10.1186/s40035-022-00308-y

Peron, C., Maresca, A., Cavaliere, A., Iannielli, A., Broccoli, V., Carelli, V., et al. (2021). Exploiting hiPSCs in leber's hereditary optic neuropathy (LHON): present achievements and future perspectives. *Front. Neurol.* 12:648916. doi: 10.3389/fneur.2021.648916

Peron, C., Mauceri, R., Cabassi, T., Segnali, A., Maresca, A., Iannielli, A., et al. (2020). Generation of a human iPSC line, FINCBi001-A, carrying a homoplasmic m.G3460A mutation in MT-ND1 associated with Leber's Hereditary optic Neuropathy (LHON). *Stem Cell Res.* 48:101939. doi: 10.1016/j.scr.2020.101939

Qi, X., Sun, L., Hauswirth, W. W., Lewin, A. S., and Guy, J. (2007). Use of mitochondrial antioxidant defenses for rescue of cells with a Leber hereditary optic neuropathy-causing mutation. *Arch. Ophthalmol.* 125, 268–272. doi: 10.1001/archopht.125.2.268

Qiu, R., Yang, M., Wang, W., Liu, J., Yang, L., and Lei, B. (2021). The protective effects of VVN001 on LPS-Induced inflammatory responses in human RPE cells and in a mouse model of EIU. *Inflammation* 44, 780–794. doi: 10.1007/s10753-020-01377-1379

Rosa, A. C., Bruni, N., Meineri, G., Corsi, D., Cavi, N., Gastaldi, D., et al. (2021). Strategies to expand the therapeutic potential of superoxide dismutase by exploiting delivery approaches. *Int. J. Biol. Macromol.* 168, 846–865. doi: 10.1016/j.ijbiomac.2020.11.149

Rovcanin, B., Jancic, J., Pajic, J., Rovcanin, M., Samardzic, J., Djuric, V., et al. (2021). Oxidative stress profile in genetically confirmed cases of leber's hereditary optic neuropathy. *J. Mol. Neurosci.* 71, 1070–1081. doi: 10.1007/s12031-020-01729-y

Sarewicz, M., Borek, A., Cieluch, E., Swierczek, M., and Osyczka, A. (2010). Discrimination between two possible reaction sequences that create potential risk of generation of deleterious radicals by cytochrome bc(1). Implications for the mechanism of superoxide production. *Biochim. Biophys. Acta* 1797, 1820–1827. doi: 10.1016/j.bbabio.2010.07.005

Schofield, J. H., and Schafer, Z. T. (2021). Mitochondrial reactive oxygen species and mitophagy: a complex and nuanced relationship. *Antioxid. Redox. Signal.* 34, 517–530. doi: 10.1089/ars.2020.8058

Sheng, Y., Abreu, I. A., Cabelli, D. E., Maroney, M. J., Miller, A. F., Teixeira, M., et al. (2014). Superoxide dismutases and superoxide reductases. *Chem. Rev.* 114, 3854–3918. doi: 10.1021/cr4005296

Singh, A., Kukreti, R., Saso, L., and Kukreti, S. (2019). Oxidative stress: a key modulator in neurodegenerative diseases. *Molecules* 24:1583. doi: 10.3390/molecules24081583

Singh, P., Bahr, T., Zhao, X., Hu, P., Daadi, M., Huang, T., et al. (2022). Creating cell model 2.0 using patient samples carrying a pathogenic mitochondrial DNA mutation: iPSC approach for LHON. *Methods Mol. Biol.* 2549, 219–231. doi: 10.1007/7651_2021_384

Tait, S. W., and Green, D. R. (2012). Mitochondria and cell signalling. *J. Cell Sci.* 125(Pt 4), 807–815. doi: 10.1242/jcs.099234

van Horssen, J., van Schaik, P., and Witte, M. (2019). Inflammation and mitochondrial dysfunction: a vicious circle in neurodegenerative disorders? *Neurosci. Lett.* 710:132931. doi: 10.1016/j.neulet.2017.06.050

Wu, Y. R., Wang, A. G., Chen, Y. T., Yarmishyn, A. A., Buddhakosai, W., Yang, T. C., et al. (2018). Bioactivity and gene expression profiles of hiPSC-generated retinal ganglion cells in MT-ND4 mutated Leber's hereditary optic neuropathy. *Exp. Cell Res.* 363, 299–309. doi: 10.1016/j.yexcr.2018.01.020

Yang, T. C., Yarmishyn, A. A., Yang, Y. P., Lu, P. C., Chou, S. J., Wang, M. L., et al. (2020). Mitochondrial transport mediates survival of retinal ganglion cells in affected LHON patients. *Hum. Mol. Genet.* 29, 1454–1464. doi: 10.1093/hmg/ddaa063

Yao, S., Zhou, Q., Yang, M., Li, Y., Jin, X., Guo, Q., et al. (2022). Multi-mtDNA variants may be a factor contributing to mitochondrial function variety in the skin-derived fibroblasts of leber's hereditary optic neuropathy patients. *Front. Mol. Neurosci.* 15:920221. doi: 10.3389/fnmol.2022.920221

Yen, M. Y., Wang, A. G., and Wei, Y. H. (2006). Leber's hereditary optic neuropathy: a multifactorial disease. *Prog. Retin. Eye Res.* 25, 381–396. doi: 10.1016/j.preteyeres.2006.05.002

Yu-Wai-Man, P., Griffiths, P. G., and Chinnery, P. F. (2011). Mitochondrial optic neuropathies - disease mechanisms and therapeutic strategies. *Prog. Retin. Eye Res.* 30, 81–114. doi: 10.1016/j.preteyeres.2010.11.002

Zhang, X. M., Li Liu, D. T., Chiang, S. W., Choy, K. W., Pang, C. P., Lam, D. S., et al. (2010). Immunopanning purification and long-term culture of human retinal ganglion cells. *Mol. Vis.* 16, 2867–2872.

Zhou, L., Chan, J. C. Y., Chupin, S., Gueguen, N., Desquiret-Dumas, V., Koh, S. K., et al. (2020). Increased Protein S-Glutathionylation in Leber's Hereditary Optic Neuropathy (LHON). *Int. J. Mol. Sci.* 21:3027. doi: 10.3390/ijms21083027

frontiers | Frontiers in Neuroscience

TYPE Original Research
PUBLISHED 30 August 2022
DOI 10.3389/fnins.2022.951491

OPEN ACCESS

EDITED BY
Arumugam R. Jayakumar,
University of Miami, United States

REVIEWED BY
Riccardo Carlo Natoli,
Australian National University, Australia
Jerry Lorren Dominic,
Jackson Memorial Hospital,
United States

*CORRESPONDENCE
Shunzong Yuan
yuanshunzong@126.com
Guang-Hua Peng
ghp@zzu.edu.cn

†These authors have contributed equally to this work

SPECIALTY SECTION
This article was submitted to Neurodegeneration, a section of the journal Frontiers in Neuroscience

RECEIVED 24 May 2022
ACCEPTED 26 July 2022
PUBLISHED 30 August 2022

CITATION
Wang S, Du L, Yuan S and Peng G-H (2022) Complement C3a receptor inactivation attenuates retinal degeneration induced by oxidative damage.
Front. Neurosci. 16:951491.
doi: 10.3389/fnins.2022.951491

Complement C3a receptor inactivation attenuates retinal degeneration induced by oxidative damage

Shaojun Wang[2†], Lu Du[2†], Shunzong Yuan[3*] and Guang-Hua Peng[1,4*]

[1]Laboratory of Visual Cell Differentiation and Regulation, Basic Medical College, Zhengzhou University, Zhengzhou, China, [2]Senior Department of Ophthalmology, Chinese People's Liberation Army (PLA) General Hospital, Beijing, China, [3]Department of Lymphoma, Head and Neck Cancer, The Fifth Medical Center, Chinese People's Liberation Army (PLA) General Hospital (Former 307th Hospital of the PLA), Beijing, China, [4]Department of Pathophysiology, Basic Medical College, Zhengzhou University, Zhengzhou, China

Retinal degeneration causes vision loss and threatens the health of elderly individuals worldwide. Evidence indicates that the activation of the complement system is associated with retinal degeneration. However, the mechanism of complement signaling in retinal degeneration needs to be further studied. In this study, we show that the expression of C3 and C3a receptor (C3ar1) is positively associated with the inflammatory response and retinal degeneration. Genetic deletion of C3 and pharmacological inhibition of C3ar1 resulted in the alleviation of neuroinflammation, prevention of photoreceptor cell apoptosis and restoration of visual function. RNA sequencing (RNA-seq) identified a C3ar1-dependent network shown to regulate microglial activation and astrocyte gliosis formation. Mechanistically, we found that STAT3 functioned downstream of the C3-C3ar1 pathway and that the C3ar1-STAT3 pathway functionally mediated the immune response and photoreceptor cell degeneration in response to oxidative stress. These findings reveal an important role of C3ar1 in oxidative-induced retinal degeneration and suggest that intervention of the C3ar1 pathway may alleviate retinal degeneration.

KEYWORDS

complement C3, C3a receptor (C3ar1), retinal degeneration, apoptosis, microglia

Introduction

Retinal degeneration threatens the vision of elderly people around the world due to the gradual degeneration of photoreceptor cells that leads to complete blindness (Handa et al., 2019). Unfortunately, no effective treatments are available for retinal degeneration (Wong et al., 2014). Retinal degeneration is often accompanied by microglial cell

activation and elevated levels of inflammatory cytokines as well as photoreceptor cell loss and retinal structure destruction (Ambati and Fowler, 2012; Menon et al., 2019; Voigt et al., 2019; Mulfaul et al., 2020; Orozco et al., 2020). These studies strongly suggest that the innate immune response plays an important role in retinal degeneration.

The complement system is a major component of the innate immune system and plays a key role in retinal development and homeostasis (Ricklin et al., 2016; Liszewski et al., 2017; Akhtar-Schafer et al., 2018). Studies have found elevated expression and deposition of C3 in damaged retinas (Chi et al., 2010; Stephan et al., 2012; Ramos de Carvalho et al., 2013; Linetsky et al., 2018). C3 activation is crucial for triggering immune responses causing retinal diseases (van Lookeren Campagne et al., 2016; Mohlin et al., 2017; Enzbrenner et al., 2021). During the activation of the classical complement pathway, C3 is cleaved into two fragments, C3a and C3b, which bind to the corresponding receptors to thereby regulate the innate immune response. The C3b-CR3 pathway has been demonstrated to be critical for the clearance of debris by microglia after CNS injury (Norris et al., 2018). In the rd10 retina, both C3 and CR3 mediate the inflammatory response and the microglial phagocytosis of apoptotic photoreceptors (Silverman et al., 2019).

Studies have also shown that the C3b-CR3 signaling pathway is involved in development, neuropathology and the inflammatory response (Litvinchuk et al., 2018). In a mouse model of AD and epilepsy, the C3a-C3ar1 axis was found to be involved in microglial activation and astrocyte gliosis formation (Lian et al., 2016; Wei et al., 2021). In addition, blockade of the C3a/C3aR axis alleviates severe acute pancreatitis-induced intestinal barrier injury by repressing inflammatory cytokines (Ye et al., 2020). Complement is also involved in orchestrating regeneration progression, as the C3ar1 signaling pathway facilitates skeletal muscle regeneration by regulating monocyte function and trafficking (Zhang et al., 2017). C3ar1 also plays an important role in chick retinal development and regeneration (Grajales-Esquivel et al., 2017).

Although C3ar1 is involved in retinal development and neuropathy, the role of the C3-C3ar1 axis in retinal degeneration is less understood. In our study, we assessed the roles of complement C3, its receptor C3aR and the downstream effector STAT3 in the regulation of retinal degeneration in a model of sodium iodate-induced oxidative stress using various techniques, such as gene knockout, immunofluorescence, RNA sequencing (RNA-seq) and functional assays. Furthermore, we identified that the C3a-C3ar1-STAT3 axis plays an important role in mediating microglial activation and photoreceptor cell injury.

Materials and methods

Animals

All studies were carried out on 8-week-old wild-type or C3-knockout (C3-KO) C57BL/6J mice. The C3-KO C57BL/6J mice were provided by Professor Yusen Zhou (State Key Laboratory of Pathogen and Biosecurity, Beijing Institute of Microbiology and Epidemiology, Beijing 100071, China). All animals were housed in a pathogen-free, temperature-controlled animal facility on a 12/12-h light/dark cycle and fed standard food and water *ad libitum*. All of the animal protocols were approved by the Institutional Animal Care and Use Committee of the General Hospital of the Chinese People's Liberation Army and Zhengzhou University and were performed in accordance with the National Institutes of Health Guidelines for the Care and Use of Laboratory Animals (Id number:2020-ky-67). All efforts were made to reduce the number of animals used and minimize the suffering caused by experimental procedures.

Treatment with sodium iodate and tissue collection

We selected sodium iodate ($NaIO_3$) (Sigma–Aldrich, United States) for the establishment of the retinal degeneration model according to a previous publication (Xiao et al., 2017). Briefly, mice in the experimental groups were administered a single dose of 35 mg/kg $NaIO_3$ dissolved in saline *via* femoral vein injection. The mice in the control group were administered an equivalent volume of saline. The $NaIO_3$-treated and control mice (n = 6 per group) were examined by electroretinography (ERG) and multifocal electroretinography (mfERG), and their eyeballs were then collected from days 1 to 28 by enucleating the mice and immersing the eyeballs in 4% paraformaldehyde in 0.1 M phosphate buffer.

Histology and immunofluorescence

After fixation for 24 h, the anterior section of the eyes was dissected, and the remaining eye cup was dehydrated and then embedded in paraffin wax. Sections (at 5 μm) were cut on a microtome (Shandon AS325; Thermo Scientific, United States). All histologic analyses of outer nuclear layer (ONL) thickness were performed using retinal sections cut along the parasagittal plane (super inferior) as described previously (Wang et al., 2014). These sections also included the ocular nerve head to maintain regional consistency between replicates and groups. H&E staining was performed, and images

were captured with a microscope (Olympus, Japan). For each section, 18 measurements spaced 200 μm apart were made to analyze ONL damage. Three measurements were made per sample and averaged.

For immunostaining, sections were dewaxed, subjected to antigen retrieval and blocked with 10% goat serum (Sigma–Aldrich Corp.) in phosphate-buffered saline containing 0.2% Triton X-100 (Sigma–Aldrich Corp.) for 1 h before being incubated with primary antibodies in a humidity chamber overnight at 40°C. The primary antibodies were as follows: anti-complement C3, 1:300; anti-Ibal, 1:300; anti-rhodopsin, 1:600; anti-C3aR, 1:300; anti-RPE65, 1:300 and anti-pSTAT3, 1:300. All antibodies were from purchased Abcam. After washing and incubation for 1 h at room temperature with secondary antibodies, the sections were counterstained with ProLong Gold with DAPI (Invitrogen) to reveal cell nuclei. Images were obtained using an Olympus FV3000 confocal microscope and were acquired at the corresponding histologically defined areas of the sections. Schematic of the retina with a sample location was shown in **Supplementary Figure 1**. All images in each individual experiment were acquired with a fixed detection gain. Images were processed and semiquantified by using ImageJ.

Electroretinography

ERG was performed using the Espion E3 console in conjunction with the ColorDome (Diagnosys LLC). ERG experiments were carried out on C57B6 wild-type or C3-KO mice at 1 week post injection. In brief, the mice were dark-adapted the night before the recordings were performed. The animals were anesthetized by a subcutaneous injection of xylazine (15 mg/kg) and ketamine (110 mg/kg). The pupils of the mice were dilated using 1% tropicamide, and the animals were positioned on a water warming pad to prevent hypothermia. For each animal, only the right eye was examined. Active gold electrodes were placed on the right eye cornea as the recording electrodes. The reference and ground electrodes were placed subcutaneously in the mid-frontal areas of the head and tail, respectively. Light stimulation was applied at a density of 0.5 log (cd·s/m^2). The amplitudes of a- and b-waves were recorded and processed using a RETI-Port device (Roland Consult). All procedures were performed in a dark room under a dim red safety light.

TdT-UTP nick end labeling staining

TdT-UTP nick end labeling (TUNEL) assays were performed with a one-step TUNEL kit according to the manufacturer's instructions (Beyond, Shanghai). Paraffin-embedded sections and cells grown in 24-well plates treated with $NaIO_3$ were fixed. Briefly, the cells were permeabilized with 0.1% Triton X-100 for 10 min at room temperature, followed by TUNEL staining for 1 h at 37°C. The FITC-labeled TUNEL-positive cells were imaged under a fluorescence microscope at 488 nm excitation and 530 nm emission wavelengths. The cells with green fluorescence were defined as apoptotic cells.

Application of drugs

A C3aR antagonist (SB290157) and STAT3 inhibitor (SH-4–54) were purchased from Selleck (S8931 and S7337) and dissolved according to the manufacturer's instructions. Mice were pretreated with SB290157 (10 mg/kg) or SH-4-54 (10 mg/kg) 3 days before the $NaIO_3$ injection and then three treated times a week *via* i.p. injection for 1 week. After the ERG assay, the mice were sacrificed, and retinal tissue was collected for immunoassay and real-time PCR assays.

Ribonucleic acid extraction and real-time polymerase chain reaction

Total RNA was extracted, and a real-time PCR assay was conducted as previously reported (Wang et al., 2019). The primer sequences are listed below:

Gene	F	R
mC3	GAAGTACCTCATGT GGGGCC	CAGTTGGGACAA CCATAAACC
mC3aR	GGAAGCTGTGATG TCCTGG	CACACATCTGTA CTCATATTGT
mStat3	CAGAAAGTGTCCTA CAAGGGCG	CGTTGTTAGACT CCTCCATGTTC
mRhodopsin	CCCTTCTCCAACGT CACAGG	GTAGAGCGTGA GGAAGTTGATG
mRecoverin	CAATGGGACCATCA GCAAA	CCTCAGGCTTG ATCATTTTGA
mTNFα	CCCTCACACTCAGATC ATCTTCT	GCTACGACGT GGGCTACAG
mIL1β	GCAACTGTTCCTGAA CTCAACT	ATCTTTTGGG GTCCGTCAACT
mIL6	TAGTCCTTCCTACCC CAATTTCC	TTGGTCCTTAG CCACTCCTTC
mβ –actin1	CGAGAAGATGACC CAGATCATGTT	CCTCGTAGAT GGGCACAGTGT

Ribonucleic acid-seq and data analysis

First, retinal tissues were collected from normal controls and wild-type mice at 7 days after $NaIO_3$ induction, and total RNA was then extracted. The RNA-seq analysis was performed on the

Illumina NovaSeq6000 platform at a depth of 60 million read pairs per sample. Three mice from each group (total of 6 mice) were analyzed. Raw reads were first aligned to the Mus musculus genome (UCSC mm10) using HISAT2 with default parameters. Then, the htseq-count function of HTSeq was used to determine the number of aligned reads that fell under the exons of the gene (union of all the exons of the gene) to present the expression of each gene. We identified differentially expressed genes (DEGs) by using the DESeq2 package in the R environment (Love et al., 2014). Finally, Gene Ontology (GO) analysis was performed.

Statistical analysis

Statistical analysis of the two groups was performed using 2-tailed paired Student's *t*-tests assuming equal variance. The results are expressed as the mean ± SEM deviation. Differences were considered significant at $P < 0.05$.

Results

Complement C3 and C3ar1 expression correlates with retinal degeneration

To further understand the molecular mechanisms underlying oxidative stress-induced retinal degeneration, we performed RNA-seq analyses of retinal tissues from 6- to 8-week-old wild-type C57BL/6J normal control and $NaIO_3$-treated C57BL/6J mice. Using principal component analysis (PCA), we identified 659 DEGs (adjusted $p < 0.01$, cutoff for LogFC is 1.754) in mice treated with $NaIO_3$ compared to the normal controls; 567 genes were upregulated and 92 were downregulated (**Figures 1A–C**). We found that the expression levels of complement genes were changed after $NaIO_3$-induced retinal degeneration. Several complement components (C1qc, C1qa, C1qb, Itgb2, C5ar1, and C3ar1) had increased expression (**Figure 1D**). The real-time PCR results confirmed that the levels of C3 and C3ar1 were increased after $NaIO_3$ treatment (**Figures 1E,F**). Immunofluorescence staining revealed prominent C3 and C3ar1 protein expression in the injured retinas but not in those of the normal control mice (**Figures 1G–J**), which provided direct evidence of oxidative stress-induced complement activation in mouse retinal tissues.

C3ar1 controls the immune interaction network

To better determine the role of C3ar1 in retinal degeneration, we searched the STRING database and constructed the protein interaction network centered on C3ar1. Based on coexpression scores determined by RNA expression patterns and on protein coregulation determined by Proteome HD, the network included a group of genes associated with retinal degeneration that are involved in the positive regulation of apoptotic cell clearance, synapse pruning, microglial activation, immune responses and complement pathway activation (**Figure 2**). For example, V-set and immunoglobulin domain-containing protein 4 (VSIG4), which is a strong negative regulator of T-cell proliferation and IL2 production, strongly interacts and coexpresses with C3ar1. The P2X purinoceptor 7 (P2RX7) receptor, a ligand-gated ion channel that responds to ATP binding, is responsible for the ATP-dependent lysis of macrophages through the formation of membrane pores permeable to large molecules. The P2RX7 receptor functions in both fast synaptic transmission and the ATP-mediated lysis of antigen-presenting cells. Together, these bioinformatics data suggest that the activation of the C3a-C3ar1 signaling pathway contribute to retinal degeneration through regulation of the inflammatory response and immune cell activation.

Knockout of C3 and C3ar1 inactivation reduce microglial activation and the inflammatory response in mice with retinal degeneration

The immune response plays an important role in photoreceptor cell degeneration (Murakami et al., 2019). To investigate the role of the C3a-C3ar1 pathway in immune regulation and retinal degeneration, immunostaining with anti-GFAP and anti-Iba1 antibodies revealed marked increases in the fluorescence intensities of GFAP and Iba1 in retinas on day 7 after $NaIO_3$ stimulation (**Figure 3**). Strikingly, C3 deficiency and C3ar1 inhibition nearly completely normalized the GFAP and Iba1 immunoreactivity levels (**Figure 3**). To identify the retinal locus of C3 on day 7 after $NaIO_3$ induction, we performed fluorescence immunostaining with multiple antibodies, including anti-GFAP, anti-Iba1, anti-CD68 and anti-C3 antibodies (**Figures 3A,B**). C3 colocalized predominantly with $Iba1^+$ cells, indicating that microglia were activation during photoreceptor cell degeneration. Triple immunostaining of CD68, C3 and Iba1 revealed the characteristics of microglial phenotypes. Oxidative stress induced an increase in the number of CD68-positive phagocytic microglia, while C3 deficiency and C3ar1 inhibition drastically decreased the number of microglial phagocytic phenotypes. Microglia and Müller glia activation is associated with an increased production of proinflammatory cytokines. To elucidate the characteristics of the inflammatory cytokines, we performed cytokine array assays using QAM-INF-1, revealing increased levels of proinflammatory factors, including TNFα, IL1, IL6, MIP1α, IFNγ, eotaxin, and IL13 (**Figure 4A**). C3 deficiency and C3ar1 inhibition obviously downregulated the expression of these inflammatory factors.

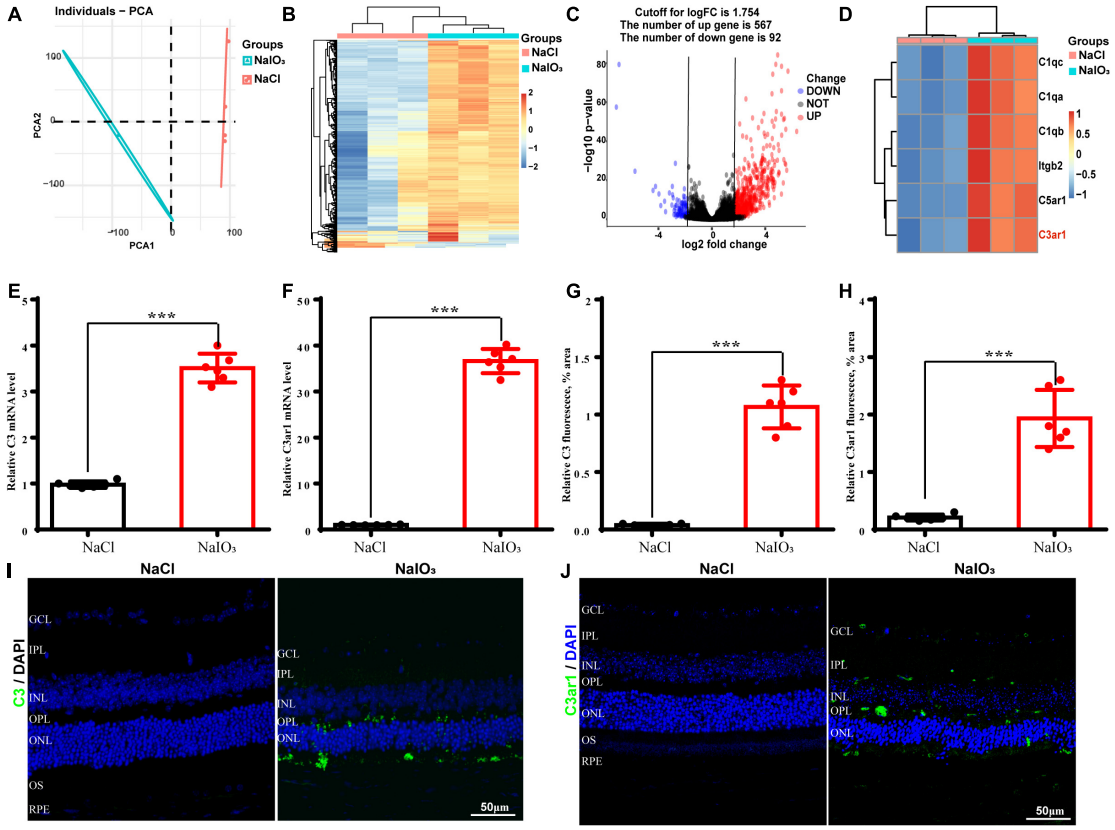

FIGURE 1
Upregulation of C3 and C3aR in the $NaIO_3$ mouse retinal degeneration model. **(A)** PCA graph showing the distribution of RNA-seq samples between the control and $NaIO_3$-treated groups. **(B)** Unsupervised clustering of the top 500 genes expressed above background levels demonstrated similar patterns of gene expression between the control and $NaIO_3$-treated groups. **(C)** Volcano plots highlighting the distributions of DEGs between the control and $NaIO_3$-treated groups. **(D)** Some differentially expressed complement component genes between the control and $NaIO_3$-treated groups are shown as a heatmap. **(E,F)** The mRNA levels of C3 and C3aR in the control and $NaIO_3$-treated groups were analyzed by real-time PCR. **(G–J)** Immunofluorescence staining and semiquantified fluorescence levels of C3 (green) and C3ar1 in saline control- and $NaIO_3$-treated retinas on day 7; nuclei were counterstained with DAPI (blue) (Bars, 50 μm). The data are expressed as the mean ± SEM ***$P < 0.001$, $n = 6$, unpaired t-test, two-tailed.

Using real-time PCR, we confirmed that the levels of TNFα, IL1, and IL6 were increased after the application of $NaIO_3$, and C3 deficiency and C3ar1 inhibition obviously downregulated the mRNA levels of these genes (Figures 4B–D). These results support that C3aR regulates astrocyte and microglial reactivity and the production of proinflammatory cytokines in retinas with oxidative stress injury.

Knockout of C3 and C3ar1 inactivation reduce photoreceptor cell apoptosis and restore visual function in mice with retinal degeneration

The above studies demonstrated the prominent role of C3a-C3ar1 in immune regulation. We also assessed the role of C3a-C3ar1 signaling in photoreceptor cell degeneration. H&E staining revealed a significant reduction in the ONL thickness on day 7 after $NaIO_3$ induction compared to that in the control group. In contrast, the ONL thickness in mice with C3 deficiency and C3ar1 inhibition did not significantly differ from that in the controls on day 7 (Figures 5A,C). Furthermore, TUNEL staining showed that the apoptosis of photoreceptor cells was significantly reduced in the C3-KO and C3ar1-inhibited groups on day 7 (Figures 5B,D). These results indicated that C3a-C3ar1 played an important role in $NaIO_3$-induced retinal photoreceptor cell degeneration and that the inactivation of C3 restored retinal function. Remarkably, the ERG a-wave and b-wave amplitudes were significantly decreased in wild-type mice on day 7 after $NaIO_3$ induction but increased in C3-deficient and C3ar1-inhibited mice (Figures 6C–F, I,J). Because rhodopsin is a key protein in the phototransduction process, we analyzed the expression levels of rhodopsin and recoverin, revealing that they were significantly downregulated in wild-type mice compared to C3-deficient and C3ar1-inhibited mice after $NaIO_3$ injection (Figures 6A,B,G,H).

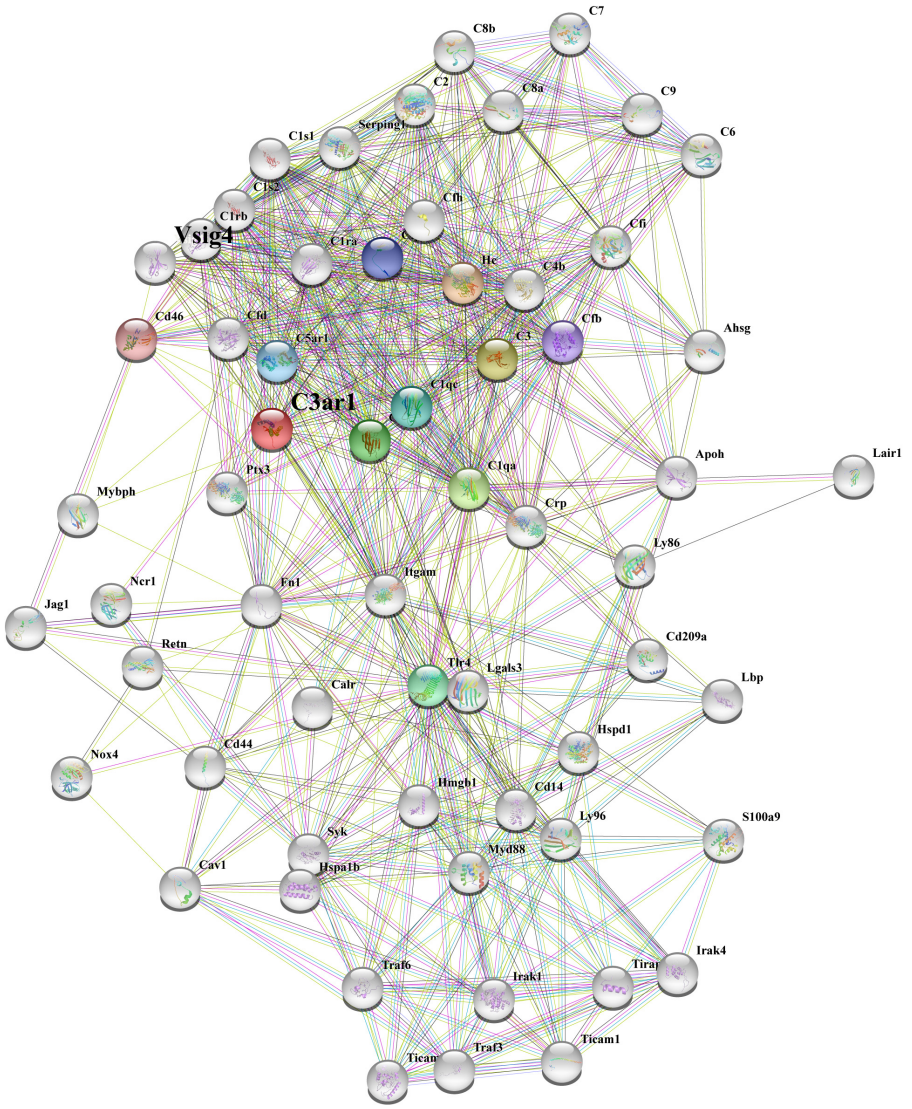

FIGURE 2
STRING network analysis reveals a C3ar1-centered immune interaction network. STRING network analysis of the C3ar1-related protein interaction network. Network nodes represent proteins. Edges represent protein–protein associations. Number of nodes: 11, number of edges: 37, average node degree: 6.73, average local clustering coefficient: 0.849, expected number of edges: 11, PPI enrichment p-value: 3.45e-10.

Involvement of the C3aR-STAT3 signaling pathway in retinal degeneration as determined by ribonucleic acid-seq

To further investigate the downstream mechanisms involving the C3a-C3ar1 pathway in photoreceptor degeneration, we compared the mRNA levels in $NaIO_3$-treated retinas on day 7 with those in control retinas by RNA-seq analysis, revealing DEGs between control and $NaIO_3$-treated retinas on day 7 (DE; fold-change > 2.0, $p < 0.05$). The downregulated DEGs included phototransduction genes, such as Arrestin3, Rhodopsin, and Rgr, while the C3, C3aR and STAT3 mRNA levels were obviously upregulated. GO enrichment analysis showed that the upregulated DEGs were involved in signaling pathways such as the STAT cascade, while the downregulated DEGs were involved in signaling pathways associated with phototransduction and visual perception (**Figure 7A**). A previous study indicated that C3ar1 regulates the expression of STAT3 and mediates inflammation during neuropathy (Litvinchuk et al., 2018), which is not clear in the retina. Real-time PCR and immunostaining confirmed the upregulation of STAT3 at both the mRNA and protein levels on day 7 after $NaIO_3$ induction (**Figures 7B–D**). Knockout of C3 and C3ar1 inhibition also normalized the

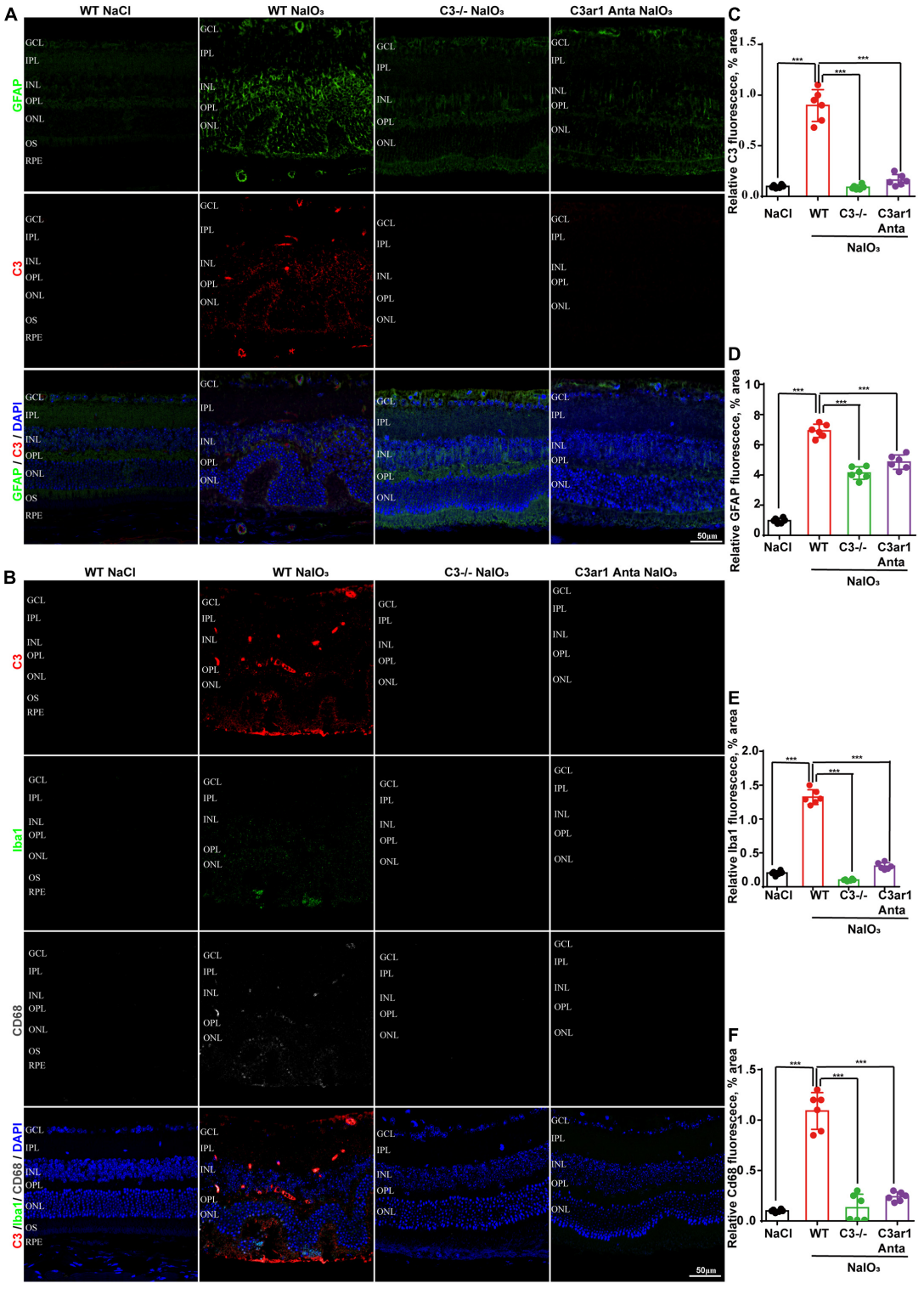

FIGURE 3
Genetic deletion of C3 and inactivation of C3ar1 attenuate reactive gliosis and microglial infiltration. **(A)** Representative GFAP and C3 multicolor immunofluorescence staining in the retinas of saline control- and NaIO3-treated WT, C3-KO and C3ar1-inhibited mice. Scale bar: 50 mm. **(B)** Representative C3, Iba1 and CD68 multicolor immunofluorescence staining in the retinas of saline control- and NaIO3-treated WT, C3-KO and C3ar1-inhibited mice. Scale bar: 50 mm. **(C–F)** Quantification of C3, GFAP, Iba1 and CD68 immunoreactivities. The data represent the mean ± SEM, $n = 6$. ***$p < 0.001$.

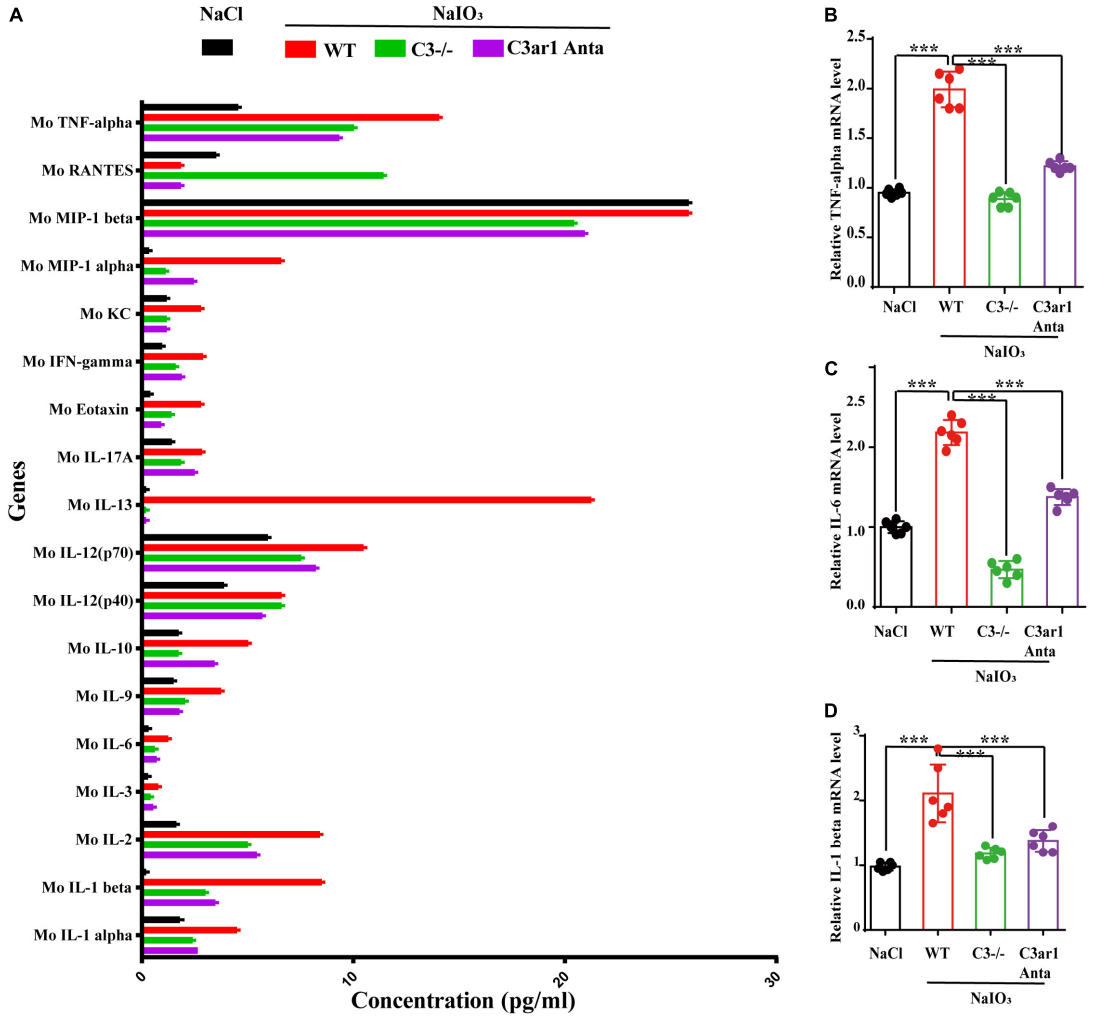

FIGURE 4
Cytokine retinal array analysis reveals high levels of proinflammatory factors. **(A)** Clustered column graph of the retinal cytokine profiles of saline control- and NaIO3-treated WT, C3-KO and C3ar1-inhibited mice obtained by using the Integral Molecular@QAM-INF-1 kit. **(B–D)** The retinal Il-6, TNF-α and TGF-β2 mRNA expression levels were determined by qRT–PCR. Each bar corresponds to the mean ± *SD*. ***$p < 0.001$.

upregulation of STAT3. Our findings suggest that the enhanced expression of STAT3 contributes to microglial activation, the inflammatory response and photoreceptor degeneration after $NaIO_3$ induction.

Inhibition of STAT3 attenuates microglial activation and rescues visual function

Previous studies have shown that the activation of the STAT pathway is involved in the immune response (Litvinchuk et al., 2018; Reichenbach et al., 2019). To better understand the role of the C3a/C3aR/STAT3 signaling pathway in photoreceptor degeneration, we pharmacologically inactivated STAT3 using the specific inhibitor SH-4-54. WT mice were pretreated with the STAT3 inhibitor SH-4-54 (10 mg/kg) 3 days before the application of $NaIO_3$. Fluorescence immunostaining revealed that SH-4-54 obviously downregulated microglial cell activation. The Iba1-positive ratio of microglial cells was alleviated after the application of SH-4-54 (**Figures 8A,E**). The H&E staining results revealed the protective effect of the ONL layer, and the ERG results showed that the a-wave and b-wave amplitudes were partially preserved, indicating the retinal protective effect of the STAT3 inhibitor (**Figures 8B,D,F,H,I**). Furthermore, TUNEL staining showed that the apoptosis of photoreceptor cells was significantly reduced after the application of SH-4-54 (**Figures 8C,G**). Overall, these results established a novel signaling pathway (C3/C3aR/STAT3) linking microglial activation and photoreceptor cell degeneration to oxidative stress conditions.

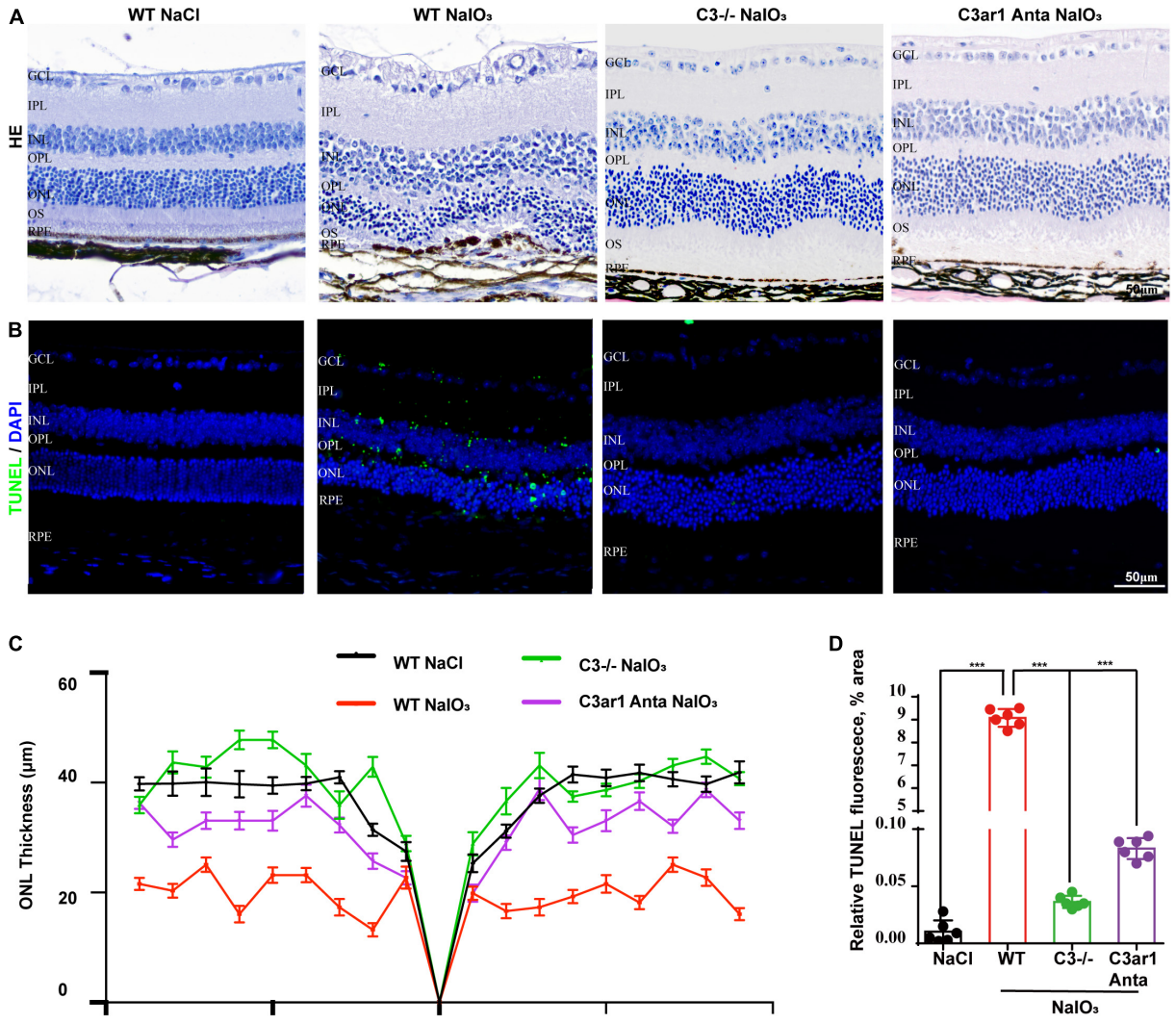

FIGURE 5
Genetic deletion of C3 and inactivation of C3ar1 protects the neural retina structure. **(A)** H&E staining of retinas of saline control- and NaIO3-treated WT, C3-KO and C3ar1-inhibited mice. **(B)** TUNEL immunofluorescence staining of retinas of saline control- and $NaIO_3$-treated WT, C3-KO and C3ar1-inhibited mice. **(C)** Quantification of ONL thickness in the retinas of saline control- and NaIO3-treated WT, C3-KO, and C3ar1-inhibited mice. **(D)** Immunofluorescence staining and quantification of TUNEL in retinas of saline control- and NaIO3-treated WT, C3-KO, and C3ar1 inhibition mice.

Discussion

The mechanism underlying retinal degeneration has not been fully elucidated, which severely restricts the development of new therapies. Strong evidence supports a key role of complement and the neuroinflammatory response in retinal diseases. Understanding the detailed mechanism will facilitate the development of potential treatments for photoreceptor cell degeneration-related diseases. In this study, we revealed that the C3a/C3aR/STAT3 pathways are important for mediating the immune response and photoreceptor cell apoptosis under oxidative stress conditions, which might be helpful for treating retinal degeneration diseases.

Complement and microglial cells mediate neural cell damage in many neural degeneration diseases, such as age-related macular degeneration (AMD), Stargard's disease and glaucoma (Jha et al., 2011; Lenis et al., 2017; Natoli et al., 2017). One previous study showed that irreversible photoreceptor cell damage in mice treated with $NaIO_3$ is related to macrophage accumulation (Moriguchi et al., 2018), and oxidative stress and complement activation have been correlated in AMD models (Pujol-Lereis et al., 2016). As the critical component of the complement system, C3 plays a role in photoreceptor cell death, but the mechanism is not clear. In this study, we observed the activation of microglial cells at 7 days after $NaIO_3$ injection, and the colocalization of C3 and microglial

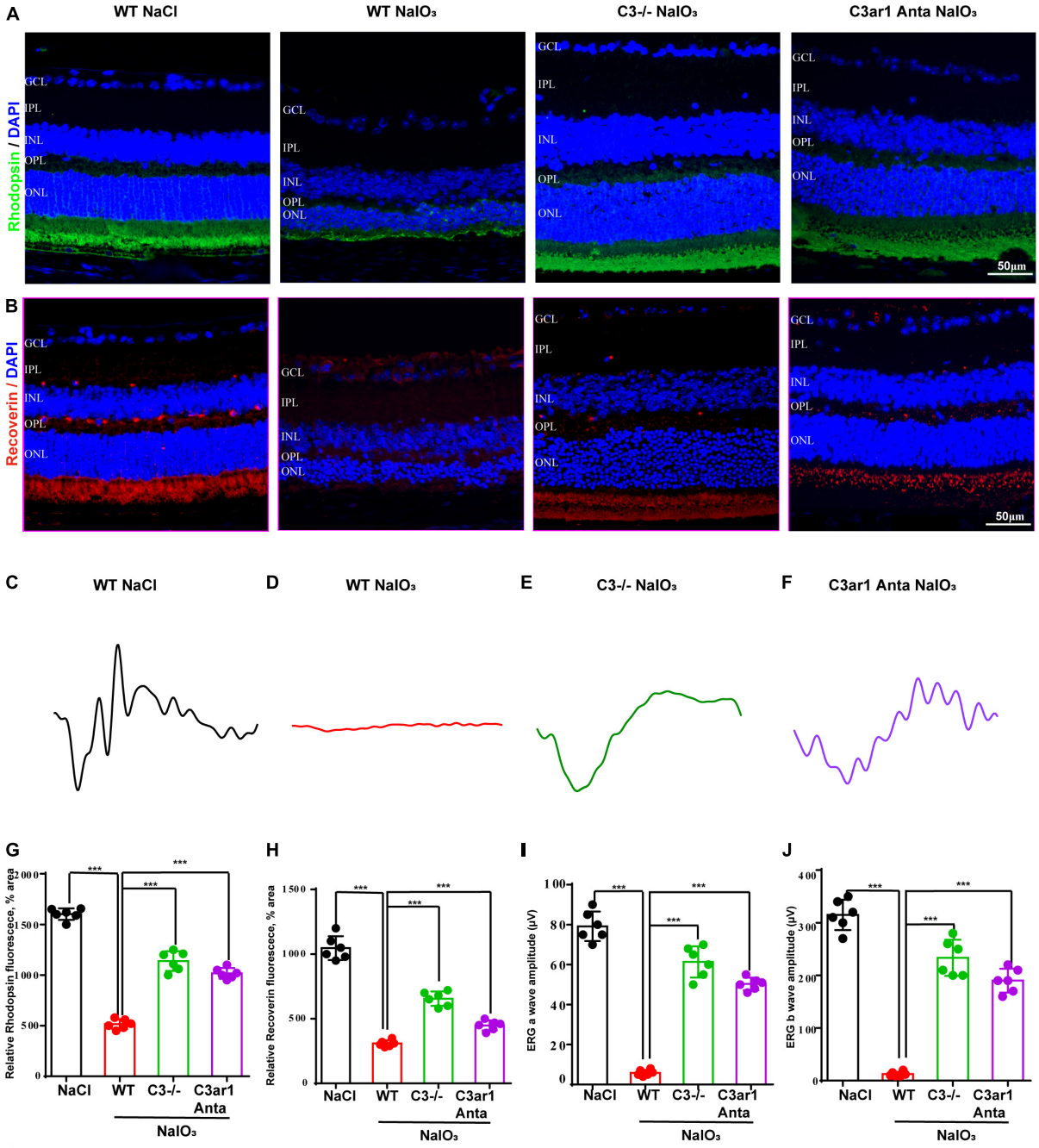

FIGURE 6
Genetic deletion of C3 and inactivation of C3ar1 rescues the retinal function of wild-type mice after $NaIO_3$ induction. **(A,B)** Immunofluorescence staining of rhodopsin and recoverin in the retinas of saline control- and NaIO3-treated WT, C3-KO and C3ar1-inhibited mice. **(C–F)** ERG analysis of retinal function in saline control- and NaIO3-treated WT, C3-KO and C3ar1-inhibited mice (dMax 3.0). **(G,H)** Quantification of rhodopsin and recoverin in the retinas of saline control- and NaIO3-treated WT, C3-KO and C3ar1-inhibited mice. **(I,J)** Bar plot of the amplitudes of a and b waves in saline control- and NaIO3 treated WT, C3-KO and C3ar1-inhibited mice (mean ± SEM, $n = 6$. ***$p < 0.001$).

cells was consistent with previous reports. We also detected the intracellular C3 expression in retinal pigment epithelium (RPE) cells at 1 day after $NaIO_3$ injection (**Supplementary Figure 2**). Furthermore, RNA-seq data revealed the upregulated expression of C3ar1 and other components under oxidative stress conditions. This inspired us to explore the role of C3a-C3ar1 in retinal injury induced by $NaIO_3$. Simultaneously, Pauly et al. (2019) were the first to explore the characteristics of

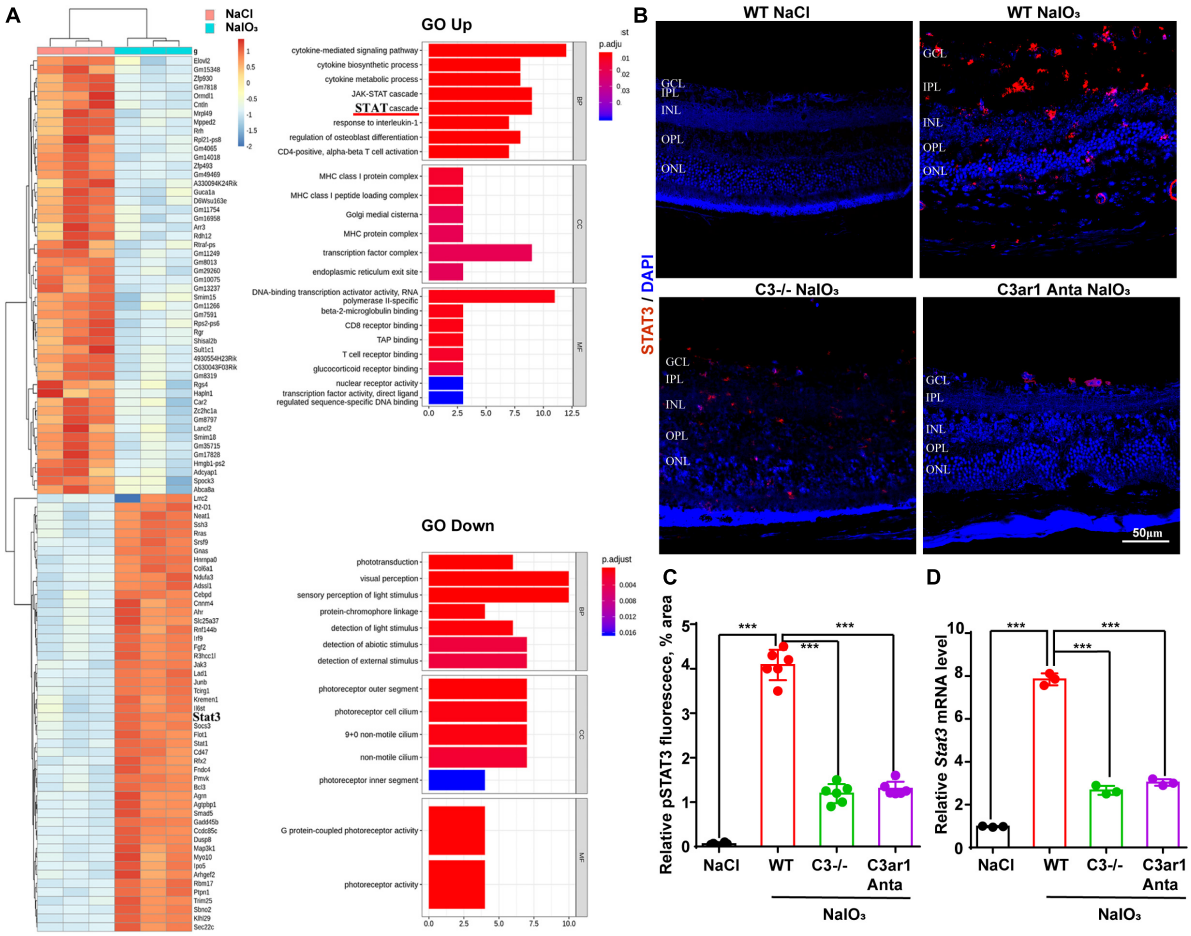

FIGURE 7
RNA-seq analysis revealed C3/C3aR/STA3 signaling pathway activation in the $NaIO_3$ mouse model. **(A)** The top 100 DEGs in wild-type mice at 0 and 7 days after $NaIO_3$ induction. Gene Ontology analysis of the signaling pathways related to up- and downregulated genes. **(B)** Immunofluorescence staining of STAT3 in the retinas of saline control- and NaIO3-treated WT, C3-KO and C3ar1-inhibited mice. **(C)** Quantification of STAT3 in the retinas of saline control- and NaIO3-treated WT, C3-KO and C3ar1-inhibited mice. **(D)** Stat3 mRNA expression in retinas as determined by qRT–PCR. Each bar corresponds to the mean ± *SD*. ***$p < 0.001$.

complement components in specific retinal cell types under normal and pathological conditions using single-cell RNA-seq analysis. Their results strongly indicate that a local retinal complement that is independent of the systemic components typically produced by the liver is activated during retinal degeneration. For the first time, we found that $NaIO_3$-induced photoreceptor apoptosis depended on C3a-C3ar1 axis activation and was partially mediated by the knockout of C3 or inhibition of C3ar1. However, the characteristics of macrophages in the peripheral infiltrating blood in the retina are not clear. One previous study found that the complement C3a signaling pathway mediates peripheral infiltrating blood monocytes and then facilitates skeletal regeneration (Zhang et al., 2017). Thus, we need to fully demonstrate the role of C3a-C3ar1 activation in macrophage infiltration and activation in the future.

Mechanistically, we identified STAT3 as a downstream gene of the C3/C3aR pathway during photoreceptor cell degeneration. Our RNA-seq analysis results revealed significant activation of the C3/C3aR/STAT cascade in the $NaIO_3$-induced retinal degeneration model. Strikingly, genetic deletion of C3 and pharmacological inhibition of C3aR or STAT3 led to the prevention of photoreceptor loss and preservation of retinal function. These findings are consistent with the previously reported critical role of C3aR in mediating CNS immune homeostasis and tau pathology by targeting a transcription factor network in human AD (Litvinchuk et al., 2018). Several studies have found that STATA3 is involved in RPE cell survival, the inflammatory response, visual cycle maintenance and cytokine release (Patel and Hackam, 2013; Patel et al., 2013). Moreover, features of the immune response, such as proinflammatory cytokine release, microglial infiltration and Muller glial reactivity, were suppressed after the C3/C3aR/STAT3 pathway was blocked in our study. Additionally, given the complexity and the degree of crosstalk

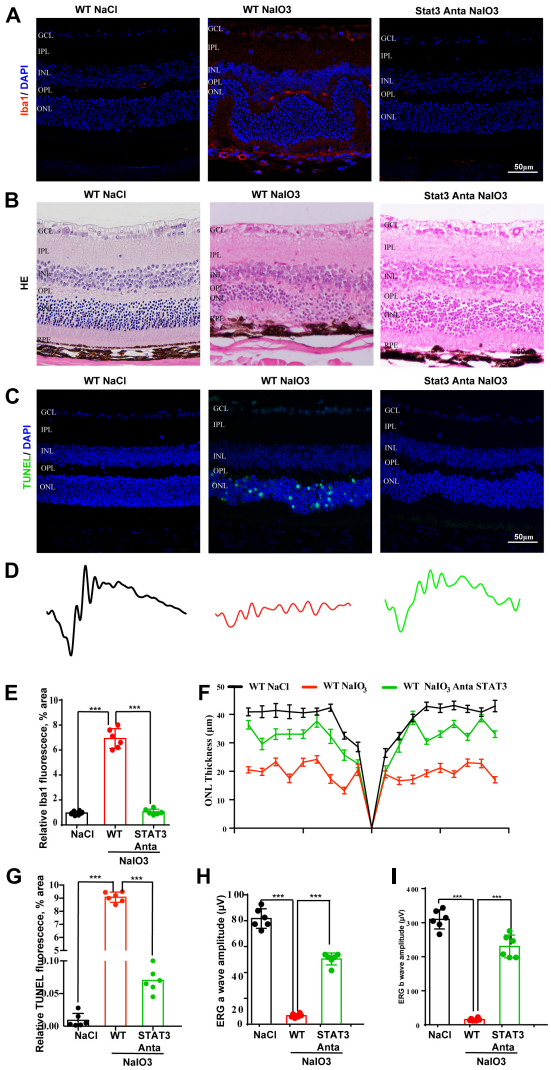

FIGURE 8
A pSTAT3 inhibitor inhibits microglial activation and rescues the retinal function of wild-type mice after $NaIO_3$ induction. **(A)** Immunostaining of Iba in the retinas of saline control- and $NaIO_3$-treated WT and pSTAT3-inhibited mice. **(B)** H&E staining of the retinas of saline control- and $NaIO_3$-treated WT and pSTAT3-inhibited mice. **(C)** TUNEL immunofluorescence staining of retinas of saline control- and $NaIO_3$-treated WT and pSTAT3-inhibited mice. **(D)** ERG analysis of retinal function in saline control- and $NaIO_3$-treated WT and pSTAT3-inhibited mice. **(E)** Quantification of Iba1 in saline control- and $NaIO_3$-treated WT and pSTAT3-inhibited mice. **(F)** Quantification of ONL thickness in the retinas of saline control- and $NaIO_3$-treated WT and pSTAT3-inhibited mice. **(G)** Quantification of TUNEL in retinas of saline control- and $NaIO_3$-treated WT and pSTAT3-inhibited mice. **(H,I)** Bar plot of the amplitudes of a and b waves in saline control- and $NaIO_3$-treated WT and pSTAT3-inhibited mice. $^{***}p < 0.001$.

between various immune pathways, other transcription factors (TFs), such as Hmox1, NFkB, and NFE2L2, might also interact with the C3a-C3ar1 pathway and be involved in retinal degeneration (Karlen et al., 2020; Potilinski et al., 2021).

Taken together, the results of this study demonstrate that the activation of the C3a/C3aR/STAT3 pathway plays an important role in mediating microglial activation and photoreceptor cell degeneration. Therefore, inhibition of local C3 and normalization of the C3a/C3aR/STAT3 pathway could be helpful for the prevention of AMD and other retinal degeneration diseases.

Data availability statement

The original contributions presented in the study are publicly available. This data can be found here: The RNA-seq data are available at: https://ngdc.cncb.ac.cn/search/?dbId=&q=CRA007710.

Ethics statement

The animal study was reviewed and approved by Institutional Animal Care and Use Committee of the General Hospital of the Chinese People's Liberation Army and Zhengzhou University. All experiments were performed in accordance with the National Institutes of Health Guidelines for the Care and Use of Laboratory Animals (Id number: 2020-ky-67).

Author contributions

SW and LD conceived and designed the study, constructed the animal, and performed the RPE cell culture and immunohistochemistry experiments. SW, LD, and SY analyzed the data and wrote the manuscript. G-HP revised the manuscript, provided support, and supervised the project. All authors read and approved the final manuscript.

Funding

This work was supported by the National Key Research and Development Program (2018YFA0107303 to G-HP), the National Natural Science Foundation of China (NSFC 81501090 to SW), and the China Postdoctoral Research Fund (Issue 2017M613396 to SW).

Acknowledgments

The C3-knockout C57BL/6J mice were a kind gift from Prof. Yusen Zhou (State Key Laboratory of Pathogen

and Biosecurity, Beijing Institute of Microbiology and Epidemiology, Beijing 100071, China).

Conflict of interest

The authors declare that the research was conducted in the absence of any commercial or financial relationships that could be construed as a potential conflict of interest.

Publisher's note

All claims expressed in this article are solely those of the authors and do not necessarily represent those of their affiliated organizations, or those of the publisher, the editors and the reviewers. Any product that may be evaluated in this article, or claim that may be made by its manufacturer, is not guaranteed or endorsed by the publisher.

Supplementary material

The Supplementary Material for this article can be found online at: https://www.frontiersin.org/articles/10.3389/fnins.2022.951491/full#supplementary-material

SUPPLEMENTARY FIGURE 1
Schematic of the retina with a sample location.

SUPPLEMENTARY FIGURE 2
Intracellular C3 activation in RPE cells after $NaIO_3$ injury *in vivo*. **(A)** Double immunofluorescent staining C3 (green) and RPE65 (red) of wild-type 0d and 1d after $NaIO_3$ injection. **(B)** Confocal assay of C3 localization of wild-type 0d and 1d after $NaIO_3$ injection. **(C)** TUNEL immunofluorescent staining of wild-type and C3-deficient mice 1d after $NaIO_3$ injection. **(D)** Quantification of **(C)**.

References

Akhtar-Schafer, I., Wang, L., Krohne, T. U., Xu, H., and Langmann, T. (2018). Modulation of three key innate immune pathways for the most common retinal degenerative diseases. *EMBO Mol. Med.* 10:e8259. doi: 10.15252/emmm.201708259

Ambati, J., and Fowler, B. J. (2012). Mechanisms of age-related macular degeneration. *Neuron* 75, 26–39.

Chi, Z. L., Yoshida, T., Lambris, J. D., and Iwata, T. (2010). Suppression of drusen formation by compstatin, a peptide inhibitor of complement C3 activation, on cynomolgus monkey with early-onset macular degeneration. *Adv. Exp. Med. Biol.* 703, 127–135. doi: 10.1007/978-1-4419-5635-4_9

Enzbrenner, A., Zulliger, R., Biber, J., Pousa, A. M. Q., Schäfer, N., Stucki, C., et al. (2021). Sodium Iodate-Induced Degeneration Results in Local Complement Changes and Inflammatory Processes in Murine Retina. *Int. J. Mol. Sci.* 22:9218. doi: 10.3390/ijms22179218

Grajales-Esquivel, E., Luz-Madrigal, A., Bierly, J., Haynes, T., Reis, E. S., Han, Z., et al. (2017). Complement component C3aR constitutes a novel regulator for chick eye morphogenesis. *Dev. Biol.* 428, 88–100. doi: 10.1016/j.ydbio.2017.05.019

Handa, J. T., Bowes Rickman, C., Dick, A. D., Gorin, M. B., Miller, J. W., Toth, C. A., et al. (2019). A systems biology approach towards understanding and treating non-neovascular age-related macular degeneration. *Nat. Commun.* 10:3347. doi: 10.1038/s41467-019-11262-1

Jha, P., Banda, H., Tytarenko, R., Bora, P. S., and Bora, N. S. (2011). Complement mediated apoptosis leads to the loss of retinal ganglion cells in animal model of glaucoma. *Mol. Immunol.* 48, 2151–2158. doi: 10.1016/j.molimm.2011.07.012

Karlen, S. J., Miller, E. B., and Burns, M. E. (2020). Microglia Activation and Inflammation During the Death of Mammalian Photoreceptors. *Annu. Rev. Vis. Sci.* 6, 149–169.

Lenis, T. L., Sarfare, S., Jiang, Z., Lloyd, M. B., Bok, D., and Radu, R. A. (2017). Complement modulation in the retinal pigment epithelium rescues photoreceptor degeneration in a mouse model of Stargardt disease. *Proc. Natl. Acad. Sci. U.S.A.* 114, 3987–3992. doi: 10.1073/pnas.1620299114

Lian, H., Litvinchuk, A., Chiang, A. C., Aithmitti, N., Jankowsky, J. L., and Zheng, H. (2016). Astrocyte-Microglia Cross Talk through Complement Activation Modulates Amyloid Pathology in Mouse Models of Alzheimer's Disease. *J. Neurosci.* 36, 577–589. doi: 10.1523/JNEUROSCI.2117-15.2016

Linetsky, M., Bondelid, K. S., Losovskiy, S., Gabyak, V., Rullo, M. J., Stiadle, T. I., et al. (2018). 4-Hydroxy-7-oxo-5-heptenoic Acid Lactone Is a Potent Inducer of the Complement Pathway in Human Retinal Pigmented Epithelial Cells. *Chem. Res. Toxicol.* 31, 666–679. doi: 10.1021/acs.chemrestox.8b00028

Liszewski, M. K., Java, A., Schramm, E. C., and Atkinson, J. P. (2017). Complement Dysregulation and Disease: Insights from Contemporary Genetics. *Annu. Rev. Pathol.* 12, 25–52. doi: 10.1146/annurev-pathol-012615-044145

Litvinchuk, A., Wan, Y.-W., Swartzlander, D. B., Chen, F., Cole, A., Propson, N. E., et al. (2018). Complement C3aR Inactivation Attenuates Tau Pathology and Reverses an Immune Network Deregulated in Tauopathy Models and Alzheimer's Disease. *Neuron* 100:1337–1353.e5. doi: 10.1016/j.neuron.2018.10.031

Love, M. I., Huber, W., and Anders, S. (2014). Moderated estimation of fold change and dispersion for RNA-seq data with DESeq2. *Genome Biol.* 15:550. doi: 10.1186/s13059-014-0550-8

Menon, M., Mohammadi, S., Davila-Velderrain, J., Goods, B. A., Cadwell, T. D., Xing, Y., et al. (2019). Single-cell transcriptomic atlas of the human retina identifies cell types associated with age-related macular degeneration. *Nat. Commun.* 10:4902.

Mohlin, C., Sandholm, K., Ekdahl, K. N., and Nilsson, B. (2017). The link between morphology and complement in ocular disease. *Mol. Immunol.* 89, 84–99.

Moriguchi, M., Nakamura, S., Inoue, Y., Nishinaka, A., Nakamura, M., Shimazawa, M., et al. (2018). Irreversible Photoreceptors and RPE Cells Damage by Intravenous Sodium Iodate in Mice Is Related to Macrophage Accumulation. *Invest. Ophthalmol. Vis. Sci.* 59, 3476–3487. doi: 10.1167/iovs.17-23532

Mulfaul, K., Ozaki, E., Fernando, N., Brennan, K., Chirco, K. R., Connolly, E., et al. (2020). Toll-like Receptor 2 Facilitates Oxidative Damage-Induced Retinal Degeneration. *Cell Rep.* 30:2209–2224.e5. doi: 10.1016/j.celrep.2020.01.064

Murakami, Y., Ishikawa, K., Nakao, S., and Sonoda, K.-H. (2019). Innate immune response in retinal homeostasis and inflammatory disorders. *Prog. Retin. Eye Res.* 74:100778.

Natoli, R., Fernando, N., Jiao, H., Racic, T., Madigan, M., Barnett, N. L., et al. (2017). Retinal Macrophages Synthesize C3 and Activate Complement in AMD and in Models of Focal Retinal Degeneration. *Invest. Ophthalmol. Vis. Sci.* 58, 2977–2990. doi: 10.1167/iovs.17-21672

Norris, G. T., Smirnov, I., Filiano, A. J., Shadowen, H. M., Cody, K. R., Thompson, J. A., et al. (2018). Neuronal integrity and complement control synaptic material clearance by microglia after CNS injury. *J. Exp. Med.* 215, 1789–1801. doi: 10.1084/jem.20172244

Orozco, L. D., Chen, H. H., Cox, C., Katschke, K. J. Jr., Arceo, R., Espiritu, C., et al. (2020). Integration of eQTL and a Single-Cell Atlas in the Human Eye Identifies Causal Genes for Age-Related Macular Degeneration. *Cell Rep.* 30:1246–1259.e6. doi: 10.1016/j.celrep.2019.12.082

Patel, A. K., and Hackam, A. S. (2013). Toll-like receptor 3 (TLR3) protects retinal pigmented epithelium (RPE) cells from oxidative stress through a STAT3-dependent mechanism. *Mol. Immunol.* 54, 122–131. doi: 10.1016/j.molimm.2012.11.005

Patel, A. K., Syeda, S., and Hackam, A. S. (2013). Signal transducer and activator of transcription 3 (STAT3) signaling in retinal pigment epithelium cells. *Jakstat* 2:e25434.

Pauly, D., Agarwal, D., Dana, N., Schäfer, N., Biber, J., Wunderlich, K. A., et al. (2019). Cell-Type-Specific Complement Expression in the Healthy and Diseased Retina. *Cell Rep.* 29, 2835–2848.e4. doi: 10.1016/j.celrep.2019.10.084

Potilinski, M. C., Tate, P. S., Lorenc, V. E., and Gallo, J. E. (2021). New insights into oxidative stress and immune mechanisms involved in age-related macular degeneration tackled by novel therapies. *Neuropharmacology* 188:108513. doi: 10.1016/j.neuropharm.2021.108513

Pujol-Lereis, L. M., Schafer, N., Kuhn, L. B., Rohrer, B., and Pauly, D. (2016). Interrelation Between Oxidative Stress and Complement Activation in Models of Age-Related Macular Degeneration. *Adv. Exp. Med. Biol.* 854, 87–93. doi: 10.1007/978-3-319-17121-0_13

Ramos de Carvalho, J. E., Klaassen, I., Vogels, I. M., Schipper-Krom, S., van Noorden, C. J., Reits, E., et al. (2013). Complement factor C3a alters proteasome function in human RPE cells and in an animal model of age-related RPE degeneration. *Invest. Ophthalmol. Vis. Sci.* 54, 6489–6501. doi: 10.1167/iovs.13-12374

Reichenbach, N., Delekate, A., Plescher, M., Schmitt, F., Krauss, S., Blank, N., et al. (2019). Inhibition of Stat3-mediated astrogliosis ameliorates pathology in an Alzheimer's disease model. *EMBO Mol. Med.* 11:e9665. doi: 10.15252/emmm.201809665

Ricklin, D., Reis, E. S., Mastellos, D. C., Gros, P., and Lambris, J. D. (2016). Complement component C3 - The "Swiss Army Knife" of innate immunity and host defense. *Immunol. Rev.* 274, 33–58. doi: 10.1111/imr.12500

Silverman, S. M., Ma, W., Wang, X., Zhao, L., and Wong, W. T. (2019). C3- and CR3-dependent microglial clearance protects photoreceptors in retinitis pigmentosa. *J. Exp. Med.* 216, 1925–1943. doi: 10.1084/jem.20190009

Stephan, A. H., Barres, B. A., and Stevens, B. (2012). The complement system: An unexpected role in synaptic pruning during development and disease. *Annu. Rev. Neurosci.* 35, 369–389.

van Lookeren Campagne, M., Strauss, E. C., and Yaspan, B. L. (2016). Age-related macular degeneration: Complement in action. *Immunobiology* 221, 733–739.

Voigt, A. P., Mulfaul, K., Mullin, N. K., Flamme-Wiese, M. J., Giacalone, J. C., Stone, E. M., et al. (2019). Single-cell transcriptomics of the human retinal pigment epithelium and choroid in health and macular degeneration. *Proc. Natl. Acad. Sci. U.S.A.* 116, 24100–24107. doi: 10.1073/pnas.1914143116

Wang, J., Iacovelli, J., Spencer, C., and Saint-Geniez, M. (2014). Direct effect of sodium iodate on neurosensory retina. *Invest. Ophthalmol. Vis. Sci.* 55, 1941–1953. doi: 10.1167/iovs.13-13075

Wang, S., Du, L., and Peng, G. H. (2019). Optogenetic stimulation inhibits the self-renewal of mouse embryonic stem cells. *Cell Biosci.* 9:73. doi: 10.1186/s13578-019-0335-6

Wei, Y., Chen, T., Bosco, D. B., Xie, M., Zheng, J., Dheer, A., et al. (2021). The complement C3-C3aR pathway mediates microglia-astrocyte interaction following status epilepticus. *Glia* 69, 1155–1169. doi: 10.1002/glia.23955

Wong, W. L., Su, X., Li, X., Cheung, C. M., Klein, R., Cheng, C. Y., et al. (2014). Global prevalence of age-related macular degeneration and disease burden projection for 2020 and 2040: A systematic review and meta-analysis. *Lancet Glob. Health* 2:e106–e116. doi: 10.1016/S2214-109X(13)70145-1

Xiao, J., Yao, J., Jia, L., Lin, C., and Zacks, D. N. (2017). Protective Effect of Met12, a Small Peptide Inhibitor of Fas, on the Retinal Pigment Epithelium and Photoreceptor After Sodium Iodate Injury. *Invest. Ophthalmol. Vis. Sci.* 58, 1801–1810. doi: 10.1167/iovs.16-21392

Ye, J., Dai, H., Liu, Y., Yu, B., Yang, J., and Fei, A. (2020). Blockade of C3a/C3aR axis alleviates severe acute pancreatitis-induced intestinal barrier injury. *Am. J. Transl. Res.* 12, 6290–6301.

Zhang, C., Wang, C., Li, Y., Miwa, T., Liu, C., Cui, W., et al. (2017). Complement C3a signaling facilitates skeletal muscle regeneration by regulating monocyte function and trafficking. *Nat. Commun.* 8:2078. doi: 10.1038/s41467-017-01526-z

frontiers | Frontiers in Neuroscience

TYPE Original Research
PUBLISHED 06 October 2022
DOI 10.3389/fnins.2022.928980

OPEN ACCESS

EDITED BY
Yang Zhang,
Chongqing University, China

REVIEWED BY
Yi Liu,
Dalian Municipal Central Hospital, China
Yameng Gu,
The Ohio State University, United States

*CORRESPONDENCE
Wei-guo Li
leeweiguo777@163.com

SPECIALTY SECTION
This article was submitted to Neurodegeneration, a section of the journal Frontiers in Neuroscience

RECEIVED 26 April 2022
ACCEPTED 08 September 2022
PUBLISHED 06 October 2022

CITATION
Zhang C, Wu Q-q, Hou Y, Wang Q, Zhang G-j, Zhao W-b, Wang X, Wang H and Li W-g (2022) Ophthalmologic problems correlates with cognitive impairment in patients with Parkinson's disease. *Front. Neurosci.* 16:928980. doi: 10.3389/fnins.2022.928980

Ophthalmologic problems correlates with cognitive impairment in patients with Parkinson's disease

Chao Zhang[1,2], Qian-qian Wu[1], Ying Hou[3], Qi Wang[4], Guang-jian Zhang[5], Wen-bo Zhao[2], Xu Wang[2], Hong Wang[6] and Wei-guo Li[1]*

[1]Department of Neurosurgery, Qilu Hospital of Shandong University, Jinan, China, [2]Institute of Brain and Brain-Inspired Science, Shandong University, Jinan, China, [3]Department of Neurology, Qilu Hospital of Shandong University, Jinan, China, [4]Department of Gerontology, Shandong Provincial Qianfoshan Hospital, Jinan, China, [5]Department of Neurology, Weifang People's Hospital, Weifang, China, [6]Department of Ophthalmology, Qilu Hospital of Shandong University, Jinan, China

Objective: Visual impairment is a common non-motor symptom (NMS) in patients with Parkinson's disease (PD) and its implications for cognitive impairment remain controversial. We wished to survey the prevalence of visual impairment in Chinese Parkinson's patients based on the Visual Impairment in Parkinson's Disease Questionnaire (VIPD-Q), identify the pathogens that lead to visual impairment, and develop a predictive model for cognitive impairment risk in Parkinson's based on ophthalmic parameters.

Methods: A total of 205 patients with Parkinson's disease and 200 age-matched controls completed the VIPD-Q and underwent neuro-ophthalmologic examinations, including ocular fundus photography and optical coherence tomography. We conducted nomogram analysis and the predictive model was summarized using the multivariate logistic and LASSO regression and verified *via* bootstrap validation.

Results: One or more ophthalmologic symptoms were present in 57% of patients with Parkinson's disease, compared with 14% of the controls (χ^2-test; $p < 0.001$). The visual impairment questionnaire showed good sensitivity and specificity (area under the curve [AUC] = 0.918, $p < 0.001$) and a strong correlation with MoCA scores (Pearson $r = -0.4652$, $p < 0.001$). Comparing visual impairment scores between pre- and post-deep brain stimulation groups showed that DBS improved visual function (U-test, $p < 0.001$). The thickness of the retinal nerve fiber layer and vessel percentage area predicted cognitive impairment in PD.

Interpretation: The study findings provide novel mechanistic insights into visual impairment and cognitive decline in Parkinson's disease. The results inform an effective tool for predicting cognitive deterioration in Parkinson's based on ophthalmic parameters.

KEYWORDS

Parkinson's disease, visual dysfunction, cognitive impairment, visual impairment in Parkinson's disease questionnaire, deep brain stimulation

Introduction

Visual impairment is a common non-motor symptom (NMS) in patients with Parkinson's disease (PD), affecting up to 78% of patients with PD (Hamedani et al., 2020). Although vision is an important determinant of quality of life, visual impairment is often underreported by patients and overlooked by their physicians (Ekker et al., 2017). Deficits in contrast sensitivity, color discrimination, and stereopsis are widespread in patients with PD and are associated with the risk of cognitive decline (Leyland et al., 2020; Murueta-Goyena et al., 2021). These parameters are not routinely assessed by ophthalmologists and neurologists. Visual dysfunction in PD is subtle and unlikely to be captured outside of the research setting. We introduced the Visual Impairment in Parkinson's Disease Questionnaire (VIPD-Q) (Borm et al., 2020) to provide insight into the relationship between ophthalmologic problems and cognitive impairment in patients with PD.

The role of visual dysfunction as a biomarker of disease and a predictor of cognitive impairment in PD has been reported in previous studies (Weil et al., 2016). These studies usually ascribe visual deficits to intracranial impairment. As the understanding of the gut–brain axis deepens, the knowledge basis for visual dysfunction in PD will likely change over time. We conducted metatranscriptomic sequencing and 16s rDNA sequencing in PD patients with and without visual impairment to identify the relationship between ophthalmology dysfunction and microbiota dysbiosis in patients with PD. To our knowledge, we have conducted the first study focusing on this issue.

We utilized optical coherence tomography (OCT) and machine learning software to analyze the ocular characteristics of patients with PD, such as retinal nerve fiber layer (RNFL) thickness and microvascular density in the fundus. These indices have been demonstrated to correlate with cognitive status in PD within a few pioneering studies (with relatively small sample sizes ranging from $n = 17$ to $n = 63$); only a limited number of ophthalmologic symptoms have been evaluated in PD (Kwapong et al., 2018; Murueta-Goyena et al., 2019, 2021).

We aimed to systematically determine the application value of VIPD-Q in patients with PD and explore the link between ophthalmology dysfunction and cognitive impairment.

Abbreviations: PD, Parkinson's Disease; VIPD-Q, Visual Impairment in Parkinson's Disease Questionnaire; DBS, Deep Brain Stimulation; RBD, rapid eye movement (REM) sleep behavior disorder; OCT, Optical Coherence Tomography; RNFL, Retinal Nerve Fiber Layer; VPA, vessel percentage area; UPDRS III, Unified Parkinson's Disease Rating Scale Section III; MoCA, Montreal Cognitive Assessment.

Methods

Study design

We used the VIPD-Q screening questionnaire to assess ophthalmologic symptoms and UPDRSIII and MoCA scores in patients with PD (Borm et al., 2020). The questionnaire was administered by two university hospitals (Qilu Hospital, First Affiliated Hospital) and scored by two clinicians (one ophthalmologist, HW and one neurologist, CZ) between June 2019 and July 2021. Participants underwent neuro-ophthalmologic examinations, including ocular fundus photography, automated perimetry, and OCT. Patients undergoing deep brain stimulation (DBS) took an extra VIPD-Q 3 months after the operation. Exclusion criteria included secondary causes of parkinsonism, prior brain surgery (except DBS), glaucoma, intraocular surgery, diabetes, and other diseases that affected the visual field or neurologic systems, and the current use of medications that affected visual function.

Ethical considerations

The study was conducted in accordance with the principles of the Declaration of Helsinki. The Ethics Committees at the Qilu Hospital (protocol KYLL-202008-065) and the First Affiliated Hospital of Shandong First Medical University (protocol S569) approved this study. Written informed consent was obtained from all participants.

Measures

RNFL and retinal thickness were measured using the Spectralis OCT device (CIRRUS 5000, Carl Zeiss, Oberkochen, Germany). Scans were performed by the same operator (HW). Image acquisition was conducted using the TruTrack eye-tracking technology that recognizes, locks onto, and follows the patient's retina. Ocular fundus photography was performed by an ophthalmologist using a digital ocular fundus camera (VISUCAM 224, Carl Zeiss, Germany) in both eyes in patients with PD. At least one reliable picture per eye was acquired for each patient. Images of ocular fundus vessels were extracted based on the U-Net model (github.com/orobix/retina-unet#retina-blood-vessel-segmentation-with-a-convolution-neural-network-u-net) (Liskowski and Krawiec, 2016) using a novel software (github.com/jellygrey/OVE/tree/master/bin). Vessel pictures were measured *via* the Angiotool software (version 0.6a) to obtain vessel-related data (Segarra et al., 2018).

We performed perivascular spaces (PVS) quantification in slices containing the maximum amount of PVS in the basal

ganglia (BG) region using ITK-SNAP software (version 3.8; the University of Pennsylvania, the University of North Carolina at Chapel Hill) (Shen et al., 2021). Boundaries of all identified PVS were delineated manually. This software automatically provides the voxel number for identified PVS in each region. PVS volume was calculated as the sum of individual volumes of the identified PVS in each region per mm^3. We then obtained PVS counts and volumes for each region.

Nomogram construction and validation

Multivariable logistic regression was applied according to sex, age, disease duration, VIPD-Q score, RNFL thickness, average vessel percentage, RBD status, hyposmia, and constipation. The "glmnet" package was used to conduct LASSO regression to screen meaningful variants, which were verified by bootstrap validation. A nomogram was generated *via* the "regplot" R package as a quantitative tool for predicting the risk of cognitive impairment. Consistency between model predictions and clinical outcomes was assessed using the concordance index (C-index). A calibration plot was generated to evaluate the accuracy of MoCA predictions. Decision curve analysis (DCA) was applied to evaluate nomogram performance using the "rmda" R package.

Statistical analysis

Statistical analyses were performed using the Prism software (version 8.0.1; San Diego, CA, USA), R (version 3.6.1), and RStudio (version 1.2.1335). Patients with PD were compared with controls using χ^2-tests for categorical variables (education, sex, comorbidity, and visual impairment) and Mann-Whitney *U*-tests for nonparametric continuous variables (age, VIPD-Q score, score per domain, MoCA score, UPDRSIII score, and levodopa equivalent dose [LED]). To explore correlations, we fit linear models and calculated Spearman's *r*-value. Univariate logistic regression was used to evaluate the statistical significance (defined as $p < 0.05$) of associations between visual function parameters and motor and non-motor symptoms.

Results

Participant characteristics

A total of 405 participants completed the questionnaire: 205 patients with PD and 200 age-matched controls (1:1 ratio). Ophthalmologic symptoms were present in 57% of patients with PD (vs. 14% of the controls; χ^2-test: $p < 0.001$). Baseline characteristics and prevalence of ophthalmologic symptoms are summarized in Table 1. The groups were well balanced for age and comorbidity.

VIPD-Q correlated with UPDRSIII, and MoCA scores

The PD group experienced more ophthalmologic symptoms, reflected by median total VIPD-Q scores (Mann-Whitney *U*-test, $p < 0.001$; Figure 1A). Figure 1B shows the number of ophthalmologic symptoms per domain (PD vs. control, χ^2-test: ocular surface, 51.7 vs. 13%; intraocular domain, 43.9 vs. 10%; oculomotor domain, 58.1 vs. 13%; optic nerve domain, 46.3 vs. 5%; $p < 0.001$).

Based on a previous study (Borm et al., 2019), we reran tests to identify the sensitivity and specificity of the VIPD-Q in the Chinese population. A receiver operating characteristic (ROC) curve indicated good sensitivity and specificity (AUC = 0.918, $p < 0.001$; Figure 1C); this result was verified using the Hosmer–Lemeshow test ($p = 0.247$). According to Youden's index, the optimal ROC cut-off value was 7 (sensitivity, 88.4%; specificity, 90.3%; Youden's index, 0.787). We divided the population into a low VIPD-Q group (score < 7; PD with normal visual function) and a high VIPD-Q group (score ≥ 7; PD with impaired visual function). The high VIPD-Q group showed higher UPDRSIII scores (Mann-Whitney *U*-test, $p = 0.0013$) and lower MoCA scores (Mann-Whitney *U*-test, $p = 0.0004$) than the low VIPD-Q group (Figure 1D). VIPD-Q scores were positively associated with UPDRSIII scores (Pearson $r = 0.3675$, $p < 0.0001$) and negatively associated with MoCA scores (Pearson $r = -0.4342$, $p < 0.0001$; Figure 1E).

STN-DBS and non-motor symptoms affected VIPD-Q scores

To determine factors influencing VIPD-Q scores in PD, we compared the LED between PD patients with and without visual impairment. No statistically significant differences were found (*t*-test, $p = 0.2689$; Figure 2A). As DBS is an option for PD treatment, we compared the improvement efficiency between the high- and low-VIPD-Q groups. The groups had similar DBS improvement (*t*-test, $p = 0.7503$; Figure 2B). However, at their 3-month follow-up, the post-DBS group showed a clear decrease in the VIPD-Q score as compared to the pre-DBS group (13.0 vs. 10.50, Mann-Whitney *U*-test, $p < 0.001$; Figure 2C). As low-frequency stimulation was reported to improve axial symptoms more effectively than high-frequency stimulation (Xie et al., 2017), we compared groups with different stimulation parameters *via* *t*-tests; no differences were found (Figure 2D).

Other NMS were shown to affect VIDP-Q scores in our study. The RBD-positive group had a higher visual impairment percentage (score > 6; chi-square: $p = 0.0139$), especially in the constipation-positive group ($p < 0.0001$; Figure 2E). Hyposmia did not seem to affect visual function (chi-square, $p = 0.0599$), although the nerve fibers were anatomically close to each other.

TABLE 1 Participant characteristics and Prevalence of ophthalmologic symptoms.

	PD ($n = 205$)	Con ($n = 200$)	*P*-value
Men, n (%)	108, (53)	106, (53)	NS
Age, y, median (IQR) [range]	63 (12) [21–82]	64 (10) [20–74]	NS
Disease duration, y, median (IQR) [range]	8 (5) [2–30]	NA	NA
Levodopa dose equivalent, mg, median (IQR) [range]	562 (375) [0–2,000]	NA	NA
Hypertension	45, (22)	36, (18)	NS
Stroke	16, (8)	14, (7)	NS
COPD	44, (22)	44, (22)	NS
Uses visual aid, n (%)	72, (35)	24, (12)	<0.001
Using a walking aid outside, n (%)	70, (34)	14, (7)	<0.001
Falls present (last 6 months)	20, (10)	4, (2)	<0.001
Ophthalmologic symptoms reported weekly or daily, *n* (%)			
Ocular surface			
1. I have blurry vision when I read or work on a computer.	93, (45)	68, (34)	<0.001
2. I have a burning sensation or gritty feeling in my eyes	24, (12)	16, (8)	<0.001
3. I have mucus/slime or particles in my eyes or eyelids.	22, (11)	16, (8)	<0.001
4. I have watery eyes.	31, (15)	34, (17)	<0.001
Intraocular			
1. When I read, some letters disappear	24, (12)	16, (8)	<0.001
2. Lines that should be straight appear to be wavy or blurred.	26, (13)	6, (3)	<0.001
3. I won't go out alone in the evening or at night because my night vision is insufficient.	21, (10)	10, (5)	<0.001
4. When I drive at night, the oncoming headlights cause more glare than before.	64, (31)	38, (19)	<0.001
Oculomotor			
1. Quick movements are hard to follow with my eyes.	112, (55)	32, (16)	<0.001
2. I have double vision.	118, (58)	40, (20)	<0.001
3. I can read better with one eye closed.	16, (8)	20, (10)	<0.001
4. I have trouble with depth perception. I find it hard to say which one of 2 objects is closer.	18, (9)	8, (4)	<0.001
Optic nerve			
1. Colors seem to be paler than before.	18, (9)	16, (8)	<0.001
2. I can't read plain text on a colored or gray background.	54, (26)	22, (11)	<0.001
3. I run into objects or people or feel that parts of my visual field are missing.	14, (7)	8, (4)	<0.001
4. I have problems with rapid changes of light intensity.	60, (29)	10, (5)	<0.001
5. I see things that other people do not see (hallucinations).	60, (29)	12, (6)	<0.001

Thinner RNFL was found in PD patients with visual impairment and cognitive dysfunction

Patients with PD were divided into a cognitively impaired group (MoCA<26) and a normal control group (MoCA≥26). OCT examination was conducted to determine the thickness of the RNFL (Figure 3A). The deviation map for RNFL is summarized in Figure 3B. Results indicate that the superior and inferior directions in the perifovea region presented a higher deviation in the visually impaired group compared to the Asian average RNFL thickness (Figure 3B). Thinner RNFL in the ocular fundus was found in the cognitively impaired group (*t*-test, $p < 0.001$; Figure 3C). We examined VIPD-Q scores according to RNFL thickness *via* Spearman correlation analysis ($p < 0.001$, Pearson $r = -0.5302$; Figure 3D). Correlations between RNFL, MoCA, and UPDRSIII were analyzed, with positive associations between RNFL thickness and MoCA score ($p < 0.001$, Pearson $r = 0.5513$; Figure 3D), and a negative correlation was found between UPDRSIII score and RNFL thickness ($p < 0.001$, Pearson $r = -0.4996$; Figure 3E).

Vessel density in ocular fundus correlated with MoCA score and PVS number in PD

The vessels in the ocular fundus were extracted and analyzed *via* software (Figure 4A). Data showed the vessel percentage area (VPA), which indicated that vessel density in the ocular fundus was obviously lower in the cognitively impaired group (*t*-test,

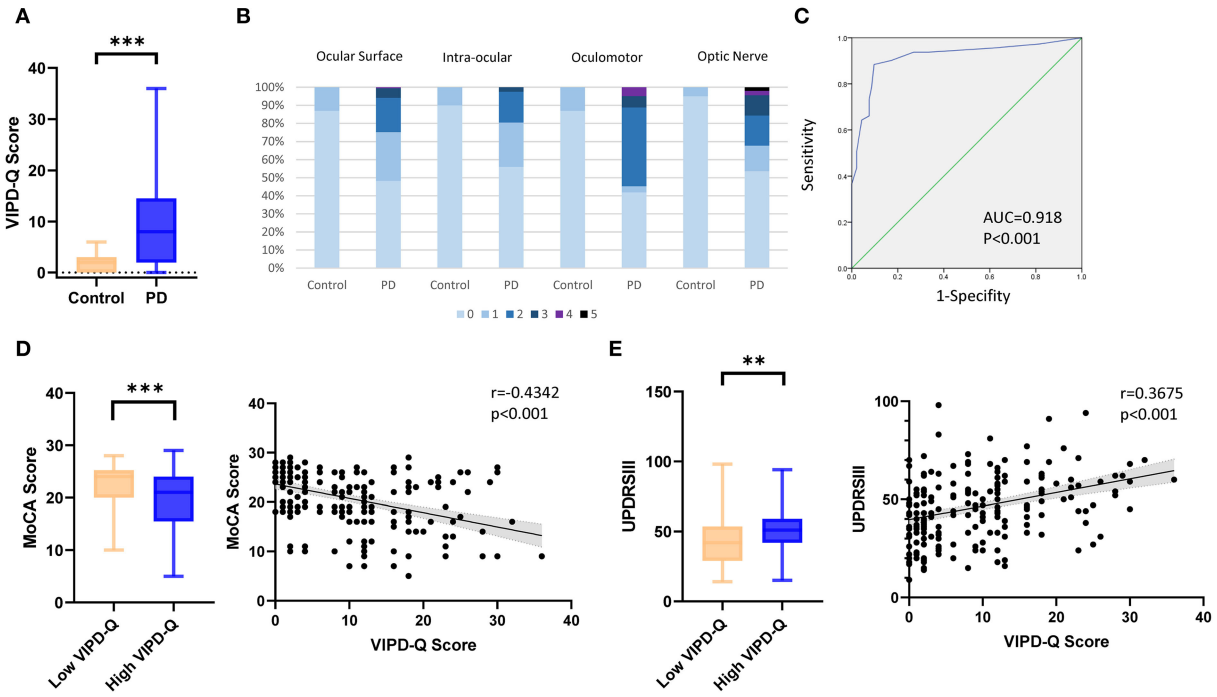

FIGURE 1
VIPD-Q scores for patients with PD in relation to MoCA and UPDRSIII scores. **(A)** Boxplot of the median total VIPD-Q score in the PD and control groups. **(B)** Number of ophthalmologic symptoms reported per domain (compared between patients with PD and controls). **(C)** The validation of sensitivity and specificity for the VIPD-Q *via* an ROC curve. **(D,E)** The VIPD-Q score was correlated with MoCA and UPDRSIII scores in PD.**$p <$ 0.01 and ***$p < 0.001$. PD, Parkinson's disease; ROC, receiver operating characteristic; VIPD-Q, Visual Impairment in Parkinson's Disease Questionnaire; UPDRS III, Unified Parkinson's Disease Rating Scale Section III; MoCA, Montreal Cognitive Assessment.

$p < 0.001$; Figure 4B). We then evaluated the relation between VIPD-Q scores and VPA *via* Spearman correlation analysis ($p = 0.001$, Pearson $r = -0.3485$; Figure 4C). Correlations between VPA and MoCA were analyzed, with positive associations between VPA and MoCA scores ($p < 0.001$, Pearson $r = 0.3338$; Figure 4C). When retrospect the MRI images, PVS counts were likewise abnormal in the visually impaired group (Figure 4D). PVS counts were higher in the high VIPD-Q group than in the control group (t-test, $p = 0.006$; Figure 4E); PVS volume did not differ (t-test, $p = 0.2679$; Figure 4E). We found negative correlations between VPA and PVS count ($p = 0.0278$, Pearson $r = -0.2009$; Figure 4F). Thus, eye examination may open a window for observing the process of intracranial disease noninvasively.

Nomogram based on ophthalmic parameters for predicting cognitive impairment risk

To evaluate the prognostic effect of ophthalmologic factors on cognitive impairment, numerous events (age, disease duration, sex, VIPD-Q score, RNFL thickness, vessel percentage area, etc.) were analyzed using multivariate logistic and LASSO regression (Figure 5A). Age, VIPD-Q score, RNFL thickness, and VPA were screened and verified *via* a bootstrap validation (Figure 5B). A nomogram was constructed based on these events (Figure 5C). The point scale in the nomogram was utilized to generate points for these variables; the risk of cognitive impairment (MoCA score < 26) was determined by accumulating the total points for all variables. The C-index of this nomogram was good, reaching 0.8373 (95% CI: 0.766–0.908). Consistency between predicted and observed clinical outcomes for patients with PD was confirmed *via* the calibration plot (Figure 5D). DCA showed a higher overall net benefit by applying the nomogram than either the "treat all" or the "treat none" approach within a range of threshold probabilities >10% (Figure 5E). These findings demonstrate that the ophthalmic event-based nomogram is an optimal model for predicting cognitive impairment in patients with PD in clinical management.

Discussion

In this study, we demonstrated that the VIPD-Q could be applied to the Chinese population. Results revealed that patients

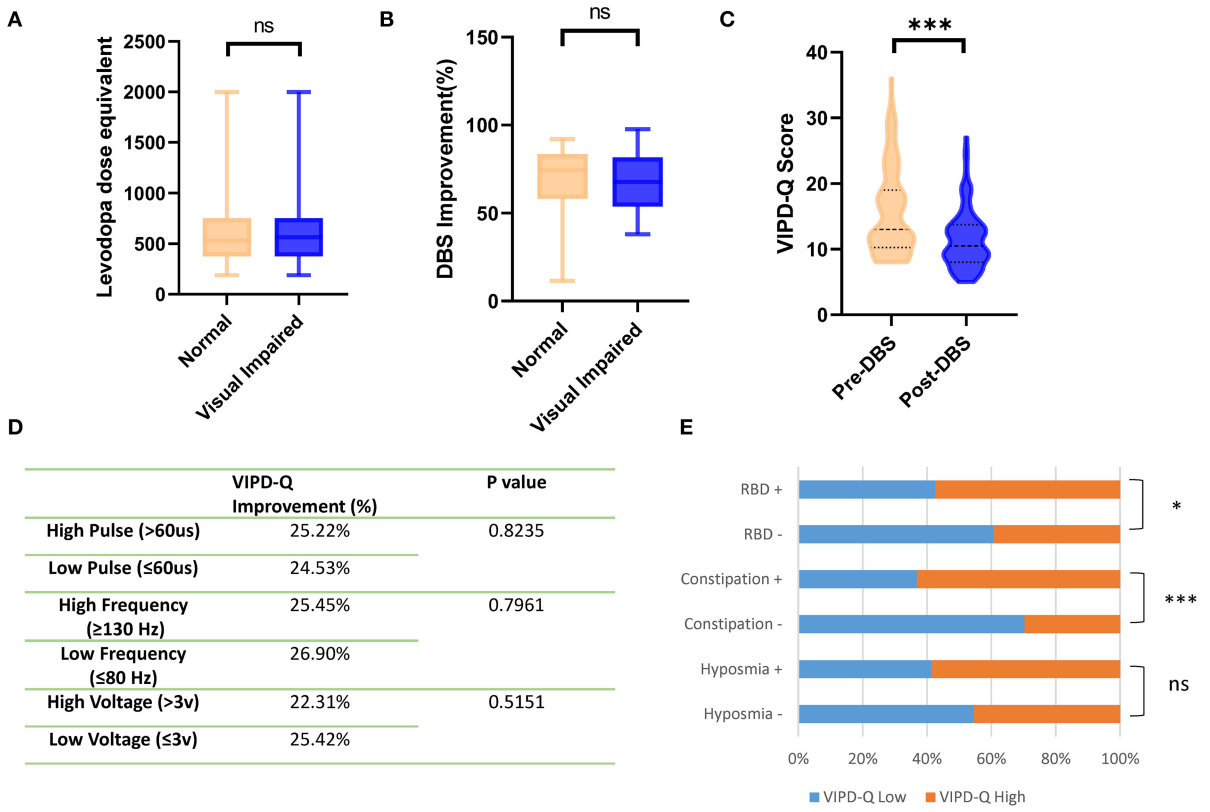

	VIPD-Q Improvement (%)	P value
High Pulse (>60us)	25.22%	0.8235
Low Pulse (≤60us)	24.53%	
High Frequency (≥130 Hz)	25.45%	0.7961
Low Frequency (≤80 Hz)	26.90%	
High Voltage (>3v)	22.31%	0.5151
Low Voltage (≤3v)	25.42%	

FIGURE 2
DBS and non-motor symptoms affected VIPD-Q scores in PD. **(A,B)** Groups with different VIPD-Q score presented similar LED and DBS improvements **(C)**. DBS improved VIPD-Q scores. **(D)** Stimulation parameter changing did not affect the VIPD-Q score. **(E)** PD patients with RBD or constipation had higher percentage of visual impairment (VIPD-Q>6). ns, no significant and ***$p < 0.001$. DBS, deep brain stimulation; RBD rapid eye movement (REM) sleep behavior disorder; VIPD-Q, Visual Impairment in Parkinson's Disease Questionnaire.

with PD have a higher prevalence of ophthalmologic symptoms, as reflected by a high VIPD-Q score, suggesting that PD itself or its treatment has an effect on an ophthalmologic function beyond the normal aging process. These results are in agreement with a previous European study (Borm et al., 2020).

To verify the sensitivity and specificity of the VIPD-Q, we plotted the ROC curve and calculated the cut-off value. We were thus able to screen PD patients with visual impairment in a large population. To our knowledge, the ideal cut-off value has not been reported previously and may provide a reference for similar studies.

An earlier study reported that visual impairment is a sensitive marker for PD (Weil et al., 2016); one study showed better discriminatory power for the early diagnosis of PD than any other NMS (Diederich et al., 2010). Our results demonstrated the predictive value of VIPD-Q for MoCA and UPDRSIII scores, echoing earlier findings that visuospatial motion perception and RNFL thickness correlate with movement disorders in PD (Beylergil et al., 2021; Murueta-Goyena et al., 2021).

The VIPD-Q scores indicated that PD or its treatment influence visual function. Studies report that oral levodopa rescues retinal morphology and improves visual function in amblyopia (Lee et al., 2019; Wang et al., 2020). We assumed that PD patients without ophthalmologic symptoms would benefit from a higher levodopa dose. However, our results conflict with this hypothesis, as different VIPD-Q score groups shared similar levodopa equivalents. DBS is another widespread treatment for PD (Weil et al., 2016), and an attractive yet less explored area is whether DBS could help patients with PD avoid visual deficits. Studies report that DBS improves saccades, smooth eye movements, and visual scanning (Murueta-Goyena et al., 2019). Others showed contradictory results (a little effect was observed after stimulation) (Kwapong et al., 2018). We evaluated the effects of DBS on ophthalmologic symptoms using the VIPD-Q. At a 3-month follow-up, we found that the VIPD-Q score declined in the post-DBS group. As oculomotor parameters were associated with axial symptoms and low frequency was reported to have a stronger effect on axial symptoms (Sidiropoulos et al., 2013; Xie et al., 2018), we compared groups with different

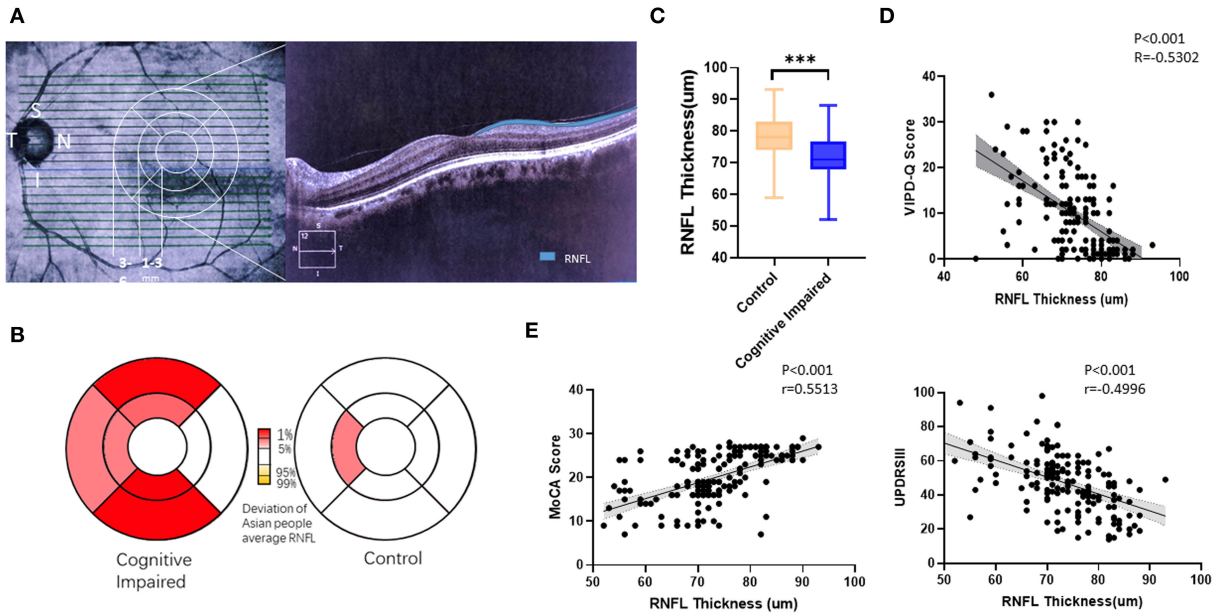

FIGURE 3
Thinner RFNL in the ocular fundus was found in the cognitively impaired group. **(A)** Representative picture of a measured RNFL. **(B)** Deviation map of RNFL indicating thinner thickness. **(C)** PD patients with cognitive impairment had, on average, a thinner RNFL. **(D)** VIPD-Q was related to RNFL thickness. **(E)** RNFL was related to MoCA and UPDRSIII scores. $^{**}p < 0.01$, $^{***}p < 0.001$, and r = Pearson r. RNFL, retinal nerve fiber layer; PD, Parkinson's disease; VIPD-Q, Visual Impairment in Parkinson's Disease Questionnaire; UPDRS III, Unified Parkinson's Disease Rating Scale Section III; MoCA, Montreal Cognitive Assessment.

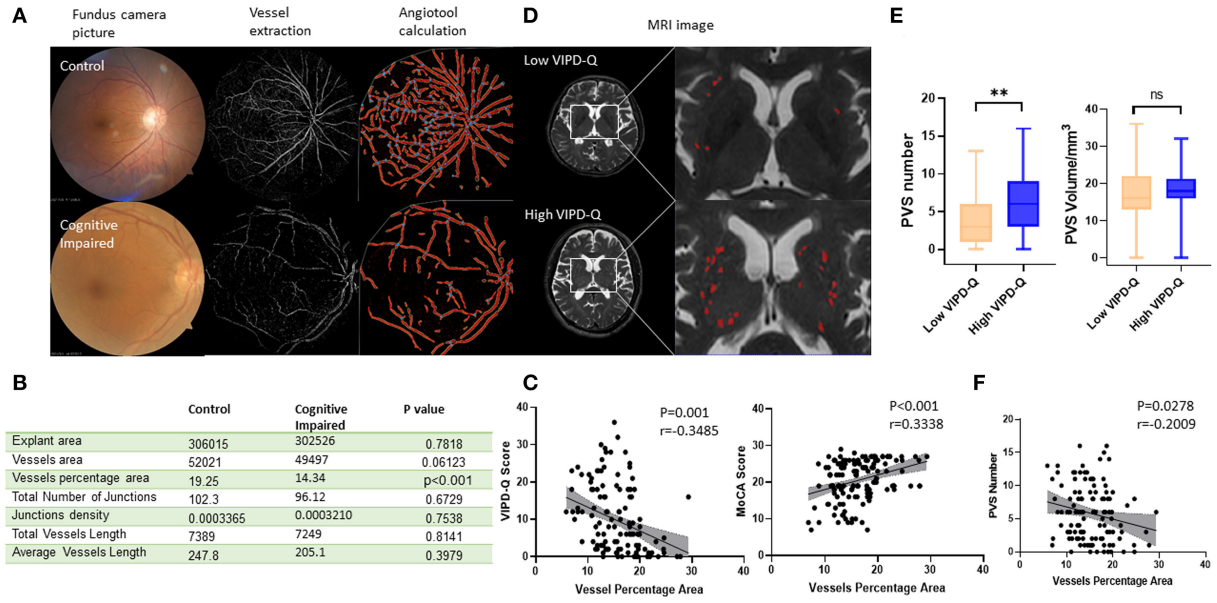

	Control	Cognitive Impaired	P value
Explant area	306015	302526	0.7818
Vessels area	52021	49497	0.06123
Vessels percentage area	19.25	14.34	p<0.001
Total Number of Junctions	102.3	96.12	0.6729
Junctions density	0.0003365	0.0003210	0.7538
Total Vessels Length	7389	7249	0.8141
Average Vessels Length	247.8	205.1	0.3979

FIGURE 4
Vascular density in ocular density predicted PVS number and cognitive status in PD. **(A)** Typical procedure for calculating vascular density in groups with or without cognitive impairment. **(B)** A table of vascular-related parameters in ocular fundus analyzed by angiotool. **(C)** The vessel percentage area was correlated with VIPD-Q and MoCA scores. **(D)** Representative MRI images for VIPD-Q high and low groups. **(E)** PVS count showed a discrepancy between VIPD-Q groups. **(F)** The vessel percentage area was correlated with PVS counts. $^{**}p < 0.01$, $^{***}p < 0.001$,and r = Pearson r. MRI, magnetic resonance imaging; PD, Parkinson's disease; PVS, perivascular spaces; VIPD-Q, Visual Impairment in Parkinson's Disease Questionnaire; MoCA, Montreal Cognitive Assessment.

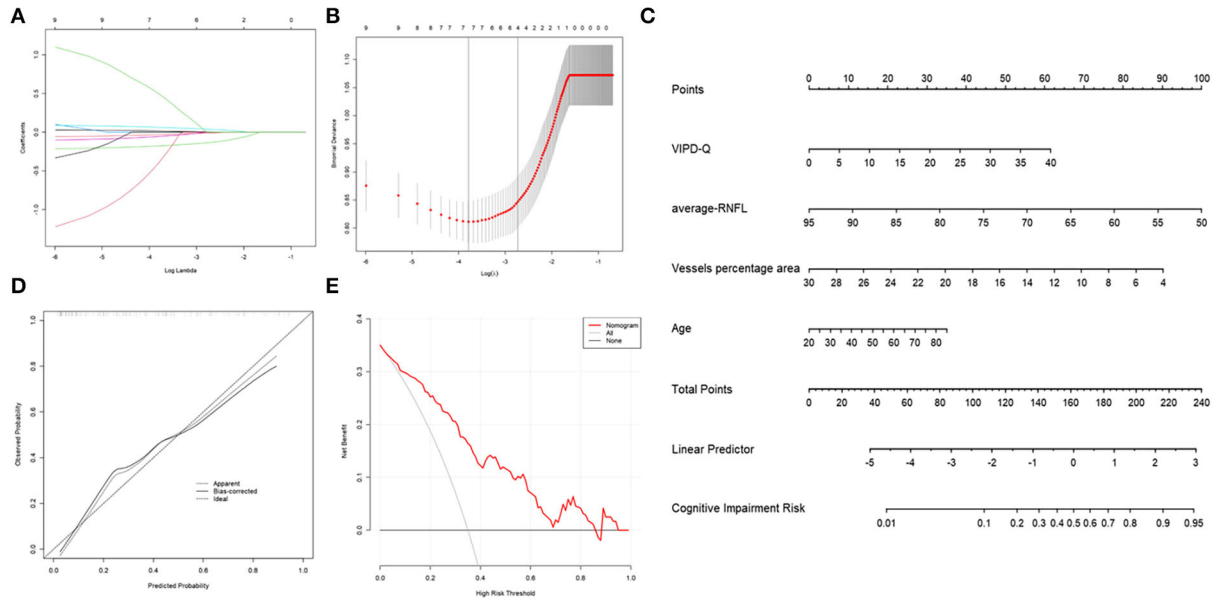

FIGURE 5
Nomogram of ophthalmic parameters predicting the risk of cognitive impairment in PD. **(A)** LASSO regression analysis was conducted to screen out MoCA score-related parameters. **(B)** Bootstrap validation was performed to verify the screened event. **(C)** A nomogram predicting the risk of cognitive impairment in PD was constructed based on ophthalmic parameters. **(D)** A calibration curve was drawn to decrease the bias of the nomogram. **(E)** A DCA curve showed that the nomogram would benefit patients with PD by accurately predicting the risk of cognitive impairment. DCA, decision curve analysis; PD, Parkinson's disease; MoCA, Montreal Cognitive Assessment.

stimulation parameters (voltage, pulse, frequency), which did not seem to influence the VIPD-Q score.

The role of NMS in PD progression has been discussed in many articles (Takeda et al., 2014; Hughes et al., 2018; Postuma et al., 2019; Cryan et al., 2020). However, few studies have focused on associations between NMS. We presumed that hyposmia would relate to visual dysfunction, as the olfactory and optic nerves are anatomically close. Strikingly, the hyposmia group in our study did not show a higher percentage of visual impairment than the control group. In contrast, the RBD-positive group showed a higher risk of visual impairment, consistent with a recently published study (Yang et al., 2016). Another vital finding in our investigation is that constipation was strongly correlated with visual impairment (percentage of visual impairment, 89 vs. 19%, $p < 0.001$). Thus, visual dysfunction in PD may originate peripherally.

Total VIPD-Q scores correlated with MoCA scores in our study, consistent with the well-established knowledge that visual dysfunction is associated with cognitive impairment. For example, thinner RNFL has predictive value as a biomarker of cognitive decline in PD (Murueta-Goyena et al., 2021). As VIPD-Q is negatively related to RNFL thickness, we consider that retinal neurodegeneration, neuronal loss, and anomalous α-synuclein deposits within the inner retinal layers may mediate this association. This hypothesis was supported by another study (Veys et al., 2019). Interestingly, the bias of thickness mainly occurred in the superior and inferior quadrants, as was observed in other Lewy body studies (Garcia-Martin et al., 2014; Murueta-Goyena et al., 2019, 2021).

Previous studies have reported that ocular microvascular patterns differ in patients with PD compared to healthy controls (Rascunà et al., 2020; Tsokolas et al., 2020; Robbins et al., 2021). We developed a software to extract the vessel from ocular fundus photography and analyze its morphology. The software was developed based on the U-Net model and uploaded to GitHub for free use. Our results showed that vessel density declined in the cognitively impaired group. This may be another explanation for the correlation between VIPD-Q scores and cognitive impairment. We also found that the PVS count in the higher VIPD-Q group exceeded that in the control group. Recent studies have indicated that PVS plays a disease-predicting role in PD, affecting cognitive status (Shibata et al., 2019; Rascunà et al., 2020; Shen et al., 2021) and motor prognosis (Chung et al., 2021). Our study demonstrated a relationship between vessel density and PVS count in PD, which, to our knowledge, has not been reported previously.

Our study was strengthened by a relatively large sample size and extensive sequencing data. This study provides powerful evidence for the positive effects of DBS on visual function. We propose a novel hypothesis that dysbiotic gut microbiota correlates with visual dysfunction in PD. Further investigation is needed to determine whether probiotics or antibiotics may help patients with PD avoid visual impairment. PVS was associated with vessel density in the ocular fundus. This work

has clinical implications, as our data suggest that ophthalmic parameters are tightly correlated with cognitive status in patients with PD. Clinicians can potentially predict the risk of cognitive impairment in PD precisely and conveniently using a nomogram.

The hypothesis that visual impairment in PD originates from dysbiosis of microbiota should be investigated further through cell-based functional studies. In addition, the follow-up time was up to 3 months, and patients with PD receiving STN-DBS may reduce their levodopa dose after this time point. As levodopa was reported to rescue retinal morphology and visual function in a murine model of human albinism (Lee et al., 2019; Vagge et al., 2020), further investigation is needed to determine whether the reduction of levodopa after DBS aggravates visual impairment. Another limitation is that 50% of the PD participants were recruited by the neurosurgery department while waiting to undergo a DBS operation. This may create selection bias regarding indications for DBS, including disease duration over 3 years and sensitivity to the levodopa challenge test. Finally, the nomogram model would benefit from external validation in a separate PD population.

In conclusion, our study demonstrated that VIPD-Q can be applied to the Chinese population and is a useful tool for screening visual impairment among patients with PD. DBS showed a positive effect on PD patients' visual function, and visual impairment was linked with cognitive decline. Thinner RNFL and lower vessel density in the ocular fundus may explain this correlation. Our study indicated that visual impairment in patients with PD may originate from the dysbiotic gut microbiota. This conclusion strongly supports the presence of interactions between gut–eye and gut–brain axes.

Data availability statement

The original contributions presented in the study are included in the article/Supplementary material, further inquiries can be directed to the corresponding author.

Ethics statement

The studies involving human participants were reviewed and approved by the Ethics Committees at Qilu Hospital (protocol KYLL-202008-065) and the First Affiliated Hospital of Shandong First Medical University (protocol S569) approved this study. The patients/participants provided their written informed consent to participate in this study. Written informed consent was obtained from the individual(s) for the publication of any potentially identifiable images or data included in this article.

Author contributions

CZ and HW performed the questionnaire including VIPD-Q, UPDRSIII, and MoCA. XW and Q-qW evaluated the status of movement disorders and made the statistics. All authors contributed to the article and approved the submitted version.

Acknowledgments

We appreciate the innovative work of Dr. Carlijn D.J.M. Borm to develop VIPD-Q and generously permit us to apply this questionnaire. We also feel grateful to Luca Antiga who shares the code for extracting the vessel in the ocular fundus.

Conflict of interest

The authors declare that the research was conducted in the absence of any commercial or financial relationships that could be construed as a potential conflict of interest.

Publisher's note

Supplementary material

The Supplementary Material for this article can be found online at: https://www.frontiersin.org/articles/10.3389/fnins.2022.928980/full#supplementary-material

References

Beylergil, S. B., Gupta, P., ElKasaby, M., Kilbane, C., and Shaikh, A. G. (2021). Does visuospatial motion perception correlate with coexisting movement disorders in Parkinson's disease? *J. Neurol.* 269, 2179–2192. doi: 10.1007/s00415-021-10804-2

Borm, C., Visser, F., Werkmann, M., de Graaf, D., Putz, D., Seppi, K., et al. (2020). Seeing ophthalmologic problems in Parkinson disease: results of a visual impairment questionnaire.

Neurology 94, e1539–e1547. doi: 10.1212/WNL.0000000000009214

Borm, C., Werkmann, M., Visser, F., Peball, M., Putz, D., Seppi, K., et al. (2019). Towards seeing the visual impairments in Parkinson's disease: protocol for a multicentre observational, cross-sectional study. *BMC Neurol.* 19, 141. doi: 10.1186/s12883-019-1365-8

Chung, S. J., Yoo, H. S., Shin, N. Y., Park, Y. W., Lee, H. S., Hong, J. M., et al. (2021). Perivascular spaces in the basal ganglia and long-term motor prognosis in newly diagnosed Parkinson disease. *Neurology* 96, e2121–e2131. doi: 10.1212/WNL.0000000000011797

Cryan, J. F., O'Riordan, K. J., Sandhu, K., Peterson, V., and Dinan, T. G. (2020). The gut microbiome in neurological disorders. *Lancet Neurol.* 19, 179–194. doi: 10.1016/S1474-4422(19)30356-4

Diederich, N. J., Pieri, V., Hipp, G., Rufra, O., Blyth, S., Vaillant, M., et al. (2010). Discriminative power of different nonmotor signs in early Parkinson's disease. A case-control study. *Mov. Disord.* 25, 882–887. doi: 10.1002/mds.22963

Ekker, M. S., Janssen, S., Seppi, K., Poewe, W., de Vries, N. M., Theelen, T., et al. (2017). Ocular and visual disorders in Parkinson's disease: common but frequently overlooked. *Parkinsonism Related Disord.* 40, 1–10. doi: 10.1016/j.parkreldis.2017.02.014

Garcia-Martin, E., Satue, M., Otin, S., Fuertes, I., Alarcia, R., Larrosa, J. M., et al. (2014). Retina measurements for diagnosis of Parkinson disease. *Retina* 34, 971–980. doi: 10.1097/IAE.0000000000000028

Hamedani, A. G., Abraham, D. S., Maguire, M. G., and Willis, A. W. (2020). Visual impairment is more common in Parkinson's disease and is a risk factor for poor health outcomes. *Mov. Disord.* 35, 1542–1549. doi: 10.1002/mds.28182

Hughes, K. C., Gao, X., Baker, J. M., Stephen, C., Kim, I. Y., Valeri, L., et al. (2018). Non-motor features of Parkinson's disease in a nested case-control study of US men. *J. Neurol. Neurosurg. Psychiatr.* 89, 1288–1295. doi: 10.1136/jnnp-2018-318275

Kwapong, W. R., Ye, H., Peng, C., Zhuang, X., Wang, J., Shen, M., et al. (2018). Retinal microvascular impairment in the early stages of Parkinson's disease. *Invest. Ophthalmol. Visual Sci.* 59, 4115–4122. doi: 10.1167/iovs.17-23230

Lee, H., Scott, J., Griffiths, H., Self, J. E., and Lotery, A. (2019). Oral levodopa rescues retinal morphology and visual function in a murine model of human albinism. *Pigment Cell Melanoma Res.* 32, 657–671. doi: 10.1111/pcmr.12782

Leyland, L. A., Bremner, F. D., Mahmood, R., Hewitt, S., Durteste, M., Cartlidge, M. R. E., et al. (2020). Visual tests predict dementia risk in Parkinson disease. *Neurol. Clin. Pract.* 10, 29–39. doi: 10.1212/CPJ.0000000000000719

Liskowski, P., and Krawiec, K. (2016). Segmenting retinal blood vessels with deep neural networks. *IEEE Trans. Med. Imaging* 35, 2369–2380. doi: 10.1109/TMI.2016.2546227

Murueta-Goyena, A., Del Pino, R., Galdós, M., Arana, B., Acera, M., Carmona-Abellán, M., et al. (2021). Retinal thickness predicts the risk of cognitive decline in Parkinson disease. *Ann. Neurol.* 89, 165–176. doi: 10.1002/ana.25944

Murueta-Goyena, A., Del Pino, R., Reyero, P., Galdós, M., Arana, B., Lucas-Jiménez, O., et al. (2019). Parafoveal thinning of inner retina is associated with visual dysfunction in Lewy body diseases. *Mov. Disord.* 34, 1315–1324. doi: 10.1002/mds.27728

Postuma, R. B., Iranzo, A., Hu, M., Högl, B., Boeve, B. F., Manni, R., et al. (2019). Risk and predictors of dementia and parkinsonism in idiopathic REM sleep behaviour disorder: a multicentre study. *Brain* 142, 744–759. doi: 10.1093/brain/awz030

Rascunà, C., Russo, A., Terravecchia, C., Castellino, N., Avitabile, T., Bonfiglio, V., et al. (2020). Retinal thickness and microvascular pattern in early Parkinson's disease. *Front. Neurol.* 11, 533375. doi: 10.3389/fneur.2020.533375

Robbins, C. B., Thompson, A. C., Bhullar, P. K., Koo, H. Y., Agrawal, R., Soundararajan, S., et al. (2021). Characterization of retinal microvascular and choroidal structural changes in Parkinson disease. *JAMA Ophthalmol.* 139, 182–188. doi: 10.1001/jamaophthalmol.2020.5730

Segarra, M., Aburto, M. R., Cop, F., Llaó-Cid, C., Härtl, R., Damm, M., et al. (2018). Endothelial Dab1 signaling orchestrates neuro-glia-vessel communication in the central nervous system. *Science* 361, eaao2861. doi: 10.1126/science.aao2861

Shen, T., Yue, Y., Zhao, S., Xie, J., Chen, Y., Tian, J., et al. (2021). The role of brain perivascular space burden in early-stage Parkinson's disease. *NPJ Parkinsons Dis.* 7, 12. doi: 10.1038/s41531-021-00155-0

Shibata, K., Sugiura, M., Nishimura, Y., and Sakura, H. (2019). The effect of small vessel disease on motor and cognitive function in Parkinson's disease. *Clin. Neurol. Neurosurg.* 182, 58–62. doi: 10.1016/j.clineuro.2019.04.029

Sidiropoulos, C., Walsh, R., Meaney, C., Poon, Y. Y., Fallis, M., Moro, E., et al. (2013). Low-frequency subthalamic nucleus deep brain stimulation for axial symptoms in advanced Parkinson's disease. *J. Neurol.* 260, 2306–2311. doi: 10.1007/s00415-013-6983-2

Takeda, A., Baba, T., Kikuchi, A., Hasegawa, T., Sugeno, N., Konno, M., et al. (2014). Olfactory dysfunction and dementia in Parkinson's disease. *J. Parkinsons Dis.* 4, 181–187. doi: 10.3233/JPD-130277

Tsokolas, G., Tsaousis, K. T., Diakonia, V. F., Matsou, A., and Tyradellis, S. (2020). Optical coherence tomography angiography in neurodegenerative diseases: a review. *Eye Brain* 12, 73–87. doi: 10.2147/EB.S193026

Vagge, A., Ferro Desideri, L., and Traverso, C. E. (2020). An update on pharmacological treatment options for amblyopia. *Int. Ophthalmol.* 40, 3591–3597. doi: 10.1007/s10792-020-01535-w

Veys, L., Vandenabeele, M., Ortuño-Lizarán, I., Baekelandt, V., Cuenca, N., Moons, L., et al. (2019). L: Retinal α-synuclein deposits in Parkinson's disease patients and animal models. *Acta Neuropathol.* 137, 379–395. doi: 10.1007/s00401-018-01956-z

Wang, S. P., Li, Q. X., and Li, S. (2020). Systematic evaluation of levodopa effect on visual improvement in amblyopia: a meta-analysis. *Clin. Neuropharmacol.* 43, 20–25. doi: 10.1097/WNF.0000000000000372

Weil, R. S., Schrag, A. E., Warren, J. D., Crutch, S. J., Lees, A. J., Morris, H. R., et al. (2016). Visual dysfunction in Parkinson's disease. *Brain* 139, 2827–2843. doi: 10.1093/brain/aww175

Xie, T., Bloom, L., Padmanaban, M., Bertacchi, B., Kang, W., MacCracken, E., et al. (2018). Long-term effect of low frequency stimulation of STN on dysphagia, freezing of gait and other motor symptoms in PD. *J. Neurol Neurosurg. Psychiatry* 89, 989–994. doi: 10.1136/jnnp-2018-318060

Xie, T., Padmanaban, M., Bloom, L., MacCracken, E., Bertacchi, B., Dachman, A., et al. (2017). Effect of low versus high frequency stimulation on freezing of gait and other axial symptoms in Parkinson patients with bilateral STN DBS: a mini-review. *Transl. Neurodegener.* 6, 13. doi: 10.1186/s40035-017-0083-7

Yang, Z. J., Wei, J., Mao, C. J., Zhang, J. R., Chen, J., Ji, X. Y., et al. (2016). Retinal nerve fiber layer thinning: a window into rapid eye movement sleep behavior disorders in Parkinson's disease. *Sleep Breath* 20, 1285–1292. doi: 10.1007/s11325-016-1366-4

frontiers | Frontiers in Neuroscience

TYPE Review
PUBLISHED 21 December 2022
DOI 10.3389/fnins.2022.1029473

OPEN ACCESS

EDITED BY
Wendy Noble,
King's College London,
United Kingdom

REVIEWED BY
Simona Piccirella,
Diadem Srl, Italy
Giulia Abate,
Brescia University, Italy

*CORRESPONDENCE
Peter Wolfrum
peter.wolfrum@gmail.com

SPECIALTY SECTION
This article was submitted to Neurodegeneration, a section of the journal Frontiers in Neuroscience

RECEIVED 27 August 2022
ACCEPTED 05 December 2022
PUBLISHED 21 December 2022

CITATION
Wolfrum P, Fietz A, Schnichels S and Hurst J (2022) The function of p53 and its role in Alzheimer's and Parkinson's disease compared to age-related macular degeneration. *Front. Neurosci.* 16:1029473. doi: 10.3389/fnins.2022.1029473

The function of p53 and its role in Alzheimer's and Parkinson's disease compared to age-related macular degeneration

Peter Wolfrum*, Agnes Fietz, Sven Schnichels and José Hurst

Centre for Ophthalmology, University Eye Hospital Tübingen, Tübingen, Germany

The protein p53 is the main human tumor suppressor. Since its discovery, extensive research has been conducted, which led to the general assumption that the purview of p53 is also essential for additional functions, apart from the prevention of carcinogenesis. In response to cellular stress and DNA damages, p53 constitutes the key point for the induction of various regulatory processes, determining whether the cell induces cell cycle arrest and DNA repair mechanisms or otherwise cell death. As an implication, aberrations from its normal functioning can lead to pathogeneses. To this day, neurodegenerative diseases are considered difficult to treat, which arises from the fact that in general the underlying pathological mechanisms are not well understood. Current research on brain and retina-related neurodegenerative disorders suggests that p53 plays an essential role in the progression of these conditions as well. In this review, we therefore compare the role and similarities of the tumor suppressor protein p53 in the pathogenesis of Alzheimer's (AD) and Parkinson's disease (PD), two of the most prevalent neurological diseases, to the age-related macular degeneration (AMD) which is among the most common forms of retinal degeneration.

KEYWORDS

p53, neurodegeneration, Alzheimer's disease, Parkinson's disease, retina, age-related macular degeneration

Introduction

Neurodegeneration describes pathological processes leading to the malfunctioning and destruction of nerve cells. With life expectancies steadily increasing, neurodegenerative diseases are a growing concern for public health (Deuschl et al., 2020). While some of the most frequent diseases concerning the brain are Alzheimer's

(AD) and Parkinson disease (PD), also retinal-related degenerative diseases such as the age-related macular degeneration (AMD) are increasingly prevalent (Checkoway et al., 2011; Li et al., 2020). The retina is an anatomical extension of the brain where certain parallels can be drawn since it is as well derived from the neuroectoderm and part of the central nervous system (CNS). Therefore, neurodegenerative diseases of the brain and the retina share characteristic damages to nerve tissue, which causes a significant loss in the self-reliance and quality of life for patients. As the diseases progress, patients can lose important functions of the nervous system or in the case of the retina, their eyesight. Although the causes of neurodegenerative diseases in general are multifactorial, some diseases are known to have a strong hereditary component (Armstrong, 2020). For instance, the early onset familial Alzheimer's disease (EOFAD) represents a subgroup of AD, whereby mutations in certain loci promote pathogenetic pathways leading to an early onset, additional neurological symptoms as well as a more severe course of disease (Wu et al., 2012). To date, the therapeutic possibilities in neurodegenerative diseases are insufficient. While PD is often progressive during treatment, the symptoms of diseases like AD can only be slightly alleviated by therapy and some forms of AMD even offer no medical therapy option at all. The therapeutic challenge results from different circumstances like pharmacokinetic problems related to the blood brain- and blood retinal-barrier, as well as diverse disease trigger factors and the poorly understood complexity of the pathogeneses (Modi et al., 2010; Duraes et al., 2018). The goal for all neurodegenerative diseases is to find novel therapeutical approaches that can prevent or decelerate the progression of these conditions. Understanding the underlying molecular and pathological mechanisms is essential for the development of such treatments. The tumor suppressor protein p53 has been shown to constitute a key point in the emergence of carcinosis (Lane, 1994). Lately, p53 has also been linked to the pathogenesis of non-cancerous diseases, which is why this review focuses on the influence of p53 in the pathogenesis of neurodegenerative diseases (Szybinska and Lesniak, 2017). Thus, in the following, the function of p53 in AD, PD and AMD is outlined and a comprehensive overview of the current state of research is offered.

The tumor suppressor protein p53

p53 was first discovered in 1979 and was named after its molecular mass of 53 kilodaltons (kDa) (Levine and Oren, 2009; Soussi, 2010). p53 acts as a transcriptional factor and is composed of the N-terminal Domain (NTD), the folded DNA-binding Domain (DBD) and tetramerization Domain (TD), as well as the regulatory Domain (RD), all together contributing to its functioning (Ho et al., 2006). The NTD thereby interacts with and activates enzymes of the transcription machinery. The DBD facilitates the process of DNA binding, together with the TD which is responsible for the tetrameric quaternary structure formation of p53 (Chene, 2001). The RD further stabilizes the tetrameric formation and is involved in the regulation of other proteins, whereby not all functions are completely resolved yet (Ho et al., 2006; Romer et al., 2006; Retzlaff et al., 2013). The correct conformation of p53 is crucial. Therefore, changes in the confirmation can lead to structural aberrations and possibly p53-unfolding accompanied by alterations of its functioning. Besides different conformational states, 12 different p53 protein-isoforms exist, which originate from alternative processes of splicing, initiation of translation or promoter activation (Khoury and Bourdon, 2011).

In more than 50% of all human cancer diseases, p53 is found to be mutated, which points out its importance in the prevention of tumor genesis (Joerger and Fersht, 2008). Besides that, ongoing research has discovered its relevance for the regulation of numerous processes in the cell. In response to cellular damages, post-translational-modifications (PTM) of p53 take place, which lead to a decreased binding affinity to the inhibitory MDM2 protein as well as an increased target gene expression. In the case of mild stress, p53 activates pathways resulting in cell cycle arrest and DNA-repair mechanisms, whereas following irreparable damages, apoptosis or senescence is initiated (**Figure 1**; Kastenhuber and Lowe, 2017). Senescence has been linked to both physiological and pathological conditions, the latter including ageing, cancer, and other age-related disorders (Munoz-Espin and Serrano, 2014). Furthermore, it has also been shown that p53 and the levels of its downstream targets are tissue specific (Burns et al., 2001; Tanikawa et al., 2017). Through different alterations such as mutations or following excessive amounts of oxidative stress, p53 mediated responses can also lead to the emergence of diseases.

p53 activation and target gene induction

To prevent possible toxic consequences under normal conditions, the basal concentration of p53 is low and regulated by the negative feedback loop of the ubiquitin ligase MDM2, which is the cellular antagonist of p53 and contributes to the critical step in mediating p53 degradation by nuclear and cytoplasmic proteasomes (Moll and Petrenko, 2003). The activation of oncogenes like the Ras oncogene as well as the accumulation of cell and DNA damages, which further lead to the induction of different kinases and transcriptional factors like *P300/CB* or *PCAF,* initiate modifications of p53 *via* phosphorylation and acetylation (Steegenga et al., 1996; Prives and Manley, 2001; Reed and Quelle, 2014). These changes lead to an increase in the DNA-binding capacity, through its DBD, as well as a reduced binding of MDM2 (Shieh et al., 1997; Kastenhuber and Lowe, 2017). Furthermore, the half-life value

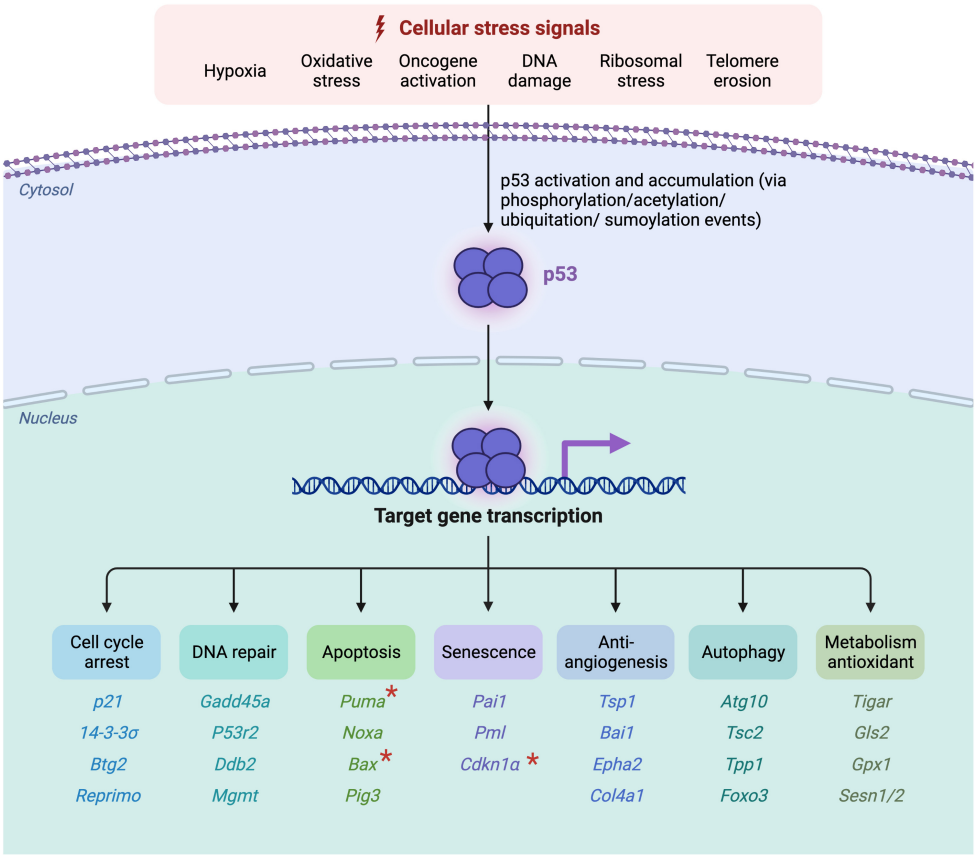

FIGURE 1
Overview of p53-activation, target gene induction and its corresponding functioning. Active oncogenes or the accumulation of cellular damages and stressors lead to the phosphorylation, acetylation, ubiquitation or sumoylation of p53 *via* the activation of kinases and transcriptional factors. Following its activation, p53 binds to its corresponding DNA-promoter-regions, through which cell cycle arrest, DNA repair mechanisms, apoptosis, senescence, anti-angiogenic, autophagic or antioxidant metabolism mechanisms are induced. The corresponding target genes are listed below the according function. The "*" marked genes represent neurodegenerative p53-influenced downstream targets, discussed in this review (Created with BioRender.com).

as well as its transcriptional activity can also be influenced by other chemical reactions like ubiquitation or sumoylation, which thereby lead to modifications of certain lysine residues in the TD and RD (Romer et al., 2006). The two reactions are again in response to cellular stress and are facilitated by the ubiquitination-proteasome system as well as proteins of the small ubiquitin-like modifier family (SUMO) (Seeler and Dejean, 2003; Li et al., 2022). Besides the four named PTMs, numerous other protein modifications exist which again lead to changes of p53-functioning (Clark et al., 2022).

Once p53 is activated, it binds *via* its DBD to the consecutive DNA-Promotor sequences of its target genes. Through the binding of one DBD dimer, consisting of two DBD monomers, the tetrameric p53-DNA-complex is formed (Romer et al., 2006). Depending on which promoter sequence p53 has bound to, different downstream genes are expressed. Thereby again, depending on various factors, the p53 mediated signal-transduction can either lead to the survival of the cell *via* cell cycle arrest and consecutive DNA repair mechanisms, the permanent cell cycle arrest *via* senescence or the lethal cell death *via* apoptosis (Mijit et al., 2020). Besides these functions, p53 can also induce anti-angiogenic, autophagic or antioxidant metabolism processes (**Figure 1**; Shu et al., 2007; Riley et al., 2008). Additional functions of p53 are also investigated, such as an influence in cell fate determination, as well as an impact in the regulation of the necrotic cell death (Crighton et al., 2006; Rozan and El-Deiry, 2007; Ying and Padanilam, 2016). Due to the large size of the protein, it is likely that even more unknown functions are also regulated by p53.

p53-mediated apoptosis regulation

The most common p53-mediated apoptosis mechanisms are the intrinsic and the extrinsic apoptosis pathway which

are mainly responsible for cell death in mammalian cells (Wang et al., 2015; Aubrey et al., 2018). In the intrinsic pathway, increased levels of p53 lead to the upregulation of the pro-apoptotic BH3-only proteins and the inhibition of anti-apoptotic proteins of the BCL-2-family. This causes increased BAX and BAK levels and further initiates the mitochondrial membrane permeabilization, Apoptosome formation and Caspase activation as part of the mitochondrial apoptotic pathway (Aubrey et al., 2018; Xu et al., 2019).

In regards to the extrinsic pathway, the activation of p53 can induce an upregulation of the death receptor density in the cell membrane (Carneiro and El-Deiry, 2020). The binding of certain ligands on these receptors, like the Fas-ligand, marks the induction of the extrinsic apoptosis pathway. Both pathways eventually lead to the activation of Caspases 3 and 7, initiating irreversible cell death. Moreover, the BH3 interacting domain death agonist (BID) is a protein that connects the extrinsic to the intrinsic apoptosis pathway which demonstrates that interferences between the two pathways can also occur (Aubrey et al., 2018; **Figure 2**).

p53 and neurodegeneration

In general, symptoms of brain-related neurodegenerative disease, like AD or PD, emerge through the decline of neuronal cells. Elevated levels of p53, cohering with neurodegeneration, have previously been observed, implying a key role of p53 in the pathogeneses of brain-related neurodegeneration (Chang et al., 2012). As a response to specific events such as DNA damage, metabolic compromises or increased oxidative stress, p53 can trigger apoptosis in neuronal cells. Thereby, depending on its stimulus, p53 induces the cell death either through the induction of the classical extrinsic and intrinsic apoptosis pathway, or through a synapses-specific cell death mechanism, whereby the apoptosis is directly triggered at the mitochondrial level, without an upstream transcriptional activity (Culmsee and Mattson, 2005).

Influence of p53 on Alzheimer's disease

Alzheimer's disease is a progressive disease affecting the cortex cerebri and hippocampus and is leading to neuronal cell loss and cerebral atrophy. As the disease progresses, cognitive impairments such as dementia, behavioral changes and disorientation symptoms occur. The pathogenesis of the accompanying neurodegeneration has been extensively studied and is associated with several events leading to β-amyloid (Aβ) plaque formation and deposition, as well as the accumulation of hyperphosphorylated Tau (p-tau) and further neurofibrillary tangle formation (**Figure 3**; Chang et al., 2012; Dos Santos Picanco et al., 2018).

As investigated in multiple studies, patients affected by AD exhibit elevated levels of p53 in several sections of their brain (de la Monte et al., 1997; Kitamura et al., 1997; Szybinska and Lesniak, 2017). One of the assumed factors leading to a p53-dependent apoptosis induction in neuronal cells is the accumulation of Aβ (Troy et al., 2000). In presence of Aβ, increased levels of the pro-apoptotic BAX, as well as decreased levels of anti-apoptotic BCL-2 proteins have been observed *in vitro*, as well as in post mortem brain analysis of AD affected patients (Paradis et al., 1996; Su et al., 1997; Chang et al., 2012). Moreover, a link between Aβ and an increase in the p53 upregulated modulator apoptosis protein (PUMA), which is another BH3-only protein that inhibits anti-apoptotic BCL-2 proteins, has been observed (Feng et al., 2015). Fogarty et al. detected that the treatment of cortical neurons with Aβ leads to the phosphorylation of p53 at serine 15, which is a well-known PTM of p53, leading to its activation and an increased transcriptional activity (Fogarty et al., 2010; Loughery et al., 2014). In the same study, an alternative cell death mechanism, operated by the process of lysosomal membrane permeabilization was observed. Thereby, the association of phosphorylated p53 with the lysosomal membrane leads to changes in its integrity and further the leakage of hydrolases into the cytosol. Subsequently, cell death is initiated, either through direct cell death, *via* the digestion of vital proteins, or indirectly *via* a caspase cascade (Boya and Kroemer, 2008; Fogarty et al., 2010).

Another nouveau theory about the role of p53 in AD pathogenesis is about the unfolded p53 modification. Uberti et al. (2002, 2008) discovered conformational changes of p53 in fibroblasts of AD affected patients (Abate et al., 2020). The thereby observed and later named "unfolded p53" protein comprises structural aberrations which can be induced through various influences. In the review of Clark et al., different factors, like reactive oxygen species (ROS), reactive nitrogen species (RNS), Aβ-amyloid or metallothionein are listed which lead to the unfolded p53 modification in context of AD pathogenesis (Clark et al., 2022). Since under its normal composition, p53 controls many processes in the cell in order to avoid cellular damages, the emergence of unfolded p53 subsequently initiates abnormal regulations like the inhibition of the SOD and GAP-43 pathway or the promotion of the CD44 and mTOR pathway, overall leading to neuronal dysfunction and the promotion of neurodegeneration (Abate et al., 2020).

One more recent finding in AD pathogenesis is the formation of p53 oligomers and fibrils followed by its colocalization with the Tau protein, which was shown in AD affected brains (Farmer et al., 2020). It is assumed that these aggregative changes of p53 lead to an endogenous p53 seeding in neurons. Furthermore, a subsequently altered p53 function, referable to the mislocalization of phosphorylated p53 outside

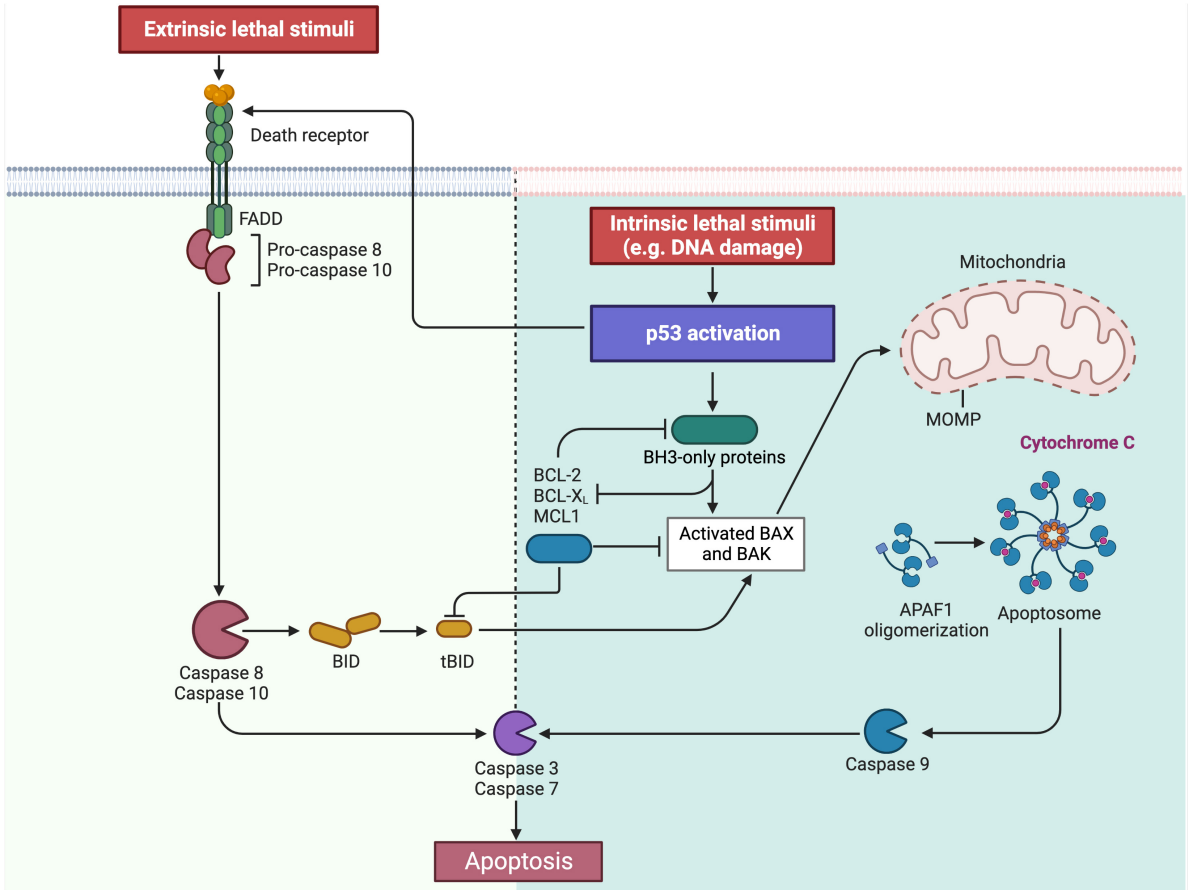

FIGURE 2
Overview on the intrinsic and extrinsic apoptosis pathway. As part of the intrinsic pathway, the activation of p53 leads to the increased expression of the BH3-only proteins, which is followed by BAX and BAK. Simultaneously the BH3-only proteins also inhibit the anti-apoptotic proteins BCL-2, BCL-X, and MCL1. This then leads to the permeabilization of the outer mitochondrial membrane (MOMP) of the mitochondria with the consequence of cytochrome c release, apoptosome formation and caspase 9-activation. Contrary, the same anti-apoptotic proteins BCL-2, BCL-X and MCL1 inhibit the BH3-only proteins under physiological conditions in order to prevent apoptosis induction. In the extrinsic pathway, p53 can upregulate so called "death receptors" in the cell membrane. Following the binding of the respective ligand, the death signal is triggered and transmitted into the cell. This then leads to the activation of caspase 8 and 10. Both pathways finally lead to the induction of caspases 3 and 7, through which the apoptosis is irreversible induced. In addition, the extrinsic and intrinsic apoptosis pathways are also connected by the BH3 interacting domain death agonist (BID), allowing a secondary activation of the intrinsic pathway (Created with BioRender.com).

of the nucleus is thereby also hypothesized, to be responsible for the progressive neurodegeneration in AD pathogenesis (Farmer et al., 2020).

Influence of p53 on Parkinson's disease

The loss of dopamine secreting neurons, as well as the accumulation of Lewy bodies, which constitute of misfolded α-synuclein, are the main events characterizing the pathogenesis of PD (**Figure 3**; Balestrino and Schapira, 2020). Patients affected by the disease experience hyperkinesia, which is accompanied with akinesis, rigor, tremor, as well as postural instability. In the further course of the disease, it can also lead to cognitive impairments and dementia (Beitz, 2014).

Different cellular stress factors such as mitochondrial dysfunction, oxidative stress or an abnormal protein aggregation have been associated with the pathogenesis of PD (Naoi and Maruyama, 1999; Luo et al., 2022). Since p53-induced cell death occurs also in response to cellular stress and p53 is able to induce cell death in dopaminergic neurons, it thus seem likely that it is involved in the pathogenesis of PD (Shu et al., 2007; Lu et al., 2017). Mogi et al. observed elevated levels of p53 as well as an increase of apoptosis-related proteins like BAX in examined parkinsonian brains (Mogi et al., 2007; Liu et al., 2019). Furthermore, phosphorylated p53 modifications have also been detected in tissue of the substantia nigra in PD

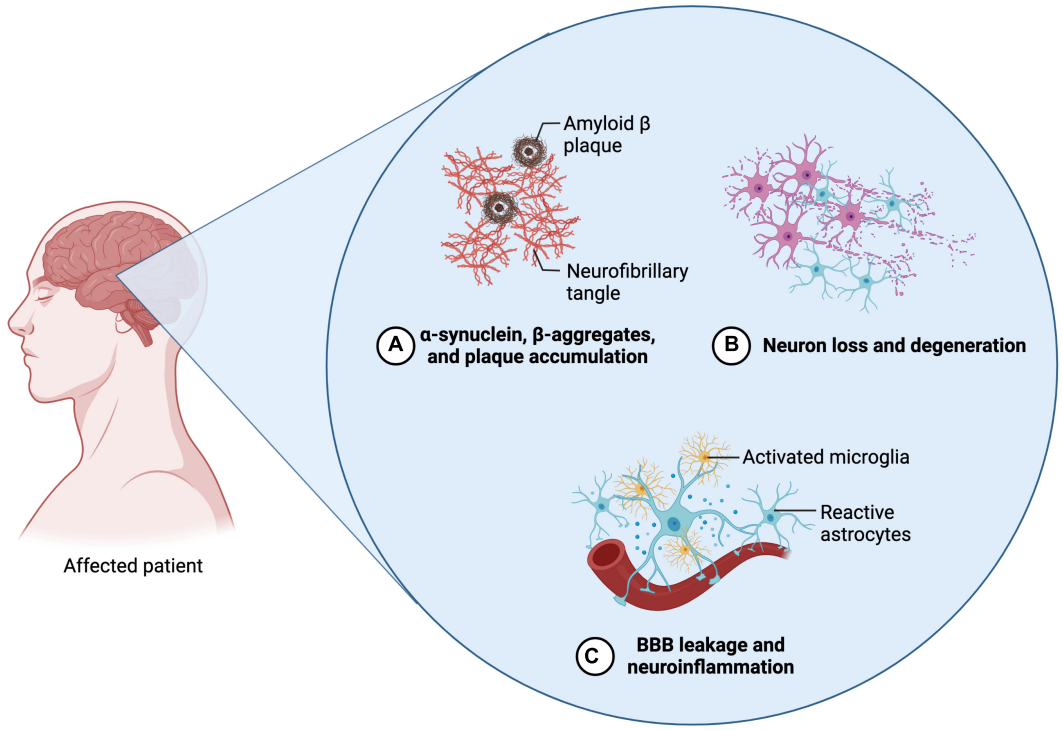

FIGURE 3
Neuropathological features of Parkinson's disease (PD) and Alzheimer's disease (AD). The two diseases exhibit similar neuropathological features. **(A)** The emergence of abnormal protein depositions can thereby be observed during the initial phases of both diseases. In regard to AD, β-amyloid plaques and Tau protein accumulations can be found, whereas in PD α-synuclein aggregates. **(B)** The abnormal accumulation then leads to the induction of apoptosis and the decline of the according neuronal cells. Regarding AD, primarily neurons in the area of the cortex and the hippocampus are affected. In PD, mainly dopaminergic neurons in the substantia nigra are affected **(C)** Alongside the progressive neuronal cell decline, neuroinflammation and the disruption of the blood-brain barrier can be observed, which is accompanied by their pathognomonic symptoms (Created with BioRender.com).

affected patients (Martire et al., 2015). Research on proteins of the BCL-2 family suggest a central role in the embryological development of dopaminergic neurons as well as its loss in disease like PD. Thereby, as part of the embryological related cell death, apoptotic processes such as the caspase 3 induced DNA fragmentation, were observed in mice-models (Jackson-Lewis et al., 2000). Additionally, the overexpression of anti-apoptotic BCL-2 proteins preserves dopaminergic neurons from toxin-induced apoptosis and leads to an increased number of dopaminergic cells postnatally (Jackson-Lewis et al., 2000; Liu et al., 2019).

Unfolded p53 protein has not been observed in PD affected patients (Abate et al., 2020). Nevertheless, a different modification of p53 has been detected in the pathogenesis of PD: 1-methyl-4-phenyl-1,2,3,6-tetrahydropyridine (MPTP) induces the cell death of dopaminergic neurons in the substantia nigra of mice which has ever since been used as model for the investigation of PD pathogenesis (Nicotra and Parvez, 2002). Mandir et al. (2002) observed that following the MPTP treatment, p53 was poly(ADP-ribosy)lated by the Poly(ADP-ribose)-Polymerase 1 (PARP). These changes thereby lead to the stabilization of p53 as well as an increase in its levels (Martire et al., 2015). During the initial phase of extensive p53-ribosylation, it was further observed that the DNA binding of p53 was inhibited. Therefore, only after the following deribosylation of p53, the binding of the according DNA target gene regions is enabled again, which finally leads to the apoptosis-induction of dopaminergic neurons (Mandir et al., 2002).

Influence of p53 in the age-related macular degeneration

AMD is a degenerative, progressive disease leading to photoreceptor degeneration in the area of the *macula lutea* and constitutes the leading cause for vision loss in elderly people from industrialized countries (Loss et al., 2018). In the development of AMD, there is a causal relationship between oxidative stress and the pathogenesis of the disease (Yildirim et al., 2011; Schnichels et al., 2021). In early disease stages, lipid deposits also called lipofuscin and drusen accumulate

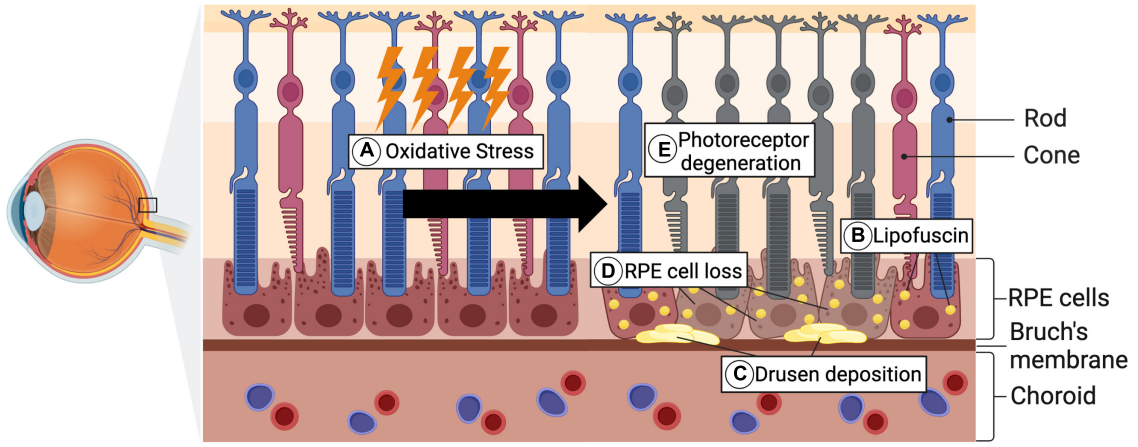

FIGURE 4
Pathological hallmarks of AMD pathogenesis. **(A)** As a consequence of genetic predispositions, environmental factors, as well as aging, oxidative stress accumulates. **(B,C)** Lipofuscin, which is composed of lipid- and protein residues, forms under increased oxidative stress levels and further accumulates in RPE cells. Alongside the lipofuscin, Drusen depositions, consisting of extracellular material, form in the area of Bruch's membrane. **(D)** Through the progredient accumulation of these depositions, the RPE cell death is subsequently triggered. **(E)** Secondary this then leads to photoreceptor degeneration and occurrence of visual impairments (Created with BioRender.com).

in the area of Bruch's membrane and RPE cells (**Figure 4**; Bowes Rickman et al., 2013). Subsequently, the accumulation leads to the functional impairment of RPE cells and thus their cell death (Mitchell et al., 2018). One of the main functions of RPE cells is the support of photoreceptor cells, hence its loss secondarily leads to photoreceptor degeneration, which is accompanied by vision impairment (Strauss, 2005; Mitchell et al., 2018). While patients affected by early forms of AMD, are mostly asymptomatic or experience slight visual function impairments reading in the dark, advanced disease stages can lead to severe vision loss (McLeod et al., 2009; Bowes Rickman et al., 2013). The later stages of AMD can further be sub-classified into the "*dry*" and the "*wet*" form. Whereas dry AMD is also referred to as atrophic AMD and accounts for 90% of all cases of AMD, the wet form is associated with neovascularization processes and coheres with rapid vision loss (Bowes Rickman et al., 2013; Akyol and Lotery, 2020). Since the RPE cell loss and consequent photoreceptor degeneration are the crucial hallmarks of AMD pathogenesis, the cell death of both cell types has been extensively investigated.

The expression of p53 in various ocular tissues, including multiple retinal layers in transgenic mice and rats, have previously been observed suggesting an overall function of p53 in the eye (Shin et al., 1999; Vuong et al., 2012). p53 is associated with retinal responses to radiation and oxidative stress. Miller et al. investigated photoreceptor cell death mechanisms by treating cells of the 661W-photoreceptor cell line with the oxidative stressor CI-1010. Elevated levels of the p53-induced caspases 3 and 8 were thereby detected without an increase of cytochrome c, suggesting a p53 dependent, non-mitochondrial cell death mechanism in photoreceptors (Miller et al., 2006). Contrary, *in vivo* studies from Lansel et al. and Marti et al. documented increased apoptosis induction in mice from extensive light exposure, independent of a p53 prevalence. In both studies, p53-wild-type mice and p53 null-mice were treated with bright light exposure treatments, following electroretinogram (ERG) and morphological analyses. Subsequently after the exposure, both mice types showed similar ERG-, as well as histochemical- and biochemical- results, suggesting that the light induced apoptosis in photoreceptors is not p53-dependent (Lansel et al., 1998; Marti et al., 1998; Vuong et al., 2012). However, increased p53-dependent apoptosis rates were observed in bright light exposed human ARPE-19 cells. The apoptosis rate was further only increased under the premise that components of the RPE lipofuscin pigment were present, which again is a concomitant factor in AMD pathogeneses (Westlund et al., 2009; Vuong et al., 2012). Furthermore, Bhattacharya et al. observed an increased basal rate of the p53-dependent apoptosis in aged human RPE cells, which could be contiguous with the progressive cell death in AMD pathogenesis. The increased p53 activity was attributed to the acetylation and phosphorylation of p53, which again leads to the loss of the negative feedback loop function of MDM2 (Bhattacharya et al., 2012). As mentioned earlier, these two modifications of p53 constitute two of the most common PTMs increasing the p53 activity levels (Aubrey et al., 2018). In conjunction with the increased p53 activity, a reduction of the anti-apoptotic BCL-2 proteins was thereby measured as well, supporting the thesis of a p53 dependent cell death (Bhattacharya et al., 2012).

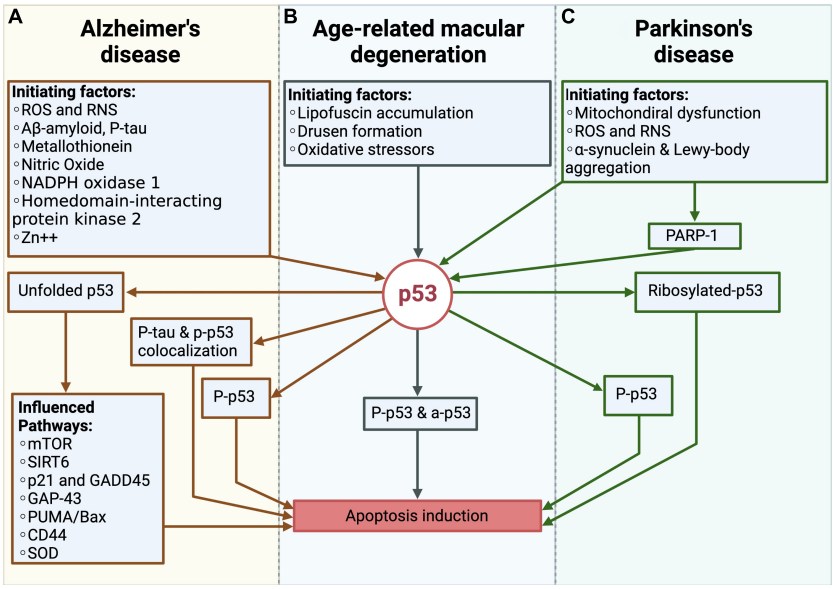

FIGURE 5
Overview over the role of p53 in Alzheimer's disease (AD), Parkinson's disease (PD) and the age-related macular degeneration (AMD). **(A)** In AD, different pathogenic factors like e.g., reactive oxygen species (ROS) and reactive nitrogen species (RNS), Aβ or p-tau, promotes the formation of unfolded p53, phosphorlyated-p53 (p-p53) as well as the colocalization of the tau protein and p-p53. Through these changes, the apoptosis of neurons is induced. **(B)** In AMD, the lipofuscin accumulation and drusen formation as well as oxidative stressors like e.g., the blue light induced ROS formation, initiate phosphorylated and acetylated p53, which further leads to the cell death of RPE cells. **(C)** In PD, mitochondrial dysfunction, ROS production and the accumulation of pathogenic proteins like α-synuclein and Lewy-bodies influence p53. Together with PARP-1 these factors promote the ribosylation and phosphorylation of p53, which is responsible for the cell death of dopaminergic neurons.

Discussion

Alzheimer's disease is the most common form of dementia and has many parallels with the pathogenesis of AMD. Thereby, both diseases primarily have an onset in elderly people and exhibit similar pathogenetic risk factors, such as smoking tobacco, hypertension or hypercholesterolemia (Armstrong, 2019; Heesterbeek et al., 2020). The cardinal features of AD include the extracellular accumulation of Aβ as well as the intracellular deposition of p-tau. Neuroinflammation and brain iron dyshomeostasis accompany Aβ and p-tau depositions and together lead to progressive neuronal cell death and dementia. In AMD patients, inflammatory processes as well as the accumulation of Aβ in drusen has also been observed, suggesting an overlapping pathology (Anderson et al., 2004). On the other hand, the pathogenesis of PD also shares several similarities with AMD. For both diseases, an increased incidence in elderly people, inflammatory processes and oxidative stress seem to play a major role (Chen et al., 2021). In a study that was conducted by Choi et al., the association of AMD with AD and PD was investigated. They show that patients affected by AMD exhibit an increased risk for also developing AD or PD, providing evidence for a linkage between retinal- and brain-related neurodegenerative diseases (Choi et al., 2020).

The before mentioned findings on p53 in AD, PD and AMD strongly suggest that the protein is critical for the pathogeneses of the three diseases (**Figure 5**). Whereas to date, the exact role of p53 in AMD pathogenesis is still unclear, much more is known about its pathogenesis in AD and PD.

In AD and PD, the direct observation of elevated p53 levels, together with the increase in pro-apoptotic BCL-2 proteins are coherent with the occurring cell death. Vice versa, increased protein levels of anti-apoptotic BCL-2 proteins seem to promote survival of the cells, which again supports the thesis of a p53-dependency. In summary, it seems likely that in AD and PD the mitochondria-dependent apoptosis is one of the assumed forms of cell death, leading to neurodegeneration. Yet, it is to expect that cell death is also initiated through further p53-dependent and independent mechanisms, like the previously described p53 dependent lysosomal membrane permeabilization (Fogarty et al., 2010). Furthermore, different PTMs have been observed for both diseases (**Figure 5**). The observation of unfolded p53, which is initiated by a variety of factors was only observed in AD patients, suggesting that the according structural changes are AD-specific (Abate et al., 2020). Otherwise, PARP-1 appears to be one of the main factors in PD, being responsible for p53-ribosylation and altering its functioning in the context of PD. One similar observation was the detection of phosphorylated p53, which was observed in both pathogeneses.

In the pathogenesis of AMD, the previously described *in vivo* and *in vitro* studies by Lansel et al. (1998); Marti et al. (1998); Miller et al. (2006) analyzing the associated photoreceptor degeneration, show contradictory results concerning the role of a p53-related photoreceptor cell death. One reason for the opposing results could be related to the fact that in the compared studies different cellular stressors were used, with the possibility of not every stressor leading to a p53-dependent apoptosis. Another cause could be the 661W cone photoreceptor cell line, which was used by Miller et al. and does not represent the actual *in vivo* situation (Miller et al., 2006). In terms of the RPE cell death findings, a p53-dependent cell death seems more likely. The described study by Bhattacharya et al., evidencing an increase in the p53 dependent apoptosis in human RPE cells, outlines a first indication of a p53-dependent cell death (Bhattacharya et al., 2012). Therefore, it is possible that in the AMD pathogenesis only the RPE cell death is p53 dependent. As with AD and PD, phosphorylated-p53 levels were found, whereas besides acetylated-p53, which constitutes a similar p53 modification, other PTMs have not yet been identified in AMD pathogenesis (**Figure 5**).

Nevertheless, the overall current state of research about the p53 dependent neurodegeneration of the retina is insufficient and further research needs to be done. For instance, the less investigated Müller cells, which have been shown to be essential for the survival of photoreceptors as well, potentially also undergo a p53-dependent apoptosis and could strengthen the link of a p53-dependent AMD pathogenesis (Dubois-Dauphin et al., 2000). If this link is further validated, new therapeutic treatment approaches could benefit from such findings. For example, a novel therapy approach could be the modulation of the p53-related pro- and anti-apoptotic BCL-2 family proteins, which is already investigated in the treatment of cancerous diseases (Thomas et al., 2013; Perini et al., 2018; Wei et al., 2020). A similar projection for the future treatment of neurodegenerative diseases has previously been described by Shacka and Roth (2005).

Conclusion

Even though p53 was discovered over 40 years ago, research about its functioning is conducted to this day. With the ongoing exploration and the growing number of p53-disease-associations outside of cancerous affections, the protein p53 is more important than ever. Altogether, the current literature strongly suggests connections between brain and retinal related neurodegenerative diseases. Besides the occurrence of the phosphorylated p53 modification, which has been detected in all three diseases, further specific modifications in AD and PD have been observed. Especially the unfolded p53 was thereby specific to AD and could potentially function as a biomarker in the future. In contrast, less is known about the role of p53 in the pathogenesis of AMD, with the current findings suggesting only a p53 dependent cell death in RPE cells and not in photoreceptor cells. More research is needed to further proof a function of p53 in the pathogenesis of AMD.

Author contributions

PW, JH, and SS devised the project. PW conceptualized and wrote the manuscript with input from JH, SS, and AF. JH, SS and AF revised the manuscript. All authors provided critical feedback and contributed to the final manuscript.

Conflict of interest

The authors declare that the research was conducted in the absence of any commercial or financial relationships that could be construed as a potential conflict of interest.

Publisher's note

All claims expressed in this article are solely those of the authors and do not necessarily represent those of their affiliated organizations, or those of the publisher, the editors and the reviewers. Any product that may be evaluated in this article, or claim that may be made by its manufacturer, is not guaranteed or endorsed by the publisher.

References

Abate, G., Frisoni, G. B., Bourdon, J. C., Piccirella, S., Memo, M., and Uberti, D. (2020). The pleiotropic role of p53 in functional/dysfunctional neurons: Focus on pathogenesis and diagnosis of Alzheimer's disease. *Alzheimers Res. Ther.* 12:160. doi: 10.1186/s13195-020-00732-0

Akyol, E., and Lotery, A. (2020). Gene, cell and antibody-based therapies for the treatment of age-related macular degeneration. *Biologics* 14, 83–94. doi: 10.2147/BTT.S252581

Anderson, D. H., Talaga, K. C., Rivest, A. J., Barron, E., Hageman, G. S., and Johnson, L. V. (2004). Characterization of beta amyloid assemblies in drusen: The deposits associated with aging and age-related macular degeneration. *Exp. Eye Res.* 78, 243–256. doi: 10.1016/j.exer.2003.10.011

Armstrong, R. (2020). What causes neurodegenerative disease? *Folia Neuropathol.* 58, 93–112. doi: 10.5114/fn.2020.96707

Armstrong, R. A. (2019). Risk factors for Alzheimer's disease. *Folia Neuropathol.* 57, 87–105. doi: 10.5114/fn.2019.85929

Aubrey, B. J., Kelly, G. L., Janic, A., Herold, M. J., and Strasser, A. (2018). How does p53 induce apoptosis and how does this relate to p53-mediated tumour suppression? *Cell Death Differ.* 25, 104–113. doi: 10.1038/cdd.2017.169

Balestrino, R., and Schapira, A. H. V. (2020). Parkinson disease. *Eur. J. Neurol.* 27, 27–42. doi: 10.1111/ene.14108

Beitz, J. M. (2014). Parkinson's disease: A review. *Front. Biosci.* 6:65–74.

Bhattacharya, S., Chaum, E., Johnson, D. A., and Johnson, L. R. (2012). Age-related susceptibility to apoptosis in human retinal pigment epithelial cells is triggered by disruption of p53-Mdm2 association. *Invest. Ophthalmol. Vis. Sci.* 53, 8350–8366. doi: 10.1167/iovs.12-10495

Bowes Rickman, C., Farsiu, S., Toth, C. A., and Klingeborn, M. (2013). Dry age-related macular degeneration: Mechanisms, therapeutic targets, and imaging. *Invest. Ophthalmol. Vis. Sci.* 54, ORSF68–ORSF80. doi: 10.1167/iovs.13-12757

Boya, P., and Kroemer, G. (2008). Lysosomal membrane permeabilization in cell death. *Oncogene* 27, 6434–6451. doi: 10.1038/onc.2008.310

Burns, T. F., Bernhard, E. J., and El-Deiry, W. S. (2001). Tissue specific expression of p53 target genes suggests a key role for KILLER/DR5 in p53-dependent apoptosis in vivo. *Oncogene* 20, 4601–4612. doi: 10.1038/sj.onc.1204484

Carneiro, B. A., and El-Deiry, W. S. (2020). Targeting apoptosis in cancer therapy. *Nat. Rev. Clin. Oncol.* 17, 395–417. doi: 10.1038/s41571-020-0341-y

Chang, J. R., Ghafouri, M., Mukerjee, R., Bagashev, A., Chabrashvili, T., and Sawaya, B. E. (2012). Role of p53 in neurodegenerative diseases. *Neurodegener. Dis.* 9, 68–80. doi: 10.1159/000329999

Checkoway, H., Lundin, J. I., and Kelada, S. N. (2011). Neurodegenerative diseases. *IARC Sci. Publ.* 163, 407–419.

Chen, P. J., Wan, L., Lai, J. N., Chen, C. S., Chen, J. J., Yen, W. M., et al. (2021). Increased risk of Parkinson's disease among patients with age-related macular degeneration. *BMC Ophthalmol.* 21:426. doi: 10.1186/s12886-021-02196-8

Chene, P. (2001). The role of tetramerization in p53 function. *Oncogene* 20, 2611–2617. doi: 10.1038/sj.onc.1204373

Choi, S., Jahng, W. J., Park, S. M., and Jee, D. (2020). Association of age-related macular degeneration on Alzheimer or Parkinson disease: A retrospective cohort study. *Am. J. Ophthalmol.* 210, 41–47. doi: 10.1016/j.ajo.2019.11.001

Clark, J. S., Kayed, R., Abate, G., Uberti, D., Kinnon, P., and Piccirella, S. (2022). Post-translational modifications of the p53 protein and the impact in Alzheimer's disease: A review of the literature. *Front. Aging Neurosci.* 14:835288. doi: 10.3389/fnagi.2022.835288

Crighton, D., Wilkinson, S., O'Prey, J., Syed, N., Smith, P., Harrison, P. R., et al. (2006). DRAM, a p53-induced modulator of autophagy, is critical for apoptosis. *Cell* 126, 121–134. doi: 10.1016/j.cell.2006.05.034

Culmsee, C., and Mattson, M. P. (2005). P53 in neuronal apoptosis. *Biochem. Biophys. Res. Commun.* 331, 761–777. doi: 10.1016/j.bbrc.2005.03.149

de la Monte, S. M., Sohn, Y. K., and Wands, J. R. (1997). Correlates of p53- and Fas (CD95)-mediated apoptosis in Alzheimer's disease. *J. Neurol. Sci.* 152, 73–83. doi: 10.1016/s0022-510x(97)00131-7

Deuschl, G., Beghi, E., Fazekas, F., Varga, T., Christoforidi, K. A., Sipido, E., et al. (2020). The burden of neurological diseases in Europe: An analysis for the Global Burden of Disease Study 2017. *Lancet Public Health* 5, e551–e567. doi: 10.1016/S2468-2667(20)30190-0

Dos Santos Picanco, L. C., Ozela, P. F., de Fatima de Brito Brito, M., Pinheiro, A. A., Padilha, E. C., Braga, F. S., et al. (2018). Alzheimer's disease: A review from the pathophysiology to diagnosis, new perspectives for pharmacological treatment. *Curr. Med. Chem.* 25, 3141–3159. doi: 10.2174/0929867323666161213101126

Dubois-Dauphin, M., Poitry-Yamate, C., de Bilbao, F., Julliard, A. K., Jourdan, F., and Donati, G. (2000). Early postnatal Muller cell death leads to retinal but not optic nerve degeneration in NSE-Hu-Bcl-2 transgenic mice. *Neuroscience* 95, 9–21. doi: 10.1016/s0306-4522(99)00313-9

Duraes, F., Pinto, M., and Sousa, E. (2018). Old drugs as new treatments for neurodegenerative diseases. *Pharmaceuticals* 11:44. doi: 10.3390/ph11020044

Farmer, K. M., Ghag, G., Puangmalai, N., Montalbano, M., Bhatt, N., and Kayed, R. (2020). P53 aggregation, interactions with tau, and impaired DNA damage response in Alzheimer's disease. *Acta Neuropathol. Commun.* 8:132. doi: 10.1186/s40478-020-01012-6

Feng, J., Meng, C., and Xing, D. (2015). Abeta induces PUMA activation: A new mechanism for Abeta-mediated neuronal apoptosis. *Neurobiol. Aging* 36, 789–800. doi: 10.1016/j.neurobiolaging.2014.10.007

Fogarty, M. P., McCormack, R. M., Noonan, J., Murphy, D., Gowran, A., and Campbell, V. A. (2010). A role for p53 in the beta-amyloid-mediated regulation of the lysosomal system. *Neurobiol. Aging* 31, 1774–1786. doi: 10.1016/j.neurobiolaging.2008.09.018

Heesterbeek, T. J., Lores-Motta, L., Hoyng, C. B., Lechanteur, Y. T. E., and den Hollander, A. I. (2020). Risk factors for progression of age-related macular degeneration. *Ophthalmic Physiol. Opt.* 40, 140–170. doi: 10.1111/opo.12675

Ho, W. C., Luo, C., Zhao, K., Chai, X., Fitzgerald, M. X., and Marmorstein, R. (2006). High-resolution structure of the p53 core domain: Implications for binding small-molecule stabilizing compounds. *Acta Crystallogr. D Biol. Crystallogr.* 62, 1484–1493. doi: 10.1107/S090744490603890X

Jackson-Lewis, V., Vila, M., Djaldetti, R., Guegan, C., Liberatore, G., Liu, J., et al. (2000). Developmental cell death in dopaminergic neurons of the substantia nigra of mice. *J. Comp. Neurol.* 424, 476–488. doi: 10.1002/1096-9861(20000828)424:3<476::aid-cne6<3.0.co;2-0

Joerger, A. C., and Fersht, A. R. (2008). Structural biology of the tumor suppressor p53. *Annu. Rev. Biochem.* 77, 557–582. doi: 10.1146/annurev.biochem.77.060806.091238

Kastenhuber, E. R., and Lowe, S. W. (2017). Putting p53 in Context. *Cell* 170, 1062–1078. doi: 10.1016/j.cell.2017.08.028

Khoury, M. P., and Bourdon, J. C. (2011). P53 isoforms: An intracellular microprocessor? *Genes Cancer* 2, 453–465. doi: 10.1177/1947601911408893

Kitamura, Y., Shimohama, S., Kamoshima, W., Matsuoka, Y., Nomura, Y., and Taniguchi, T. (1997). Changes of p53 in the brains of patients with Alzheimer's disease. *Biochem. Biophys. Res. Commun.* 232, 418–421. doi: 10.1006/bbrc.1997.6301

Lane, D. P. (1994). P53 and human cancers. *Br. Med. Bull.* 50, 582–599. doi: 10.1093/oxfordjournals.bmb.a072911

Lansel, N., Hafezi, F., Marti, A., Hegi, M., Reme, C., and Niemeyer, G. (1998). The mouse ERG before and after light damage is independent of p53. *Doc. Ophthalmol.* 96, 311–320. doi: 10.1023/a:1001795526628

Levine, A. J., and Oren, M. (2009). The first 30 years of p53: Growing ever more complex. *Nat. Rev. Cancer* 9, 749–758. doi: 10.1038/nrc2723

Li, J. Q., Welchowski, T., Schmid, M., Mauschitz, M. M., Holz, F. G., and Finger, R. P. (2020). Prevalence and incidence of age-related macular degeneration in Europe: A systematic review and meta-analysis. *Br. J. Ophthalmol.* 104, 1077–1084. doi: 10.1136/bjophthalmol-2019-314422

Li, Y., Li, S., and Wu, H. (2022). Ubiquitination-proteasome system (UPS) and autophagy two main protein degradation machineries in response to cell stress. *Cells* 11:851. doi: 10.3390/cells11050851

Liu, J., Liu, W., and Yang, H. (2019). Balancing apoptosis and autophagy for Parkinson's disease therapy: Targeting BCL-2. *ACS Chem. Neurosci.* 10, 792–802. doi: 10.1021/acschemneuro.8b00356

Loss, J., Muller, D., Weigl, J., Helbig, H., Brandl, C., Heid, I. M., et al. (2018). Views of ophthalmologists on the genetics of age-related macular degeneration: Results of a qualitative study. *PLoS One* 13:e0209328. doi: 10.1371/journal.pone.0209328

Loughery, J., Cox, M., Smith, L. M., and Meek, D. W. (2014). Critical role for p53-serine 15 phosphorylation in stimulating transactivation at p53-responsive promoters. *Nucleic Acids Res.* 42, 7666–7680. doi: 10.1093/nar/gku501

Lu, T., Kim, P. P., Greig, N. H., and Luo, Y. (2017). Dopaminergic neuron-specific deletion of p53 Gene attenuates methamphetamine neurotoxicity. *Neurotox. Res.* 32, 218–230. doi: 10.1007/s12640-017-9723-z

Luo, Q., Sun, W., Wang, Y. F., Li, J., and Li, D. W. (2022). Association of p53 with neurodegeneration in Parkinson's disease. *Parkinsons Dis.* 2022:6600944. doi: 10.1155/2022/6600944

Mandir, A. S., Simbulan-Rosenthal, C. M., Poitras, M. F., Lumpkin, J. R., Dawson, V. L., Smulson, M. E., et al. (2002). A novel in vivo post-translational modification of p53 by PARP-1 in MPTP-induced parkinsonism. *J. Neurochem.* 83, 186–192. doi: 10.1046/j.1471-4159.2002.01144.x

Marti, A., Hafezi, F., Lansel, N., Hegi, M. E., Wenzel, A., Grimm, C., et al. (1998). Light-induced cell death of retinal photoreceptors in the absence of p53. *Invest. Ophthalmol. Vis. Sci.* 39, 846–849.

Martire, S., Mosca, L., and d'Erme, M. (2015). PARP-1 involvement in neurodegeneration: A focus on Alzheimer's and Parkinson's diseases. *Mech. Ageing Dev.* 14, 53–64. doi: 10.1016/j.mad.2015.04.001

McLeod, D. S., Grebe, R., Bhutto, I., Merges, C., Baba, T., and Lutty, G. A. (2009). Relationship between RPE and choriocapillaris in age-related macular degeneration. *Invest. Ophthalmol. Vis. Sci.* 50, 4982–4991. doi: 10.1167/iovs.09-3639

Mijit, M., Caracciolo, V., Melillo, A., Amicarelli, F., and Giordano, A. (2020). Role of p53 in the regulation of cellular senescence. *Biomolecules* 10:420. doi: 10.3390/biom10030420

Miller, T. J., Schneider, R. J., Miller, J. A., Martin, B. P., Al-Ubaidi, M. R., Agarwal, N., et al. (2006). Photoreceptor cell apoptosis induced by the 2-nitroimidazole radiosensitizer, CI-1010, is mediated by p53-linked activation of caspase-3. *Neurotoxicology* 27, 44–59. doi: 10.1016/j.neuro.2005.06.001

Mitchell, P., Liew, G., Gopinath, B., and Wong, T. Y. (2018). Age-related macular degeneration. *Lancet* 392, 1147–1159. doi: 10.1016/S0140-6736(18)31550-2

Modi, G., Pillay, V., and Choonara, Y. E. (2010). Advances in the treatment of neurodegenerative disorders employing nanotechnology. *Ann. N. Y. Acad. Sci.* 1184, 154–172. doi: 10.1111/j.1749-6632.2009.05108.x

Mogi, M., Kondo, T., Mizuno, Y., and Nagatsu, T. (2007). P53 protein, interferon-gamma, and NF-kappaB levels are elevated in the parkinsonian brain. *Neurosci. Lett.* 414, 94–97. doi: 10.1016/j.neulet.2006.12.003

Moll, U. M., and Petrenko, O. (2003). The MDM2-p53 interaction. *Mol. Cancer Res.* 1, 1001–1008.

Munoz-Espin, D., and Serrano, M. (2014). Cellular senescence: From physiology to pathology. *Nat. Rev. Mol. Cell Biol.* 15, 482–496. doi: 10.1038/nrm3823

Naoi, M., and Maruyama, W. (1999). Cell death of dopamine neurons in aging and Parkinson's disease. *Mech. Ageing Dev.* 111, 175–188. doi: 10.1016/s0047-6374(99)00064-0

Nicotra, A., and Parvez, S. (2002). Apoptotic molecules and MPTP-induced cell death. *Neurotoxicol. Teratol.* 24, 599–605. doi: 10.1016/s0892-0362(02)00213-1

Paradis, E., Douillard, H., Koutroumanis, M., Goodyer, C., and LeBlanc, A. (1996). Amyloid beta peptide of Alzheimer's disease downregulates Bcl-2 and upregulates bax expression in human neurons. *J. Neurosci.* 16, 7533–7539.

Perini, G. F., Ribeiro, G. N., Pinto Neto, J. V., Campos, L. T., and Hamerschlak, N. (2018). BCL-2 as therapeutic target for hematological malignancies. *J. Hematol. Oncol.* 11:65. doi: 10.1186/s13045-018-0608-2

Prives, C., and Manley, J. L. (2001). Why is p53 acetylated? *Cell* 107, 815–818. doi: 10.1016/s0092-8674(01)00619-5

Reed, S. M., and Quelle, D. E. (2014). P53 acetylation: Regulation and consequences. *Cancers* 7, 30–69. doi: 10.3390/cancers7010030

Retzlaff, M., Rohrberg, J., Kupper, N. J., Lagleder, S., Bepperling, A., Manzenrieder, F., et al. (2013). The regulatory domain stabilizes the p53 tetramer by intersubunit contacts with the DNA binding domain. *J. Mol. Biol.* 425, 144–155. doi: 10.1016/j.jmb.2012.10.015

Riley, T., Sontag, E., Chen, P., and Levine, A. (2008). Transcriptional control of human p53-regulated genes. *Nat. Rev. Mol. Cell Biol.* 9, 402–412. doi: 10.1038/nrm2395

Romer, L., Klein, C., Dehner, A., Kessler, H., and Buchner, J. (2006). P53–a natural cancer killer: Structural insights and therapeutic concepts. *Angew. Chem. Int. Ed. Engl.* 45, 6440–6460. doi: 10.1002/anie.200600611

Rozan, L. M., and El-Deiry, W. S. (2007). P53 downstream target genes and tumor suppression: A classical view in evolution. *Cell Death Differ.* 14, 3–9. doi: 10.1038/sj.cdd.4402058

Schnichels, S., Paquet-Durand, F., Loscher, M., Tsai, T., Hurst, J., Joachim, S. C., et al. (2021). Retina in a dish: Cell cultures, retinal explants and animal models for common diseases of the retina. *Prog. Retin. Eye Res.* 81:100880. doi: 10.1016/j.preteyeres.2020.100880

Seeler, J. S., and Dejean, A. (2003). Nuclear and unclear functions of SUMO. *Nat. Rev. Mol. Cell Biol.* 4, 690–699. doi: 10.1038/nrm1200

Shacka, J. J., and Roth, K. A. (2005). Regulation of neuronal cell death and neurodegeneration by members of the Bcl-2 family: Therapeutic implications. *Curr. Drug Targets CNS Neurol. Disord.* 4, 25–39. doi: 10.2174/1568007053005127

Shieh, S. Y., Ikeda, M., Taya, Y., and Prives, C. (1997). DNA damage-induced phosphorylation of p53 alleviates inhibition by MDM2. *Cell* 91, 325–334. doi: 10.1016/s0092-8674(00)80416-x

Shin, D. H., Lee, H. Y., Lee, H. W., Kim, H. J., Lee, E., Cho, S. S., et al. (1999). In situ localization of p53, bcl-2 and bax mRNAs in rat ocular tissue. *Neuroreport* 10, 2165–2167. doi: 10.1097/00001756-199907130-00030

Shu, K. X., Li, B., and Wu, L. X. (2007). The p53 network: p53 and its downstream genes. *Colloids Surf. B Biointerfaces* 55, 10–18. doi: 10.1016/j.colsurfb.2006.11.003

Soussi, T. (2010). The history of p53. A perfect example of the drawbacks of scientific paradigms. *EMBO Rep.* 11, 822–826. doi: 10.1038/embor.2010.159

Steegenga, W. T., van der Eb, A. J., and Jochemsen, A. G. (1996). How phosphorylation regulates the activity of p53. *J. Mol. Biol.* 263, 103–113. doi: 10.1006/jmbi.1996.0560

Strauss, O. (2005). The retinal pigment epithelium in visual function. *Physiol. Rev.* 85, 845–881. doi: 10.1152/physrev.00021.2004

Su, J. H., Deng, G., and Cotman, C. W. (1997). Bax protein expression is increased in Alzheimer's brain: Correlations with DNA damage, Bcl-2 expression, and brain pathology. *J. Neuropathol. Exp. Neurol.* 56, 86–93. doi: 10.1097/00005072-199701000-00009

Szybinska, A., and Lesniak, W. (2017). P53 dysfunction in neurodegenerative diseases - the cause or effect of pathological changes? *Aging Dis.* 8, 506–518. doi: 10.14336/AD.2016.1120

Tanikawa, C., Zhang, Y. Z., Yamamoto, R., Tsuda, Y., Tanaka, M., Funauchi, Y., et al. (2017). The transcriptional landscape of p53 signalling pathway. *EBioMedicine* 20, 109–119. doi: 10.1016/j.ebiom.2017.05.017

Thomas, S., Quinn, B. A., Das, S. K., Dash, R., Emdad, L., Dasgupta, S., et al. (2013). Targeting the Bcl-2 family for cancer therapy. *Expert Opin. Ther. Targets* 17, 61–75. doi: 10.1517/14728222.2013.733001

Troy, C. M., Rabacchi, S. A., Friedman, W. J., Frappier, T. F., Brown, K., and Shelanski, M. L. (2000). Caspase-2 mediates neuronal cell death induced by beta-amyloid. *J. Neurosci.* 20, 1386–1392.

Uberti, D., Carsana, T., Bernardi, E., Rodella, L., Grigolato, P., Lanni, C., et al. (2002). Selective impairment of p53-mediated cell death in fibroblasts from sporadic Alzheimer's disease patients. *J. Cell Sci.* 115, 3131–3138. doi: 10.1242/jcs.115.15.3131

Uberti, D., Lanni, C., Racchi, M., Govoni, S., and Memo, M. (2008). Conformationally altered p53: A putative peripheral marker for Alzheimer's disease. *Neurodegener. Dis.* 5, 209–211. doi: 10.1159/000113704

Vuong, L., Conley, S. M., and Al-Ubaidi, M. R. (2012). Expression and role of p53 in the retina. *Invest. Ophthalmol. Vis. Sci.* 53, 1362–1371. doi: 10.1167/iovs.11-8909

Wang, X., Simpson, E. R., and Brown, K. A. (2015). P53: Protection against tumor growth beyond effects on cell cycle and apoptosis. *Cancer Res.* 75, 5001–5007. doi: 10.1158/0008-5472.CAN-15-0563

Wei, Y., Cao, Y., Sun, R., Cheng, L., Xiong, X., Jin, X., et al. (2020). Targeting Bcl-2 proteins in acute myeloid leukemia. *Front. Oncol.* 10:584974. doi: 10.3389/fonc.2020.584974

Westlund, B. S., Cai, B., Zhou, J., and Sparrow, J. R. (2009). Involvement of c-Abl, p53 and the MAP kinase JNK in the cell death program initiated in A2E-laden ARPE-19 cells by exposure to blue light. *Apoptosis* 14, 31–41. doi: 10.1007/s10495-008-0285-7

Wu, L., Rosa-Neto, P., Hsiung, G. Y., Sadovnick, A. D., Masellis, M., Black, S. E., et al. (2012). Early-onset familial Alzheimer's disease (EOFAD). *Can. J. Neurol. Sci.* 39, 436–445. doi: 10.1017/s0317167100013949

Xu, X., Lai, Y., and Hua, Z. C. (2019). Apoptosis and apoptotic body: Disease message and therapeutic target potentials. *Biosci. Rep.* 39:BSR20180992. doi: 10.1042/BSR20180992

Yildirim, Z., Ucgun, N. I., and Yildirim, F. (2011). The role of oxidative stress and antioxidants in the pathogenesis of age-related macular degeneration. *Clinics* 66, 743–746. doi: 10.1590/s1807-59322011000500006

Ying, Y., and Padanilam, B. J. (2016). Regulation of necrotic cell death: p53, PARP1 and cyclophilin D-overlapping pathways of regulated necrosis? *Cell. Mol. Life Sci.* 73, 2309–2324. doi: 10.1007/s00018-016-2202-5

frontiers | Frontiers in Neuroscience

TYPE Review
PUBLISHED 03 February 2023
DOI 10.3389/fnins.2023.1021152

OPEN ACCESS

EDITED BY
Sandra Kuehn,
University of Oslo, Norway

REVIEWED BY
Shelby Hetzer,
University of Cincinnati, United States
Nathan Evanson,
Cincinnati Children's Hospital Medical Center, United States

*CORRESPONDENCE
Matthew A. Reilly
✉ reilly.196@osu.edu

SPECIALTY SECTION
This article was submitted to Neurodegeneration, a section of the journal Frontiers in Neuroscience

RECEIVED 17 August 2022
ACCEPTED 13 January 2023
PUBLISHED 03 February 2023

CITATION
Ryan AK, Rich W and Reilly MA (2023) Oxidative stress in the brain and retina after traumatic injury.
Front. Neurosci. 17:1021152.
doi: 10.3389/fnins.2023.1021152

Oxidative stress in the brain and retina after traumatic injury

Annie K. Ryan[1], Wade Rich[1] and Matthew A. Reilly[1,2]*

[1]Department of Biomedical Engineering, The Ohio State University, Columbus, OH, United States, [2]Department of Ophthalmology and Visual Sciences, The Ohio State University, Columbus, OH, United States

The brain and the retina share many physiological similarities, which allows the retina to serve as a model of CNS disease and disorder. In instances of trauma, the eye can even indicate damage to the brain *via* abnormalities observed such as irregularities in pupillary reflexes in suspected traumatic brain injury (TBI) patients. Elevation of reactive oxygen species (ROS) has been observed in neurodegenerative disorders and in both traumatic optic neuropathy (TON) and in TBI. In a healthy system, ROS play a pivotal role in cellular communication, but in neurodegenerative diseases and post-trauma instances, ROS elevation can exacerbate neurodegeneration in both the brain and the retina. Increased ROS can overwhelm the inherent antioxidant systems which are regulated *via* mitochondrial processes. The overabundance of ROS can lead to protein, DNA, and other forms of cellular damage which ultimately result in apoptosis. Even though elevated ROS have been observed to be a major cause in the neurodegeneration observed after TON and TBI, many antioxidants therapeutic strategies fail. In order to understand why these therapeutic approaches fail further research into the direct injury cascades must be conducted. Additional therapeutic approaches such as therapeutics capable of anti-inflammatory properties and suppression of other neurodegenerative processes may be needed for the treatment of TON, TBI, and neurodegenerative diseases.

KEYWORDS

trauma, optic neuropathy, traumatic brain injury, ROS, neurodegeneration

1. Introduction

The eye and the brain are closely connected and thus share many similarities. Many researchers have focused on studying ocular phenomena *via* examination of the retina since the eye is much more accessible and yet shares many of the same physiological, anatomical, and developmental characteristics as the brain (Cheung et al., 2017; Bernardo-Colón et al., 2018). The eye allows for close observation of the central nervous system (CNS) as both the neurons and blood vessels can be directly monitored (Nguyen et al., 2021). As Ptito et al. (2021) state, "no other part of the central nervous system is amenable to direct observation" (2021, p. 7). This unique relationship between the eye and the brain allows the eye to serve as a model for CNS disease. Also, many neurodegenerative diseases such as Alzheimer's Disease (AD), Parkinson's Disease (PD), and Multiple Sclerosis (MS) present with changes in ocular physiology (Blanks et al., 1989; Archibald et al., 2009; Green et al., 2010; Lee et al., 2020; Nguyen et al., 2021). The eye is often referred to as an extension of the brain, and this can be exemplified through the optic nerve developmental process. By examining how the retina develops one can see how interlinked the brain and the retina are. **Figure 1** depicts the retinal layers with the RGC axons joining to form the optic nerve. During development, the retinal ganglion cell (RGC) axons begin to extend through the optic nerve and toward the brain

(Nickells, 1996). Once the RGC axons reach the brain they then form synaptic connections with their respective target sites before uptaking brain-derived neurotrophic factor (BDNF), which is produced by neuronal cells (Nickells, 1996; Brooks et al., 1999). Before this point, developing RGCs did not need BDNF to survive, but once the first synaptic connection is made between the brain and the retina, BDNF is transported to the retina (Nickells, 1996; Brooks et al., 1999). From this developmental point onward RGCs will need BDNF in order to survive (Nickells, 1996; Brooks et al., 1999). The brain and retina also share high concentrations of the same forms of neurotransmitters, such as glutamate (Nickells, 1996; Wu and Maple, 1998). Both the brain and retina have high physiological energy requirements, which require many mitochondria in order to produce the necessary energy requirements (Rango and Bresolin, 2018; Eells, 2019; Singh et al., 2019; Nascimento-dos-Santos et al., 2020). As well as providing energy, mitochondria also help to regulate other essential cellular functions such as apoptosis, reactive oxygen species (ROS) production, antioxidant regulation *via* the mitochondrial thioredoxin system, intracellular calcium regulation, and many other roles (Forred et al., 2017; Angelova and Abramov, 2018; Robicsek et al., 2018). Mitochondria serve a crucial role in maintaining homeostatic conditions in cells, and thus, when they function irregularly, disastrous consequences arise. Dysfunctions in mitochondria have been linked to several neurodegenerative diseases in both the brain and the retina, which can lead to over production of ROS (Angelova and Abramov, 2018; Singh et al., 2019; Nascimento-dos-Santos et al., 2020).

The means in which trauma presents to the brain can also be translated to the eye. Traumatic brain injury (TBI) develops after direct or indirect trauma to the brain and can present as changes in consciousness, impaired cognitive ability, memory deficits, changes in vision, and even death (Rodgers et al., 2012; Mohan et al., 2013; Ohta et al., 2013; Brooks et al., 2014; Rubiano et al., 2015; Galgano et al., 2017; Gupta et al., 2019). Traumatic optic neuropathy (TON) is an irreversible vision-loss condition that is often developed after TBI (Sarkies, 2004; Sherwood et al., 2014). Similar to TBI, TON can develop after either direct or indirect injury. Direct TON (dTON) develops when the optic nerve is directly impacted (e.g., optic nerve crush or severing), while indirect TON (iTON) develops as a result of blunt force injury and the neuroinflammatory process that arises afterward (Sarkies, 2004; DeJulius et al., 2021).

The eye can be used to glean information about the brain. For example, the eye has been used screen for potential TBIs by medical professionals for years through the observation of pupillary reflexes (Adoni and McNett, 2007). One of the first tests done to a suspected TBI patient is to shine a light into their eyes and note if there are any abnormalities in the way their pupils respond to the light. An abnormal pupillary response is linked to TBI (Adoni and McNett, 2007).

The brain and retina also share a similar mechanism in order to protect themselves known as the blood-brain and blood-retina barrier (BBB and BRB) (Streit et al., 2004; Bond and Rex, 2014). As such, these barriers keep unwanted cells and other pathogens out of the CNS, but if these barriers are disrupted, as is the case in injury, then immune cells can migrate into both the brain and retina (Streit et al., 2004; Bond and Rex, 2014; DeJulius et al., 2021). Macroglia, such as astrocytes, are important glial cells responsible for maintenance of the BBB (Cabezas et al., 2014). The mature brain and retina both contain astrocytes and microglial cells (Kolb, 2001; Purves et al., 2001). One form of macroglia that is unique to the brain is the oligodendrocytes, which serve to build myelin around certain axons (Purves et al., 2001). The retina also has a unique macroglia, which is known as the Müller glia and is depicted in **Figure 1** (Kolb, 2001). The Müller glial cells are the main glial cell of the retina and help to maintain homeostasis while providing environmental protection (Kolb, 2001).

The damage mechanisms in TBI and traumatic optic neuropathy (TON) are not fully understood; however, it is known that their neuroinflammatory processes tend to occur secondary to initial injury (Rodgers et al., 2012; Zhou et al., 2021; Priester et al., 2022). It has also been concluded that ROS play a major role in the observed neurodegeneration after TON and TBI (Bernardo-Colón et al., 2018; DeJulius et al., 2021; Priester et al., 2022). The specific pathways in which traumatic injury initiates neurodegeneration and how increased levels of ROS are produced are not fully understood. In addition, the means to treat neurodegeneration after TBI and TON remain elusive with many attempts at antioxidant therapeutics ultimately failing at the clinical level (Angelova and Abramov, 2018; Priester et al., 2022). In order to determine efficacious therapeutics, we must first determine the means in which neurodegeneration progresses after injury.

2. The role of ROS in the healthy brain and retina

Reactive oxygen species are a group of unstable molecules which are produced under normal physiologic conditions through the partial reduction of molecular oxygen (Hsieh et al., 2014; Nita and Grzybowski, 2016; Sies and Jones, 2020; Yang and Lian, 2020). Such molecules include hydroxyl radical (OH), superoxide (O_2^-), hydrogen peroxide (H_2O_2), and singlet oxygen ($^1O_2$) (Hsieh et al., 2014; Sies and Jones, 2020; Yang and Lian, 2020). Reactive nitrogen species (RNS) also play a role as signaling molecules and in unbalanced systems can result in disease states (Hsieh et al., 2014). Common examples of RNS include nitric oxide (NO), peroxynitrite ($OONO^-$), and nitrogen dioxide (NO_2^-) (Hsieh et al., 2014). Under normal physiological conditions NO can be produced *via* shear stress and plays an important role in the regulation of vasculature (Metea and Newman, 2006; Attwell et al., 2010; Mishra and Newman, 2010; Hsieh et al., 2014; Someya et al., 2019). ROS in small concentrations are beneficial and highly necessary for daily functioning in cells (Dröge, 2002) as signaling molecules and are involved in feedback inhibition loops, which help to maintain redox balance within cells (Angelova and Abramov, 2018). In neuronal cells ROS play a vital role in neuronal differentiation through neuronal growth factor (NGF) induced differentiation (Suzukawa et al., 2000). The functionality of ROS as a beneficial signaling agent at low concentrations and damaging oxidative stressor at high concentrations appears to be present systemically, and certainly can be found within the brain and retina. One study investigating diabetic retinopathy concluded that ROS generation in retinal cells is regulated by glucose concentration in a concentration dependent manner (Zhang et al., 2019). Low levels of glucose led to retinal pigment epithelium mitophagy, which could have potentially protective effects, with no impact to cell proliferation or apoptosis, while high levels of glucose inhibited cell proliferation, induced apoptosis, and initiated ROS mediated gene inactivation (Zhang et al., 2019).

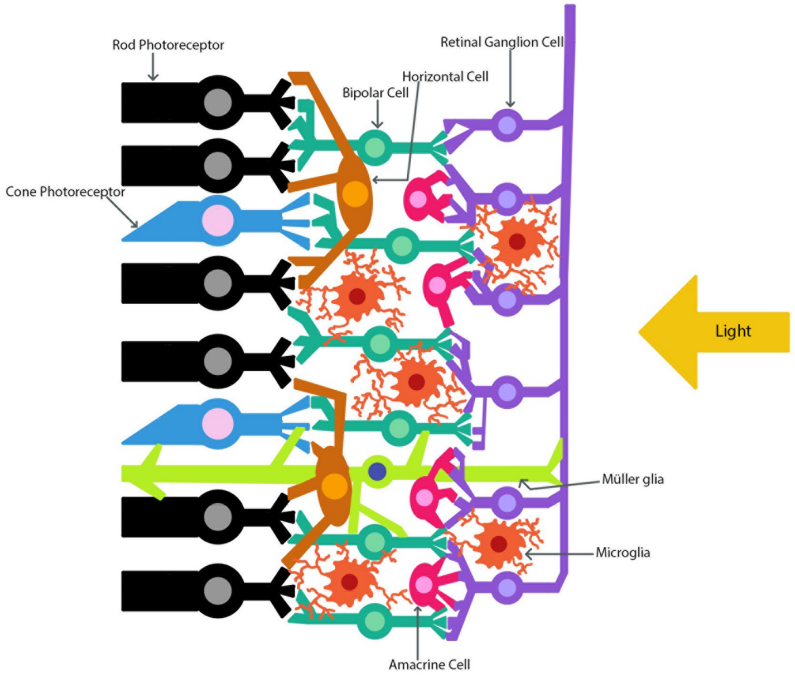

FIGURE 1
The retinal layers. The path of light as it travels through the retina to the photoreceptors is indicated. The retinal ganglion cell axons combine to form the optic nerve.

Healthy mitochondria play an important role in helping to maintain redox homeostasis balance in cells *via* the mitochondrial thioredoxin system and are usually protected by this system (Forred et al., 2017; Angelova and Abramov, 2018). The mitochondria is a large producer of ROS as it is a by-product of ATP synthase (Yang and Lian, 2020). Scortegagna et al. (2003) examined the relationship between hypoxia inducible factor-2 alpha (HIF-2α), antioxidant enzymes, and ROS concentrations. Their results suggest ROS regulation in the mitochondria may be partially controlled by HIF-2α (Scortegagna et al., 2003). Other enzymes and antioxidants for downregulation of ROS include vitamins E and C, superoxide dismutase 2 (SOD2), and glutathione peroxidase 1 (GPx1) (Bernardo-Colón et al., 2018; Yang and Lian, 2020). If these antioxidants fail at maintaining homeostatic concentrations of ROS, then deleterious effects can be observed. While the mitochondria is a large producer of ROS, it can also become the target of ROS damage (Angelova and Abramov, 2018). One group observed that an increase in mitochondrial ROS was triggered by excess levels of tumor necrosis factor (TNF) (Roca and Ramakrishnan, 2013). The mitochondria can also experience ROS-induced ROS release (Hiebert et al., 2015). Under normal conditions, the mitochondria can maintain ROS concentrations through the regulation of mitochondrial permeability transition pore (mPTP) openings (Hiebert et al., 2015). However, when ROS levels become too high for the mPTP openings to sufficiently regulate the levels, and the antioxidant enzymes become overwhelmed, the mitochondria can then release a burst of ROS (Hiebert et al., 2015). This excessive release of ROS damages the mitochondria, and potentially neighboring mitochondria, and leads to a decrease in ATP synthesis and increase in apoptotic processes (Hiebert et al., 2015). In a rodent TBI model, it was observed that mitochondrial bioenergetics in the form of respiration are significantly decreased after injury as compared to sham control animals (Pandya et al., 2014). Sullivan et al. (2004) described how the change in ATP production after TBI may arise. They summarize that after TBI calcium levels rise, followed by mitochondrial channel openings increasing to allow an increased flux of calcium into the mitochondrion (Sullivan et al., 2004). This then destabilizes the electron transport chain which is followed by a decrease in ATP production, mitochondrial membrane potential, and increased levels of ROS (Sullivan et al., 2004). During this process, the mitochondria swell, which results in the release of proapoptotic proteins. In summary, when the mitochondria become the site of ROS-induced damage, it fails to function properly, which can cause unwanted affects to the mitochondria's role of energy production.

Nitric oxide can also be beneficial or detrimental depending on concentration. While low levels of NO are necessary for signaling, higher concentrations can be harmful to neurons (Singh et al., 2019; Mueller-Buehl et al., 2021). In the retina, small concentrations of NO are utilized for light adaptation, visual processing, and amplification of visual responses in various retinal cell types (Vielma et al., 2012; Mueller-Buehl et al., 2021). NO can be produced by peroxisomes as well as other sources and is an indispensable messenger molecule responsible for regulating vascular tone, blood clotting, inflammation, and serving as a cardiovascular protectant (Naseem, 2005). Both the brain and the retina utilize NO signaling pathways to regulate vascular dilation and constriction (Metea and Newman, 2006; Someya et al., 2019). Someya et al. (2019) determined stimulated retinal neuronal cells release NO which then act as an important messenger to activate glial cell secretion of vasodilatory metabolites. Similar to Someya et al. (2019), Attwell et al. (2010) determined active neurons stimulate an increase in blood flow into their locations. They observed this phenomenon, which is termed hyperemia, and observed secreted glutamate triggers NMDA receptors which results in increased flux of calcium into neurons

(Attwell et al., 2010). This increase of intracellular calcium then activates neuronal nitric oxide synthase (nNOS), which results in a higher concentration of NO which then leads to vasodilation (Attwell et al., 2010). NO can also regulate vasoconstriction as detailed by Metea and Newman (2006). They observed increased levels of NO resulted in greater vasoconstriction and decreased levels resulted in vasodilation (Metea and Newman, 2006). The authors do note that in general NO is considered a vasodilating agent; however, their results indicated NO promoted vasoconstriction in the retina (Metea and Newman, 2006). Mishra and Newman (2010) also determined that glial cell and light stimulation can induce vasoconstrictions through elevated NO.

Reactive oxygen species found in peroxisomes assist animal cells with the critical function of fatty acid oxidation which allows for metabolic energy release. Peroxisomes also utilize ROS during the synthesis of lipids such as cholesterol (Cooper, 2000). Peroxisomes, originally thought to be merely a sink for excess cellular hydrogen peroxide, are now known to be involved in many complex metabolic pathways and are an essential source of reactive nitrogen species (RNS) including NO. Oversaturation of ROS and RNS can lead to chemical stress, but low concentrations such as those found in healthy peroxisomes are essential for cellular signaling. One study found that peroxisomes can sense and respond to environmental cues from ROS and redox changes and play a key role in maintaining redox homeostasis (Sandalio and Romero-Puertas, 2015). The study demonstrated that signaling pathways involving peroxisomes both sensed ROS change in the environment and responded by manipulating target genes involved in the cellular response to oxidative stress. Peroxisomes were also found to be involved in hormone production (Sandalio and Romero-Puertas, 2015). Another study found that peroxisomes are present and active within the murine retina (Das et al., 2019). Significantly, different retinal cells expressed different levels of peroxisome activity suggesting that peroxisomes may have unique roles within different retinal tissues (Das et al., 2019).

Another organelle which utilizes ROS is the lysosome. Lysosomes are required for cellular digestive processes, waste removal, and molecular scavenging from damaged or outdated cellular matter. Similarly, to the peroxisome, lysosomes are involved in metabolic signaling and require a low concentration of ROS to perform their cellular function (Lim and Zoncu, 2016). High levels of ROS, however, have been shown to inhibit lysosomal activity, reduce lysosomal motility, and prevent lysosomal fusion with target molecules (Saffi et al., 2021). Lysosomes are also active in the retina and assist with regulation of autophagy. Autophagy is known to decrease with age which can result in accumulation of waste or a decrease to cellular organization. This age associated reduction to beneficial autophagy, essentially acting as cellular cleaning, may be linked to development of disease such as age associated macular degeneration (Sinha et al., 2016). Lysosomal activity and autophagy with associated ROS is also linked with synaptic pruning in the brain (Song et al., 2008).

Peroxisomes and lysosomes are present in both the retinal cells and brain cells. In the brain, peroxisomes have been detected in all neural cell types and specifically measured in neurons, oligodendrocytes, astrocytes, microglia, and endothelial cells (Berger et al., 2016). Within the brain peroxisomes appear as single membrane-bound organelles and are smaller than peroxisomes found in other tissues (Berger et al., 2016). Peroxisomes contribute to lipid metabolism, and are membrane associated in neural cells, so healthy peroxisomal function is crucial for proper development and health of myelin sheaths in the brain white matter (Kassmann, 2014). Lysosomes are also found within neurons including pyramidal cell, mitral cell, hippocampal granule, and olfactory bulb neurons (Roberts and Gorenstein, 1987). Lysosomal distribution within the neuron; clustering within the dendrites, axon, or cell body; was shown to fluctuate across the lifespan of an organism as well (Roberts and Gorenstein, 1987; Ferguson, 2019). Lysosomes are present in glial cells and assist with glial functions such as molecular secretion, uptake, and degradation in astrocytes, oligodendrocytes, and microglia (Kreher et al., 2021). Peroxisomes have been detected within every retinal cell layer, although their distribution is not uniform (Das et al., 2019). Lysosomes have been studied within retinal pigmented epithelial cells (Sinha et al., 2016), linked to photoreceptor cell homeostasis (Santo and Conte, 2021), and lysosomal localization in the retinal pigmented epithelia linked to downstream photoreceptor health (el-Hifnawi et al., 1994). Within the retina, lysosomes appear to be most concentrated in the retinal pigmented epithelia, and are found within photoreceptors (Strauss, 2005). Lysosomal function within the retinal pigmented epithelia can have downstream effects on the neuronal retina and photoreceptor cells (Strauss, 2005).

It is evident that ROS are ubiquitous throughout the body and hold critical roles in cellular signaling, metabolism, digestion, organization, and energy economics. ROS are found in the healthy retina and brain carrying out similar functions as they do throughout the body. There also appears to be a nearly universal trend exhibited by ROS in the body in which their effects on cellular function switch from supportive to harmful as ROS concentration increases. These species are necessary in low concentrations for healthy tissue function, but in large doses can induce oxidative stress or damage tissues. The homeostatic balance of ROS is vital to proper cellular function. When focusing on ROS accumulation with age, it may seem at first that elimination of ROS and their damaging properties entirely would be desired. Under further scrutiny, however, it is apparent that the functionality of ROS at low concentrations is conductive to proper cell health.

3. Role of ROS in TBI, TON, and other neurodegenerative diseases

3.1. Traumatic brain injury (TBI)

Traumatic brain injury is one of the leading forms of death as a result of trauma related injury (Rubiano et al., 2015; Priester et al., 2022). About 69 million people worldwide develop a TBI each year with children and young adults making up the majority of cases (Galgano et al., 2017; Dewan et al., 2018; Priester et al., 2022). TBI can result in death, changes in vision, impaired cognitive attention, issues with function, memory deficits, and changes in behavior (Rodgers et al., 2012; Mohan et al., 2013; Ohta et al., 2013; Brooks et al., 2014; Rubiano et al., 2015; Gupta et al., 2019). TBI has two parts: primary and secondary injury (Galgano et al., 2017; Tan et al., 2018; Priester et al., 2022). Primary injury occurs due to direct physical forces impacting the brain (Galgano et al., 2017; Tan et al., 2018; Priester et al., 2022). Secondary injury can occur several minutes to weeks after primary injury and encompasses cortical edema, BBB breakdown, ROS release, calcium imbalances, inflammatory cascades, and other cellular and molecular changes (Galgano et al., 2017; Priester et al., 2022). Post-TBI brains can

develop swollen neurons, vacuolar changes, uncentered nuclei, and the loss of both white and gray matter (Sen, 2017; Tan et al., 2018). Tissue degeneration can be tracked through silver staining in brains (Deng et al., 2007). Deng et al. (2007) observed a significantly increased volume of silver staining with a maximal peak occurring at 48 h after injury. They observed the silver staining and subsequent neurodegeneration continued even at 7 days post injury (Deng et al., 2007). This is one example of how secondary TBI can exacerbate neurodegeneration even days after primary injury. After TBI, changes in ocular tissues can be observed as well. Models of TBI have reported changes in retinal nerve fiber layer (RNFL) thickness along with a decrease in oligodendrocyte precursor cells (OPCs) and subsequent reduction in myelination (Gupta et al., 2019). Currently there are no effective neuroprotective pharmaceutical therapeutics (Galgano et al., 2017; Priester et al., 2022).

3.2. Traumatic optic neuropathy (TON)

Eye related injuries encompass ~2.5 million emergency department visits per year in the US alone, and account for 13% of battlefield injuries (Sherwood et al., 2014). TON is an irreversible vision-threatening complication of blunt force trauma, often affiliated with a TBI (Sarkies, 2004; Sherwood et al., 2014). TON is divided into two main categories: direct and indirect. Direct TON (dTON) occurs when the eye has been penetrated and encompasses injuries such as foreign bodies piercing the optic nerve, or orbital fractures crushing and/or severing the optic nerve (Sarkies, 2004). Indirect TON (iTON) is the more common form; however, it may not be detected as quickly (Sarkies, 2004). iTON is the result of blunt force trauma of the head, or TBI (Sarkies, 2004; DeJulius et al., 2021). About 0.5–5% of closed head TBIs result in TON (Sarkies, 2004). Currently, intervention relies on corticosteroids and/or surgical decompression (Sarkies, 2004). However, both have limited success and more importantly there is a growing concern of utilizing corticosteroids in the presence of TBI (Roberts et al., 2004; Sarkies, 2004; Steinsapir and Goldberg, 2011). In addition, translational animal models remain limited. TON is correlated with a deficit of RGCs and axon degeneration, but the exact disease progression and cell death pathways are not fully understood (Tse et al., 2018; Khan et al., 2021). ROS have been observed to increase while antioxidant enzymes, such as SOD, decrease after injury (Bernardo-Colón et al., 2018). Bernardo-Colón et al. (2018) also observed blast induced TON, caused vacuolization and hyper-myelination in optic nerves. Myelin injury, decreases in retinal nerve fiber layer thickness, and overall changes in retinal thickness have also been noted in TON models (Brooks et al., 2014; Jones et al., 2016; Evanson et al., 2018). It has also been noted that ROS plays a major effect in the degeneration of axons and subsequent vision loss after iTON (Bernardo-Colón et al., 2018; DeJulius et al., 2021).

3.3. ROS and the disease progression in TON and TBI

Like TBI, the vision loss associated with iTON is usually a secondary injury event (Tandon and Maapatra, 2017; Zhou et al., 2021). Li et al. (2020) conducted a study in which they modeled different blunt force head injuries to determine how iTON may be induced. From their study they determined a blunt force impact to the center of the forehead (0°) and a blunt force impact to the right frontal region of the forehead (45°) resulted in injury to the optic nerve *via* a shearing form of injury (Li et al., 2020). They determined blunt force impact to the head can result in stress wave propagation through the orbital rim to the optic canal (Li et al., 2020). In their model they observed the translation of impact energy propagated along the orbital ceiling to the top rim of the optic canal, which lead to optic canal diameter reduction (Li et al., 2020). This reduction may also play a role in facilitating secondary injury events, especially in the intracanalicular optic nerve as this area normally has limited space, and further reduction mixed with the start of neuroinflammatory responses could facilitate further compression of the optic nerve (Sarkies, 2004; Li et al., 2020). After the primary injury, secondary neurodegeneration occurs as neuroinflammation and ROS species accumulate near the site of injury (**Figure 2**) (Dröge, 2002; Bond and Rex, 2014). Before injury, the CNS and eye lack systemic macrophages due to their strict BBB/BRB, but they have microglia which act as immune cells and work to maintain the neurological tissue (Dröge, 2002; Bond and Rex, 2014; Tao et al., 2017; Thompson and Tsirka, 2017; McMenamin et al., 2019; DeJulius et al., 2021). After injury, the BBB/BRB can break down and allow for infiltration of peripheral immune cells such as macrophages, neutrophils, and leukocytes (Bond and Rex, 2014; Brooks et al.,

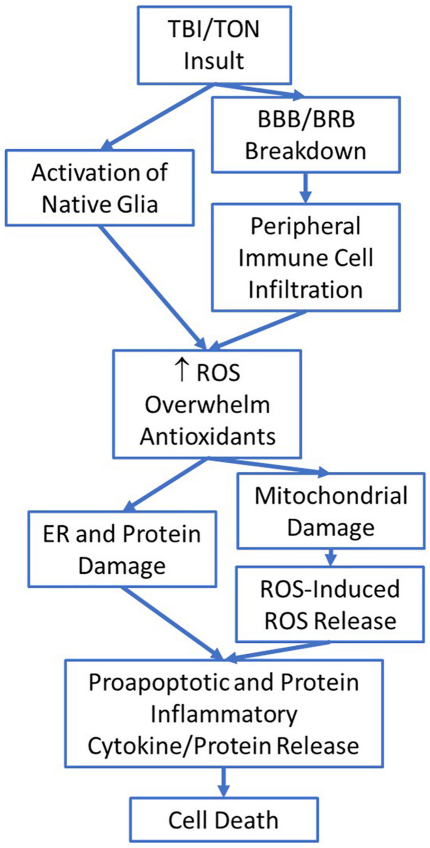

FIGURE 2
The potential flow of injury mechanisms and steps involved after traumatic brain injury (TBI)/traumatic optic neuropathy (TON) which eventually lead to cell death.

2014; Galgano et al., 2017; McMenamin et al., 2019; DeJulius et al., 2021). As a result, ROS levels can become increasingly elevated as activated macrophages and other immune cells release large amounts of ROS when in inflammatory environments (Dröge, 2002). In TON it may be that RGC and axonal degeneration progress due to the breakdown of the BRB and subsequent infiltration of systemic immune cells which then produce large quantities of ROS. Once macrophages infiltrate the damaged CNS, they take on an active microglial morphology and begin to produce pro-inflammatory cytokines alongside the native active microglial cells (Bond and Rex, 2014; DeJulius et al., 2021). Elevated ROS may be too much for the mitochondria to combat *via* their redox homeostasis system, leading to mitochondrial damage and genetic alterations (Deng et al., 2007; Gupta et al., 2019).

Injury may cause mitochondrial dysfunction, which alters the mitochondrial redox homeostasis system, with respect to overproduction of ROS, and alterations of ROS-mediated gene expression (Dröge, 2002; Angelova and Abramov, 2018). When ROS is being overproduced by the mitochondria it can cause lipid peroxidation to start and in turn activate microglia (Angelova and Abramov, 2018). The dysfunction in the mitochondria limits the cells' ability to combat the rising ROS with natural antioxidants, which then can lead to neurological degeneration and subsequent cell death (Angelova and Abramov, 2018). One study even observed irregularities in the shape of mitochondria after TBI (Tan et al., 2018). In this study, mitochondria in cortical neurons were observed to be swollen and misshaped with alterations and disruptions present in their cristae (Tan et al., 2018). Mueller-Buehl et al. (2021) also observed swollen mitochondria in their H_2O_2 induced retinal degeneration model. In addition, Tan et al. (2018) also examined endoplasmic reticulum (ER) stress and dysfunction in the context of TBI.

The ER is a large organelle in the cell and is responsible for several key functions including protein synthesis and transport, lipid synthesis, protein folding, steroid synthesis, and calcium storage (Schwarz and Blower, 2016). ER stress occurs when there is an accumulation of unfolded or misfolded proteins and as a result the unfolded protein response (UPR) is initiated to return the ER to normal function (Nakka et al., 2016; Schwarz and Blower, 2016; Tan et al., 2018). Activation of ER stress pathways have been observed to promote the formation of ROS through inducible nitric oxide synthase (iNOS)- dependent and -independent pathways (Hsieh et al., 2007). If function cannot be restored, then cell death and apoptosis occur (Schwarz and Blower, 2016). ER stress has also been observed in neurological cells after TBI (Deng et al., 2007; Logsdon et al., 2014, 2016; Hylin et al., 2018; Tan et al., 2018). Tan et al. (2018, p. 832) noted proteins related to ER stress were activated immediately after TBI and peaked 3 h after the injury. A separate study found ER stress related markers were increased 24 h after blast induced TBI (Logsdon et al., 2014). Similarly, Dash et al. (2015) observed significantly increased levels of eIF2α, a known marker of ER stress, at 24 h after injury in their rodent TBI model. Both Lucke-Wold et al. (2016) and Logsdon et al. (2016) noted an elevation in C/EBP homologous protein (CHOP) expression 24 h after their rodent blast injury model, indicating ER stress was induced. Lucke-Wold et al. (2016) also observed increased levels in human brain samples of patients inflicted with chronic traumatic encephalopathy (CTE), which further promotes ER stress's role in neurodegeneration after neurotrauma (Lucke-Wold et al., 2016). Interestingly, Hylin et al. (2018) observed an increase in CHOP and binding immunoglobulin protein (BiP), another marker of ER stress, were significantly increased as early as 4 h after TBI in their juvenile rodent TBI model. Tan et al. (2018, p. 833) found that ER were abnormally shaped and swollen in cortical neurons after TBI. This same study observed the apoptotic ER stress pathway was maximally activated 6 h after injury followed by activation of the mitochondrial apoptotic pathway, which occurred 6 h after TBI (Tan et al., 2018). Tan et al. (2018, p. 835) determined that inhibition of ER stress *via* the ER stress modulator salubrinal (Sal) could stop apoptosis and restore normal function to dysfunctional mitochondria. Logsdon et al. (2014) also investigated administration of Sal for the treatment of TBI and the associated neuropsychiatric symptoms. Logsdon et al. (2014, p. 12) also concluded that ER stress regulation *via* Sal was capable of reducing apoptosis while also limiting impulse-like behavior in rats afflicted with TBI.

Glial cell activation remains a common factor in secondary neurodegeneration following the initial injury in both TBI and TON (Rodgers et al., 2012; Bond and Rex, 2014; Choi et al., 2014; Tao et al., 2017; Evanson et al., 2018; DeJulius et al., 2021; Hetzer et al., 2021; Zhou et al., 2021; Priester et al., 2022). As previously stated, after injury the BBB/BRB can break down, allowing for systemic macrophages to invade the CNS and take on an active microglial morphology (Bond and Rex, 2014; Brooks et al., 2014; McMenamin et al., 2019; DeJulius et al., 2021). Injury also activates the resting microglia cells, which then activate the neuroinflammatory response (Bond and Rex, 2014; DeJulius et al., 2021; Zhou et al., 2021; Priester et al., 2022). Activated glial cells will release proinflammatory cytokines and phagocytose cells; however, they do this while releasing large amounts of ROS (Dröge, 2002; Bond and Rex, 2014; DeJulius et al., 2021). In an overall healthy environment, this neuroinflammatory response serves to heal tissue, but when the level of ROS begins to outcompete the cells' ability to produce antioxidants this chain of events can lead to neural degeneration (Bond and Rex, 2014; Priester et al., 2022). One study determined the BBB was disrupted as early as 30 min after blast-induced TBI (Logsdon et al., 2014). They also observed astrocyte activation after an increase in ER stress and subsequent upregulation of UPR (Logsdon et al., 2014). Logsdon et al. (2014, p. 7) noted the activation of astrocytes is characteristic of neuroinflammation and cell death. Studies examining astrocyte activation tend to utilize glial fibrillary acidic protein (GFAP) (Choi et al., 2014; Evanson et al., 2018). GFAP immunoreactivity was increased after TBI in both Choi et al. (2014), Evanson et al. (2018). Interestingly Evanson et al. (2018) observed an increase in size of microglial cells 24 h after injury in the optic track only, but at 24 h after injury they did not observe increased GFAP immunoreactivity (Evanson et al., 2018). This would indicate a shape change in microglia occur prior to increased astrocyte activation. At 7 days post injury the microglial cells were still increased in size, but only in the optic tract, while GFAP immunoreactivity was found to be increased at this timepoint in the optic tract, LGN, and SC (Evanson et al., 2018). A separate study determined GFAP immunoreactivity was increased in both the retina and optic nerve after single and repeated blast overpressure induced trauma (Choi et al., 2014). It may be that glial cell activation plays an important role in the accumulation of ROS and subsequent neurodegeneration observed in both the brain and retina following traumatic injury. The infiltration of systemic macrophages, upon the disruption of the BBB/BRB, in addition to the native CNS activated glial cells may overwhelm the antioxidant systems in place for normal glial cell response (Zhou et al., 2021). This may ultimately lead to neurodegeneration after injury.

4. Current therapeutic approaches

There are many different therapeutic studies being conducted targeting not only antioxidant mechanisms, but also other elements in the injury and neurodegenerative cascade. One such promising therapeutic is tauroursodeoxycholic acid (TUDCA). TUDCA is comprised of taurine, which is a common amino acid in the retina that retinal cells need to uptake for cellular function (Daruich et al., 2019). TUDCA has been shown to have anti-inflammatory, anti-apoptotic, antioxidant, and neuroprotective effects (Elia et al., 2015; Gómez-Vicente et al., 2015; Daruich et al., 2019). TUDCA was observed to promote RGC survival after optic nerve crush in rats and has also been utilized in several studies for the treatment of neurodegenerative disorders such as ALS, PD, AD, and HD (Vang et al., 2014; Elia et al., 2015; Daruich et al., 2019; Kitamura et al., 2019). TUDCA has been observed to reduce ROS, limit microglial cell activation, reduce ER stress, and suppress inflammatory processes (Vang et al., 2014; Gómez-Vicente et al., 2015; Daruich et al., 2019). It has also been reported that TUDCA can preserve the BRB (Daruich et al., 2019).

Another promising therapeutic is ibudilast, which is a cAMP phosphodiesterase (PDE) inhibitor (Cueva Vargas et al., 2016). Ibudilast works to attenuate ROS production by inhibiting phosphodiesterase which in turn increases cAMP levels (Tahvilian et al., 2019). The increase of cAMP suppresses the expression of sigma (σ) receptors, which can be responsible for increasing ROS (Ostenfeld et al., 2005; Tahvilian et al., 2019). In addition, ibudilast reduces glial cell activation and subsequently reduces pro-inflammatory cytokines (Lee et al., 2012; Cueva Vargas et al., 2016). Ibudilast is known to suppress the proinflammatory protein macrophage migration inhibitory factor (MIF), while also increasing the concentration of anti-inflammatory cytokines and neurotrophic factors (Cho et al., 2010; Lee et al., 2012). Like TUDCA, ibudilast has been investigated in neurodegenerative diseases such as MS and ALS (Fox et al., 2018; Oskarsson et al., 2021). Rodgers et al. (2012) examined the connection between post-injury neuroinflammation and post-traumatic anxiety in a TBI rat model. In this study they utilized OX-42 to determine microglia activation and GFAP to determine astrocyte activation (Rodgers et al., 2012). They observed increased labeling for both microglia and astrocytes after injury (Rodgers et al., 2012). Rodgers et al. (2012) utilized ibudilast and determined ibudilast was capable of reducing reactive gliosis while also attenuating anxiety behaviors in post-TBI rats (Rodgers et al., 2012). Based on these studies, ibudilast may be a promising therapeutic toward the reduction of microglial and astrocyte activation and subsequent reduction of ROS production.

Erythropoietin (EPO) is another potential therapeutic that may be able to reduce elevated ROS in neurodegenerative cells (Bond and Rex, 2014). EPO can limit the immune cell response and migration, and thus may be beneficial in attenuating the elevation of ROS and proinflammatory cytokines through this process (Bond and Rex, 2014). EPO has been utilized in a TON model to reduce ROS (DeJulius et al., 2021). In this study, they determined sustained release of EPO *via* poly(propylene sulfide) (PPS) and poly(lactic-co-glycolic acid) (PLGA) microspheres resulted in neuroprotective properties after iTON (DeJulius et al., 2021). EPO has also been examined for neuroprotective effects in a mouse model of Parkinson's Disease (Dhanushkodi et al., 2012). In this study they determined EPO may result in increased axonal sprouting and neuroprotective effects in PD (Dhanushkodi et al., 2012).

Researchers have begun analyzing whether attenuation of pro-inflammatory cytokines such as tumor necrosis factor (TNF) can result in neuroprotective effects. TNF concentrations are elevated after traumatic injury and in several neurodegenerative diseases such as AD, MS, and PD (Fontaine et al., 2002). TNF is one of the most important proinflammatory cytokines that is upregulated after TON (Tse et al., 2018). TNF helps to regulate immune cell function and plays a pivotal role in the pathogenesis of almost all neurodegenerative diseases (Tse et al., 2018; Chen et al., 2022). TNF-α has been observed to increase ROS through the activation of cyclin-dependent kinase 5 (Cdk5) (Sandoval et al., 2018). TNF's ability to increase ROS may be why it is found to play a role in so many neurodegenerative diseases. Fontaine et al. (2002) analyzed whether the upregulation of the molecule TNF was causing the degeneration or whether which TNF receptor the molecule bound to was causing the degeneration. They determined TNF Receptor 2 (TNF-R2) may promote neuroprotection while TNF Receptor 1 (TNF-R1) may promote neurodegeneration (Fontaine et al., 2002). In a healthy environment, the rate of activity between the two receptors should be relatively balanced, but if TNF-R2 were to become overactive then neurodegeneration could occur (Fontaine et al., 2002). Fontaine et al. (2002) tried blocking the TNF molecule itself but observed no significant difference in cell death or survival. When they created a TNF-R2 deficit they observed an increase in retinal cell death *via* TNF; however, when they created a deficit in TNF-R1 they observed a neuroprotective response from TNF (Fontaine et al., 2002). Since TNF is upregulated in many ocular disorders and neurodegenerative diseases, it may be beneficial to attenuate TNF levels and TNF-R1 activity as a means to promote neuroprotection.

Other researchers have focused on replacing the abnormal mitochondria. As previously explained, mitochondria are a major source of ROS production and a site for ROS damage. In a rodent model one group was able to transfer isolated and normally functioning mitochondria into neuronal schizophrenia cells (Robicsek et al., 2018). The addition of normal mitochondria reduced the neurological deficits associated with schizophrenia in their rodent model (Robicsek et al., 2018). This technique has also been applied to the ocular environment by Nascimento-dos-Santos et al. (2020) in their optic nerve injury model. In this study, liver mitochondria were transplanted into the retina and were successful in regulating the oxidative metabolism of these cells (Nascimento-dos-Santos et al., 2020). They observed successful protection of RGCs and an increase amount of optic nerve axons with the transplanted mitochondria (Nascimento-dos-Santos et al., 2020).

5. Discussion

The brain and retina are uniquely connected, which allows for the ocular environment to serve as a model for CNS degeneration and disease. In addition, traumatic brain injury can often result in disturbances or total loss to the visual system (Sarkies, 2004; DeJulius et al., 2021). Trauma nurses are even tasked with checking a patient's pupillary reflex when TBI is suspected (Adoni and McNett, 2007). The unique relationship between the retina and the brain allows us to glean neurodegenerative processes in an accessible environment (Cheung et al., 2017; Bernardo-Colón et al., 2018).

As described in this paper, much can be learned about the cellular response to traumatic brain injury through examination of the retina after injury. Both TBI and TON experience secondary injury *via* neuroinflammatory responses that can occur several hours to days after injury. Treatment protocols must be determined to suppress harmful over production of ROS, and up regulation of glial cells, proinflammatory cytokines, and other cellular elements responsible for increased neurodegeneration in the unbalanced system. Current treatment options are limited and have had minimal success. Determination of why these treatments fail will allow researchers to determine not only the maximal therapeutic intervention but will also allow researchers to better understand the disease progression.

5.1. Why might antioxidant treatments fail?

It is clear that ROS plays a pivotal role in neurodegeneration in both the brain and retina. Thus, it would make sense to limit the concentration of ROS *via* antioxidants for preservation of the neurological system from degeneration. Many have tried this approach, but unfortunately most antioxidant therapeutics tend to fail during clinical trials (Priester et al., 2022). The question then becomes why do antioxidant therapeutics fail if ROS play such a major role in neurodegeneration? Dröge (2002) states that utilizing large concentrations of antioxidants to combat ROS may actually be damaging as the body does need some small concentrations of ROS to continue normal cellular functions and processes. It may be excessive use of antioxidants end up resulting in no change to neurodegeneration because they are over limiting ROS, and the homeostatic balance has shifted in the opposite direction. Grotegut et al. (2020) examined minocycline's ability to reduce inflammation in a retinal degeneration model. Minocycline acts as a microglial inhibitor, which can lower ROS by suppressing the amount of active microglia (Grotegut et al., 2020). In their study they concluded that the low dose of minocycline resulted in better neuroprotection and suppression of inflammatory and apoptotic processes than the higher dosage (Grotegut et al., 2020). On the other hand, Schnichels et al. (2021) examined cyclosporine A's ability to protect RGCs after hypoxia. In this study, they did not observe a significant protective effect for RGCs when a 6 μg/mL dosage was utilized (Schnichels et al., 2021). They did observe a significant protective effect when the higher dosage, 9 μg/mL, was utilized (Schnichels et al., 2021). To achieve proper neuroprotection from ROS *via* antioxidant therapeutics it is necessary to fully understand the degenerative processes occurring during trauma and disease mediated neurodegeneration. The means in which we can treat these disorders depends on the ways ROS interacts with the cellular environment to exacerbate damage. In some instances, it may be necessary to utilize lower doses rather than flood the CNS with antioxidant therapeutics. The means in which each therapeutic acts upon the CNS must also be established in order to determine the dosage required to obtain neuroprotective properties.

Determining the dosage dependent manner of antioxidant therapeutics is only one piece of the puzzle. Neurodegeneration through ROS is multifaceted and includes elements such as BBB/BRB breakdown, infiltration of systemic macrophages, activation of glial cells, mitochondrial dysfunction, and redox imbalance. The struggle of treating neurodegeneration after injury is determining which section of the injury process needs attention. In order to answer this question, it may depend on the timing of therapeutic intervention. Tao et al. (2017) determined ROS elevation started to rise around 30 min after sonication-induced TON. Logsdon et al. (2014) reported BBB breakdown around 30 min after TBI and then increased mRNA stress response genes at 3 h after injury. They also noted DNA damage-inducible protein 34 (GADD34) was upregulated at 24 h after injury with astrocyte activation occurring afterward (Logsdon et al., 2014). Deng et al. (2007) also noted an increase in oxidative stress markers around 30 min after TBI with these levels remaining elevated for 3–6 h before returning to control levels. It may be that in order for antioxidant therapeutics to work, they need to be administered as close to the injury event as possible. If therapeutic intervention is delayed, the ROS elevation event may have already created substantial damage and the body may have moved toward activation of other cellular cascades that result in further neurodegeneration, such as activation of astrocytes. From the research presented, it appears ROS elevation and oxidative stress is one of the first mechanisms to occur after the injury event; however, due to polytrauma and the fact that noticeable vision loss does not always occur immediately after injury, patients with TON/TBI may not seek treatment until well after this crucial window of time. Therefore, the therapeutic intervention utilized must take into account the injury timeline and how the secondary neurodegenerative cascade has progressed. In some instances, ROS reductive treatments may be ineffective if the injury process has moved downstream; therefore, targeting other cellular cascades in addition to the ROS reductive therapeutics in a mixed approach may be the best course of action when treatment after injury has been delayed.

Further research is needed to determine the best approach to mitigate neurodegenerative processes in the CNS. In traumatic injury the BBB/BRB has been observed to breakdown, this breakdown may actually help facilitate the delivery of therapeutic intervention methods such as antioxidants as some antioxidant therapeutics cannot cross the BBB/BRB under normal physiological conditions (Singh et al., 2019). In other neurodegenerative disorders, this breakdown may not occur, or may occur at a different time points after the beginning of neurodegeneration. Additional research is also warranted to further determine the pathophysiological time course of both traumatic and genetic forms of neurodegeneration. The determination of this time course may allow researchers to develop efficacious treatment protocols for individuals afflicted with neurodegenerative processes in both the brain and retina.

Author contributions

AR and WR drafted the manuscript. MR edited the manuscript. All authors contributed to the literature review and discussions and approved the submitted version.

Funding

This work was supported by the US Department of Defense Vision Research Program Awards W81XWH-15-1-0074 and W81XWH-22-1-0989.

Conflict of interest

The authors declare that the research was conducted in the absence of any commercial or financial relationships that could be construed as a potential conflict of interest.

Publisher's note

All claims expressed in this article are solely those of the authors and do not necessarily represent those of their affiliated organizations, or those of the publisher, the editors and the reviewers. Any product that may be evaluated in this article, or claim that may be made by its manufacturer, is not guaranteed or endorsed by the publisher.

Author disclaimer

The opinions or assertions contained herein are the private views of the authors and are not to be construed as official or as reflecting the views of the Department of the Army or the Department of Defense.

References

Adoni, A., and McNett, M. (2007). The pupillary response in truamatic brain injury: A guide for trauma nurses. *J. Trauma Nurs.* 14, 191–196. doi: 10.1097/01.jtn.0000318921.90627.fe

Angelova, P. R., and Abramov, A. Y. (2018). Role of mitochondrial ROS in the brain: From physiology to neurodegeneration. *FEBS Lett.* 592, 692–702. doi: 10.1002/1873-3468.12964

Archibald, N. K., Clarke, M. P., Mosimann, U. P., and Burn, D. J. (2009). The retina in Parkinson's disease. *Brain* 132, 1128–1145. doi: 10.1093/brain/awp068

Attwell, D., Buchan, A. M., Charpak, S., Lauritzen, M., MacVicar, B. A., and Newman, E. A. (2010). Glial and neuronal control of brain blood flow. *Nature* 468, 232–243. doi: 10.1038/nature09613

Berger, J., Dorninger, F., Forss-Petter, S., and Kunze, M. (2016). Peroxisomes in brain development and function. *Biochim. Biophys. Acta* 1863, 934–955. doi: 10.1016/j.bbamcr.2015.12.005

Bernardo-Colón, A., Vest, V., Clark, A., Cooper, M. L., Calkins, D. J., Harrison, F. E., et al. (2018). Antioxidants prevent inflammation and preserve the optic projection and visual function in experimental neurotrauma. *Cell Death Discov.* 9:1097. doi: 10.1038/s41419-018-1061-4

Blanks, J. C., Hinton, D. R., Sadun, A. A., and Miller, C. A. (1989). Retinal ganglion cell degeneration in Alzheimer's disease. *Brain Res.* 501, 364–372. doi: 10.1016/0006-8993(89)90653-7

Bond, W. S., and Rex, T. S. (2014). Evidence that erythropoietin modulates neuroinflammation through differential action on neurons, astrocytes, and microglia. *Front. Immunol.* 5:523. doi: 10.3389/fimmu.2014.00523

Brooks, D. E., Komàromy, A. M., and Källberg, M. E. (1999). Comparative retinal ganglion cell and optic nerve morphology. *Vet Ophthalmol.* 2, 3–11. doi: 10.1046/j.1463-5224.1999.00047.x

Brooks, D. E., Plummer, C. E., Craft, S. L. M., and Struthers, J. D. (2014). Traumatic brain injury manifested as optic neuropathy in the horse: A commentary and clinical case. *Equine Vet. Educ.* 26, 527–531. doi: 10.1111/eve.12214

Cabezas, R., Ávila, M., Gonzalez, J., El-Bachá, R. S., Báez, E., García-Segura, L. M., et al. (2014). Astrocytic modulation of blood brain barrier: Perspectives on Parkinson's disease. *Front. Cell. Neurosci.* 8:211. doi: 10.3389/fncel.2014.00211

Chen, B., Zhang, H., Li, H., Wang, C., and Wang, Y. (2022). Traumatic optic neuropathy: A review of current studies. *Neurosurg. Rev.* 45, 1895–1913. doi: 10.1007/s10143-021-01717-9

Cheung, C. Y. L., Kamran Ikram, M., Chen, C., and Wong, T. Y. (2017). Imaging retina to study dementia and stroke. *Prog. Retin. Eye Res.* 57, 89–107. doi: 10.1016/j.preteyeres.2017.01.001

Cho, Y., Crichlow, G. V., Vermeire, J. J., Leng, L., Du, X., Hodsdon, M. E., et al. (2010). Allosteric inhibition of macrophage migration inhibitory factor revealed by ibudilast. *Proc. Natl. Acad. Sci. U.S.A.* 107, 11313–11318. doi: 10.1073/pnas.1002716107

Choi, J. H., Greene, W. A., Johnson, A. J., Chavko, M., Cleland, J. M., McCarron, R. M., et al. (2014). Pathophysiology of blast-induced ocular trauma in rats after repeated exposure to low-level blast overpressure. *Clin. Exp. Ophthalmol.* 43, 239–246. doi: 10.1111/ceo.12407

Cooper, G. M. (2000). *The cell: A molecular approach*, 2nd Edn. Sunderland, MA: Sinauer Associates.

Cueva Vargas, J. L., Belforte, N., and Di Polo, A. (2016). The glial cell modulator ibudilast attenuates neuroinflammation and enhances retinal ganglion cell viability I glaucoma through protein kinase a signaling. *Neurobiol. Dis.* 93, 156–171. doi: 10.1016/j.nbd.2016.05.002

Daruich, A., Picard, E., Boatright, J. H., and Cohen-Behar, F. (2019). Review: The bile acids urso- and tauroursodeoxycholic acid as neuroprotective therapies in retinal disease. *Mol. Vis.* 25, 610–624.

Das, Y., Roose, N., De Groef, L., Fransen, M., Moons, L., Van Veldhoven, P. P., et al. (2019). Differential distribution of peroxisomal proteins points to specific roles of peroxisomes in the murine retina. *Mol. Cell. Biochem.* 456, 53–62. doi: 10.1007/s11010-018-3489-3

Dash, P. K., Hylin, M. J., Hood, K. N., Orsi, S. A., Zhao, J., Redell, J. B., et al. (2015). Inhibition of eukaryotic initiation factor 2 alpha phosphatase reduces tissue damage and improves learning and memory after experimental traumatic brain injury. *J. Neurotrauma* 32, 1608–1620. doi: 10.1089/neu.2014.3772

DeJulius, C. R., Bernardo-Colón, A., Naguib, S., Backstrom, J. R., Kavanaugh, T., Gupta, M. K., et al. (2021). Microsphere antioxidant and sustained erythropoietin-R76E release functions cooperate to reduce traumatic optic neuropathy. *J. Control. Release* 329, 762–773. doi: 10.1016/j.jconrel.2020.10.010

Deng, Y., Thompson, B. M., Gao, X., and Hall, E. D. (2007). Temporal relationship of peroxynitrite-induced oxidative damage, calpain-mediated cytoskeletal degradation and neurodegeneration after traumatic brain injury. *Exp. Neurol.* 205, 154–165. doi: 10.1016/j.expneurol.2007.01.023

Dewan, M. C., Rattani, A., Gupta, S., Baticulon, R. E., Hung, Y., Punchak, M., et al. (2018). Estimating the global incidence of traumatic brain injury. *J. Neurosurg.* 130, 1080–1097. doi: 10.3171/2017.10.JNS17352

Dhanushkodi, A., Akano, E. O., Roguski, E. E., Xue, Y., Rao, S. K., Matta, S. G., et al. (2012). A single intramuscular injection of rAAV-mediated mutant erythropoietin protects against MPTP-induced Parkinsonism. *Genes Brain Behav.* 12, 224–233. doi: 10.1111/gbb.12001

Dröge, W. (2002). Free radicals in the physiological control of cell function. *Physiol. Rev.* 82, 47–95. doi: 10.1152/physrev.00018.2001

Eells, J. T. (2019). Mitochondrial dysfunction in the aging retina. *Biology* 8:31. doi: 10.3390/biology8020031

el-Hifnawi, E., Kühnel, W., el-Hifnawi, A., and Laqua, H. (1994). Localization of lysosomal enzymes in the retina and retinal pigment epithelium of RCS rats. *Ann. Anat.* 176, 505–513. doi: 10.1016/s0940-9602(11)80384-5

Elia, A. E., Lalli, S., Monsurrò, M. R., Sagnelli, A., Taiello, A. C., Reggiori, B., et al. (2015). Tauroursodeoxycholic acid in the treatment of patients with amyotrophic lateral sclerosis. *Eur. J. Neurol.* 23, 45–52. doi: 10.1111/ene.12664

Evanson, N. K., Guilhaume-Correa, F., Herman, J. P., and Goodman, M. D. (2018). Optic tract injury after closed head traumatic brain injury in mice: A model of indirect traumatic optic neuropathy. *PLoS One* 13:e0197346. doi: 10.1371/journal.pone.0197346

Ferguson, S. M. (2019). Neuronal lysosomes. *Neurosci. Lett.* 697, 1–9. doi: 10.1016/j.neulet.2018.04.005

Fontaine, V., Mohand-Said, S., Hanoteau, N., Fuchs, C., Pfizenmaier, K., and Eisel, U. (2002). Neurodegenerative and neuroprotective effects of tumor necrosis factor (TNF) in retinal ischemia: Opposite roles of TNF receptor 1 and TNF receptor 2. *J. Neurosci.* 22:RC216. doi: 10.1523/JNEUROSCI.22-07-j0001.2002

Forred, B. J., Daugaard, D. R., Titus, B. K., Wood, R. R., Floen, M. J., Booze, M. L., et al. (2017). Detoxification of mitochondrial oxidants and apoptotic signaling are facilitated by thioredoxin-2 and peroxiredoxin-3 during hyperoxic injury. *PLoS One* 12:e0168777. doi: 10.1371/journal.Pone.0168777

Fox, R. J., Coffey, C. S., Conwit, R., Cudkowicz, M. E., Gleason, T., Goodman, A., et al. (2018). Phase 2 trial of ibudilast in progressive multiple sclerosis. *N. Engl. J. Med.* 379, 846–855. doi: 10.1056/NEJMoa1803583

Galgano, M., Toshkezi, G., Qiu, X., Russell, T., Chin, L., and Zhao, L. (2017). Traumatic brain injury: Current treatment strategies and future endeavors. *Cell Transplant.* 26, 1118–1130. doi: 10.1177/0963689717714102

Gómez-Vicente, V., Lax, P., Fernández-Sánchez, L., Rondón, N., Esquiva, G., Germain, F., et al. (2015). Neuroprotective effect of tauroursodeoxycholic acid on n-methyl-d-aspartate-induced retinal ganglion cell degeneration. *PLoS One* 10:e0137826. doi: 10.1371/journal.pone.0137826

Green, A. J., McQuaid, S., Hauser, S. L., Allen, I. V., and Lyness, R. (2010). Ocular pathology in multiple sclerosis: Retinal atrophy and inflammation of disease duration. *Brain* 133, 1591–1601. doi: 10.1093/brain/awq080

Grotegut, P., Perumal, N., Kuehn, S., Smit, A., Dick, H. B., Grus, F. H., et al. (2020). Minocycline reduces inflammatory response and cell death in a S100B degeneration model. *J. Neuroinflamm.* 17:375. doi: 10.1186/s12974-020-02012-y

Gupta, R., Saha, P., Sen, T., and Sen, N. (2019). An augmentation in histone dimethylation at lysine nine residues elicits vision impairment following traumatic brain injury. *Free Radic. Biol. Med.* 134, 630–643. doi: 10.1016/j.freeradbiomed.2019.02.015

Hetzer, S. M., Shalosky, E. M., Torrens, J. N., and Evanson, N. K. (2021). Chronic histological outcomes of indirect traumatic optic neuropathy in adolescent mice: Persistent degeneration and temporally regulated glial responses. *Cells* 10:3343. doi: 10.3390/cells10123343

Hiebert, J. B., Shen, Q., Thimmesch, A. R., and Pierce, J. D. (2015). Traumatic brain injury and mitochondrial dysfunction. *Am. J. Med. Sci.* 350, 132–138. doi: 10.1097/MAJ.0000000000000506

Hsieh, H. J., Liu, C. A., Huang, B., Tseng, A. H., and Wang, D. L. (2014). Shear-induced endothelial mechanotransduction: The interplay between reactive oxygen species (ROS) and nitric oxide (NO) and the pathophysiological implications. *J. Biomed. Sci.* 21:3. doi: 10.1186/1423-0127-21-3

Hsieh, Y. H., Su, I. J., Lei, H. Y., Lai, M. D., Chang, W. W., and Huang, W. (2007). Differential endoplasmic reticulum stress signaling pathways mediated by iNOS. *Biochem. Biophys. Res. Commun.* 359, 643–648. doi: 10.1016/j.bbrc.2007.05.154

Hylin, M. J., Holden, R. C., Smith, A. C., Logsdon, A. F., Qaiser, R., and Lucke-Wold, B. P. (2018). Juvenile traumatic brain injury results in cognitive deficits associated with impaired endoplasmic reticulum stress and early tauopathy. *Dev. Neurosci.* 40, 175–188. doi: 10.1159/000488343

Jones, K., Choi, J., Sponsel, W. E., Gray, W., Groth, S. L., Glickman, R. D., et al. (2016). Low-level primary blast causes acute ocular trauma in rabbits. *J. Neurotrauma* 33, 1194–1201. doi: 10.1089/neu.2015.4022

Kassmann, C. M. (2014). Myelin peroxisomes - essential organelles for the maintenance of white matter in the nervous system. *Biochimie* 98, 111–118. doi: 10.1016/j.biochi.2013.09.020

Khan, R. S., Ross, A. G., Aravand, P., Dine, K., Selzer, E. B., and Shindler, K. S. (2021). RGC and vision loss from traumatic optic neuropathy induced by repetitive closed head trauma is dependent on timing and force of impact. *Transl. Vis. Sci. Technol.* 10:8. doi: 10.1167/tvst.10.1.8

Kitamura, Y., Bikbova, G., Baba, T., Yamamoto, S., and Oshitari, T. (2019). *In vivo* effects of single or combined topical neuroprotective and regenerative agents on degeneration of retinal ganglion cells in rat optic nerve crush model. *Sci. Rep.* 9:101. doi: 10.1038/s41598-018-36473-2

Kolb, H. (2001). "Glial cells of the retina," in *Webvision: The organization of the retina and visual system*, eds H. Kolb, E. Fernandez, and R. Nelson (Salt Lake City, UT: University of Utah Health Sciences Center).

Kreher, C., Favret, J., Maulik, M., and Shin, D. (2021). Lysosomal functions in glia associated with neurodegeneration. *Biomolecules* 11:400. doi: 10.3390/biom11030400

Lee, J., Cho, E., Ko, Y. E., Kim, I., Lee, K. J., Kwon, S. U., et al. (2012). Ibudilast, a phosphodiesterase inhibitor with anti-inflammatory activity, protects against ischemic brain injury in rats. *Brain Res.* 1431, 97–106. doi: 10.1016/j.brainres.2011.11.007

Lee, S., Jiang, K., Mcllmoyle, B., To, E., Xu, Q. A., Hirsch-Reinshagen, V., et al. (2020). Amyloid beta immunoreactivity in the retinal ganglion cell layer of the Alzheimer's eye. *Front. Neurosci.* 14:758. doi: 10.3389/fnins.2020.00758

Li, Y., Singman, E., McCulley, T., Wu, C., and Daphalapurkar, N. (2020). The biomechanics of indirect traumatic optic neuropathy using a computational head model with a biofidelic orbit. *Front. Neurol.* 11:346. doi: 10.3389/fneur.2020.00346

Lim, C. Y., and Zoncu, R. (2016). The lysosome as a command-and-control center for cellular metabolism. *J. Cell Biol.* 214, 653–664. doi: 10.1083/jcb.201607005

Logsdon, A. F., Lucke-Wold, B. P., Nguyen, L., Matsumoto, R. R., Turner, R. C., Rosen, C. L., et al. (2016). Salubrinal reduces oxidative stress, neuroinflammation and impulse behavior in a rodent model of traumatic brain injury. *Brain Res.* 1643, 140–151. doi: 10.1016/j.brainres.2016.04.063

Logsdon, A. F., Turner, R. C., Lucke-Wold, B. P., Robson, M. J., Naser, Z. J., Smith, K. E., et al. (2014). Altering endoplasmic reticulum stress in a model of blast-induced traumatic brain injury controls cellular fate and ameliorates neuropsychiatric symptoms. *Front. Cell Neurosci.* 8:421. doi: 10.3389/fncel.2014.00421

Lucke-Wold, B. P., Turner, R. C., Logsdon, A. F., Nguyen, L., Bailes, J. E., Lee, J. M., et al. (2016). Endoplasmic reticulum stress implicated in chronic traumatic encephalopathy. *J. Neurosurg.* 124, 687–702. doi: 10.3171/2015.3.JNS141802

McMenamin, P. G., Saban, D. R., and Dando, S. J. (2019). Immune cells in the retina and choroid: Two different tissue environments that require different defenses and surveillance. *Prog. Retin. Eye Res.* 70, 85–98. doi: 10.1016/j.preteyeres.2018.12.002

Metea, M. R., and Newman, E. A. (2006). Glial cells dilate and constrict blood vessels: A mechanism of neurovascular coupling. *J. Neurosci.* 26, 2862–2870. doi: 10.1523/JNEUROSCI.4048-05.2006

Mishra, A., and Newman, E. A. (2010). Inhibition of inducible nitric oxide synthase reverses the loss of functional hyperemia in diabetic retinopathy. *Glia* 58, 1996–2004. doi: 10.1002/glia.21068

Mohan, K., Kecova, H., Hernandez-Merino, E., Kardon, R. H., and Harper, M. M. (2013). Retinal ganglion cell damage in an experimental rodent model of blast-mediated traumatic brain injury. *Invest. Ophthalmol. Vis. Sci.* 54, 3440–3450. doi: 10.1167/iovs.12-11522

Mueller-Buehl, A. M., Tsai, T., Hurst, J., Theiss, C., Peters, L., Hofmann, L., et al. (2021). Reduced retinal degeneration in an oxidative stress organ culture model through an iNOS-Inhibitor. *Biology* 10:383. doi: 10.3390/biology10050383

Nakka, V. P., Prakash-babu, P., and Vemuganti, R. (2016). Crosstalk between the endoplasmic reticulum stress, oxidative stress, and autophagy: Potential therapeutic targets for acute CNS injuries. *Mol. Neurobiol.* 53, 532–544. doi: 10.1007/s12035-014-9029-6

Nascimento-dos-Santos, G., de-Souza-Ferreira, E., Lani, R., Faria, C. C., Araújo, V. G., Teixeira-Pinheiro, L. C., et al. (2020). Neuroprotection from optic nerve injury and modulation of oxidative metabolism by transplantation of active mitochondria to the retina. *Biochim. Biophys. Acta Mol. Basis Dis.* 1866:165686. doi: 10.1016/j.bbadis.2020.165686

Naseem, K. M. (2005). The role of nitric oxide in cardiovascular diseases. *Mol. Asp. Med.* 26, 33–65. doi: 10.1016/j.mam.2004.09.003

Nguyen, C. T. O., Acosta, M. L., Di Angelantonio, S., and Salt, T. E. (2021). Editorial: Seeing beyond the eye: The brain connection. *Front. Neurosci.* 15:719717. doi: 10.3389/fnins.2021.719717

Nickells, R. W. (1996). Retinal ganglion cell death in glaucoma: The how, the why, and the maybe. *J. Glaucoma* 5, 345–356.

Nita, M., and Grzybowski, A. (2016). The role of the reactive oxygen species and oxidative stress in the pathomechanism of the age-related ocular diseases and other pathologies of the anterior and posterior eye segments in adults. *Oxid. Med. Cell. Longev.* 2016:3164734. doi: 10.1155/2016/3164734

Ohta, M., Higashi, Y., Yawata, T., Kitahara, M., Nobumoto, A., Ishida, E., et al. (2013). Attenuation of axonal injury and oxidative stress by edaravone protects against cognitive impairments after traumatic brain injury. *Brain Res.* 1490, 184–192. doi: 10.1016/j.brainres.2012.09.011

Oskarsson, B., Maragakis, N., Bedlack, R. S., Goyal, N., Meyer, J. A., Genge, A., et al. (2021). MN-166 (ibudilast) in amyotrophic lateral sclerosis in a phase IIb/III study: COMBAT-ALS study design. *Neurodegener. Dis. Manag.* 11, 431–443. doi: 10.2217/nmt-2021-0042

Ostenfeld, M. S., Fehrenbacher, N., Høyer-Hansen, M., Thomsen, C., Farkas, T., and Jäättelä, M. (2005). Effective tumor cell death by sigma-2 receptor ligand siramesine involves lysosomal leakage and oxidative stress. *Cancer Res.* 65, 8975–8983. doi: 10.1158/0008-5472.CAN-05-0269

Pandya, J. D., Readnower, R. D., Patel, A. P., Yonutas, H. M., Pauly, J. R., Goldstein, G. A., et al. (2014). N-acetylcysteine amide confers neuroprotection, improves bioenergetics and behavioral outcome following TBI. *Exp. Neurol.* 257, 106–113. doi: 10.1016/j.expneurol.2014.04.020

Priester, A., Waters, R., Abbott, A., Hilmas, K., Woelk, K., Miller, H. A., et al. (2022). Theranostic copolymers neutralize reactive oxygen species and lipid peroxidation products for the combined treatment of traumatic brain injury. *Biomacromolecules* 22, 1703–1712. doi: 10.1021/acs.biomac.1c01635

Ptito, M., Bleau, M., and Bouskila, J. (2021). The retina: A window into the brain. *Cells* 10:3269. doi: 10.3390/cells10123269

Purves, D., Augustine, G. J., Fitzpatrick, D., Katz, L. C., LaMantia, A. S., McNamara, J. O., et al. (eds) (2001). *Neuroscience*, 2nd Edn. Sunderland, MA: Sinauer Associates.

Rango, M., and Bresolin, N. (2018). Brain mitochondria, aging, and Parkinson's disease. *Genes* 9:250. doi: 10.3390/genes9050250

Roberts, I., Yates, D., Sandercock, P., Farrell, B., Wasserberg, J., Lomas, G., et al. (2004). Effect of intravenous corticosteroids on death within 14 days in 10008 adults with clinically significant head injury (MRC CRASH trial): Randomised placebo-controlled trial. *Lancet* 364, 1321–1328. doi: 10.1016/S0140-6736(04)17188-2

Roberts, V. J., and Gorenstein, C. (1987). Examination of the transient distribution of lysosomes in neurons of developing rat brains. *Dev. Neurosci.* 9, 255–264. doi: 10.1159/000111628

Robicsek, O., Ene, H. M., Karry, R., Ytzhaki, O., Asor, E., McPhie, D., et al. (2018). Isolated mitochondria transfer improves neuronal differentiation of schizophrenia-derived induced pluripotent stem cells and rescues deficits in a rat model of the disorder. *Schizophr. Bull.* 44, 432–442. doi: 10.1093/schbul/sbx077

Roca, F. J., and Ramakrishnan, L. (2013). TNF dually mediates resistance and susceptibility to mycobacteria via mitochondrial reactive oxygen species. *Cell* 153, 521–534. doi: 10.1016/j.cell.2013.03.022

Rodgers, K. M., Bercum, F. M., McCallum, D. L., Rudy, J. W., Frey, L. C., Johnson, K. W., et al. (2012). Acute neuroimmune modulation attenuates the development of anxiety-like freezing behavior in an animal model of traumatic brain injury. *J. Neurotrauma* 29, 1886–1897. doi: 10.1089/neu.2011.2273

Rubiano, A. M., Carney, N., Chesnut, R., and Puyana, J. C. (2015). Global neurotrauma research challenges and opportunities. *Nature* 527, S193–S197. doi: 10.1038/nature16035

Saffi, G. T., Tang, E., Mamand, S., Inpanathan, S., Fountain, A., Salmena, L., et al. (2021). Reactive oxygen species prevent lysosome coalescence during PIKfyve inhibition. *PLoS One* 16:e0259313. doi: 10.1371/journal.pone.0259313

Sandalio, L. M., and Romero-Puertas, M. C. (2015). Peroxisomes sense and respond to environmental cues by regulating ROS and RNS signaling networks. *Ann. Bot.* 116, 475–485. doi: 10.1093/aob/mcv074

Sandoval, R., Lazcano, P., Ferrari, F., Pinto-Pardo, N., González-Billault, C., and Utreras, E. (2018). TNF-α increases production of reactive oxygen species through Cdk5 activation in nociceptive neurons. *Front. Physiol.* 9:65. doi: 10.3389/fphys.2018.00065

Santo, M., and Conte, I. (2021). Emerging lysosomal functions for photoreceptor cell homeostasis and survival. *Cells* 11:60. doi: 10.3390/cells11010060

Sarkies, N. (2004). Traumatic optic neuropathy. *Eye* 18, 1122–1125. doi: 10.1038/sj.eye.6701571

Schnichels, S., Schultheiss, M., Klemm, P., Blak, M., Herrmann, T., Melchinger, M., et al. (2021). Cyclosporine a protects retinal explants against hypoxia. *Int. J. Mol. Sci.* 22:10196. doi: 10.3390/ijms221910196

Schwarz, D. S., and Blower, M. D. (2016). The endoplasmic reticulum: Structure, function and response to cellular signaling. *Cell. Mol. Life Sci.* 73, 79–94. doi: 10.1007/s00018-015-2052-6

Scortegagna, M., Ding, K., Oktay, Y., Gaur, A., Thurmond, F., Yan, L. J., et al. (2003). Multiple organ pathology, metabolic abnormalities and impaired homeostasis of reactive oxygen species in Epas1$^{-/-}$ mice. *Nat. Genet.* 35, 331–340. doi: 10.1038/ng1266

Sen, N. (2017). An insight into the vision impairment following traumatic brain injury. *Neurochem. Int.* 11, 103–107. doi: 10.1016/j.neuint.2017.01.019

Sherwood, D., Sponsel, W. E., Lund, B. J., Gray, W., Watson, R., Groth, S. L., et al. (2014). Anatomical manifestations of primary blast ocular trauma observed in a postmortem porcine model. *Invest. Ophthalmol. Vis. Sci.* 55, 1124–1132. doi: 10.1167/iovs.13-13295

Sies, H., and Jones, D. P. (2020). Reactive oxygen species (ROS) as pleiotropic physiological signalling agents. *Nat. Rev. Mol. Cell Biol.* 21, 363–383. doi: 10.1038/s41580-020-0230-3

Singh, A., Kukreti, R., Saso, L., and Kukreti, S. (2019). Oxidative stress: A key modulator in neurodegenerative diseases. *Molecules* 24:1583. doi: 10.3390/molecules24081583

Sinha, D., Valapala, M., Shang, P., Hose, S., Grebe, R., Lutty, G. A., et al. (2016). Lysosomes: Regulators of autophagy in the retinal pigmented epithelium. *Exp. Eye Res.* 144, 46–53. doi: 10.1016/j.exer.2015.08.018

Someya, E., Akagawa, M., Mori, A., Morita, A., Yui, N., Asano, D., et al. (2019). Role of neuron- glia signaling in regulation of retinal vascular tone in rats. *Int. J. Mol. Sci.* 20:1952. doi: 10.3390/ijms20081952

Song, J. W., Misgeld, T., Kang, H., Knecht, S., Lu, J., Cao, Y., et al. (2008). Lysosomal activity associated with developmental axon pruning. *J. Neurosci.* 28, 8993–9001. doi: 10.1523/JNEUROSCI.0720-08.2008

Steinsapir, K. D., and Goldberg, R. A. (2011). Traumatic optic neuropathy: An evolving understanding. *Am. J. Ophthalmol.* 151, 928–933.e2. doi: 10.1016/j.ajo.2011.02.007

Strauss, O. (2005). The retinal pigment epithelium in visual function. *Physiol. Rev.* 85, 845–881. doi: 10.1152/physrev.00021.2004

Streit, W. J., Mrak, R. E., and Griffin, W. S. T. (2004). Microglia and neuroinflammation: A pathological perspective. *J. Neuroinflamm.* 1:14. doi: 10.1186/1742-2094-1-14

Sullivan, P. G., Rabchevsky, A. G., Waldmeier, P. C., and Springer, J. E. (2004). Mitochondrial permeability transition in CNS trauma: Cause or effect of neuronal cell death? *J. Neurosci. Res.* 79, 231–239. doi: 10.1002/jnr.20292

Suzukawa, K., Miura, K., Mitsushita, J., Resau, J., Hirose, K., Crystal, R., et al. (2000). Nerve growth factor-induced neuronal differentiation requires generation of Rac1-regulated reactive oxygen species. *J. Biol. Chem.* 275, 13175–13178. doi: 10.1074/jbc.275.18.13175

Tahvilian, R., Amini, K., and Zhaleh, H. (2019). Signal transduction of improving effects of ibudilast on methamphetamine induced cell death. *Asian Pac. J. Cancer Prev.* 20, 2763–2774.

Tan, H. P., Guo, Q., Hua, G., Chen, J. X., and Liang, J. C. (2018). Inhibition of endoplasmic reticulum stress alleviates secondary injury after traumatic brain injury. *Neural Regen. Res.* 13, 827–836. doi: 10.4103/1673-5374.232477

Tandon, V., and Maapatra, A. K. (2017). Current management of optic nerve injury. *Indian J. Neurosurg.* 6, 83–85. doi: 10.1055/s-0037-1606314

Tao, W., Dvoriantchikova, G., Tse, B. C., Pappas, S., Chou, T. H., Tapia, M., et al. (2017). A novel mouse model of traumatic optic neuropathy using external ultrasound energy to achieve focal, indirect optic nerve injury. *Sci. Rep.* 7:11779. doi: 10.1038/s41598-017-12225-6

Thompson, K. K., and Tsirka, S. E. (2017). The diverse roles of microglia in the neurodegenerative aspects of central nervous system (CNS) autoimmunity. *Int. J. Mol. Sci.* 18:504. doi: 10.3390/ijms18030504

Tse, B. C., Dvoriantchikova, G., Tao, W., Gallo, R. A., Lee, J. Y., Pappas, S., et al. (2018). Tumor necrosis factor inhibition in the acute management of traumatic optic neuropathy. *Invest. Ophthalmol. Vis. Sci.* 59, 2905–2912. doi: 10.1167/iovs.18-24431

Vang, S., Longley, K., Steer, C. J., and Low, W. C. (2014). The unexpected uses of urso- and tauroursodeoxycholic acid in the treatment of non-liver diseases. *Glob. Adv. Health Med.* 3, 58–69. doi: 10.7453/gahmj.2014.017

Vidal, L., Díaz, F., Villena, A., Moreno, M., Campos, J. G., and Pérez de Vargas, I. (2010). Reaction of Müller cells in an experimental rat model of increased intraocular pressure following timolol, latanoprost and brimonidine. *Brain Res. Bull.* 82, 18–24. doi: 10.1016/j.brainresbull.2010.02.011

Vielma, A. H., Retamal, M. A., and Schmachtenberg, O. (2012). Nitric oxide signaling in the retina: What have we learned in two decades? *Brain Res.* 1430, 112–125. doi: 10.1016/j.brainres.2011.10.045

Wu, S. M., and Maple, B. R. (1998). Amino acid neurotransmitters in the retina: A functional overview. *Vis. Res.* 38, 1371–1384. doi: 10.1016/s0042-6989(97)00296-4

Yang, S., and Lian, G. (2020). ROS and diseases: Role in metabolism and energy supply. *Mol. Cell. Biochem.* 467, 1–12. doi: 10.1007/s11010-019-03667-9

Zhang, Y., Xi, X., Mei, Y., Zhao, X., Zhou, L., Ma, M., et al. (2019). High-glucose induces retinal pigment epithelium mitochondrial pathways of apoptosis and inhibits mitophagy by regulating ROS/PINK1/Parkin signal pathway. *Biomed. Pharmacother.* 111, 1315–1325. doi: 10.1016/j.biopha.2019.01.034

Zhou, Y., Fan, R., Botchway, B. O. A., Zhang, Y., and Liu, X. (2021). Infliximab can improve traumatic brain injury by suppressing the tumor necrosis factor alpha pathway. *Mol. Neurobiol.* 58, 2803–2811. doi: 10.1007/s12035-021-02293-1

Frontiers in Neuroscience

Provides a holistic understanding of brain function from genes to behavior

Part of the most cited neuroscience journal series which explores the brain - from the new eras of causation and anatomical neurosciences to neuroeconomics and neuroenergetics.

Discover the latest Research Topics

See more →

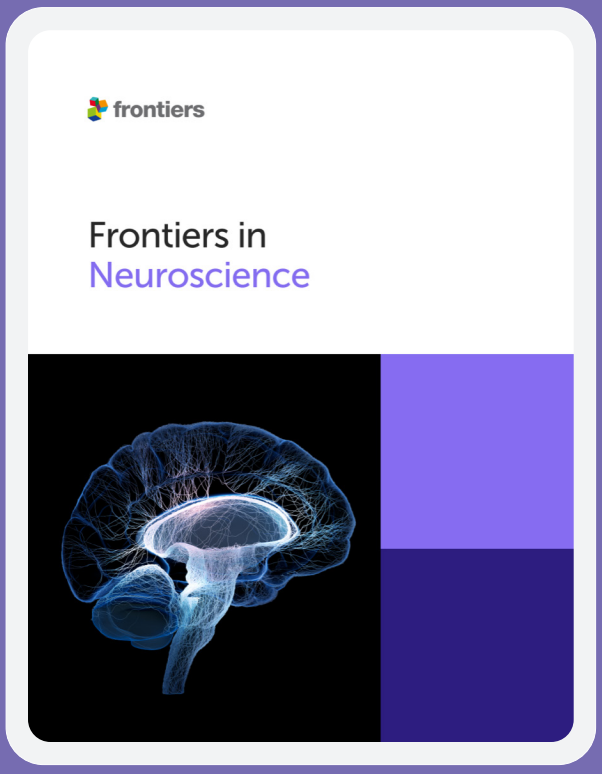

Frontiers

Avenue du Tribunal-Fédéral 34
1005 Lausanne, Switzerland
frontiersin.org

Contact us

+41 (0)21 510 17 00
frontiersin.org/about/contact